

THE BIOLOGICAL ROLE OF REDOX SIGNALLING BY THE TUMOUR
SUPPRESSOR PTEN

SARAH LOUISE SMITH
Doctor of Philosophy

ASTON UNIVERSITY
SEPTEMBER 2022

© Sarah Louise Smith, 2022

Sarah Louise Smith asserts their moral right to be identified as the author of this thesis.

This copy of the thesis has been supplied on condition that anyone who consults it is understood to recognise that its copyright belongs to its author and that no quotation from the thesis and no information derived from it may be published without appropriate permission or acknowledgement.

Abstract

Phosphatase and tensin homologue (PTEN) is an antagonist of the Akt pathway through its phosphatase activity against phosphatidylinositol-3,4,5-phosphate (PIP₃). The Akt pathway modulates numerous metabolic and cell survival processes. PTEN is redox sensitive and oxidation by reactive oxygen species (ROS) causes catalytic inactivation and changes to its interactome. ROS can oxidise phospholipids resulting in lipid oxidation products, such as acrolein and 4-hydroxynonenal (4-HNE). Whilst the effect of 4-HNE on PTEN has previously been studied, there is limited data for acrolein. The research presented in this thesis aimed to further characterise the effect of lipoxidation on PTEN by investigating the effect of acrolein on PTEN's activity, structure and interactions using a range of proteomic techniques.

In the first chapter, recombinant human PTEN-V5-His was overexpressed in *Escherichia coli* and purified using immobilised metal affinity chromatography. In the second chapter, PTEN-V5-His was treated *in vitro* with acrolein, from 0.2:1 to 20:1 acrolein:PTEN. Phosphatase activity and SDS-PAGE analysis showed dose-dependent inactivation and aggregation. Analysis using tandem mass spectrometry showed a greater susceptibility of cysteine residues to modification, with lysine modifications detected at higher acrolein concentrations. The third chapter involved affinity pull down with PTEN-V5-His, where acrolein treatment was performed prior to challenge with HCT-116 cell lysates. Proteomic analysis of the captured proteins identified changes in the interactome between untreated and acrolein-treated PTEN. HECTD1, an E3 ubiquitin ligase, was validated *in vitro* as a novel interactor of PTEN that showed increased binding on acrolein treatment of PTEN. The final chapter characterised the *in cellulo* effect of acrolein treatment, where a dose- and time-dependent loss of cell viability was identified for HCT-116 cells. On treatment with sublethal acrolein concentrations, the levels of active phosphoAkt increased whereas inactive Akt remained constant. Taken together, these results demonstrate that acrolein causes a functional change in the activity, structure and interactions of PTEN.

Acknowledgements

Firstly, I would like to thank my supervisor Prof. Corinne Spickett and my co-supervisors, Prof. Andrew Pitt and Dr Alex Cheong. Corinne, thank for welcoming me into the group and for your guidance and advice over the last 3 years. Andy, thank you for sharing your mass spectrometry knowledge with me and for continuing to support me after your move. Alex, thank you for the moral support and advice. I would also like to thank Dr Ivana Milic for her practical help and support with running my samples on the mass spectrometer and for her patience with all my questions!

MB360 would not have been the same without Bita Hosseini and Idoia Company-Marin. I couldn't have asked for better company and I wish you both the very best. I would also like to thank the other researchers that have been members of the Oxidative Stress group during my time at Aston University.

To my best friends Shaheda, Emma, Fadoua and Radmila, I am so lucky to have you four and thank you for all the love you've given me from afar. To Tiago, thank you for all that you have brought to my life and the support you have given me. To my parents, Pauline and Mark Hengeveld and Peter and Lisa Smith, thank you for everything. Without your never-ending supply of love and words of advice, I would not be where I am today. To my brother, Tom, and sisters, Elisabeth and Maria, thank you for always cheering me on.

Table of Contents

Abstract	2
Acknowledgements.....	3
List of Abbreviations.....	9
List of Figures.....	12
List of Tables.....	15
1 Chapter 1 – Introduction	17
1.1 Oxidative Stress and Redox Signalling.....	17
1.1.1 Reactive Oxygen Species	17
1.1.2 Lipid Oxidation Products	17
1.2 PTEN is a Tumour Suppressor and Metabolic Regulator	19
1.2.1 The Structure of PTEN	19
1.2.2 The Phosphatase Activity of PTEN	22
1.2.3 PTEN's Role in the Akt Signalling Pathway	23
1.2.4 The Subcellular Localisation of PTEN Determines its Physiological Role	25
1.2.5 Isoforms of PTEN	25
1.2.6 Regulation of PTEN by Post-translational Modification	26
1.2.7 PTEN's Interactome	34
1.3 Aims and Hypotheses	35
1.3.1 Research Aim 1: Characterise the Effect of Acrolein on PTEN's Phosphatase Activity	35
1.3.2 Research Aim 2: Characterise the Effect of Acrolein on PTEN's Structure.....	37
1.3.3 Research Aim 3: Characterise the Effect of Acrolein on PTEN's Interactions.....	38
2 Chapter 2 – General Materials and Methods	40
2.1 Materials	40
2.2 Mammalian Cell Culture	40
2.2.1 Thawing, Subculture and Cryopreservation of HCT-116 cells	40
2.2.2 Cell Count and Viability Assessment	41
2.2.3 Mammalian Cell Harvest	41
2.2.4 Mammalian Cell Lysis	41
2.3 Protein Detection and Analysis	42
2.3.1 Molecular weight and extinction coefficient determination.....	42

2.3.2	Protein Quantification	42
2.3.3	Sodium Dodecyl Sulfate Polyacrylamide Gel Electrophoresis (SDS-PAGE)	43
2.3.4	Western Blot Analysis	44
2.4	Mass Spectrometry.....	44
2.4.1	Reconstitution and Dilution of Proteases	44
2.4.2	In-gel Digestion	45
2.4.3	In-solution Digestion.....	45
2.4.4	High Performance Liquid Chromatography with Tandem Mass Spectrometry (HPLC-MS/MS)	46
2.4.5	Mascot Search Parameters.....	47
3	Chapter 3 – Expression, Purification and Characterisation of Recombinant PTEN.....	48
3.1	Introduction.....	48
3.1.1	Protein Production for <i>In Vitro</i> Studies	48
3.1.2	Expression and Purification of Recombinant PTEN.....	49
3.1.3	Identification of Proteins using Mass Spectrometry	50
3.1.4	Aims	52
3.2	Materials and Methods	53
3.2.1	Materials	53
3.2.2	Expression of PTEN-V5-His in <i>E. coli</i>	53
3.2.3	Purification of PTEN-V5-His.....	55
3.2.4	Protein Detection and Analysis	57
3.2.5	Phosphatase Activity Analysis	58
3.2.6	Statistical Analysis.....	59
3.3	Results.....	60
3.3.1	Plasmid Preparation from TOP10 <i>E. coli</i> Resulted in Supercoiled Plasmid Suitable for Transformation and Expression	60
3.3.2	Expression in BL21 (DE3) Successfully Produced Soluble PTEN-V5-His	61
3.3.3	Characterisation of Purified PTEN-V5-His Confirmed Correct Sequence and Phosphatase Activity	63
3.4	Discussion.....	71
4	Chapter 4 – Effect of Acrolein on the Activity and Structure of Recombinant PTEN.....	77
4.1	Introduction.....	77
4.1.1	Lipoxidation of PTEN	77
4.1.2	Approaches to the Detection of Lipid Oxidation Product Adducts	78

4.1.3	Mass Spectrometry Analysis of Acrolein Protein Modifications	79
4.1.4	Aims and Hypotheses	80
4.2	Methods.....	81
4.2.1	Optimisation of the OMFP Activity Assay for Acrolein-Treated PTEN.....	81
4.2.2	<i>In vitro</i> Lipoxidation of PTEN-V5-His.....	81
4.2.3	Proteomic Analysis of the Effect of Lipoxidation on PTEN	82
4.2.4	Incubation of PTEN-V5-His at 37°C with and without DTT	84
4.2.5	Statistical Analysis.....	84
4.3	Results.....	85
4.3.1	The OMFP Phosphatase Activity of Purified PTEN-V5-His Decreases with Decreasing DTT Concentration	85
4.3.2	Sodium Borohydride Reduction Does Not Affect the OMFP Phosphatase Activity of PTEN-V5-His.....	86
4.3.3	The Time-Independent Inactivation of PTEN's Phosphatase Activity by Acrolein after 10 minutes.....	87
4.3.4	The Dose-Dependent Inactivation of PTEN's Phosphatase Activity by Acrolein.....	88
4.3.5	The Cross-linking Effect of Acrolein on PTEN-V5-His	89
4.3.6	Incubation of PTEN-V5-His in the Absence of DTT Results in Oxidation and Cross-linking	91
4.3.7	PTEN's Cysteine and Lysine Residues are the Most Susceptible to Acrolein Modification	92
4.3.8	Cysteine and Lysine Residues across PTEN's Structure are Susceptible to Acrolein Modification	95
4.3.9	Increasing the Sequence Coverage of Potential Modification Sites using Alternative Proteases	99
4.3.10	Digestion of Acrolein-treated PTEN with Chymotrypsin Revealed Additional Lysine Modifications at High Treatment Concentrations	102
4.3.11	Digestion of Acrolein-treated PTEN with Trypsin/Glu-C Found No Modification to the Catalytic Cysteine	105
4.3.12	Lipoxidative Modification Mapping to the 3D Structure of PTEN and Solvent Accessibility Analysis	110
4.4	Discussion.....	114
5	Chapter 5 – Effect of Acrolein on the Global Interactome of Recombinant PTEN.....	126
5.1	Introduction.....	126
5.1.1	Protein Interactomes and the Effect of Post-translational modification	126
5.1.2	Methods to Identify Post-translational Modification-Associated Protein-Protein Interactions.....	126

5.1.3	PTEN's Interactome	129
5.1.4	Redox-Sensitive Interactors of PTEN	131
5.1.5	Aims and Hypotheses	133
5.2	Methods.....	135
5.2.1	Preparation of Recombinant PTEN Bait	135
5.2.2	Preparation of HCT-116 Lysate Prey	135
5.2.3	Pull Down Assay Optimisation	135
5.2.4	Pull Down Assay with Untreated and Acrolein-treated Recombinant PTEN	137
5.2.5	Proteomic Analysis of the Effect of Lipoxidation on PTEN's interactome.....	138
5.3	Results.....	140
5.3.1	Increasing the Concentration of Imidazole in the Affinity Pull Down Buffers Reduces Non-specific Binding to the Nickel Resin	140
5.3.2	Acrolein Treatment did not have an Adverse Effect on the Affinity Pull Down Assays 143	
5.3.3	Acrolein Treatment of Immobilised PTEN=V5-His Successfully Modified Susceptible Residues 147	
5.3.4	PTEN-specific Interactors were Identified from the Affinity Pull Down Assays.....	147
5.3.5	PTEN-specific Interactors Showed a Change in Abundance Between the Untreated and Acrolein-treated PTEN Pull Downs	148
5.3.6	Validation of an Acrolein-sensitive Interactor using Western Blotting.....	153
5.4	Discussion.....	157
6	Chapter 6 – Effects of Acrolein on the Function of PTEN In Cellulo.....	167
6.1	Introduction.....	167
6.1.1	Approaches to Assessment of Cell Viability.....	167
6.1.2	Effect of Oxidation and Lipoxidation on PTEN's Regulation of the Akt Signalling Pathway 168	
6.1.3	Protein-Protein Interaction (PPI) Validation	169
6.1.4	Aims and Hypotheses	171
6.2	Methods.....	173
6.2.1	MTT Assay and Optimisation	173
6.2.2	Trial Immunoprecipitation of PTEN and α,β -tubulin from HCT-116 and MCF-7 cells. 173	
6.2.3	Co-immunoprecipitation of Endogenous PTEN and HECTD1 from Untreated and Acrolein-treated HCT-116 Cells	175
6.2.4	Mammalian Cell Lysis Optimisation for Western Blotting	176
6.2.5	Acrolein Treatment of HCT-116 Cells for Western Blot Analysis.....	177
6.2.6	Statistical Analysis.....	178
6.3	Results.....	179

6.3.1	The Use of Acidified IPA as an MTT Solubilisation Solution Increases the Absorbance in Comparison to the use of Acidified SDS	179
6.3.2	Acrolein Treatment has a Dose- and Time-dependent Effect on Cell Viability	180
6.3.3	Immunoprecipitation of Endogenous PTEN from HCT-116 cells.....	181
6.3.4	Detection of Endogenous PTEN in HCT-116 Lysate and Optimisation of Lysis for Western Blot Analysis	186
6.3.5	Repeat IP of Endogenous PTEN from HCT-116 WT and MCF-7 Cells.....	187
6.3.6	CoIP of Endogenous PTEN from Untreated and Acrolein-treated HCT-116 Cells.....	190
6.3.7	Acrolein Treatment Increases the Level of pAkt whilst levels of total Akt Remain Stable	194
6.4	Discussion.....	196
7	Chapter 7 – General Discussion.....	206
7.1	Knowledge Gap and Key Findings	206
7.2	Inactivation of PTEN by Acrolein <i>In Vitro</i> and <i>In Cellulo</i>	207
7.3	Acrolein-treated PTEN showed Changes in its Interactome.....	211
7.4	Conclusion and Future Directions.....	213
8	References	215
9	Appendices	236

List of Abbreviations

4-HNE	4-hydroxynonenal
Ala	Alanine
ALP	Alkaline phosphatase
ANOVA	Analysis of variance
Anxa2	Annexin A2
APD	Affinity pull down
APS	Ammonium persulfate
Arg	Arginine
ASA	Absolute solvent accessibility
Asp	Aspartic acid
ATIR-FTIR	Attenuated total reflectance-fourier transform infrared
BCA	Bicinchoninic acid
BRET	Bioluminescence resonance energy transfer
BSA	Bovine serum albumin
CD	Circular dichroism
CID	Collision-induced dissociation
CoIP	Co-immunoprecipitation
CSP	Chemical shift perturbation
CV	Column volume
Cys	Cysteine
DDA	Data-dependent analysis
DDB1	DNA damage binding protein 1
DIA	Data-independent analysis
DMF	Dimethylformamide
DMSO	Dimethyl sulfoxide
DNPH	2,4-dinitrophenylhydrazine
DTT	Dithiothreitol
DUP	Dual specificity phosphatases
ECL	Enhanced chemiluminescence
EDTA	Ethylenediaminetetraacetic acid
EI	Electron ionisation
ELISA	Enzyme-linked immunosorbent assay
ESI	Electrospray ionisation
FA	Formic acid
FBS	Fetal bovine serum
FLIM	Fluorescence lifetime imaging microscopy
FOXO	Forkhead Box O
FRET	Fluorescence resonance energy transfer
FT	Flow-through
FTIC	Fourier transform ion cyclotron
GFP	Green fluorescent protein
Glu	Glutamic Acid
Gly	Glycine
GSK3	Glycogen synthase kinase 3
GST	Glutathione-S-transferase
HA	Haemagglutinin
His	Histidine
His tag	6-Histidine fusion tag
HPLC	High performance liquid chromatography
HRP	Horse radish peroxidase

IAM	Iodoacetamide
IDR	Intrinsically disordered region
Ile	Isoleucine
IMAC	Immobilised metal affinity chromatography
InsP	Inositol phosphate
IP	Immunoprecipitation
IPA	Isopropanol
IPTG	Isopropyl β -D-1-thiogalactopyranoside
K_a	Acid dissociation constant
LB	Luria broth
LB-Amp	Luria broth supplemented with ampicillin
LC-MS/MS	Tandem mass spectrometry
LPS	Lipopolysaccharide
Lys	Lysine
m/z	Mass-to-charge ratio
MALDI	Matrix-assisted laser desorption/ionisation
MBP	Maltose-binding protein
MDA	Malondialdehyde
MPO	Myeloperoxidase
mTORC1	Mammalian target of rapamycin complex 1
MTS	3-(4,5-dimethylthiazol-2-yl)-5-(3-carboxymethoxyphenyl)-2-(4-sulfophenyl)-2H-tetrazolium
MTT	3-(4,5-dimethylthiazol-2-yl)-2,5 diphenyl tetrazolium bromide
NMR	Nuclear magnetic resonance
O/N	Overnight
OMF	3-O-methylfluorescein
OMFP	3-O-methylfluorescein phosphate
oxPTEN	oxidised PTEN
P loop	Phosphate binding loop
pAkt	Phosphorylated Akt
PAP	Parallel affinity purification
PBS	Phosphate-buffered saline
PK1	3-phosphoinositide-dependent protein kinase 1
Phe	Phenylalanine
PI3K	Phosphoinositide 3-kinases
PIC	Protease inhibitor cocktail
PIP₃	Phosphatidylinositol (3,4,5)-trisphosphate
PKC	Protein kinase C
PMA	Phorbol 12-myristate 13-acetate
PMSF	Phenylmethylsulfonyl fluoride
pNPP	Paranitrophenyl phosphate
PPI	Protein-protein interaction
Prdx1	Peroxiredoxin
Pro	Proline
PTB	Phosphotyrosine domain
PTEN	Phosphatase and tensin homologue
PTM	Post-translational modification
PTP	Protein tyrosine phosphatase
PUFA	Polyunsaturated fatty acids
PVDF	Polyvinylidene difluoride
RCML	Reduced, carboxamidomethylated and maleylated lysozyme
ROS	Reactive oxygen species
RPM	Revolutions per minute

RSA	Relative solvent accessibility
RT	Room temperature
RT-PCR	Real time-polymerase chain reaction
SC	Spin column
SDS-PAGE	Sodium dodecyl sulfate polyacrylamide gel electrophoresis
SEC	Size exclusion chromatography
SEM	Standard error of the mean
Ser	Serine
SMOX	Spermine oxidase
SOC	Super optimal broth with catabolite repression
SPR	Surface plasmon resonance
Sy.x	Standard error of the estimate
TAE	Tris-acetate-ethylenediaminetetraacetic acid
TAP	Tandem affinity purification
TBS	Tris-buffered saline
TBS-T	Tris-buffered saline with tween
TEMED	Tetramethylethylenediamine
TFA	Trifluoroacetic acid
Thr	Threonine
TOF	Time of flight
Trdx	Thioredoxin
Trp	Tryptophan
Tyr	Tyrosine
UV	Ultraviolet
Val	Valine
WDR5	WD repeat-containing protein 5
WT	Wild type
XIC	Extracted ion chromatogram
XTT	2,3-bis-(2-methoxy-4-nitro-5-sulfophenyl)-2H-tetrazolium-5-carboxanilide
Y2H	Yeast-2-hybrid

List of Figures

Figure 1.1 The N- and C- terminal domains of PTEN (reproduced with permission from Smith et al. (2021)).....	20
Figure 1.2 An overview of the metabolic and cell survival signalling pathways downstream from the action of PTEN (reproduced with permission from Smith et al. (2021)).....	23
Figure 3.1 Agarose gel separation of intact and restriction digested purified plasmid.	61
Figure 3.2 Western Blot analysis of PTEN-V5-His expression after induction with 1.0 mM IPTG at 20°C for 2-24 hours.	62
Figure 3.3 SDS-PAGE analysis of purified PTEN-V5-His expressed for different times.....	63
Figure 3.4 Representative SDS-PAGE analysis of the IMAC purification of PTEN-V5-His.....	64
Figure 3.5 Representative SDS-PAGE and densitometry analysis of PTEN-V5-His.....	65
Figure 3.6 Representative sequence coverage of PTEN-V5-His.....	67
Figure 3.7 Representative OMF calibration curve.	68
Figure 3.8 Effect of pre-incubation on the linearity of the increase in fluorescence during the OMFP phosphatase activity assay.	69
Figure 3.9 Effect of buffer exchange and concentration on the OMFP phosphatase activity of PTEN-V5-His.....	70
Figure 4.1 Effect of DTT on the OMFP phosphatase activity of PTEN-V5-His.....	85
Figure 4.2 Effect of NaBH ₄ reduction on the OMFP phosphatase activity of PTEN-V5-His.....	86
Figure 4.3 OMFP Phosphatase Activity Analysis of PTEN-V5-His Treated with Increasing Acrolein Concentrations for 10 minutes, 1 hour and 4 hours.....	88
Figure 4.4 OMFP Phosphatase Activity Analysis of PTEN-V5-His Treated with Increasing Acrolein Concentrations for 10 minutes.....	89
Figure 4.5 SDS-PAGE and Densitometry Analysis of PTEN-V5-His Treated with Increasing Acrolein Concentrations for 10 minutes, 1 hour and 4 hours.....	90
Figure 4.6 SDS-PAGE Analysis of the Effect of Incubation with and without DTT at 37°C on PTEN-V5-His.....	92
Figure 4.7 Representative Mascot Peptide Output for an Unmodified and a True and False Positive Hit for Acrolein-modified Cys71.	96
Figure 4.8 Representative Mascot Peptide Sequencing of Unmodified and Acrolein-modified Hit for the Cys124 Peptide.....	97
Figure 4.9 Representative Mascot Peptide Identification of Unmodified and a False Positive Hit for an Acrolein-modified Lysine Residue (Lys164) and a True Positive Hit for an Acrolein-modified Lysine Residue (Lys6).....	98
Figure 4.10 Comparison of the Sequence Coverage of PTEN-V5-His Digested with Trypsin or Chymotrypsin.....	102

Figure 4.11 Acrolein Modified Residues Mapped to the Crystal Structure of PTEN.	110
Figure 4.12 Acrolein Modified Residues Mapped to the Crystal Structure of PTEN and coloured according to their accessible surface area.	113
Figure 4.13 Structure of Acrolein and 4-HNE.....	124
Figure 5.1 An overview of the steps involved in high-throughput investigations of the interactome of PTEN (reproduced with permission from Smith et al. (2021)).....	131
Figure 5.2 Comparison of APD Techniques and the Effect of Imidazole on PTEN-V5-His Immobilisation to Nickel Affinity Resin.	141
Figure 5.3 Quantification and SDS-PAGE Analysis of the Effect of Imidazole on Non-Specific Binding of HCT-116 Lysate Proteins to Nickel Resin.....	142
Figure 5.4 SDS-PAGE Analysis of the Fractions Obtained During Nickel Affinity Pull Down Assays with and without Acrolein Treatment of PTEN-V5-His.	145
Figure 5.5 Representative SDS-PAGE Analysis of the Proteins Obtained from the Elution Fractions during the Pull Down Assay.	146
Figure 5.6 Overview of the Number of Proteins Obtained during the Pull Down Assays with and without Acrolein.....	148
Figure 5.7 Comparison of the Maximum Fold Change in Abundance of Interactors of Interest between Control and Acrolein-treated PTEN.	152
Figure 5.8 Western Blot Analysis of HCT-116 WT lysate against HECTD1 and α/β -Tubulin.....	154
Figure 5.9 Representative Western Blot Analysis of a Potential Acrolein-Sensitive PTEN Interactor; HECTD1.....	156
Figure 5.10 The number of potential PTEN interactors, validated PTEN interactors and interactors with a proposed functional role for the interaction with PTEN.....	164
Figure 5.11 A diagram showing the E3 ubiquitin ligases that have been identified as potential interactors of PTEN, in previous high- and low-data content studies (blue) and the current study (green).	166
Figure 6.1 Effect of Acidified IPA vs Acidified SDS in the Solubilisation of MTT when Assaying for Cell Viability.....	180
Figure 6.2 Effect of Acrolein Treatment on the Cell Viability of HCT-116 cells after 1 and 24 hours ...	181
Figure 6.3 Initial IP of PTEN showed successful binding of the anti-PTEN Ab to the Protein A resin but no observable detection of PTEN.	182
Figure 6.4 SDS-PAGE Analysis of the PTEN and α/β -Tubulin IP Fractions.....	184
Figure 6.5 Western Blot Analysis of the PTEN and α/β -Tubulin CoIP Elution Fractions.....	185
Figure 6.6 Western Blot Analysis of the Detection of PTEN and α/β -Tubulin Under Different Lysis Conditions	187
Figure 6.7 Western Blot Analysis of PTEN IP from HCT-116 WT and MCF-7 Cells	189
Figure 6.8 SDS-PAGE Analysis of the PTEN CoIP Fractions from Untreated and Acrolein-Treated HCT-116 Lysates.....	191

Figure 6.9 Western Blot Analysis of PTEN CoIP from HCT-116 WT and MCF-7 cells	193
Figure 6.10 Western Blot Analysis of the Detection of Akt (pan), phosphoAkt (Ser403) and α/β -Tubulin with Increasing Acrolein Treatment Concentration	195

List of Tables

Table 2.1 Cell Culture Volumes	41
Table 2.2 Parameters chosen for MS/MS analysis	47
Table 2.3 Parameters chosen for Default Mascot Daemon searches	47
Table 3.1. Fusion Tags Previously Used in the Production of Recombinant PTEN for <i>In Vitro</i> Studies	49
Table 3.2. Parameters chosen for Mascot Daemon searches	58
Table 3.3 Quantification of the purified commercial plasmid	60
Table 3.4 Yield, Purity and Phosphatase Activity Analysis of PTEN-V5-His Expressed from 2-24 hours.	63
Table 3.5 LC-MS/MS Protein Identification of Purified PTEN-V5-HIS and Additional Co-purified <i>E. coli</i> Host Proteins.....	66
Table 3.6. Enzyme Assays Used to Quantify the Phosphatase Activity of PTEN	75
Table 4.1 Parameters used for Mascot searches for Protease Comparison.....	83
Table 4.2 Parameters chosen for Mascot searches for Acrolein Modification Analysis	84
Table 4.3 LC-MS/MS Identification of Acrolein Modifications of PTEN-V5-His after In-gel Digestion with Trypsin.....	94
Table 4.4 Mascot Analysis of PTEN-V5-His Digested with Alternative Proteases	101
Table 4.5 Representative Catalytic Cysteine Coverage of PTEN-V5-His Digested with Alternative Proteases	101
Table 4.6 LC-MS/MS Identification of Acrolein Modifications of PTEN-V5-His after In-gel Digestion with Chymotrypsin	104
Table 4.7 Results for a Search of Acrolein-modified Cys124 Peptides with Increasing Charge States in the LC-MS Data of Acrolein-treated and Untreated PTEN-V5-His digested with Trypsin/Glu-C In-solution	106
Table 4.8 Identification and Quantification of the Peptides Containing Carbamidomethylated or Acrolein Modified Cysteines from Untreated and Maximally Acrolein-treated PTEN-V5-His after In-solution Digestion with Trypsin/Glu-C.....	108
Table 4.9 Solvent Accessibility Analysis of Acrolein-Modified PTEN-V5-His Residues	112
Table 4.10 Inactivation of Recombinant PTEN with Acrolein and 4-HNE	118
Table 4.11 Modification of Recombinant PTEN with Acrolein and 4-HNE Identified using LC-MS/MS	122
Table 5.1 Summary of the Content PTEN Interactome Studies (modified from Smith et al. (2021)) ..	130
Table 5.2 Parameters chosen for Mascot searches for Acrolein Modification Analysis	138
Table 5.3 Parameters chosen for Mascot searches for Interactor Analysis.....	139
Table 5.4 Quantification of the Total Protein in the Fractions collected during the Pull Down Assays	144
Table 5.5 Acrolein Modification of Immobilised PTEN-V5-His Identified by LC-MS/MS	147

Table 5.6 PTEN-Specific Interactors Identified by the Pull Down Assay that met the Threshold Parameters.....	149
Table 5.7 Summary of APD Methods for Bait Preparation and PPI Isolation (modified from Smith et al. (2021)).....	158
Table 5.8 Advantages and Disadvantages of Affinity Chromatography Methods for PPI Isolation (reproduced with permission from Smith et al. (2021)).....	160
Table 6.1 Previous Studies Utilising the MTT Assay to Test Acrolein Cytotoxicity on Mammalian Cell Lines	168
Table 6.2 Previous Cell Viability for Different Cell Lines after Treatment with 100 μ M Acrolein for 24 hours using the MTT Assay.....	200
Table 6.3 Methods for Coimmunoprecipitation of PTEN from Mammalian Cell Lines from Previous PTEN Interactome Studies.....	202

Chapter 1 – Introduction

1.1 Oxidative Stress and Redox Signalling

Maintaining a balance between oxidation and reduction is critical for many cellular processes (Birben et al., 2012, Sies et al., 2017). This includes regulation of cell signalling through oxidative modification of proteins, such as protein kinases and protein tyrosine phosphatases, which can be inactivated by oxidation and subsequently re-activated by reduction. This reversible inactivation provides an element of control beyond phosphorylation state and is part of reduction-oxidation (redox) signalling (Sies et al., 2017, Corcoran and Cotter, 2013).

1.1.1 Reactive Oxygen Species

Oxidative stress occurs during a redox imbalance, where the capacities of the physiological antioxidant systems are reached, resulting in an excess of reactive oxygen species (ROS) (Birben et al., 2012). ROS include radicals such as superoxide anion ($\bullet\text{O}_2^-$) and hydroxyl radicals ($\text{OH}\bullet$) as well as the non-radical species hydrogen peroxide (H_2O_2) and hypochlorous acid (HOCl) (Adam Whaley-Connell, 2011, Sies et al., 2017). Oxidative stress is a pro-inflammatory condition and is apparent in pathological conditions such as cancer and diabetes (Adam Whaley-Connell, 2011). Protein modification by oxidation occurs most commonly at cysteine and methionine residues, but also occurs at a lower rate for histidine, lysine, and tryptophan residues (Davies, 2016). In addition to ROS, there are reactive species of different origins: nitrogen, sulfur and carbon (Sies et al., 2017).

1.1.2 Lipid Oxidation Products

Lipid oxidation can occur enzymatically by lipoxygenases and cyclooxygenases and non-enzymatically by free radical and non-radical oxidants (Yamamoto, 1992, Porter et al., 1995, Niki et al., 2005, Reis and Spickett, 2012, Viedma-Poyatos et al., 2021). With respect to the redox focus of this thesis, the formation of lipid oxidation products during oxidative stress will be expanded further below.

Lipid peroxidation is the process by which the unsaturated carbon-carbon double bonds of polyunsaturated fatty acids (PUFAs), in the phospholipid cell membrane for example, are attacked by free radical oxidants (Esterbauer et al., 1991, Pizzimenti et al., 2013, Viedma-Poyatos et al., 2021). There are three phases of free radical mediated PUFA peroxidation: initiation, propagation and termination (Porter et al., 1995, Guéraud et al., 2010). The free radicals produced by lipid peroxidation during the initiation and propagation phases are

considered to have local effects due to their short half-life. However, the resultant breakdown products formed at the termination phase of PUFA peroxidation, known as lipid peroxidation end products, have a longer half-life and an ability to diffuse away from their site of production (Guéraud et al., 2010). There are 5 distinct groups of lipid peroxidation end products: alkanals, 2-alkenals, 4-hydroxy-2-alkenals, keto-alkenals and alkanedials (Domingues et al., 2013). Of particular interest and the subject of extensive studies is acrolein, due to its high reactivity, as well as 4-hydroxy-2-nonenal (4-HNE) and malondialdehyde (MDA) due to their high abundance (Esterbauer et al., 1991, Pizzimenti et al., 2013, Ayala et al., 2014, Sousa et al., 2017, Viedma-Poyatos et al., 2021).

Acrolein, 2-propenal, is produced endogenously in cells as a byproduct of lipid peroxidation, polyamine metabolism and myeloperoxidase function, and exogenously, as an environmental pollutant and manufacturing bi-product (Esterbauer et al., 1991, LoPachin et al., 2009, Myers et al., 2011). Acrolein is formed when carbohydrates, fats and amino acids are heated during food preparation, as well as during combustion of fuel, smoking of tobacco and production of plastics (Esterbauer et al., 1991, Stevens and Maier, 2008). In consideration of the risk posed by the different acrolein exposure routes described above and their relevance to human health, acrolein exposure during cooking, smoking and manufacturing have previously been reviewed (Stevens and Maier, 2008).

Acrolein is a reactive aldehyde that is characterised by the presence of an α,β -unsaturated carbon-carbon bond and a carbonyl group (LoPachin et al., 2009). The mobility of acrolein's electron density, due to the electronegative oxygen in its carbonyl group, denotes acrolein to be a soft electrophile (LoPachin et al., 2009). Despite acrolein's relatively low abundance in cells as a lipid peroxidation product in comparison to 4-HNE and MDA, it has a high reactivity as the strongest electrophile and as it is relatively small it could give increased access to modification sites (Esterbauer et al., 1991, Pizzimenti et al., 2013, Spickett and Pitt, 2020). Acrolein preferentially reacts with soft nucleophiles, such as the thiol group of cysteines, through Michael addition (Stevens and Maier, 2008, LoPachin et al., 2009, Cai et al., 2009, Myers et al., 2011). Acrolein can also react with harder nucleophiles such as histidine by Michael addition and lysine by Michael addition or Schiff base formation, but these reactions are slower and require higher concentrations of acrolein (Esterbauer et al., 1991, LoPachin et al., 2009, Cai et al., 2009). Modification of lysine residues can also result in the formation of more complex adducts such as $N\epsilon$ -(3-formyl-3,4-dehydropiperidino)lysine adduct (FDP-lysine) and the $N\epsilon$ -(3-methylpyridinium)lysine (MP-lysine) adduct (Uchida et al., 1998, Furuhashi et al., 2003). Michael addition of acrolein occurs through the reaction of its β -carbon with a protein's nucleophilic group, such as a thiol group or a nitrogen lone pair, to give an

addition via acrolein's double bond (Cai et al., 2009, Viedma-Poyatos et al., 2021, Domingues et al., 2013, Spickett and Pitt, 2020). Schiff base modification occurs when acrolein's carbonyl carbon reacts with primary amino groups (Cai et al., 2009, Domingues et al., 2013, Viedma-Poyatos et al., 2021). Whilst both types of modifications are reversible, Schiff base modification is more unstable and is readily reversed under acidic conditions (Cai et al., 2009, Afonso et al., 2018, Spickett and Pitt, 2020, Viedma-Poyatos et al., 2021). In addition to Michael addition and Schiff base formation, acrolein can cause protein crosslinking (Requena et al., 1996, Stevens and Maier, 2008, LoPachin et al., 2009, Reis and Spickett, 2012, Domingues et al., 2013, Pizzimenti et al., 2013, Viedma-Poyatos et al., 2021). This covalent modification of proteins by lipid oxidation products is an example of post-translational modification known as lipoxidation (Spickett and Pitt, 2020, Viedma-Poyatos et al., 2021).

1.2 PTEN is a Tumour Suppressor and Metabolic Regulator

Phosphatase and tensin homologue (PTEN) was discovered by three independent groups in 1997 (Li et al., 1997, Li and Sun, 1997, Steck et al., 1997). Alternative names for PTEN (Li et al., 1997) are tensin-like phosphatase-1 (TEP1) (Li and Sun, 1997) and mutated in multiple advanced cancers-1 (MMAC-1) (Steck et al., 1997). PTEN was identified to be frequently deleted in cancer, including in 31% of glioblastoma cell lines, 100% of prostate cell lines and 6% of the breast cancer cell lines tested (Li et al., 1997). Correlations were made between the homology of PTEN to protein tyrosine/dual specificity phosphatases and tensin, an actin-interacting protein, and its potential function as a tumour suppressor and regulator of metastasis respectively was proposed (Li et al., 1997).

1.2.1 The Structure of PTEN

The gene encoding PTEN has 9 exons and 1209 nucleotides and generates a 403 amino acid protein. The protein is divided into two major domains, an N-terminal domain and a C-terminal domain (Lee et al., 1999). The secondary structure of the N-terminal domain consists of 5 beta-sheets and 6 alpha-helices whilst the C-terminal domain is comprised of 2 beta-sheets linked with 2 alpha-helices (Lee et al., 1999). Figure 1.1 illustrates the structure of PTEN, as well as common modification sites.

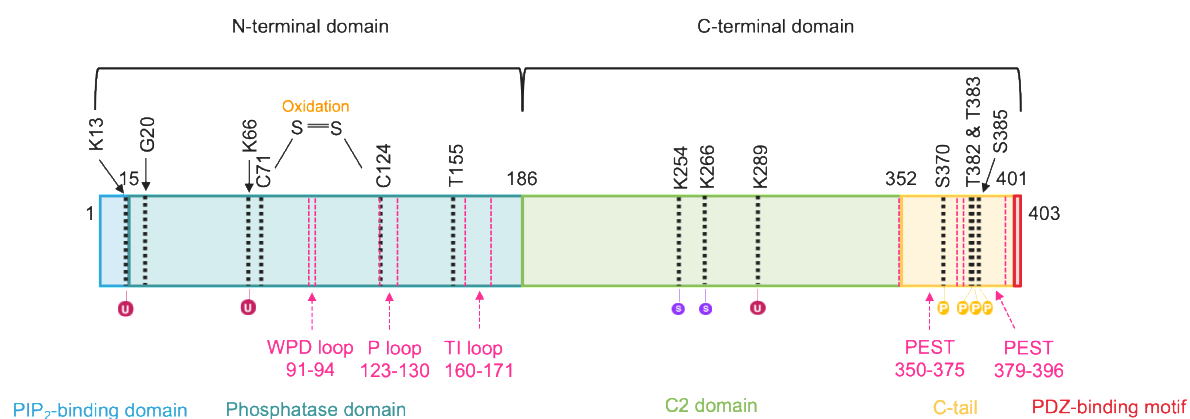


Figure 1.1 The N- and C- terminal domains of PTEN (reproduced with permission from Smith et al. (2021))

The N-terminal Domain

The N-terminal domain contains three regions that are homologous to protein tyrosine phosphatases (PTPs) and dual specificity phosphatases (DUPs) (Yuvaniyama et al., 1996, Lee et al., 1999). There are three regions of conserved residues that are essential for catalysis and conformation, including the phosphate binding (P) loop (amino acids 121-131), the TI loop (amino acids 160-171) and the WPD loop (amino acids 88-98). The P loop contains the 8 residue PTP signature motif, HCXXGXXR (Lee et al., 1999). The HCXXGXXR motif contains several residues essential for function; Cys124 and Arg130 are involved in catalysis while His123 and Gly127 contribute to the P-loop conformation and Ala126 plays a role in substrate specificity (Barford et al., 1994, Stuckey et al., 1994, Leitner et al., 2018, Lee et al., 1999). During catalysis, Cys124, the nucleophilic catalytic cysteine, forms a thiol-phosphate intermediate through which the 3' phosphoryl group is transferred from its substrate, PIP₃ (Denu and Dixon, 1998, Barford et al., 1998, Zhang, 2003, Xiao et al., 2007, Chia et al., 2010). The main difference between PTEN's active site and those of other PTPs, such as PTP1B, is its larger width due to a 4 amino acid insertion in the TI loop, giving an extension of the substrate pocket (Lee et al., 1999). This additional space allows the accommodation of PIP₃ which is a larger substrate than those of other DUPs (Lee et al., 1999). The conserved Thr167-Ile168 amino acids have been shown to have a role in substrate specificity (Leitner et al., 2018). The WPD loop contains a 3 amino acid motif (Phe90-Glu91-Asp92) which is followed by a histidine residue, His93, which contributes to the basic environment of the active site (Lee et al., 1999). The WPD loop is also denoted as a 'moveable loop' as on binding of PTEN by a substrate there is a conformational change whereby the WPD loop moves into the active site (Chia et al., 2010). This movement from an 'open' to a 'closed' conformation permits the active site residue Asp92 to participate in catalysis, with a role in the hydrolysis of the Cys124 thiol-phosphate intermediate (Zhang, 2003, Chia et al., 2010).

The C-terminal Domain

The C-terminal domain is important for several biological functions, such as signal transduction, substrate binding and stability (Rizo and Südhof, 1998). The region is subdivided into the C2 domain, the C-terminal tail and the PDZ-motif. The C2 domain has structural similarity to the C2 domain of protein kinase C (PKC) (Nalefski and Falke, 1996). The C2 domain is a calcium binding motif which can bind several targets, from phospholipids and inositol polyphosphates to other protein domains, such as the phosphotyrosine domain (PTB) (Nalefski and Falke, 1996, Rizo and Südhof, 1998). *In vitro* testing of the PTEN C2 domain and its affinity for phospholipid vesicles demonstrated the domain's affinity for phospholipid membranes (Lee et al., 1999). In addition to facilitating the electrostatic binding of PTEN to the cell membrane, the C2 domain is also associated with the N-terminal phosphatase domain and is proposed to have a role in the orientation and productive positioning of PTEN for catalysis (Lee et al., 1999, Das et al., 2003, Georgescu et al., 2000).

The C-terminal tail is an intrinsically disordered region (IDR) and it plays a role in the stability, autoregulation and protein-protein interactions of PTEN (Malaney et al., 2013). Correlation of the stability of PTEN to the PEST sequences present in the C-terminal tail has been reported (Georgescu et al., 1999). PEST sequences are proline, serine, threonine and glutamic acid rich polypeptide sequences which are directly related to a protein's half-life (Rechsteiner and Rogers, 1996). Through labelling and detection of its half-life, "tail-less" PTEN was present at four-fold lower levels in cells when compared to wild-type PTEN (Vazquez et al., 2000). Due to the size and acidic nature of the amino acids flanking Thr383, similarities were drawn to the nature of PTEN's substrates, leading to conclusions that Thr383 could be a site of auto-dephosphorylation (Raftopoulou et al., 2004, Myers et al., 1997). C-terminal tail threonine and serine residues (Thr366, Ser370, Ser380, Thr382, Thr383 and Ser385) are targets of phosphorylation and are involved in the regulation of PTEN, the mechanism of which is discussed below in section 1.2.6 (Myers et al., 1997, Bolduc et al., 2013).

Three terminating residues at the C-terminus, Thr⁴⁰¹, Lys⁴⁰² and Val⁴⁰³, denote the PDZ-motif, a series of amino acids that permit interaction with protein interaction modules called PDZ domains (Lee and Zheng, 2010, Teng et al., 1997, Lee et al., 1999). The PDZ-motif has strong interactions with the phosphatase domain in the N-terminal, through both hydrogen bonding and hydrophobic interactions, aiding correct conformation (Lee et al., 1999). Additionally, the PDZ-motif has been reported to be important for protein-protein interactions (PPIs) (Waite and Eng, 2002, Fanning and Anderson, 1999).

1.2.2 The Phosphatase Activity of PTEN

As introduced above, structural similarities were drawn between PTEN and protein tyrosine phosphatases (PTPs) (Li and Sun, 1997, Li et al., 1997, Steck et al., 1997). PTEN homology with the dual-specificity phosphatase *Vaccinia* H1-related (VHR) was identified in the N-terminal domain of PTEN, with a phosphate binding (P) loop, a TI loop and a WPD loop (Yuvaniyama et al., 1996, Li and Sun, 1997, Lee et al., 1999). The identification of correlations between PTEN and PTPs lead to studies investigating the phosphatase activity of PTEN against phosphorylated protein substrates (Myers et al., 1997). Whilst PTEN was shown to have low catalytic activity against the proteinaceous substrates tested, activity was demonstrated against phosphorylated serine, threonine and tyrosine residues, denoting PTEN as a dual-specificity phosphatase (DUP) (Li and Sun, 1997, Myers et al., 1997). With the highest activity against polyGluTyr, acidic substrates were proposed to be preferred by PTEN (Myers et al., 1997). This led to investigations into acidic non-proteinaceous substrates, including the landmark study determining phosphatidylinositol (3,4,5)-trisphosphate (PIP₃) as PTEN's physiological substrate (Maehama and Dixon, 1998). The lipid phosphatase activity of PTEN against PIP₃ gives it regulatory control over the Akt pathway and this catalytic activity is essential for PTEN's role as a tumour suppressor and metabolic regulator (Myers et al., 1998, Chen et al., 2018).

PTEN mutation is present in many types of human cancer (Eng, 2003, Chalhoub and Baker, 2009). Mechanistic studies have been performed into the role of commonly mutated N-terminal residues in the phosphatase activity of PTEN. These include the catalytic cysteine, Cys124, as well as other surrounding residues including Asp92, Ala126, Gly129, Thr167 and Ile168, (Maehama and Dixon, 1998, Xiao et al., 2007). A systematic evaluation of the phosphatase activity of mutated PTEN reported that 74% of the 42 missense mutations evaluated resulted in lipid phosphatase inactivity (Han et al., 2000, Chia et al., 2010). As discussed above, Asp 92 and Cys124 are essential for both lipid and protein phosphatase activity (Xiao et al., 2007, Denu and Dixon, 1998, Barford et al., 1998, Zhang, 2003, Chia et al., 2010). Gly129 is a common PTEN mutation in patients with Cowden syndrome. Interestingly, while a Gly129 mutation abolishes lipid phosphatase activity, PTEN's protein phosphatase function remains active (Maehama and Dixon, 1998, Han et al., 2000, Waite and Eng, 2002). Studies into substrate specificity showed the importance of Ala126, Thr167 and Ile168 (Leitner et al., 2018).

1.2.3 PTEN's Role in the Akt Signalling Pathway

The downstream effects of PTEN's regulation of the Akt signalling pathway have been previously reviewed (Song et al., 2012, Lee et al., 2018, Hopkins et al., 2014). PIP₃ is responsible for the positioning of Akt at the plasma membrane where it can be subsequently activated by phosphorylation by 3-phosphoinositide-dependent protein kinase 1 (PDK1) (Hemmings and Restuccia, 2012). PTEN downregulates the levels of the PIP₃ and therefore the levels of active Akt, phosphorylated Akt (pAkt). Figure 1.2 provides context of where PTEN acts in the cell and downstream signalling effects of Akt activation, highlighted by the blue box, and shows the important regulatory role PTEN has on key cellular processes, such as cell survival and metabolism.

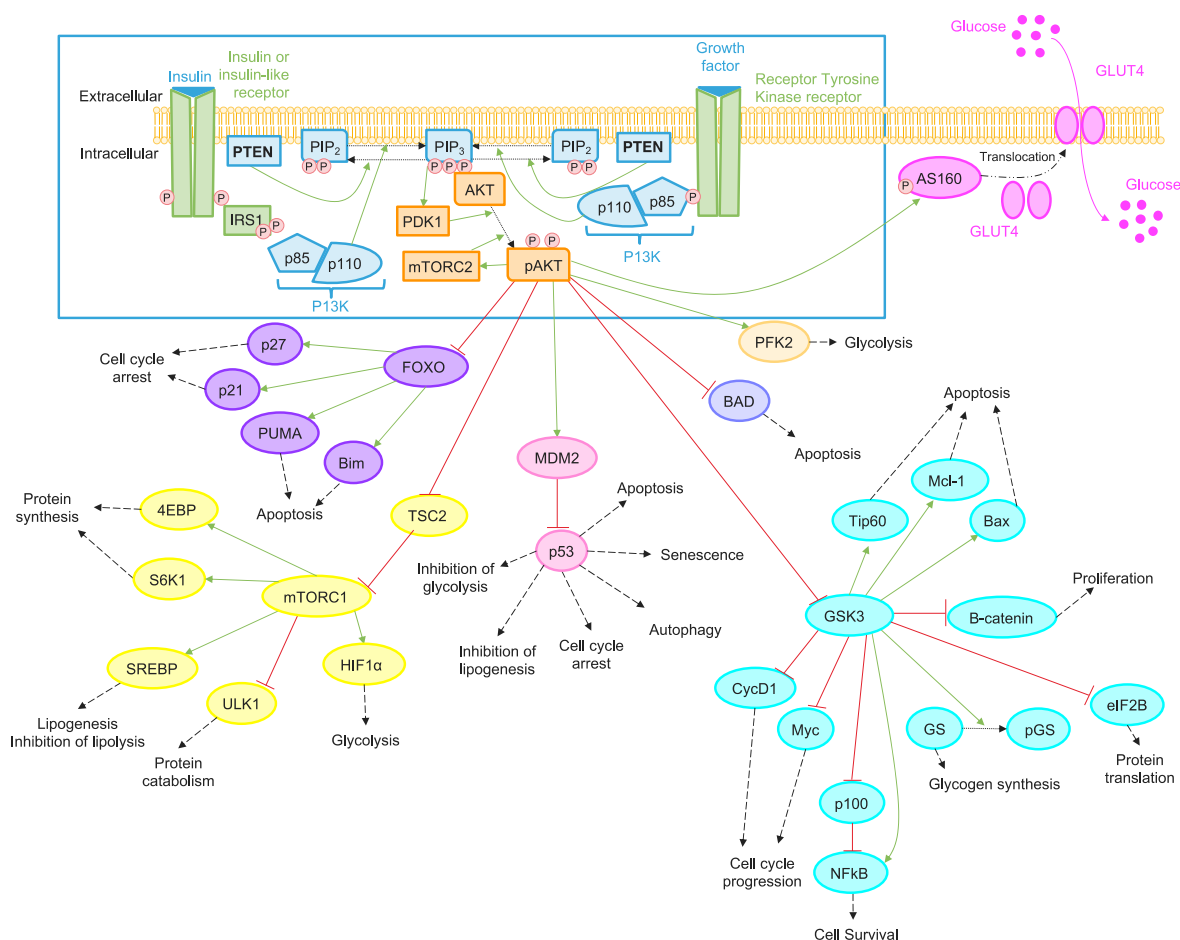


Figure 1.2 An overview of the metabolic and cell survival signalling pathways downstream from the action of PTEN (reproduced with permission from Smith et al. (2021)).

The first identified substrate of Akt was glycogen synthase kinase 3 (GSK3), a highly conserved, ubiquitous protein kinase (Cross et al., 1995, Kaidanovich-Beilin and Woodgett, 2011). Sharing 85% sequence homology, GSK3 has two isoforms, α and β , both of which

have a central role in a variety of signalling pathways, including some that are distinct from the Akt pathway (Manning and Toker, 2017). GSK3 is active in under resting conditions, in the absence of cellular stimulation, but N-terminal serine phosphorylation of GSK3 by Akt results in inhibition (Kaidanovich-Bellin and Woodgett, 2011, Sutherland et al., 1993, Manning and Toker, 2017). Depending on cellular status, GSK3 activates a range of downstream targets involved in diverse pathways including apoptosis (Tip60, Mcl-1 and Bax), cell survival (NF κ B) and glycogen synthesis (glycogen synthase). Inhibition by GSK3 results in the downregulation of downstream targets involved in proliferation (β -catenin), protein translation (eIF2B) and cell cycle progression (CycD1, Myc) (Manning and Toker, 2017, Evangelisti et al., 2020, Beurel et al., 2015).

Forkhead Box O (FOXO) transcription factors are another target for Akt (Manning and Toker, 2017). Phosphorylation of FOXO by Akt facilitates the translocation of FOXO to the cytosol from the nucleus, downregulating the transcription of FOXO associated gene targets (Brunet et al., 1999). Examples of these gene targets include the pro-apoptotic proteins PUMA and Bim, as well as those associated with the induction of cell cycle arrest, such as the cell cycle inhibitors p27 and p21 (van der Vos and Coffey, 2010).

Mammalian target of rapamycin complex 1 (mTORC1) is activated through the inhibition of the mTORC-1 inhibitor tuberous sclerosis complex 2 (TSC2) on phosphorylation by Akt (Inoki et al., 2002). The removal of mTORC1 inhibition upregulates downstream targets involved in metabolic processes, including protein synthesis (via 4EBP and S6L1), lipogenesis and inhibition of lipolysis (via SREBP) and glycolysis (via HIF1 α) (Saxton and Sabatini, 2017, Düvel et al., 2010, Altomare and Khaled, 2012, Porstmann et al., 2008, Caron et al., 2015). mTORC1 regulates protein turnover through inhibition of downstream targets involved in protein catabolism (via ULK1) and promotion of proteolysis through the ubiquitin-proteasome system (UPS) (Kim et al., 2011, Zhao et al., 2015, Zhang et al., 2014).

The tumour suppressor p53 is a central transcription factor acting to inhibit cell proliferation through apoptosis, cell cycle arrest, senescence and autophagy in a context dependent manner (Zilfou and Lowe, 2009). p53 is activated through stabilisation and tetramer formation to allow DNA binding and transcriptional activation for gene expression (Yee and Vousden, 2005). Ubiquitination and degradation of p53 is promoted by the ubiquitin ligase MDM2, which is upregulated by Akt activation (Ogawara et al., 2002).

1.2.4 The Subcellular Localisation of PTEN Determines its Physiological Role

Whilst initial studies of PTEN focused on its lipid phosphatase activity at the cell membrane and its cytoplasmic localisation, discussed above, additional studies have identified alternative subcellular localisations of PTEN and uncovered additional functions (Lian and Di Cristofano, 2005, Bononi and Pinton, 2015). Additional subcellular localisations include: nucleus (Liu et al., 2005, Trotman et al., 2007), nucleolus (Li et al., 2014, Liang et al., 2017), mitochondria (Liang et al., 2014, Zhu et al., 2006), endoplasmic reticulum (Bononi et al., 2013) and extracellular (Hopkins et al., 2013, Putz et al., 2012). The regulation of PTEN's subcellular localisation has recently been reviewed (Liu et al., 2019). Additional translational isoforms of PTEN have demonstrated fundamental differences in subcellular localisation and their functional roles are discussed in detail below.

1.2.5 Isoforms of PTEN

Whilst the focus of this study is on canonical PTEN (referred to in this thesis as 'PTEN'), there are two alternative isoforms of PTEN: PTEN- α and PTEN- β . These differ from PTEN in both structure and subcellular localisation. Both isoforms have additional N-terminal residues, where PTEN- α is extended by 173 residues and PTEN- β is extended by 146 residues (Hopkins et al., 2013, Liang et al., 2014, Liang et al., 2017). Whilst both isoforms have additional functions related to their subcellular localisation, it has been confirmed that both PTEN- α and PTEN- β retain lipid phosphatase activity and the ability to downregulate the Akt pathway (Liang et al., 2017). Despite this, a tumour promotor function has recently been proposed for both PTEN- α and PTEN- β after they were identified as interactors of WD repeat-containing protein 5 (WDR5) which is a scaffold protein for histone H3 lysine 4 (H3K4) promoting H3K4 trimethylation and the subsequent transcription of oncogenes (Shen et al., 2019). Expression of PTEN- α and PTEN- β was seen to accelerate tumour progression, but on depletion of PTEN- α and PTEN- β tumour progression was inhibited (Liang and Yin, 2019, Shen et al., 2019). A higher sensitivity to proteasomal degradation has also been demonstrated for both translational isoforms (Shen et al., 2019)

PTEN- α has been identified as a secreted form of PTEN (Hopkins et al., 2013). This membrane permeable isoform of PTEN was found to exert functional tumour suppression in recipient cells through the downregulation of the Akt pathway via its lipid phosphatase activity (Hopkins et al., 2013). In addition, PTEN- α has been identified as co-localised with mitochondria at the outer mitochondrial membrane and was found to have a role in the regulation of mitochondrial function and energy metabolism (Liang et al., 2014, Wang et al., 2018). More recently, through dephosphorylation of ubiquitin, PTEN- α was identified as an

inhibitor of mitophagy, which is a mechanism to remove damaged mitochondria through selective autophagy (Wang et al., 2018). In addition, a role in immune suppression has been identified for PTEN- α leading to the promotion of immune resistance in PTEN-mutant cancer by counteracting CD8⁺ T cell-mediated cytotoxicity (Sun et al., 2021).

PTEN- β is localised to the nucleolus and was found to regulate cellular proliferation through the association with and dephosphorylation of nucleolin (Liang et al., 2017). The N-terminal extension of PTEN- β is rich in arginine and arginine rich regions are often found in nucleolar-localisation signals (Liang et al., 2017). This was proposed as the mechanism through which PTEN- β is localised to the nucleolus (Liang et al., 2017). The use of pull down assays against PTEN- β identified nucleolin as a novel interactor with a role in ribosome biogenesis (Liang et al., 2017). The phosphorylation state of nucleolin is key to its function in the regulation of rDNA transcription and PTEN was shown to dephosphorylate nucleolin through its protein phosphatase activity (Liang et al., 2017).

1.2.6 Regulation of PTEN by Post-translational Modification

Phosphorylation

One method of protein phosphatase regulation is phosphorylation (Barford et al., 1998). PTEN is a constitutively phosphorylated protein, with a C-terminal tail region rich in serine and threonine residues (Vazquez et al., 2000). Phosphorylation sites Ser360, Thr382 and Thr383 have been denoted as sites of regulation, as on deletion of these residues PTEN activity is increased (Vazquez et al., 2000). Recruitment of PTEN to a multimeric complex was hypothesised to be the regulatory process by which PTEN is localised to the cell membrane, where PIP₃ is located (Vazquez et al., 2001). Phosphorylation of PTEN prevents this recruitment through conformational changes that result in 'closed' PTEN, masking the PDZ binding domain and reducing interactions with PDZ-domain containing proteins (Vazquez et al., 2001). Identification of the co-purification of protein kinase CK2 with PTEN from cells identified CK2 as a PTEN kinase (Vazquez et al., 2001). Due to the constitutive action of CK2, dephosphorylation of PTEN was put forward as the mechanism of regulation, switching the conformation of PTEN from closed to open, allowing recruitment to the membrane and subsequent access to PIP₃ (Vazquez et al., 2001, Torres and Pulido, 2001).

Phosphorylation state also affects PTEN's stability. Transfection of cultured mammalian cells with wild type or phosphorylation-mutants of PTEN identified that when known Ser/Thr phosphorylation sites were mutated to alanine, the degradation of PTEN was slower in comparison to wild type PTEN (Torres and Pulido, 2001). When the PTEN-transfected cells

were treated with both a proteasome inhibitor (MG132) and a protein kinase CK2 inhibitor (DRB), the levels of phosphorylation of PTEN decreased whilst the levels of PTEN remained unchanged (Torres and Pulido, 2001). These findings indicated that the phosphorylation state of PTEN affects the degradation of PTEN and degradation of PTEN is mediated by the proteasome (Torres and Pulido, 2001).

Ubiquitination and Small Ubiquitin-like Modifiers (SUMO)-ylation

Ubiquitination is the process by which proteins are covalently modified through the ligation of ubiquitin, a 76 amino acid protein, to lysine residues by the action of three proteins; an activating enzyme (E1), a ubiquitin-carrier protein (E2) and a ubiquitin-protein ligase (E3) (Hershko and Ciechanover, 1998). Ubiquitination is an important post-translational modification in determining the fate of a protein. Initially ubiquitination was identified as a route for proteolytic degradation via the ubiquitination-proteasome system but important non-proteolytic functions have since been identified (Hershko and Ciechanover, 1998, Callis, 2014). As introduced above, the proteasome was shown to have a role in the degradation of PTEN (Torres and Pulido, 2001). This was further supported during a study of the effect of Zn^{2+} on the levels of PTEN and activation of the Akt pathway (Wu et al., 2003). As Zn^{2+} activates signalling cascades, such as the PI3K/Akt pathway, and can inhibit protein tyrosine phosphatases, the effect of Zn^{2+} on PTEN was investigated (Wu et al., 2003, Kim et al., 2000b). It was found that exposure of cells to Zn^{2+} , using cultured airway epithelial cells and *in vivo* in rats, gave a reduction in PTEN levels and an increase in pAkt, indicating activation of the Akt pathway (Wu et al., 2003). Cells that were pre-treated with the proteasome inhibitor MG132 prior to exposure to Zn^{2+} showed no reduction in PTEN levels or increase in pAkt levels (Wu et al., 2003). This role of the proteasome in PTEN degradation was expanded by Wang et al. (2007) with the observation that the C-terminal domain of PTEN contains two signature PEST motifs for proteins that are degraded by the ubiquitin pathway, as introduced above. Co-transfection of cells with haemagglutinin (HA)-tagged ubiquitin and his-tagged PTEN protein and subsequent pull downs against the his-tagged PTEN can show polyubiquitination of PTEN by immunoblotting against HA (Wang et al., 2007). Isolation by purification and subsequent mass spectrometric analysis identified NEDD4-1, a HECT-E3 ligase, as a PTEN interactor and this interaction was confirmed with co-immunoprecipitation (Wang et al., 2007). Co-transfection of HA-ubiquitin and His-PTEN with NEDD4-1 gave an increase in PTEN polyubiquitination and reduction of PTEN levels, which taken together confirmed NEDD4-1 as an E3 ligase for PTEN, responsible for targeting PTEN for proteasomal degradation (Wang et al., 2007). Since the identification of NEDD4-1 as an E3 ligase for PTEN, several additional E3 ligases have been identified as interactors of PTEN. At the time of writing, BioGRID details 11 different E3 ligases as interactors of PTEN, with NEDD4 and

WWP2 as the E3 ligases with the strongest evidence, with the highest numbers of different publications identifying this interaction (Stark et al., 2006).

While polyubiquitination plays an essential role in the degradation of PTEN, monoubiquitination has been found to play a role in determination of subcellular localisation and trafficking of PTEN. Whilst a Lys289Glu mutation did not affect the phosphatase activity or membrane recruitment of PTEN, the PTEN mutant was excluded from the nucleus, while wild type PTEN was found in both the cytoplasm and nucleus (Trotman et al., 2007). *In vitro* ubiquitination assays identified Lys289 as a major ubiquitination site and an additional lysine residue located in the N-terminal (Lys13) was identified as a second site of ubiquitination, also promoting nuclear import of PTEN (Trotman et al., 2007). Monoubiquitination at these two lysine sites was demonstrated *in vivo* and whilst wild type PTEN and the Lys13Glu and Lys289Glu mutants all showed polyubiquitination, there was a loss of monoubiquitination for both the mutants (Trotman et al., 2007). When co-expressing ubiquitin with PTEN there was an increase in both the rate of nuclear import and the amount of nuclear PTEN (Trotman et al., 2007). Interestingly, nuclear PTEN was not found to be ubiquitinated, which indicates that once shuttled de-ubiquitination is required to retain PTEN in the nucleus (Trotman et al., 2007). Taken together, these findings suggest that both Lys13 and Lys289 are key target residues for monoubiquitination and control of nuclear import of PTEN. Further to the nuclear import of PTEN, monoubiquitination has also been shown to have a role in the secretion of PTEN in exosomes (Putz et al., 2012). Secreted PTEN can be internalised by neighbouring cells and exert fully functional tumour suppression (Putz et al., 2012). Analysis of PTEN from patient-derived glioblastoma cells revealed a high frequency of mutations that affect localisation of PTEN to the plasma membrane and the nucleus, while catalytic activity often remained unaffected (Yang et al., 2017). Several lysine residues (Lys13, Lys254, Lys260, Lys263, Lys266, Lys267, Lys269 and Lys289) were tested due to previous evidence of modification by ubiquitin or SUMO, but mutation at Lys13 was the only mutation that showed reduced nuclear import of PTEN (Yang et al., 2017). This latest evidence contraindicates initial statements that Lys289 is a key site for monoubiquitination and promotion of nuclear import. Additional N-terminal sites of ubiquitination at Lys66, Lys80 and Lys289 have been identified as potential ubiquitination sites (Gupta and Leslie, 2016). A Lys66Arg mutation resulted in an increase of intracellular PTEN, demonstrating a link between ubiquitination at this residue and PTEN degradation (Gupta and Leslie, 2016). It was shown through *in vitro* ubiquitination assays that whilst mutation at Lys66, Lys80 and Lys289 gave some reduction in polyubiquitination, the Lys66 mutation showed the greatest reduction (Gupta and Leslie, 2016).

SUMO proteins are structurally similar to ubiquitin and the ligation of SUMO, known as SUMOylation, commonly occurs at lysine residues found within a consensus motif ψ -Lys-X-Asp/Glu (ψ : a large hydrophobic amino acid, X: any amino acid) (Rodriguez et al., 2001). Modification of PTEN by SUMO has been demonstrated at C-terminal residues Lys266 and Lys289 (Huang et al., 2012, González-Santamaría et al., 2012). Mutation of Lys266 and 289 did not result in the complete ablation of SUMOylation, indicating that there are additional lysine residues that can act as SUMO acceptors that are not present in a consensus sequence (González-Santamaría et al., 2012). This could be explained by the identification of Lys254 as an additional SUMOylation site (Bassi et al., 2013). SUMOylation of PTEN was found to reduce nuclear PTEN and facilitate membrane recruitment, with Lys266 found as the critical residue for membrane association (Huang et al., 2012, González-Santamaría et al., 2012). A mechanism was proposed whereby the electropositive nature SUMO-PTEN interacts with the electronegative cell membrane (Huang et al., 2012). Lys289 has been previously identified as a monoubiquitination site and is essential for nuclear import, as discussed above. It has been proposed that ligation by ubiquitin and SUMO are in competition with each other and that this could explain the accumulation of Lys266-SUMOylated PTEN in the cytoplasm and the reduction of nuclear PTEN, as PTEN cannot therefore be monoubiquitinated (González-Santamaría et al., 2012, Trotman et al., 2007). In addition to Lys266 and Lys289, Lys254 has been shown to have a role in nuclear retention of PTEN (Bassi et al., 2013). Mutation of Lys254Glu reduced the amount of nuclear PTEN, which was recovered in the presence of a nuclear export inhibitor suggesting that whilst this mutant can be shuttled to the nucleus it is unable to remain there (Bassi et al., 2013). SUMOylation and ubiquitination show similarity beyond having lysine as their target residues, as SUMOylated PTEN has been demonstrated to accumulate on inhibition of the proteasome, suggesting that SUMOylation could also trigger proteasomal degradation (González-Santamaría et al., 2012)

Oxidation

In addition to phosphorylation, reversible redox mechanisms are important for the regulation of PTEN activity (Lee et al., 2002). The phosphatase activity of PTEN relies on its nucleophilic catalytic cysteine (Cys124) which, as introduced above, is found within PTEN's P loop as part of a conserved HCXXGXXR motif (Denu and Dixon, 1998, Barford et al., 1998, Xiao et al., 2007, Chia et al., 2010). Whilst free cysteine residues have a theoretical pK_a of 8.6, PTEN's catalytic cysteine has a calculated pK_a of 4.5, which is consistent with the pK_a s of the catalytic cysteines of other PTPs with the conserved HCXXGXXR motif (Lee et al., 2002). This is due to the presence of positively charged neighbouring residues (Lee et al., 2002). When the neutral thiol group (-SH) becomes a charged thiolate ion ($-S^-$), under conditions in which the pH is above the pK_a of cysteine, the nucleophilicity of the cysteine increases (Roos et al.,

2012). As such, the thiol group (-SH) of Cys124 exists as a thiolate ion ($-S^-$) at physiological pH (Denu and Dixon, 1998, Roos et al., 2012, Kim et al., 2000a). This increase in nucleophilicity is critical for catalytic activity due to the resultant increase in reactivity with electrophiles (Poole, 2015, Winterbourn and Hampton, 2008). Whilst facilitating the formation of the phosphate-thiol intermediate, this increased reactivity means that PTEN's catalytic cysteine is also more susceptible to attack by oxidants and electrophiles, including reactive aldehydes (Winterbourn and Hampton, 2008, Myers et al., 2011, Roos et al., 2012, Forman et al., 2004, Forman and Torres, 2002).

Redox reactions have been implicated in regulation of PTEN activity. Exposure to hydrogen peroxide (H_2O_2) causes both time- and dose-dependent inactivation of PTEN's catalytic activity (Lee et al., 2002). On exposure to an oxidant, such as H_2O_2 , the thiolate ion is oxidised to sulfenic acid (-SOH) which is then able to form disulfide bonds with proximal cysteines, which for PTEN is its resolving cysteine, Cys71 (Lee et al., 2002, Leslie et al., 2003). Whilst this inactivates PTEN, the disulfide bond can be reduced and the activity of PTEN can be recovered (Lee et al., 2002). This reversible disulfide bond prevents PTEN from becoming further oxidised to sulfonic acid ($-SO_3H$), which can be irreversible (Lim et al., 2008). The formation a reversible intramolecular disulfide bond is proposed to be a protective mechanism that can prevent this overoxidation. Treatment of PTEN with 1 mM H_2O_2 resulted in an increase in cellular PIP_3 levels, indicating that PTEN is inhibited by oxidation and thus uncovering a redox regulatory mechanism (Leslie et al., 2003). Endogenous production of H_2O_2 by stimulation of mammalian cells with growth factors, such as EGF and PDGF, has also been shown to increase the amount of pAkt alongside the detection of oxidised PTEN and a loss of phosphatase activity (Kwon et al., 2004). Oxidised PTEN was also detected after stimulation of mammalian cells with lipopolysaccharide (LPS) and phorbol 12-myristate 13-acetate (PMA), where acute exposure of both resulted in the endogenous production of oxidants (Leslie et al., 2003). However, it is worth noting that the authors stated that stimulation with either treatment alone did not always produce a statistically significant increase in the level of oxidised PTEN (Leslie et al., 2003).

Hypochlorous acid has also been shown to cause oxidative modifications to PTEN on key residues for activity. Whilst a low-level exposure had a reversible effect on PTEN's activity, this was unrecoverable when the levels of HOCl were increased to >60:1 molar ratio of HOCl:PTEN. HOCl modification of C-terminal domain residues was detected in aggregated PTEN, indicating modification of these residues caused destabilisation of PTEN's conformation (Verrastro et al., 2018). Additional effects of the HOCl exposure included chlorination and hydroxylation modifications (Verrastro et al., 2018). Other oxidants that have

been shown to modify PTEN include reactive nitrogen species, such as CSNO and NO (Kwak et al., 2010, Yu et al., 2005).

Thioredoxin plays a major role in the reduction and re-activation of PTEN, and has been found to be more efficient than glutaredoxin through co-immunoprecipitation of both proteins with PTEN and exposure to either thioredoxin or glutaredoxin inhibitors (Lee et al., 2002). There was a delay in reduction of oxPTEN on exposure to the thioredoxin inhibitor but not the glutaredoxin inhibitor, indicating that thioredoxin is a lead reductant for PTEN (Lee et al., 2002). The relationship between thioredoxin and PTEN has since been evidenced further (Meuillet et al., 2004, Schwertassek et al., 2014, Song et al., 2007, Sadeghirizi et al., 2016). Peroxiredoxin-1 is another reductant that has been shown to form a complex with PTEN and has been seen to protect PTEN's phosphatase activity during mild oxidative stress (Cao et al., 2009). On exposure to high levels of oxidative stress, this protection was lost and a decrease in interaction was identified between peroxiredoxin-1 and PTEN (Cao et al., 2009). The redox regulation of PTEN has been previously reviewed (Zhang et al., 2020, Nguyen Huu et al., 2021).

Lipoxidation

Reactive aldehydes have been shown to inactivate PTEN and the effect on the Akt pathway has previously been investigated *in vitro*, *in cellulo* and *in vivo* with a mouse model (Shearn et al., 2011, Covey et al., 2010, Shearn et al., 2013). MCF-7 and HEK-293 cells were treated with 10 μ M reactive carbonyls, including 4-HNE, acrolein and cyclopentenone-biotin analogues (Covey et al., 2010). Covalent modification of PTEN was demonstrated by selective tagging of oxidised or carbonylated thiols (Covey et al., 2010). Detection of carbonylated PTEN was achieved by labelling oxidised or carbonylated thiols with NEM-biotin before isolation of modified protein by precipitation with NA-beads and subsequent western blot detection of PTEN (Covey et al., 2010). As stated by the authors, a limitation of this technique is that there is no distinction between carbonylation or oxidation of residues (Covey et al., 2010). Additionally, the proposed vulnerability of Cys124 for alkylation due to its nucleophilicity could not be investigated as the modifications could not be mapped to specific residues. However, this experimental approach does demonstrate that cells can take up exogenous β -enones and that this exposure results in the modification of several intracellular proteins, including PTEN (Covey et al., 2010). The effect of two cyclopentenone-biotin analogues on PTEN's activity was inferred through analysis of the levels of pAkt, where inactivation of PTEN would result in an increase in cellular pAkt due to the loss of PTEN downregulation of the levels of PIP₃. Time- and dose-dependent suppression of PTEN's downregulation of the Akt signalling pathway was seen on treatment of cells with 2-20 μ M of the cyclopentenone-biotin

analogue, $\Delta 12$ PGJ₂-biotin, with the 20 μ M treatment taken forward for an additional time-course experiment for 10-120 minutes (Covey et al., 2010). This suppression was demonstrated by an increase in the levels of pAKT, detected by western blotting and expressed as a function of total Akt (Covey et al., 2010). Downregulation of the levels of pAkt was recovered on inhibition of the kinase activity of PI3K (Covey et al., 2010). Time-dependent suppression of Akt by acrolein and 4-HNE treatment was also demonstrated, but dose-dependent suppression was not tested (Covey et al., 2010). Isolation of PTEN from treated cells showed inactivation of its phosphatase activity to various degrees, where treatment with 1 μ M of the electrophilic PG-analogues demonstrated a similar inhibition to the treatment of 10 μ M of the two electrophilic reactive aldehydes, acrolein and 4-HNE, and exposure to the non-electrophilic PG-analogue showed minimal inhibition of activity (Covey et al., 2010). An increase in pAkt was accompanied by an increase in Akt-dependent proliferation for 5 and 10 μ M $\Delta 12$ PGJ₂-biotin, demonstrating its effect on cellular proliferation (Covey et al., 2010).

Additional studies have focused on the effect of 4-HNE exposure on PTEN, with a small amount of additional data on the effect of acrolein (Shearn et al., 2011, Shearn et al., 2013). These two studies sought to further investigate the link between oxidative stress and lipid metabolism, of which PTEN is a central regulator. In line with the focus of this thesis, this section will discuss only the data attempting to characterise the effect of lipoxidation on the structure and activity of PTEN. However, it is worth noting that these authors also used *in cellulo* techniques to demonstrate the accumulation of lipids in hepatocytes and *in vivo* techniques with mouse models to demonstrate the effect of reactive aldehydes from chronic ethanol administration as a model for alcoholic liver disease (Shearn et al., 2011, Shearn et al., 2013). As with the previous study from Covey et al. (2010), the initial study by Shearn et al. (2011) analysed the effect of exogenous treatment of whole cells on the Akt pathway by probing for pAkt and total Akt by Western Blot. Shearn et al. (2011) assessed the effect of increasing concentrations of 4-HNE (0-100 μ M) on the amount of pAkt, for both phosphorylation states pSer473 and pSer473/pThr308, and the highest concentration of 4-HNE (100 μ M) was taken forward for time course analysis from 5 to 120 minutes. There was an increase in the amount of both forms of pAkt as the concentration of 4-HNE increased and whilst there was an initial increase as the time of exposure increased, this plateaued after 30 minutes (Shearn et al., 2011). An advantage of the study by Shearn et al. (2011) over the study by Covey et al. (2010) is that the effect of the exogenous 4-HNE treatment on the amount of ROS was investigated, eliminating any cross-attribution of ROS-mediated inhibition of PTEN's regulation of the Akt pathway, which was important as 4-HNE has previously been shown to increase intracellular ROS levels. By quantifying the amount of intracellular PIP₃ in

addition to the levels of pAkt, Shearn et al. (2011) demonstrated targeted analysis on the effect of 4-HNE exposure on PTEN's activity *in cellulo*. As would be expected from the increase in pAkt, cellular treatment with 4-HNE gave a statistically significant increase in the levels of PIP₃, and as the physiological substrate of PTEN this increase suggests an inactivation of PTEN's phosphatase activity. Carbonylation of PTEN *in cellulo* was demonstrated on exogenous treatment of cells with 100 µM 4-HNE using the same pull-down approach used previously by Covey et al., (2010) (Shearn et al., 2011). *In vitro* analysis confirmed reduction of PTEN's phosphatase activity and adduction of PTEN by 4-HNE was evidenced with both western blot and MALDI-TOF mass spectrometry (Shearn et al., 2011). However, the use of intact mass analysis and MALDI-TOF meant only a mass shift for a single adduction was detected, due to the limits of the instrument resolution at this m/z ratio, and this could not be mapped to any specific residue (Shearn et al., 2011).

The use of proteomic digestion and tandem mass spectrometry (LC-MS/MS) identified specific sites of modification that could be mapped to the structure of PTEN (Shearn et al., 2013). Several cysteine and lysine residues were found to be modified after exposure of PTEN to 4-HNE at a 1:1 and 10:1 ratio of 4-HNE:PTEN, but no modification to the catalytic cysteine was identified. The application of computational modelling identified a potential mechanism of inhibition of catalytic activity by steric hindrance of the active site by the 4-HNE adduct on the resolving cysteine, Cys71, or inhibition of C2 domain on modification of Lys327 (Shearn et al., 2013). The LC-MS/MS data from the initial digestion of 4-HNE-treated PTEN with trypsin resulted in a long Cys124 peptide as there was no cleavage at Lys102, which is followed by Pro103, due to the Keil rule where trypsin does not cleave at lysine residues that are preceded by a proline residue (Keil, 1992). This results in a peptide of 41 residues that is difficult to detect due to its large size, requiring multiple charge states to bring the mass to within the data acquisition parameters of the study. Double digestion with trypsin/chymotrypsin was used to try to increase the sequence coverage of the active site, where chymotrypsin cleaves preferentially at Trp, Tyr and Phe residues, and whilst a Cys124 peptide was detected in the untreated control, this peptide was not detected in the 4-HNE-treated sample (Shearn et al., 2013). The authors hypothesised that this could be due to an alternative post-translational modification to Cys124 or due to the modification of surrounding proximal lysine residues by 4-HNE resulting in a missed cleavage. The vulnerability of Cys124 to modification by electrophiles, and the increased vulnerability of cysteine residues in comparison to lysine residues, suggests that it would be preferentially modified in favour of any proximal lysine residues. The issue of unrecognisable peptides due to modified lysine missed cleavages could be mitigated by using less stringent peptide search parameters to increasing the number of missed cleavages allowed. Whilst this may increase the number of false positives, it could

have given an idea as to the likelihood of additional missed cleavages as an explanation to the lack of detection of Cys124. Several residues across the structure of PTEN were identified as modified by 4-HNE and, in an attempt to characterise residue vulnerability, Shearn et al. (2013) carried out a time-course experiment using a 10:1 ratio of 4-HNE to PTEN to provide a molar excess of treatment. However, utilising a lower range of treatment concentrations may have provided more targeted evidence to the most vulnerable sites of modification, as this would have provided information on the residues that are modified first in the presence of a limited amount of 4-HNE. Adduction of 4-HNE to endogenous PTEN was demonstrated on PTEN immunoprecipitation from cellular lysates with western blotting and further characterisation to map the *in cellulo* modifications using LC-MS/MS was attempted, but no PTEN peptides were detected which was attributed to an insufficient amount of protein (Shearn et al., 2013).

The role of spermine oxidase (SMOX) and myeloperoxidase (MPO) in acrolein production and the effect on PTEN has also been investigated (Al-Salihi et al., 2015, Uemura et al., 2017). On induction of acrolein production, both Al-Salihi et al. (2015) and Uemura et al. (2017) identified acrolein adduction of PTEN and a corresponding increase in pAkt. A recent paper has been published on the general effect of acrolein on cells and its contribution to tumourgenesis outside of the specific context of PTEN, where acrolein was seen to induce oncogenic transformation through activation of the Akt pathway (Tsai et al., 2021).

1.2.7 PTEN's Interactome

As is highlighted above, protein-protein interactions are essential to many facets of PTEN regulation. In addition to specific investigations into single interactors, global interactome studies have identified an even broader range of interacting proteins, from primary to secondary interactors. The BioGrid identifies, at the time of writing, 476 published physical interactions for PTEN (Stark et al., 2006). There are 7 previously published high-throughput studies of PTEN's interactome (Gorbenko et al., 2004, Herlevsen et al., 2007, Crockett et al., 2005, Gorbenko et al., 2010, Gunaratne et al., 2011, Maddika et al., 2011, Verrastro et al., 2016). In each of these cases, techniques such as the yeast2hybrid assay or pull-down assays have identified a large number of potential primary or secondary interactors, from 12-400 per study (Herlevsen et al., 2007, Gorbenko et al., 2010). However, far fewer of these interacting proteins, between 1 and 4 for each study, were validated and physiological functions hypothesised. We have recently published a review evaluating the approaches that were used in these studies to investigate the protein interactome of PTEN (Smith et al., 2021).

Redox plays an important role in the regulation of PTEN and oxidative post-translational modifications can alter critical residues for conformation and catalysis. Of the 7 interactome studies mentioned above, one investigated the effect of oxidative modification on the interactome of PTEN (Verrastro et al., 2016). This is an important investigation as key regulators of PTEN interact with PTEN in an oxidation-dependent manner (Verrastro et al., 2016). Recombinant PTEN was expressed with a glutathione-S-transferase (GST) tag, and the recombinant protein was purified and was subsequently used as bait, with and without prior treatment with H₂O₂, in a pull down assay to isolate interacting proteins (Verrastro et al., 2016). Tandem mass spectrometry was used to identify any changes in the interactome on oxidation; 97 total potential interactors were identified with 14 found to vary with oxidation state (Verrastro et al., 2016). 4 primary interactors were validated using western blot analysis with peroxiredoxin 1 (Prdx1), thioredoxin and annexin A2 (Anxa2) interactions varying with oxidation state (Verrastro et al., 2016). DNA damage binding protein 1 (DDB1) was also validated as a novel interactor, however there was no difference in binding with redox state (Verrastro et al., 2016).

1.3 Aims and Hypotheses

Previous studies into the effect of lipoxidation on the activity and structure of PTEN have focused on 4-HNE and cyclopentenones, although some preliminary data for acrolein has been published. Covey et al. (2010) demonstrated inhibition of phosphatase activity on exogenous treatment of cells with acrolein and modification of endogenous PTEN was detected by western blot, but no further characterisation has been attempted. This could include time- or dose-dependent investigations into the effect on PTEN's phosphatase activity and mapping of modifications to the structure of PTEN using LC-MS/MS. The effect of lipoxidation on the protein interactions of PTEN has not been investigated but a previous oxidation study provides a theoretical framework for the potential of lipoxidation to affect interactions as well. This thesis aims to build upon previous efforts to investigate the effect of lipoxidation on PTEN.

1.3.1 Research Aim 1: Characterise the Effect of Acrolein on PTEN's Phosphatase Activity

Section 1.2.6 introduced the previous studies into how modification of PTEN by reactive aldehydes affects its catalytic activity and these studies have included the use of both *in vitro* and *in cellulo* techniques. The previous evidence for the inactivation of PTEN by acrolein is from exposure of PTEN to a single concentration of acrolein for a defined treatment time where a reduction in activity was seen (Covey et al., 2010). Whilst exposure of PTEN to 4-HNE has

shown a time-dependent loss of activity *in vitro* and a dose-dependent loss of activity *in cellulo* (Shearn et al., 2011), this has not been tested for acrolein. Both acrolein and 4-HNE possess a reactive aldehyde group through which they can modify proteins and as such it was hypothesised that acrolein's effect on PTEN's activity would mirror the time- and dose-dependent inactivation seen by 4-HNE. Whilst previous studies investigating the effect of reactive aldehydes on the activity of PTEN have used an *in vitro* phosphatase assay with PTEN's physiological substrate PIP₃, 3-O-methylfluorescein phosphate (OMFP) is a phosphorylated artificial substrate that has been successfully used to quantify the effect of oxidation on PTEN's activity for two reactive oxygen species, hydrogen peroxide and hypochlorous acid (Covey et al., 2010, Shearn et al., 2011, Verrastro et al., 2016, Verrastro et al., 2018). Studies characterising the phosphatase activity of PTEN demonstrated that whilst PTEN's activity was highest for PIP₃, PTEN can also dephosphorylate proteinaceous and artificial substrates (Myers et al., 1997, Maehama and Dixon, 1998, Mak and Woscholski, 2015). *In cellulo* approaches have included the application of exogenous reactive aldehydes to whole cells, before precipitation of endogenous PTEN and subsequent analysis of the phosphatase activity of the isolated PTEN *in vitro* or the measurement the amount of pAkt (Covey et al., 2010, Shearn et al., 2011, Shearn et al., 2013).

The first objective was to quantify the effect of acrolein directly using an *in vitro* activity assay with recombinant PTEN using OMFP as a substrate. This required the overexpression and purification of a recombinant PTEN protein before treatment *in vitro* with increasing concentrations of acrolein from 0.2:1 to 10:1 acrolein:PTEN for 10 minutes, 1 hour and 4 hours. By using increasing concentrations of acrolein and increasing the exposure time, both the time- and dose-dependency of inactivation could be quantified. The second objective was to assess the effect of acrolein *in cellulo* by treating mammalian cells with exogenous acrolein and detecting any changes in the amount of pAkt in reference to the total amount of Akt. Sublethal concentrations of acrolein would first be established using a cell viability assay before application of increasing acrolein concentrations to whole cells and measurement of the amount of pAkt and Akt from the cell lysates, using a housekeeping protein, α,β -tubulin, as a loading control. The key advantages to the *in vitro* treatment of recombinant PTEN in comparison to the *in cellulo* approach, is the ability to apply treatments in a defined ratio and to monitor the effect of acrolein modification of PTEN in a targeted manner without any potential interference by other cellular effects of the acrolein treatment. However, this could also be seen as a disadvantage as that the treatment does not take place within the physiological context of the cell. Monitoring the amount of pAkt as a way to demonstrate the inactivation of PTEN is well established by its use in numerous published studies, and whilst western blotting is not a quantitative technique, the use of image software allows quantification

of the intensity of the individual target bands which can then be compared across different treatments. Care must be taken when attempting to quantify any changes in pAkt that the cellular load of each lane on the gel is equivalent for each treatment, and confidence can be increased by normalisation of the target band intensity to the intensity of a housekeeping protein before quantifying the amount of pAkt as an expression of the amount of total Akt. This aim to characterise the inactivation of PTEN is linked to the next aim to identify modification sites using of SDS-PAGE and LC-MS/MS, which may shed light on the mechanism of inactivation by acrolein.

1.3.2 Research Aim 2: Characterise the Effect of Acrolein on PTEN's Structure

The presence of the same reactive aldehyde group in both 4-HNE and acrolein means that the two lipid oxidation products are likely to modify similar residues on the same protein. Previous mapping of the 4-HNE modification sites for PTEN has identified several vulnerable cysteine and lysine residues across the structure of PTEN (Shearn et al., 2013). As discussed in section 1.1.2, cysteine residues are the most vulnerable amino acids to modification by acrolein, with lysine and histidine residues requiring higher treatment concentrations or longer treatment times (Stevens and Maier, 2008, LoPachin et al., 2009, Cai et al., 2009, Myers et al., 2011). The first hypothesis was that cysteine residues would be modified first, appearing at the lowest treatment concentrations, with lysine modifications appearing at higher treatment concentrations. The second hypothesis was that the catalytic cysteine would be particularly susceptible to modification as it has a higher nucleophilicity, as discussed in section 1.2.6, and would be expected to be the most reactive to electrophiles such as acrolein (Winterbourn and Hampton, 2008, Forman et al., 2004). This matches the previous hypothesis by Shearn et al. (2013) for PTEN and 4-HNE. The third hypothesis was that due to the smaller size of acrolein in comparison to 4-HNE, it was thought that acrolein may also be able to modify less accessible residues. Finally, it was hypothesised that as the treatment concentrations increased, the likelihood of cross-linking would increase due to the increased number of modifications as the acrolein adduct's carbonyl group can further react with neighbouring lysine residues (Burcham et al., 2007). There would also be an increased risk of aggregate formation as the number of modifications increases due protein unfolding from an increase in hydrophobicity on the introduction of additional carbonyl groups (Spickett and Pitt, 2020). The first attempt to further characterise the modification of PTEN by 4-HNE beyond western blotting used matrix-assisted laser desorption ionisation/time of flight (MALDI-TOF) mass spectrometry for intact mass analysis (Shearn et al., 2011). Whilst this approach confirmed the adduction of PTEN by 4-HNE through detection of a 156 Da mass shift, there was no further information on the site of modification. Expansion to tandem mass spectrometry with

electrospray ionisation mapped the sites of 4-HNE modification to residues across the structure of PTEN (Shearn et al., 2013).

The first objective was to visualise the acrolein-treated protein from each time-point using SDS-PAGE to identify the profile of cross-linking and aggregation. The second objective was to analyse the PTEN bands to map modifications using in-gel digestion with trypsin and LC-MS/MS analysis. Whilst western blotting has previously been used to identify modification of endogenous PTEN isolated from acrolein-treated cells, this is not required to analyse the profile of crosslinking where an overexpressed recombinant protein is purified and treated *in vitro*. Whilst SDS-PAGE cannot confirm any modification at the monomeric band, as the shift in molecular weight on adduction with acrolein would not be detectable, it can identify potential cross-links with the appearance of bands at 2(+) times the molecular weight of monomeric PTEN. Coupling the SDS-PAGE with LC-MS/MS would allow confirmation of modification at the monomeric band with the advantage over western blotting alone that the modification can also be mapped. Trypsin is a gold standard protease for proteomics as the average size of the resultant peptide falls within the ideal range for fragmentation and its cleavage at the C-terminal of Arg and Lys residues results in a positive charge at the C-terminus of the peptide, which is advantageous for LC-MS/MS separation and identification (Tsiatsiani and Heck, 2015). As the expected sites of modification are Cys, Lys and His residues, the disadvantage of using trypsin for protein digestion is that it preferentially cleaves at Lys and Arg residues. Modification to a Lys residue would result in a missed cleave, which may lead to larger resultant peptides which could be difficult to analyse by LC-MS/MS. This limitation would be exacerbated at higher treatment concentrations where lysine modifications would be more likely to occur. Despite the ability to map the modifications to specific residues for different treatment concentrations, it is likely that there will be different proteoforms in each band with a different population of modifications, but due to the resultant mixed peptide pool from each SDS-PAGE band it would not be possible to differentiate which modifications occurred together on a single protein. This second aim is linked to the third and final aim to identify changes in PTEN's interactome on acrolein modification as it is required to know the profile and extent of modification to choose conditions under which PTEN is sufficiently modified that changes in interactions might be expected, but not so modified that the protein becomes unfolded, which could result in non-physiological interactions.

1.3.3 Research Aim 3: Characterise the Effect of Acrolein on PTEN's Interactions

Due to the structural changes that are likely to occur on adduction of PTEN by acrolein, based on the previous data from 4-HNE, it was hypothesised that the introduction of acrolein

modifications may facilitate or inhibit interactions through changes to an interaction site or overall conformation. Low-data content studies, using approaches such as co-immunoprecipitation, are hypothesis-driven and are suitable for in depth characterisation of a known interaction. High-data content studies, such as the yeast2hybrid (Y2H) assay or affinity pull down (APD) assay, are suited for broader interactome investigations and result in the generation of new routes of investigation (Smith et al., 2021). APD involves the immobilisation of a bait protein and capture of potential interactors on exposure to a pool of prey proteins which can then be identified by LC-MS/MS (Louche et al., 2017). The Y2H assay relies on the introduction of two functional domains of a single transcription factor which are brought together on the interaction of two fusion-proteins to produce an observable effect (Fields and Song, 1989). Both techniques have previously been used to study PTEN's interactome (Gorbenko et al., 2004, Herlevsen et al., 2007, Crockett et al., 2005, Gorbenko et al., 2010, Gunaratne et al., 2011, Maddika et al., 2011, Verrastro et al., 2016). Co-immunoprecipitation relies on a similar chromatographic concept, but the bait is precipitated from the same environment as the prey before confirmation of protein identity with western blotting. This technique has been used to confirm potential PTEN interactors identified by APD and Y2H (Ahn et al., 2008, Gunaratne et al., 2011, Maddika et al., 2011, Gorbenko et al., 2010).

The first objective was to characterise the effect of acrolein on PTEN's interactions by performing an APD assay with an *in vitro* lipoxidation treatment step for global interaction analysis of the effect of acrolein on the interactions of PTEN. The second objective was to take forward an interesting candidate that showed a change in interaction for acrolein-treated PTEN and validate the interaction *in cellulo* using co-immunoprecipitation. APD has previously been used to investigate the effect of oxidation on the interactome of PTEN (Verrastro et al., 2016). Due to the chromatographic nature of APD, different buffers can be easily introduced and removed and as such it is well suited to the incorporation of a treatment step, as was required for this study. It is worth considering that lipoxidation has been shown to alter the subcellular localisation of proteins and changes in localisation are likely to facilitate changes to interactions due to the differences in proximal proteins (Zorrilla et al., 2019). This effect would not be identified by an *in vitro* interaction study as the pool of prey is a mixed cell lysate homogenate, with no distinction of subcellular localisation. An *in cellulo* APD approach would address this limitation but adds complication to the analysis as both the bait and prey would be modified.

Chapter 2 – General Materials and Methods

2.1 Materials

All materials were purchased from Merck, ThermoFisher or FisherScientific, unless otherwise stated. HCT-116 cells were obtained from Rudiger Woscholski's lab at Imperial College London.

2.2 Mammalian Cell Culture

All processes relating to cell culture, with the exception of microscopy, cell counting with a haemocytometer and cell lysis, were performed using aseptic technique under a laminar flow hood. For maintenance of the cell line and cell harvest, all reagents were pre-warmed to 37°C prior to use. For cell lysis, all reagents were pre-cooled on ice.

2.2.1 Thawing, Subculture and Cryopreservation of HCT-116 cells

HCT-116 cells were thawed by gentle agitation in a 37°C waterbath before centrifugation at 125 x g for 5 minutes at RT. The pellet was gently resuspended in 500 µl of complete McCoy's 5a media (McCoy's 5a with 10% (v/v) fetal bovine serum (FBS), 100 U/ml penicillin and 100 µg/ml streptomycin) before further dilution to 10 ml. The cells were transferred to a 25cm² flask and incubated in a humidified incubator at 37°C with 5% CO₂. Once the cells reached 75-80% confluence they were expanded to a 75 cm².

To maintain the cells, once they had reached approximately 75-80% confluence they were subcultured. The old media was aspirated and the cells were washed twice with PBS (10 mM Na₂HPO₄, 1.8 mM KH₂PO₄, 137 mM NaCl and 2.7 mM KCl, pH 7.4). The cells were then incubated with 1X trypsin-EDTA (0.5 mg/ml trypsin with 0.2 mg/ml EDTA pH 7.0-7.6) (Merck, UK) in PBS for 5 minutes at 37°C, as per the volumes in Table 2.1. The trypsin was inactivated with an equal volume of McCoy's 5a Complete media and the cells were resuspended. For general maintenance of the cell line, the cells were diluted between 1:8 and 1:12 with complete McCoy's 5a media, depending on the cell density, before final addition of McCoy's 5a Complete media to the flask as per the volumes in Table 2.1.

For cryopreservation, the cells were washed with PBS, detached with trypsin as above and diluted to 2.5 x 10⁶ cells/ml in freezing medium (5% dimethyl sulfoxide (DMSO) in FBS). 1 ml aliquots were prepared in cryovials, before freezing overnight at -80°C using a MrFrosty Freezing Container with RT isopropanol. The aliquots were then transferred to the vapour phase of liquid nitrogen for long term storage.

Table 2.1 Cell Culture Volumes

Flask Size (cm ²)	Reagent Volume (ml)			
	PBS	Trypsin	Trypsin Deactivation with Media	Final Total Media
25	2	2	2	7.5
75	5	5	5	25
150	10	10	10	50

2.2.2 Cell Count and Viability Assessment

Cell number and viability was determined by counting cells stained with trypan blue. 50 µl of a cell suspension was mixed with 50 µl of 0.1% Trypan Blue and 10 µl was applied to the haemocytometer. The number of phase bright (live) cells was then taken as a percentage of the total cells (live + dead (blue cells)) to calculate the cell viability. The cells were then diluted in the appropriate buffer or media to the desired concentration.

2.2.3 Mammalian Cell Harvest

The cells were grown to 75-80% confluence before harvesting, as per section 2.2.1. The detached cells were pelleted by centrifugation at 125 x g for 10 minutes at RT and the pellet was washed twice in PBS to remove any excess media and trypsin. The cells were diluted in PBS to a concentration of 5 x 10⁶ cells/ml and 1 ml aliquots were pelleted at 1000 x g for 10 minutes at 4°C. The pellets were frozen at -80°C for future use or lysed for immediate use as per section 2.2.4.

2.2.4 Mammalian Cell Lysis

When the cell pellet was frozen, the cells were thawed on ice prior to lysis. When the cell pellet was not frozen, the cells were placed on ice prior to lysis. 250 µl mammalian lysis buffer (25 mM NaPO₄ pH 7.4 with 150 mM NaCl and 1% Triton X-100 and 5% glycerol) with 10 µl 25X protease inhibitor cocktail without EDTA (PIC) was added per 5 x 10⁶ cells/ml cell pellet. The cell pellet was homogenised by resuspension with a 1 ml syringe and needle. The cells were incubated on an end-over-end rotator for 30 minutes at 4°C. The lysate was centrifuged at 13,000 x g for 10 minutes at 4°C and the supernatant was carefully aspirated and transferred to a pre-cooled tube. The lysate was quantified using the bicinchoninic acid (BCA) assay as per section 2.3.2.

2.3 Protein Detection and Analysis

2.3.1 Molecular weight and extinction coefficient determination

The nucleotide sequence of the open reading frame for PTEN-V5-His was converted to an amino acid sequence using SnapGene software. The amino acid sequence was analysed using the ExPASy Protein Parameter software to determine the estimated molecular weight and extinction coefficient (Artimo et al., 2012). For PTEN-V5-His, the molecular weight was 52 kDa and the extinction coefficient was 93,500.

2.3.2 Protein Quantification

For purified protein, the Nanodrop 2000 was used for protein quantification. For more complex protein samples, such as those from cell lysates or purification processing samples, a Bradford or BCA assay was used.

Using the protein settings of a Nanodrop 2000, and taking into account the theoretical molecular weight and extinction coefficient of the target protein, the absorbance at 280 nm was determined for each purified sample in duplicate or triplicate and converted to protein concentration. For protein purification samples, which were complex mixtures of proteins in the presence of a reducing agent, the fractions were quantified using a Bradford assay using the Pierce™ Coomassie Plus (Bradford) Assay Reagent (ThermoFisher Scientific, UK) according to the manufacturer's instructions for a 96-well plate format. Briefly, 300 µl of the Bradford reagent was added to 10 µl of sample, before incubation for 10 minutes at RT and measurement of absorbance at 595 nm. For mammalian lysate samples, where there was a complex mixture of proteins in the presence of detergent, the protein was quantified using the Pierce™ BCA Protein assay kit (ThermoFisher Scientific, UK) in a 96-well plate format, according to the manufacturer's instructions. Briefly, the mammalian cell lysates were diluted 1:5 and 1:10 in 1X PBS in a final volume of 25 µl before addition of 200 µl of working BCA reagent. The plate was mixed and incubated at 37°C for 30 minutes before cooling to RT for 10 minutes and the absorbance was measured at 562 nm. For affinity pull down assay fractions, where the protein concentration was low, the enhanced cuvette-based BCA protocol was used, where 100 µl of sample was mixed with 2 ml of the working BCA reagent and heated at 60°C for 2 hours before cooling to RT and measurement of absorbance at 562 nm.

For each of the assays, a standard curve using bovine serum albumin (BSA) was created by diluting a 2 mg/ml stock of Pierce™ BSA Standard (ThermoFisher Scientific, UK) in PBS to the following concentrations: 2000, 1500, 1000, 750, 500, 250, 125 and 25 µg/ml. For each sample in a different buffer, a blank was included where 25 µl of sample buffer was used in

place of the unknown sample, diluted as appropriate, in triplicate. To estimate the protein concentration, the absorbance of the appropriate sample buffer blank was subtracted from the absorbance of the unknown sample. Using the standard curve, the blank-adjusted absorbance was converted to protein concentration. Where two different sample dilutions were used, an average was taken.

2.3.3 Sodium Dodecyl Sulfate Polyacrylamide Gel Electrophoresis (SDS-PAGE)

Polyacrylamide gels were prepared at with 4.5 ml of 8, 10 or 12% resolving gel overlaid with a 4% stacking gel. The composition of the resolving gel was 375 mM Tris pH 8.8 with 1% sodium dodecyl sulfate (SDS), 0.1% tetramethylethylenediamine (TEMED) and 0.1% ammonium persulfate (APS). The composition of the stacking gel was 126 mM Tris pH 6.8 with 1% SDS, 0.1% TEMED and 0.1% APS. To store, the cast gels were individually wrapped in damp paper towel before sealing with clingfilm and storing at 4°C.

For purification analysis, protein samples were prepared on the basis of volume for crude, unpurified protein samples and on the basis of concentration for purification protein samples. For mammalian cell lysate quantification, the protein samples were prepared on the basis of concentration. For reducing samples, proteins were diluted 1:1 in 2X reducing Laemmli loading dye (125 mM Tris-HCl pH 6.8 with 4% SDS, 20% glycerol, 10% β -mercaptoethanol with 0.004% bromophenol blue) (Merck, UK) and heated at 95°C for 5 min. For non-reducing samples, proteins were diluted 1:1 in 2X non-reducing loading dye (62.5 mM Tris-HCl pH 6.8 with 2.5 % SDS, 10 % glycerol and 0.002 % bromophenol blue) and heated at 72°C for 10 minutes. Prior to adding the samples, the wells flushed with running buffer (25 mM Tris pH 8.3 with 192 mM glycine and 0.1% SDS) using a 200 μ l pipette. 5 μ l of molecular weight ladder was added to one lane of the gel and the protein samples were loaded onto the gel. The gel was run at 50V for 30 minutes until the loading dye had run through the stacking gel. The voltage was then increased to 100V for 1.5 hours until the dye front had reached the bottom of the gel.

The polyacrylamide gel was stained with Coomassie Stain (0.1 % (w/v) Coomassie Brilliant Blue in 40 % (v/v) methanol with 10 % (v/v) glacial acetic acid) for 1 hour at RT and 50 rpm before destaining overnight with 7.5% acetic acid with 10% ethanol. Alternatively, the polyacrylamide gel was stained with PageBlue™ Protein Staining Solution (ThermoFisher Scientific), as per manufacturer instructions, for 1-18 hours at RT at 50 rpm before destaining overnight in water. The gel was imaged using the GBox imaging system and GeneSys

software (Syngene, UK). For purity analysis, ImageJ software was used with a light background subtraction and 50 rolling pixels.

2.3.4 Western Blot Analysis

All wash steps were performed at 50 rpm at RT unless otherwise stated. The SDS-PAGE gel was washed in ice-cold transfer buffer (25 mM Tris with 190 mM glycine and 20% methanol) for 10 minutes. PVDF membrane was activated in methanol for 1 minute before washing with ice-cold transfer buffer for 10 minutes. The gel was transferred using the MiniBlot system (BioRad, USA) at 100 V for 60 minutes on ice, or 30 V for 18 h at 4°C. The membrane was stained with Ponceau Stain (0.1% Ponceau Red in 7.5% acetic acid) for 5 minutes before destaining in Type 2 H₂O for 1 minute and imaging to check for effective transfer. The membrane was completely detained in TBS-T (20 mM Tris pH 7.5 with 150 mM NaCl and 0.1% Tween-20) for 5 minutes before a further 3 x 5-minute washes in TBS-T. The membrane was blocked with 5% skimmed milk powder or 5% bovine serum albumin (BSA) in TBS-T for 1h at RT or 18-20h at 4°C. The membrane was rinsed in TBS-T before washing for 5 minutes with TBS-T. The membrane was incubated with an appropriate dilution of primary antibody in 5% milk powder or 5% BSA in TBS-T for 1h at RT or 18-20 h at 4°C. To detect PTEN, a 1:5,000 dilution of Mouse Anti-PTEN IgG (Cell Signalling Technologies, UK) was used. The membrane was washed in TBS-T for 5 minutes 3 times before incubation with an appropriate dilution of secondary antibody in 5% milk powder or 5% BSA in TBS-T for 1h at RT. For PTEN, the secondary antibody was a 1:10,000 dilution Goat Anti-Mouse IgG-HRP antibody (BioRad, UK) was used. The membrane was washed in TBS-T for 10 minutes 3 times, before rinsing in TBS (20 mM Tris pH 7.5 with 150 mM NaCl). The membrane was incubated with SuperSignal West Pico Chemiluminescent Substrate (ThermoScientific, UK) or Clarity Western Enhanced Chemiluminescence (ECL) Substrate (BioRad, UK), prepared as per the corresponding manufacturer's instructions, for 5 minutes at RT before imaging using the GBox imaging system and GeneSys software (Syngene, UK).

2.4 Mass Spectrometry

2.4.1 Reconstitution and Dilution of Proteases

Prior to use, the proteases were reconstituted, as per manufacturer instructions, to 1 µg/ml and stored in their reconstitution buffer at -20°C or diluted for use in the digestion protocols below. Trypsin Gold (Mass Spectrometry Grade) was reconstituted in 50 mM acetic acid and diluted to 20 µg/ml with 40mM NH₄HCO₃ with 10% ACN for use. Chymotrypsin was reconstituted in 1 mM HCl and diluted to 20 µg/ml with 40mM NH₄HCO₃. Glu-C (Sequencing

Grade) (Promega, UK) and Lys-C (Mass Spectrometry Grade) (Promega, UK) were reconstituted in Type 1 H₂O and diluted to 20 or 200 µg/ml in 25 mM NH₄HCO₃.

2.4.2 In-gel Digestion

For selected samples, an in-gel digestion was performed to allow mass spectrometric analysis. Target SDS-PAGE gel bands were excised and cut into 2-3 mm sized pieces. The gel pieces were first washed with 500 µl of 100 mM NH₄HCO₃ for 1h on a shaker, and then with 500 µl of 50% ACN with 100 mM NH₄HCO₃ for 1h on a shaker. 150 µl of 100 mM NH₄HCO₃ and 10 µl of 45 mM DTT were added to the gel pieces before incubation at 60°C for 30 minutes. The samples were allowed to cool to RT for 10 minutes before addition of 10 µl of 100 mM iodoacetamide (IAM) and incubation in the dark for 30 minutes at RT. The buffer was removed and the gel pieces washed with 500 µl of 50% ACN with 100 mM NH₄HCO₃ for 1h on a shaker. 50 µl of ACN was added to dehydrate and shrink the gel pieces for 10 minutes. The solvent was removed and the gel pieces were dried in a vacuum centrifuge for 10 minutes at 30°C, or until visibly dry. 20 µl of 20 µg/ml trypsin (prepared as per section 2.4) or chymotrypsin (prepared as per section 2.4) was added to each gel pieces and overlaid with 25 mM NH₄HCO₃ to cover the gel pieces. The gel pieces were heated at 37°C overnight for trypsin or 25°C for 4 hours for chymotrypsin. The gel pieces were centrifuged briefly and all of the liquid sample was transferred to a fresh centrifuge tube. To improve recovery of the digested proteins, 20 µl of 5% formic acid was added to each of the gel pieces and heated at 37°C for 20 minutes. 40 µl of ACN was then added to the gel pieces and heated at 37°C for 20 minutes. The solvent was transferred to the fresh sample tubes already containing the first portion of the sample. The samples were dried in a vacuum centrifuge for approximately 1h at 30°C. The dried samples were then stored at -20°C.

2.4.3 In-solution Digestion

The protein sample to be digested was buffer exchanged into 25 mM NH₄HCO₃ using a Zeba Spin Desalting Column with a 7 kDa molecular weight cut off (ThermoFisher Scientific, UK). For sample volumes <30 µl, a 75 µl desalting column was used, while for sample volumes >30 µl, a 0.5 ml desalting column was used. The buffer exchanged sample was quantified using the Nanodrop 2000, as described in section 2.3.2, and mixed 1:1 in *RapiGest* SF surfactant (Waters, US), which was previously diluted to 0.2% in 25 mM NH₄HCO₃. 5 mM DTT was added and the sample was incubated at 60°C for 30 minutes. The sample was cooled to RT for 10 minutes before incubation with 15 mM IAM in the dark at RT for 30 minutes. For digestion trials and optimisation, the reduced and alkylated purified PTEN-V5-His was aliquoted into 5 µg aliquots and frozen at -80°C at this stage. For the digestion, the protease was diluted to 1

µg/ml with the appropriate resuspension buffer, as per manufacturer instructions and section 2.4.1, before dilution to 20 or 200 µg/ml in 25 mM ammonium bicarbonate. The protease was added at a ratio of 20:1 protein:protease. During the digestion optimisation experiments, 0.25 µg of protease was used for 5 µg protein 0.25 µg and for the final digestions, 0.4 µg of protease was used for 10 µg of protein. For trypsin, lys-C or glu-C, the samples were digested overnight at 37°C. For chymotrypsin, the samples were digested at 25°C for 4 hours. To terminate the digestion and precipitate the *RapiGest* surfactant, 1% trifluoroacetic acid (TFA) was added and the sample was incubated for 45 minutes at 37°C. The sample was centrifuged at 13,000 x g for 10 minutes and the supernatant was carefully aspirated and transferred to a new tube. The sample was then applied to a Pierce™ C18 spin column (ThermoFisher Scientific), as per manufacturer instructions, to concentrate and clean up the peptides. The peptides were then dried using a vacuum centrifuge at 37°C and frozen at -20°C for future mass spectrometry analysis.

2.4.4 High Performance Liquid Chromatography with Tandem Mass Spectrometry (HPLC-MS/MS)

The digest extracts were thawed at RT for 10 minutes before being re-suspended in 25-50 µL of high performance liquid chromatography (HPLC) Solvent A (2% ACN with 0.1% formic acid (FA)) by vigorous vortexing before transfer to autosampler vials. Initial samples were analysed using an Ultimate 3000 system (ThermoScientific, UK) coupled to a 5600 TripleTOF mass spectrometer (Sciex, UK). 10 µl of sample was loaded onto a desalting trap (PepMap™ C18, 0.5 x 5 mm) and washed at 20 µl/min for 4 minutes. The sample was then separated at 300 nl/min on a C18 column (PepMap™, 15 cm x 75 µm) at 35°C. Peptides were eluted with a 45-minute gradient from 2% to 45% HPLC Solvent B (98% ACN with 0.1% formic acid). The column was then washed for 4 minutes with 90% HPLC Solvent B, before re-equilibrating with 2% B for 8 minutes prior to the next sample run. Later samples were analysed using a Waters M-class LC system (Waters, US) coupled to a 5600 TripleTOF mass spectrometer (Sciex, UK). 5 µl of sample was loaded onto a nanoEase MZ Symmetry C18 Trap (180 µm x 20 mm) (Waters, UK) and washed at 20 µl/min for 4 minutes. The sample was then separated at 500 nl/min on a nanoEase MZ Peptide C18 column (15 cm x 75 µm) (Waters, UK) at 35°C. Peptides were eluted with a 45-minute gradient from 2% to 45% HPLC Solvent B (99% ACN from 0.1% FA). The column was then washed for 4 minutes with 90% HPLC Solvent B, before re-equilibrating with 1% B for 8 minutes prior to the next sample run. The resolved peptides were subjected to tandem mass spectrometry using the parameters in Table 2.2.

Table 2.2 Parameters chosen for MS/MS analysis

Setting	Parameters used
Source	Nanospray
Spray Voltage	2.4 kV
Source Temperature	150°C
Declustering Potential	50 V
Curtain Gas	15
<i>Survey Scan Settings</i>	
Mode	Positive Mode
Mass range	350-1250 Da
Scan time	200 ms
Resolution	High
<i>MS/MS IDA Settings</i>	
Number of ions selected	10
Charge	+2 to +5
Dynamic exclusion time	12 s
Energy Setting	Rolling Collision Energy

2.4.5 Mascot Search Parameters

Protein identification was performed using the Mascot Daemon to access the Mascot search engine, using the settings in Table 2.3. Further information about the parameters for specific proteases and acrolein post-translational modifications are given in Section 4.2.3. The resultant peptides in the search results were filtered with a threshold of an ion score of 40. Further details on how the Mascot results were interpreted for protein identification are given in Section 3.2.4 and post-translational modification analysis are given in Section 4.2.3

Table 2.3 Parameters chosen for Default Mascot Daemon searches

Setting	Parameters Chosen
Taxonomy	Mammalia
Database	SwissProt 2021_03 (565,254 sequences, 203,850,821 residues)
Fixed Modifications	Carbamidomethyl (C)
Variable Modifications	Oxidation (M)*
Enzyme	Enzyme dependent [!]
Maximum Missed Cleavages	Enzyme dependent [!]
Peptide Charge	+1
Peptide Tolerance	± 0.5 Da
MS/MS Ions Search	✓
Data Format	Mascot generic
MS/MS Tolerance	± 0.5 Da

Key:

*: Depending on the experiment, additional modifications may be included here (for example Acrolein Michael addition).

!: See specific method sections for further details.

Chapter 3 – Expression, Purification and Characterisation of Recombinant PTEN

3.1 Introduction

3.1.1 Protein Production for *In Vitro* Studies

There are a variety of proteins that can be produced recombinantly, from enzymes and antibodies to virus-like particles and membrane proteins. Currently, there are multiple cell-based expression systems that can be used for protein production depending on their suitability for the desired target protein and downstream applications. These expression systems include both eukaryotic and prokaryotic cells. Eukaryotic expression systems, such as mammalian, yeast, insect or plant cells, are most suitable for large proteins with multiple domains and post-translational modifications (PTMs). When the target protein is smaller and simpler with no requirement of eukaryotic PTMs, prokaryotic systems such as *E. coli* can be used. The advantages and disadvantages of the different expression systems have been reviewed extensively (Demain and Vaishnav, 2009, Chen, 2012, Liu et al., 2012, McKenzie and Abbott, 2018, Schillberg et al., 2019). More recently, cell-free approaches for protein synthesis have been more widely used, having its own advantages and disadvantages (Hunter et al., 2018). To date, cell-free expression has not yet been utilised for recombinant PTEN, and so this approach will not be discussed further here.

To permit production of an endogenous protein, a suitable expression plasmid with the target protein must be incorporated into the desired expression host. During plasmid construction, there is an opportunity to encode a fusion tag on the N- or C- terminal of a protein of interest which aids in several important factors for protein production (Ki and Pack, 2020). The characteristics of commonly used fusion tags have previously been evaluated (Jia and Jeon, 2016). Fusion tags can range in size, from as small as 6-8 amino acids for polyhistidine (His₆) and FLAG tags, respectively, whereas larger tags can include glutathione-S-transferase (GST) of 220 amino acids and green fluorescent protein (GFP) of 228 amino acids. Tandem tags involving more than one fusion tag on one terminus, or a tag on both the N- and C-terminus have also been used (Bernier et al., 2018). The use of different tags, either alone or in combination, affects expression, with regards to both yield and solubility of the target protein (Young et al., 2012, Bernier et al., 2018). In addition, fusion tags provide the opportunity to use specific chromatography strategies, giving an easier route of purification and higher purity of the purified protein in one step when compared to non-specific chromatography, such as ion exchange or size exclusion chromatography (Zhao et al., 2013, Jia and Jeon, 2016). The use of a fusion tag also permits the possibility of downstream experiments such as pull-down

assays for detecting PPIs, which offers an advantage over the use of a native protein and a corresponding antibody for co-immunoprecipitation as the protein of interest is pulled down with a specific antibody or affinity resin against the tag (Bell et al., 2013).

3.1.2 Expression and Purification of Recombinant PTEN

Recombinant PTEN has been used extensively for studies in the characterisation of PTEN. Recombinant proteins are commonly expressed in prokaryotic expression systems, such as *Escherichia coli* (*E. coli*) (Maehama and Dixon, 1998, Crockett et al., 2005, Redfern et al., 2008, Verrastro et al., 2016) and eukaryotic expression systems, including human cell lines (Myers et al., 1998, Herlevsen et al., 2007, Gunaratne et al., 2011, Maddika et al., 2011) and insect cells (Gajewski et al., 2007, Naguib et al., 2015, Liang et al., 2017, Dempsey and Cole, 2018).

A variety of fusion tags have been used to aid the production of PTEN by facilitating expression and simplifying purification. Table 3.1 shows a non-exhaustive list of the recombinant PTEN fusion proteins that have been utilised in studies into the structure and function of PTEN. GST is the most used fusion tag for production of recombinant PTEN *in vitro*, but His₆ has also been used (Table 3.1).

Table 3.1. Fusion Tags Previously Used in the Production of Recombinant PTEN for *In Vitro* Studies

Study Authors (Year)	Fusion Tag
Li and Sun (1997)	His ₆
Myers et al. (1997)	GST
Maehama and Dixon (1998)	GST
Myers et al. (1998)	GST
Lee et al. (1999)	GST
Lee et al. (2002)	His ₆
Leslie et al. (2003)	GST
Campbell et al. (2003)	GST
Redfern et al. (2008)	His ₆
Mak et al. (2010)	GST
Spinelli and Leslie (2015)	GST
Lee et al. (2015)	GST
Mak and Woscholski (2015)	GST
Arora and Ghosh (2016)	GST
Verrastro et al. (2018)	GST

Abbreviations:
His₆: 6-Histidine fusion tag
GST: Glutathione-**S**-transferase fusion tag

3.1.3 Identification of Proteins using Mass Spectrometry

Protein identification can be achieved by analysis of their resulting peptides after protein digestion, known as bottom-up proteomics (Zhang et al., 2013). Broadly, this involves protein extraction, with optional enrichment steps, and fractionation prior to protein digestion, either in-gel or in-solution, and tandem mass spectrometry (LC-MS/MS) analysis (Rogers and Bomgarden, 2016). The methods of protein extraction and the decision to include an enrichment step, such as immunoprecipitation, will depend on the application and the nature and abundance of the target protein (Dupree et al., 2020). Protein extraction takes the form of cell or tissue lysis, with a combination of enzymatic, detergent-based and physical lysis techniques (Rogers and Bomgarden, 2016). There is potential interference of common extraction reagents, including salts and detergents, with the chromatography performance and sensitivity of the MS/MS and these require removal prior to MS analysis (Rogers and Bomgarden, 2016). During in-gel digestion this occurs during the PAGE fractionation step and for in-solution digestion this involves a protein precipitation or buffer exchange step (Rogers and Bomgarden, 2016). The samples can also be cleaned up at the peptide level, after digestion, with the use of specialised pipette tips or spin columns packed with chromatography resin, to remove salts and concentrate the sample prior to analysis. Trypsin is the gold standard protease for bottom-up proteomics, but there are some considerations to its use that are introduced in section 1.3.2 and expanded further in section 3.4 and Chapter 4. The use of alternative proteases has been previously reviewed (Zhang et al., 2013, Tsiatsiani and Heck, 2015, Giansanti et al., 2016).

LC-MS/MS involves the separation of peptides using high performance liquid chromatography (LC) techniques prior to MS/MS. LC techniques can include reversed phase chromatography, which separates peptides on the basis of hydrophobicity, ion exchange chromatography, which separates peptides on the basis of isoelectric point (pI) and size exclusion chromatography, which separates peptides on the basis of size (Dupree et al., 2020). Incorporation of an LC step conveys an advantage as there is an additional fractionation step prior to MS analysis by the elution of peptides over a gradient. This reduces the complexity of the samples and maximises on the potential for protein identification by minimising the ion suppression that can occur when attempting to identify many proteins from a complex sample at the same time (Dupree et al., 2020). Both the mass and charge of an analyte affect its ability to suppress a co-eluting analyte (Annesley, 2003).

A mass spectrometer has three key components: an ion source to generate charged analyte species, a mass analyser to measure the mass-to-charge (m/z) ratio, and a detector to measure the intensity (Dupree et al., 2020). Ionisation is used to transfer the analytes into the

gas phase and for biological samples soft ionisation techniques, such as electrospray ionisation (ESI) and matrix-assisted laser desorption ionisation (MALDI), are the most suitable (Challen and Cramer, 2022, Feider et al., 2019). Biological samples, such as peptides, are susceptible to degradation with harder ionisation techniques, such as electron ionisation (EI) (Li et al., 2015). The use of soft ionisation techniques reduces this risk, keeping the peptide intact for more predictable fragmentation in the mass spectrometer that can be attributed to a diagnostic ion (Li et al., 2015, Fuchs and Schiller, 2016). ESI has the advantage over MALDI as it can be more easily coupled to an LC system as the analytes are ionised and transferred from the liquid phase directly on elution. ESI involves the formation of a fine droplet spray of the charged analytes by nebulisation on application of voltage to the analyte liquid and exposure to heat and an inert gas, which promote desolvation (Ho et al., 2003). The solvent is evaporated from droplets and the analyte ions within them are electrostatically repelled due to the repulsive Coulomb force between species of the same charge type, which eventually overcome the opposing surface tension force, resulting in smaller and smaller droplets until the droplets are so small that the analyte ions are ejected into the gas phase (Ho et al., 2003, Bruins, 1998, Banerjee and Mazumdar, 2012). MALDI involves the co-crystallisation of the analyte with a matrix which is then dried onto a conductive plate and on exposure of the sample spot to a laser, the crystal decomposes and the ions are transferred to the gas phase (Israr et al., 2020).

There are four mass analysers that are commonly used in proteomics, either alone or in conjunction with each other: ion trap, time of flight (TOF), quadrupole and fourier transform ion cyclotron (FTIC) (Aebersold and Mann, 2003). There are several types of analysis that can be performed, including data-dependent analysis (DDA), where the ions are selected on the basis of their abundance, and data-independent (DIA) analysis, where ions within a defined mass range are selected (Dupree et al., 2020). Although the reproducibility of DIA is higher than for DDA, DDA is commonly used during bottom-up proteomics for discovery experiments to maximise protein sequence coverage (Bateman et al., 2014). The selected ions are taken forward to fragmentation, and whilst collision-induced dissociation (CID) is the most common in bottom-up proteomics due to its predictable fragmentation pattern, there are other techniques including electron-transfer and electron-capture dissociation (Dupree et al., 2020). The spectra of the peptide fragments is assigned to a protein based on a database of proteins digested *in silico*, giving protein identification (Zhang et al., 2013).

3.1.4 Aims

The aim of the work reported in this chapter was to produce recombinant PTEN, PTEN-V5-His, in *E. coli* with an acceptable yield, purity and phosphatase activity against OMFP. The first objective was to identify suitable conditions to express soluble PTEN-V5-His using the protein expression *E. coli* strain, BL21 (DE3). The second objective was to purify the expressed PTEN-V5-His. The third objective was to characterise the purity and catalytic activity of the purified PTEN-V5-His, using SDS-PAGE, LC-MS/MS and *in vitro* phosphatase activity assays. Due to the presence of a His affinity tag and use of a complementary metal affinity resin for purification, it was hypothesised that the purity of the purified PTEN-V5-His would be sufficient for use in *in vitro* experiments described in Chapter 4 and 5. The final purity of PTEN-V5-His is important when considering the subsequent protein-protein interaction (PPI) experiments, as contaminating proteins may have their own interacting proteins which would be found in the interactor fraction that do not interact with PTEN, giving false positive interactors. *E. coli* has previously been used as a protein expression system for PTEN during characterisation studies of PTEN's structure and activity, and so it was also hypothesised that the purified PTEN-V5-His would be catalytically active. The production of an active protein was essential for the subsequent lipoxidation experiments, to allow assessment of the effect of acrolein treatment on PTEN's phosphatase activity.

3.2 Materials and Methods

3.2.1 Materials

All materials were purchased from Merck, ThermoFisher or FisherScientific, unless otherwise stated. JpExpress404 PTEN was a gift from Ramon Parsons (Addgene plasmid #49420; <http://n2t.net/addgene:49420>; RRID:Addgene_49420). The DNA sequence of the plasmid is detailed in Supplementary Figure 1.

3.2.2 Expression of PTEN-V5-His in *E. coli*

Plasmid Purification

TOP10 *E. coli* transformed with a plasmid encoding PTEN-V5-His (JpExpress404 PTEN) was obtained as a stab culture and plated on Luria Broth (LB) agar plates (10 g/L sodium chloride (NaCl), 10 g/L tryptone, 5 g/L yeast extract) with 100 µg/µl ampicillin (LB-Amp) and 12 g/l agar plates (Hopkins et al., 2013). The plates were incubated at 37°C for 18-24h. Single colonies were picked and expanded in 6 ml of LB-Amp at 37°C and 180 rpm until an OD₆₀₀ of between 0.5 and 1.0 was obtained. 100-200 ml of LB-Amp were inoculated with a 1:200 dilution of the primary culture and incubated at 37°C 180 rpm for 18-20h. The remaining primary culture was diluted 1:1 in sterile 50% glycerol and stored at -80°C. The secondary cultures were harvested at 4,816 x g for 10 minutes at room temperature (RT). The plasmid was purified using the PureYield™ Maxi Prep System (Promega, UK) using the manufacturers recommended protocol.

Plasmid Quantification

The purified plasmid was quantified in duplicate using a NanoDrop 2000 system (ThermoFisher Scientific, UK) measuring absorbance at 230, 260 and 280 nm. If the absorbance at 260 nm was > 1.0 the plasmid was diluted 1:10 in nuclease free water before re-measurement. The absorbance was converted automatically by the Nanodrop 2000 software to DNA concentration in ng/ml by normalisation of the path length to 1 cm from 1 mm and modification of the Beer-Lambert equation to include a factor of 50 ng-cm/µl for double-stranded DNA, as described by the manufacturer.

Plasmid Restriction Digest

To linearise the plasmid, the restriction enzyme EcoRI (New England Biosciences, UK) or Xho1 (New England Biosciences, UK) and its corresponding buffer, was used as per manufacturer instructions. 1 Unit (U) of restriction enzyme was combined with 1 µg of purified plasmid and 1X reaction buffer in a final reaction volume of 50 µL. The reaction mix was incubated at 37°C for 1h.

Agarose DNA gel

100 ng of linearised and intact plasmid was loaded onto separate lanes of a 12-well 0.9% agarose gel with 1x BlueJuice loading dye (Invitrogen™, ThermoFisher Scientific, UK) in a final volume of 15 µL. The gel was run at 100 V for 90 minutes before staining with 1x SybrSafe dye (Invitrogen™, ThermoFisher Scientific, UK) in 1x Tris-acetate-ethylenediaminetetraacetic acid (EDTA) (TAE) buffer (40 mM Tris pH 8.3 with 20 mM acetic acid and 1 mM EDTA) in the dark at 50 rpm. The gel was imaged using GeneSys GBox system (Syngene, UK).

Transformation of PTEN-V5-His into BL21 (DE3) E. coli

Once plasmid quality was confirmed, competent cells of a protein expression strain of *E. coli*, BL21 (DE3) (SigmaAldrich, Merck, UK), were transformed with the JpExpress404 plasmid using heat shock according to the manufacturer instructions. A 40 µl suspension of competent BL21 (DE3) cells (Sigma Aldrich, UK) was thawed on ice and 5 µg of plasmid in 10 µl of nuclease free water was added. The suspension was incubated on ice for 30 minutes before heat shocking at 42°C for 30 seconds. A 250 µl aliquot of pre-warmed Super Optimal broth with Catabolite repression (SOC) media (SigmaAldrich, Merck, UK) was added and the cell suspension was incubated at 37°C for 1 h with shaking. 20 µl and 200 µl of culture was plated on LB-Amp agar plates. The plates were incubated at 37°C for 18-20h. Single colonies were picked and used to inoculate 6 ml of LB-Amp. The primary culture was incubated at 37°C at 180 rpm until an OD₆₀₀ of 0.5-1.0 was reached, then it was diluted 1:1 in sterile 50% glycerol and frozen at -80°C.

Small Scale Expression of PTEN-V5-His

A glycerol stock of BL21 (DE3) transformed with PTEN-V5-His was streaked on LB-Amp agar plates and incubated for 18-20h at 37°C. Single colonies were used to inoculate 6 ml of LB-Amp and incubated for 18-20h at 20°C at 180 rpm, until an OD₆₀₀ of 0.5-1.0 was reached. The primary culture was used to inoculate a secondary culture using a 1:200 dilution in 100 ml of LB-Amp. The secondary culture was incubated for 3-4h at 37°C with shaking at 220 rpm until an OD₆₀₀ of 0.5-0.6 was reached. Protein expression was then induced by the addition of isopropyl β-D-1-thiogalactopyranoside (IPTG) to a final concentration of 1 mM. The induced cultures were incubated at 20°C or 37°C with shaking at 220 rpm. To assess protein expression a 1 ml sample was taken at 2h, 4h, 18h and 24h and the cells were harvested by centrifugation at 5,000 x g for 5 minutes at RT and the cell pellets were stored at -20°C. The remaining culture from each time point was harvested at 4,816 x g for 30 minutes at 4°C before resuspension in ice cold 50 mM Tris-HCl, pH 7.4 with 1 mM phenylmethylsulfonyl fluoride (PMSF). The suspension was transferred to a fresh tube and centrifuged at 4,816 x g for 30

minutes at 4°C, the supernatant was discarded and the pellets were stored at - 20°C. These pellets were then used for small scale purification to analyse yield and activity of PTEN-V5-His at the different expression time points and temperature.

Small scale lysis of the time point samples was achieved by re-suspending the pellets from the 1 ml pellet from each expression time point and temperature in 50% v/v of ice-cold lysis buffer (50 mM Tris-HCl, pH 7.4, with 150 mM NaCl, 1 mM EDTA, 1 mM DTT, 1 mM PMSF and 200 µg/mL lysozyme). The cell suspension was incubated at 37°C for 30 minutes before the addition of 50% w/v of 0.11 mm acid-washed glass beads and vortexing vigorously for 5 minutes. The resulting lysate was centrifuged at 20,000 x g for 30 minutes at 4°C and the supernatant aspirated. A Bradford assay was performed on the supernatant and 15 µg of protein was incubated at 95°C for 5 minutes with 1X reducing loading dye (SigmaAldrich, UK) and run on a 12% reducing SDS-PAGE for 30 minutes at 50 V and 90 minutes at 100 V. A western blot was performed, as per section 2.3.4 to detect PTEN-V5-His at each expression time point and temperature.

Large Scale Expression of PTEN-V5-His

A glycerol stock of BL21 (DE3) transformed with PTEN-V5-His was streaked on LB-Amp agar plates and incubated for 18-20h at 37°C. Single colonies were used to inoculate 6 ml of LB-Amp and incubated for 18-20h at 20°C at 180 rpm, until an OD600 of 0.5-1.0 was reached. The primary culture was used to inoculate secondary culture using a 1:200 dilution in 400 ml of LB-Amp. The secondary culture was incubated for 3-4h at 37°C with shaking at 220 rpm until an OD600 of 0.5-0.7 was reached. Protein expression was then induced by the addition of IPTG to a final concentration of 0.5 mM. The induced cultures were incubated at 20°C with shaking at 220 rpm. The remaining culture from each time point was harvested at 4,816 x g for 30 minutes at 4°C before resuspension in ice cold 50 mM NaPO₄ pH 7.4 with 1 mM PMSF. The suspension was transferred to a fresh tube and centrifuged at 4,816 x g for 30 minutes at 4°C, the supernatant was discarded and the pellets were stored at - 20°C.

3.2.3 Purification of PTEN-V5-His

Lysis of the E. coli pellet

Pellets were thawed on ice for 1h before resuspension in ice cold lysis buffer (50 mM sodium phosphate pH 8.0 with 500 mM NaCl, 0.1% Triton X-100, 1 mM PMSF, 1 mM DTT, 1 mg/ml lysozyme). The cell suspension was incubated on a roller at 60 rpm at 4°C for 2h, until the lysate was translucent. The lysate was sonicated on ice using a handheld sonicator with an MSF-7 probe at 50% amplitude in 10 second bursts with a 20 second rest in between, a total

of 10 times. The sonicated lysate was centrifuged at 30,000 x g for 60 minutes at 4°C. The supernatant was passed through with a needle using a manual syringe to reduce viscosity before filtration with a 0.8 µm syringe filter on ice.

Immobilised Metal Affinity Chromatography

Due to the presence of the His-tag in PTEN-V5-His, immobilised metal affinity chromatography (IMAC) was used to purify the protein. The binding buffer (25 mM NaPO₄ pH 8.0 with 500 mM NaCl, 0.1% Triton X-100, 1 mM PMSF, 1 mM DTT and 1 mM imidazole), wash buffer (25 mM NaPO₄ pH 8.0 with 500 mM NaCl, 1 mM PMSF, 1 mM DTT and 1 mM imidazole) and elution buffer (25 mM NaPO₄ pH 8.0 with 500 mM NaCl, 0.1% Triton X-100, 1 mM DTT and 250 mM imidazole) were prepared fresh and kept on ice. All steps of the purification were performed at room temperature with ice-cold buffers and supernatant. Where resin was pipetted, a wide-bore pipette tip was used. For initial purifications, where the yield was unknown, 0.5% w/v resin to culture was used. For subsequent purifications, 0.25 ml resin was used per 1l culture. An appropriate amount of HisSelect Affinity Gel resin (MilliPore, SigmaAldrich, UK) was loaded into an empty gravity flow column before equilibration. During the equilibration steps, the resin was washed with 5 column volumes (CV) type 2 H₂O, 5CV of elution buffer and 10CV of binding buffer. The bottom of the gravity column was partially occluded with a 10 µl pipette tip to slow the flowrate and increase the exposure time of the lysate to the resin. The clarified lysate was applied to the column before washing with 20CV binding buffer 1 to wash out any unbound proteins and 10CV wash buffer to remove the Triton X-100. 1CV of wash buffer was applied to a capped column and the column was stored at 4°C overnight. Initially, 20CV elution buffer was applied 2CV at a time, allowing the buffer to completely pass through the column before application of the next 2CV. For future purifications, 10CV of elution buffer was applied in full and the eluate collected together. 200 µl of each purification step, except the eluate, was taken and frozen at -20°C for subsequent purification process analysis. The elution fractions were quantified for protein concentration and analysed using reducing SDS-PAGE and a phosphatase assay, as described below in section 3.2.4 and 3.2.5. For select samples, in-gel digestion and LC-MS/MS was performed as described below in section 3.2.4.

Buffer Exchange, Concentration and Storage

To remove any leached nickel resin and fully reduce the purified protein, 1 mM EDTA and 10 mM DTT were added to the elution fraction pool prior to buffer exchange into the storage buffer (25 mM sodium phosphate pH 7.4 with 150 mM NaCl and 10 mM DTT) before short-term storage at 4°C. For long term storage, glycerol was added to a final concentration of 25% before storage at -80°C. If the protein concentration was <1 mg/ml the PTEN-V5-His was

concentrated using a 10 kDa centrifugal filtration unit (Cytiva, UK). The concentrator was prepared by flushing the membrane with appropriate buffer by centrifugation at 4,000 x g at 4°C for 2 minutes. The protein was concentrated at 4,000 x g at 4°C until the desired volume was reached. The concentrate was collected by inverting the centrifugal filter into the collection cap and centrifuging at 3,000 x g for 2 minutes at 4°C.

IMAC Resin Cleaning and Regeneration

After each use the resin was washed with 5CV of Type 2 H₂O before cleaning with 5CV of 6M guanidine-hydrochloride (HCl). The column was then washed with 5CV of Type 2 H₂O, 5CV of binding buffer, 10CV of Type 2 H₂O and finally 10CV of 20% ethanol for storage. The resin was then kept at 4°C. If the resin appeared grey or brown after cleaning it was stripped and re-charged as per manufacturer instructions using 0.1 M EDTA and 10 mg/ml nickel (II) sulfate before washing and storing as above.

3.2.4 Protein Detection and Analysis

Protein Quantification

Using the Nanodrop 2000 protein settings with the estimated theoretical molecular weight and extinction coefficient of the protein, the absorbance at 280 nm was measured and the protein concentration determined for each sample in duplicate or triplicate. For PTEN-V5-His, the molecular weight was 52 kDa and the extinction coefficient was 93,500.

Sodium Dodecyl Sulfate Polyacrylamide Gel Electrophoresis (SDS-PAGE)

Sample preparation and SDS-PAGE analysis was performed as described in section 2.3.3.

LC-MS/MS and Protein Identification

In-gel digestion and LC-MS/MS analysis were performed as per section 2.4. Protein identification was performed using the Mascot Daemon to access the Mascot search engine, using the settings in Table 3.2.

Table 3.2. Parameters chosen for Mascot Daemon searches

Setting	Parameters Chosen
Taxonomy	Mammalia
Database	SwissProt 2021_03 (565,254 sequences, 203,850,821 residues)
Fixed Modifications	Carbamidomethyl (C)
Variable Modifications	Oxidation (M)
Enzyme	Trypsin
Maximum Missed Cleavages	1
Peptide Charge	+1
Peptide Tolerance	± 0.5 Da
MS/MS Ions Search	✓
Data Format	Mascot generic
MS/MS Tolerance	± 0.5 Da

3.2.5 Phosphatase Activity Analysis

OMFP Phosphatase Activity Assay

The following assay reagents were pre-warmed to 30°C: 10X assay buffer (250 mM sodium phosphate, 1.5 M NaCl, pH 8.0), Type 2 H₂O, 100 mM DTT and 10 mM EDTA were prewarmed to 30°C. An OMF standard curve was produced in triplicate at 0, 0.1, 0.25, 0.5, 0.75, 1, 2.5, 5, 7.4 and 10 µM in 1X assay buffer in triplicate with a final volume of 200 µl. 20 µg of PTEN recombinant protein was prepared in a black, flat bottomed 96-well plate in triplicate, in 1X assay buffer with 10 mM DTT and 1 mM EDTA, to a final volume of 200 µl. Ten units (U) of alkaline phosphatase (ALP) with OMFP reaction mix was used as the positive control, where OMFP reaction mix without any enzyme, PTEN or ALP, was used as the negative control. The plate was mixed for 10 seconds on low speed and pre-warmed for 10 minutes at 30°C. Initial preliminary assays did not include an incubation for 10 minutes at 30°C. 50 µl of OMFP reaction mix was added to each well before measurement before being shaken on low speed for 10 seconds to mix. The fluorescence was measured with 485 nm excitation and 538 nm emission, with a 515 nm cut off, every minute for 20 minutes. For each sample the fluorescence increase was adjusted for background by subtracting the fluorescence at time point 0 from the fluorescence at time point 20. This fluorescence increase was adjusted for non-specific, background hydrolysis of OMFP by subtracting the fluorescence increase of the negative control.

Enzyme Kinetic Linearity Analysis

The effect of pre-incubation on the linearity PTEN-V5-His enzyme activity was analysed using the OMFP phosphatase assay, as described above, with the following amendments. The samples were prepared in the 96-well plate and the assay was performed with and without a 10-minute pre-incubation inside the fluorimeter at 30°C prior to the addition of the OMFP

reaction mix. The fluorescence increase from three experimental replicates was adjusted for the background fluorescence before the mean was plotted against the time \pm standard error of the mean (SEM). A simple linear regression analysis was performed using GraphPad Prism 8.0 to report the R^2 value and the standard error of the estimate ($Sy.x$) to determine the goodness of fit.

3.2.6 Statistical Analysis

Data from three experimental replicates with three or more variables was analysed using GraphPad Prism 8.0 to perform one-way ANOVA analysis, correcting, where applicable, for multiple comparisons using the Tukey test. Statistical significance defined as $P < 0.05$. The P value style was as follows: (ns) >0.5 (ns), <0.05 (*), <0.005 (**), <0.0005 (**), <0.0005 (***), <0.0005 (****). Raw data is shown as mean values \pm SEM.

3.3 Results

3.3.1 Plasmid Preparation from TOP10 *E. coli* Resulted in Supercoiled Plasmid Suitable for Transformation and Expression

Isolation of the commercial plasmid from TOP10 (PTEN-V5-His) *E. coli* was required to transform BL21 (DE3) *E. coli* for expression of PTEN-V5-His. Once purified using the MaxiPrep Promega system, the plasmid was analysed by spectrophotometry and agarose gel electrophoresis to determine the plasmid's suitability for transformation. Spectrophotometry analysis of the purified plasmid showed little contamination with protein, indicated by an A_{260}/A_{280} ratio of approximately 1.8 (Table 3.3). The A_{260}/A_{230} was above 1.8, indicating no contamination of buffer reagents such as ethanol, used in the plasmid purification process (Table 3.3). Once the plasmid was shown to be free of contaminants, the length and conformation of the plasmid was confirmed using agarose gel analysis of uncut and restriction digested plasmid (Figure 3.1). It could be seen from the lane containing the uncut plasmid PTEN-V5-His that the majority of the plasmid was in the supercoiled conformation, the optimal conformation for transformation. A proportion of the uncut plasmid was in the open coiled conformation, where a single strand nick has occurred (Figure 3.1). Additionally, the restriction digests (RD) performed with Xho1 or EcoRI were incomplete and show some supercoiled DNA present. However, the plasmid that was successfully digested in the RD lanes was the correct length at approximately 5.3 kbp (Figure 3.1).

Table 3.3 Quantification of the purified commercial plasmid

Plasmid	JpExpress 404 PTEN
Recombinant Protein	PTEN-V5-His
A₂₆₀/A₂₈₀	1.84 ± 0.02 [£]
A₂₆₀/A₂₃₀	1.94 ± 0.08 [£]
Plasmid DNA Concentration (ng/µl)	282 ± 3.00 [£]
Total Plasmid (µg)	211.5

[£] The data is presented as the mean value of technical triplicates ± SEM

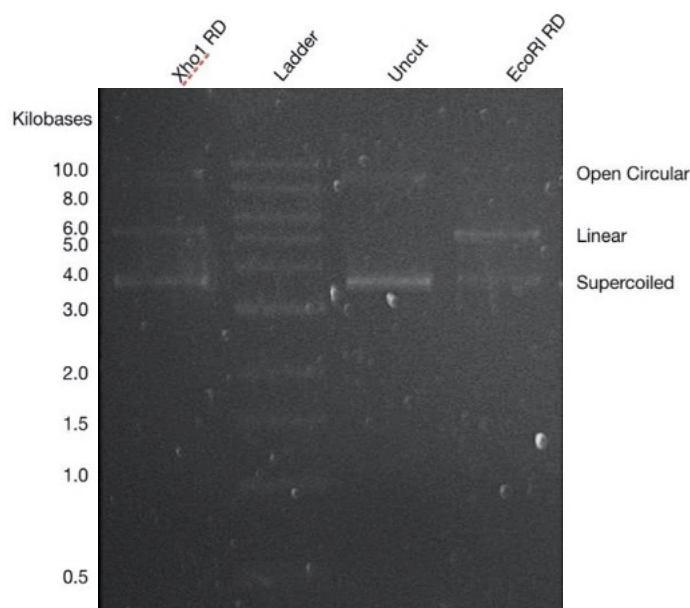


Figure 3.1 Agarose gel separation of intact and restriction digested purified plasmid.

One hundred ng of DNA was run on a 0.9% agarose gel and stained with SybrSafe. Purified JpExpress404 PTEN plasmid encoding PTEN-V5-His was restriction digested with either Xho1 or EcoRI. The correct length of the plasmid was 5.3 kbp.

3.3.2 Expression in BL21 (DE3) Successfully Produced Soluble PTEN-V5-His

The optimal expression conditions were then tested for PTEN-V5-His, by induction of cultures grown to mid-log phase with an OD_{600} of 0.5-0.7, by addition of 1.0 mM IPTG and incubation at 20°C for 2-24 hours. The lysate obtained from each expression time point had a major band at approximately 60 kDa, corresponding to PTEN-V5-His recombinant protein which has an expected molecular weight of 50 kDa (Figure 3.2). There was an 80 kDa band in the purified PTEN-GST positive control. This was also present in the negative control, which was clarified lysate from uninduced transformed BL21 (DE3) with a PTEN-GST bacterial expression plasmid, indicating that some basal expression had occurred (Figure 3.2). However, the negative control did not contain a band at 60 kDa, confirming that there was no cross reactivity of the anti-PTEN antibody against any of the native BL21 (DE3) proteins present in lysate at the expected molecular weight of the target protein, PTEN-V5-His (Figure 3.2). There were additional, smaller molecular weight bands present at each of the expression time points (Figure 3.2), which due to their reactivity with an anti-PTEN could correspond to mistranslated PTEN-V5-His protein.

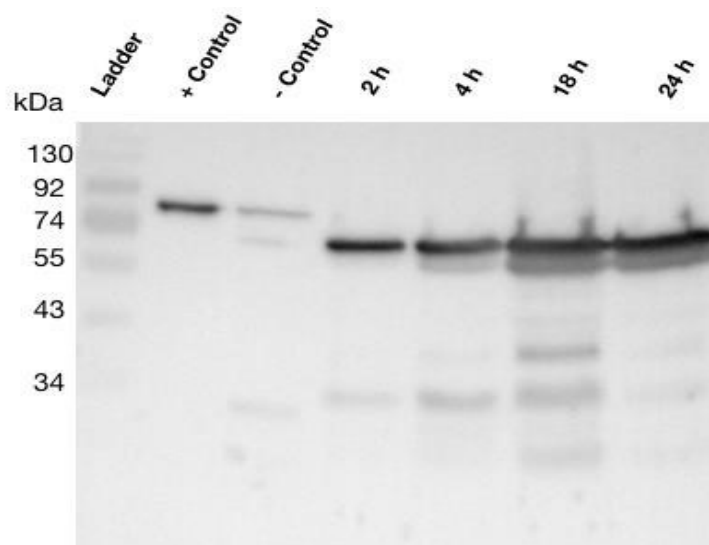


Figure 3.2 Western Blot analysis of PTEN-V5-His expression after induction with 1.0 mM IPTG at 20°C for 2-24 hours.

20 μ l of purification samples in 1X reducing loading dye were resolved on a 10% polyacrylamide gel before transfer to a PVDF membrane. After blocking, the blot was incubated with 1:5,000 Mouse Anti-PTEN primary antibody and subsequently 1:10,000 Goat Anti-Mouse IgG-HRP conjugated secondary antibody. The positive control is purified PTEN-GST and the negative control is uninduced BL21 (DE3) transformed with a plasmid encoding PTEN-GST.

Figure 3.3 shows the SDS-PAGE analysis of the elution fractions from each expression time point. PTEN-V5-His, corresponding to a 60 kDa band, was present in each fraction and the purity level was quantified using densitometry (Table 3.4). There was an increase in the size of the 60 kDa PTEN-V5-His band (Figure 3.3) and the purity of the fraction (Table 3.4) as the expression time increased. There were some smaller molecular weight contaminants at 25-30 kDa, 50 kDa and some larger molecular weight contaminants at 75-80 kDa, at each of the time points (Figure 3.3). The purified protein from each expression time point was analysed for phosphatase activity by testing the fractions by the OMFP assays. The OMFP assay shows OMFP phosphatase activity increased as the expression time point increased (Table 3.4).

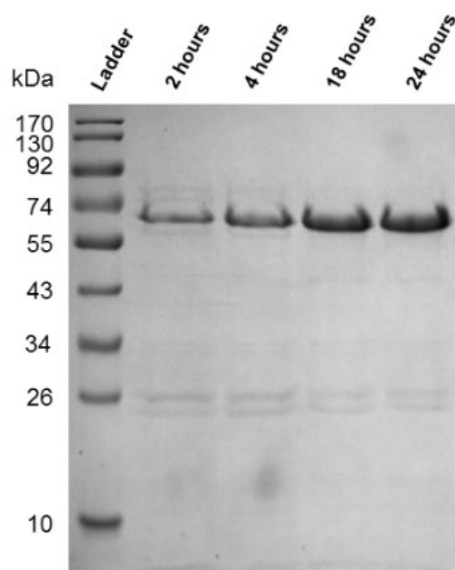


Figure 3.3 SDS-PAGE analysis of purified PTEN-V5-His expressed for different times.

20 μ l of purified PTEN-V5-His from lysate of induced BL21 (DE3) expressed for 2-24 hours was analysed by reducing SDS-PAGE on a 12.5% polyacrylamide gel and stained with Coomassie blue. PTEN-V5-His is a 50 kDa protein present here as an approximately 60 kDa band.

Table 3.4 Yield, Purity and Phosphatase Activity Analysis of PTEN-V5-His Expressed from 2-24 hours.

Expression (hours)	Yield (mg of protein per L of bacterial culture)	PTEN-V5-His Purity (%)	OMFP Activity (nmol OMF/min/mg protein)
2	3.09 [§]	30 [♦]	0.21 \pm 0.01 [£]
4	3.12 [§]	41 [♦]	0.32 \pm 0.00 [£]
18	4.04 [§]	65 [♦]	0.72 \pm 0.02 [£]
24	4.16 [§]	65 [♦]	0.83 \pm 0.02 [£]

[§] The data is presented as the mean value of technical triplicates.

[♦] The data is presented as the result from one technical replicate.

[£] The data is presented as the mean value of technical triplicates \pm SEM

3.3.3 Characterisation of Purified PTEN-V5-His Confirmed Correct Sequence and Phosphatase Activity

PTEN-V5-His can be expressed successfully in BL21 (DE3) and purified using immobilised metal affinity chromatography

Samples taken during lysis and purification were analysed by SDS-PAGE to ensure the washes were sufficient to remove unbound proteins whilst retaining PTEN-V5-His on the column (Figure 3.4). As expected, proteins of various molecular weights were visible in the lanes containing clarified lysate and flow-through, corresponding to host proteins of *E. coli* (Figure 3.4). Washes 1 and 2 showed minimal protein, indicating that the washes are sufficient to remove unbound proteins whilst retaining PTEN-V5-His on the resin (Figure 3.4). There were some proteins of higher and lower molecular weights than PTEN-V5-His present in the

overnight incubation in wash buffer 2, shown in the wash overnight (O/N) lane (Figure 3.4), indicating that an overnight incubation with 1 mM imidazole removes some contaminating proteins whilst retaining the majority of the PTEN-V5-His. The eluate shows one major band corresponding to PTEN-V5-His with some smaller molecular weight bands. The average yield of three representative purifications of PTEN-V5-His from 2l of culture was 1.66 ± 0.16 mg/l of culture ($n=3$, Mean \pm SEM). Quantifications of loss during buffer exchange and the concentration step showed an average protein loss of $14 \pm 2\%$ and $20 \pm 5\%$ ($n=3$, Mean \pm SEM), respectively.

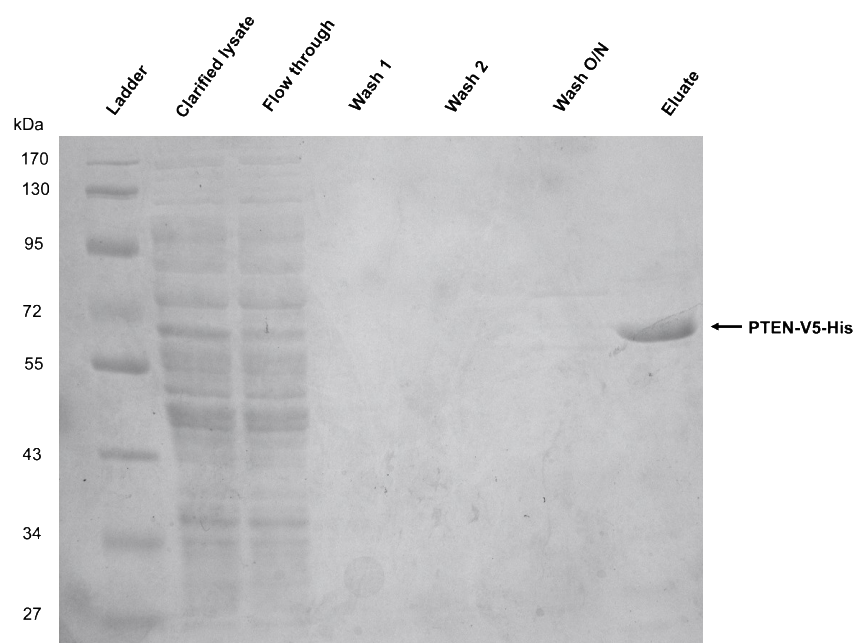


Figure 3.4 Representative SDS-PAGE analysis of the IMAC purification of PTEN-V5-His.

10 μ l of clarified lysate, flow-through, wash 1 and wash 2 was analysed with 2 μ g of wash O/N and the eluate fraction by reducing SDS-PAGE on a 10% polyacrylamide gel stained with Coomassie blue.

To ensure the purification strategy facilitated the production of monomeric PTEN-V5-His with sufficiently high purity for the desired downstream applications, the purified protein was analysed by SDS-PAGE. Figure 3.5A shows PTEN-V5-His (Band 2) to be the largest band, with one higher (Band 1) and two lower (Band 3 and Band 4) molecular weight impurities in the reducing and non-reducing gel. Band 2, corresponding to PTEN-V5-His, appears as an approximately 60 kDa protein using both reducing and non-reducing SDS-PAGE. Band 1 appears as a 75-80 kDa protein, band 3 appears as an approximately 45 kDa protein and band 4 appears as an approximately 35 kDa protein (Figure 3.5A). The lack of higher molecular weight impurities (>100 kDa) in the non-reducing or reducing gel shows that there is no cross-linking or aggregation. Figure 3.5B shows the plot of the densitometry analysis of the reducing sample, which maps to the additional molecular weights apparent in Figure 3.5A.

The purity of PTEN-V5-His, as determined by the densitometry plot (Figure 3.5B), was $67 \pm 4\%$.

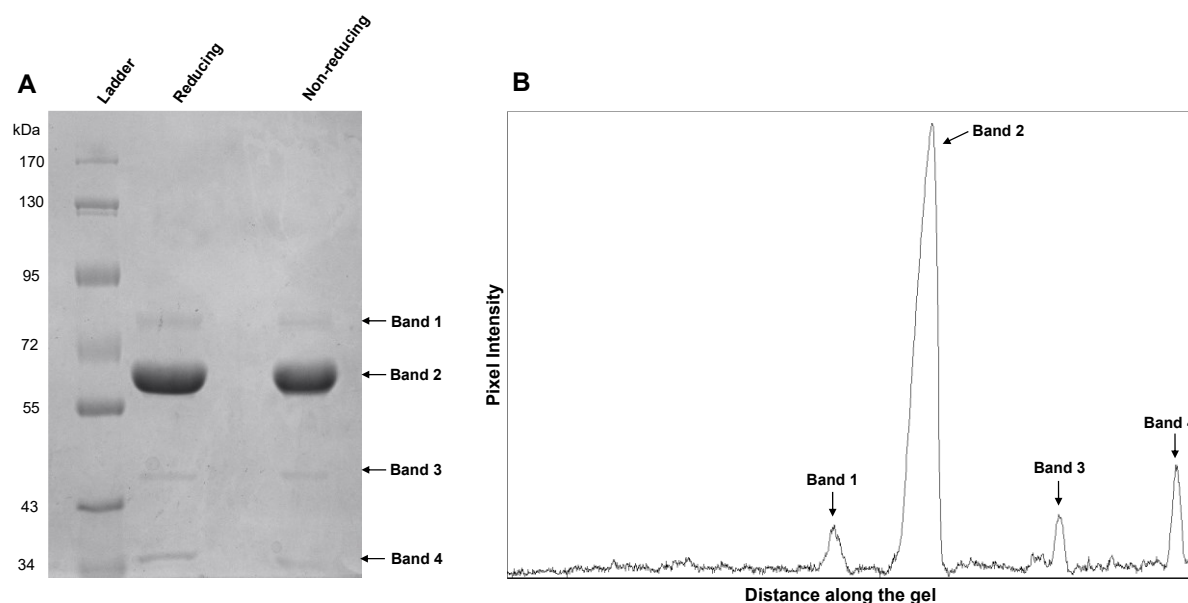


Figure 3.5 Representative SDS-PAGE and densitometry analysis of PTEN-V5-His.

A) 5 μg of purified PTEN-V5-His was analysed by reducing and non-reducing SDS-PAGE on an 8% polyacrylamide gel stained with Coomassie blue. B) The stained gel was imaged using a GBox and the reducing lane was analysed using ImageJ with the background adjusted using a light background and 50 pixels.

LC-MS/MS analysis of the in-gel digest samples from the reducing SDS-PAGE bands 1-4 (Figure 3.5), identified PTEN-V5-His as human PTEN (Figure 3.5 Band 2) and the additional co-purified contaminant bands (Figure 3.5 Bands 1, 3 and 4) to be from *E. coli* (Table 3.5). Whilst confirmation that the expressed fusion protein was human PTEN is important, the sequence coverage of the digested protein was key to the future work of this thesis. To map acrolein modification to the structure of PTEN a high sequence coverage is needed, and it is desirable to cover key residues of interest such as the resolving cysteine (Cys71) and catalytic cysteine (Cys124). Figure 3.6 shows the sequence coverage of PTEN-V5-His obtained using an in-gel digestion with trypsin. Whilst the sequence coverage of the human PTEN region of the purified PTEN-V5-His was high at 86%, the overall sequence coverage of PTEN-V5-His was 77%, as the V5-His portion of the sequence was not included in the SwissProt database that was used to perform the Mascot search.

Table 3.5 LC-MS/MS Protein Identification of Purified PTEN-V5-HIS and Additional Co-purified *E. coli* Host Proteins

Gel Band	Band Intensity (%)	Protein ID	Protein	Taxonomy	Database	Score	Mass (Mr)	Sequence Coverage (%)	Peptide no. (non-duplicate / duplicates)
1	5	ARNA_ECOBW	Bifunctional polymyxin resistance protein ArnA	<i>E. coli (K12)</i>	SwissProt	58423	74869	45	1380 (36/1344)
2	87	PTEN_HUMAN	Phosphatase and tensin homolog	<i>H. sapiens</i>	SwissProt	122676	47706	81	2724 (60/2664)
3	3	ASTC_ECOBW	Succinylornithine transaminase	<i>E. coli (K12)</i>	SwissProt	61338	43980	57	1113 (31/1082)
4	5	RL2_ECOBW	50S ribosomal protein L2	<i>E. coli (K12)</i>	SwissProt	66173	29956	55	1456 (32/1424)

Chapter 3 – Expression, Purification and Characterisation of Recombinant PTEN

1	2	3	4	5	6	7	8	9	10	11	12	13	14	15	16	17	18	19	20		
M	T	A	I	I	K	E	I	V	S	R	N	K	R	R	Y	Q	E	D	G		
												Nuclear Localisation Sequence									
												PL binding				CL				CL	
21	22	23	24	25	26	27	28	29	30	31	32	33	34	35	36	37	38	39	40		
F	D	L	D	L	T	Y	L	I	Y	P	N	I	I	A	M	G	F	P	A	E	
Nuclear Localisation Sequence																					
CL	CL	CL	CL	CL																	
41	42	43	44	45	46	47	48	49	50	51	52	53	54	55	56	57	58	59	60		
R	L	E	G	V	Y	R	N	N	I	D	D	V	V	R	F	L	D	S	K		
61	62	63	64	65	66	67	68	69	70	71	72	73	74	75	76	77	78	79	80		
H	K	N	H	Y	K	I	Y	N	L	C	A	E	R	H	Y	D	T	A	K		
81	82	83	84	85	86	87	88	89	90	91	92	93	94	95	96	97	98	99	100		
F	N	C	R	V	A	Q	Y	P	F	E	D	H	N	P	P	Q	L	E	L		
												WPD loop									
												Protonation									
101	102	103	104	105	106	107	108	109	110	111	112	113	114	115	116	117	118	119	120		
I	K	P	F	C	E	D	L	D	Q	W	L	S	E	D	D	N	H	V	A		
121	122	123	124	125	126	127	128	129	130	131	132	133	134	135	136	137	138	139	140		
A	I	H	C	K	A	G	K	G	R	T	G	V	M	I	C	A	Y	L	L		
P loop																					
Conformatic Catalysis												Basic				Catalysis					
141	142	143	144	145	146	147	148	149	150	151	152	153	154	155	156	157	158	159	160		
H	R	G	K	F	L	K	A	Q	E	A	L	D	F	Y	G	E	V	R	T		
												TI loop									
161	162	163	164	165	166	167	168	169	170	171	172	173	174	175	176	177	178	179	180		
R	D	K	K	G	V	T	I	P	S	Q	R	R	Y	V	Y	Y	Y	S	Y		
												TI loop									
												Extension				Extension					
181	182	183	184	185	186	187	188	189	190	191	192	193	194	195	196	197	198	199	200		
L	L	K	N	H	L	D	Y	R	P	V	A	L	L	F	H	K	M	M	F		
201	202	203	204	205	206	207	208	209	210	211	212	213	214	215	216	217	218	219	220		
E	T	I	P	M	F	S	G	G	T	C	N	P	Q	F	V	V	C	Q	L		
221	222	223	224	225	226	227	228	229	230	231	232	233	234	235	236	237	238	239	240		
K	V	K	I	Y	S	S	N	S	G	P	T	R	R	E	D	K	F	M	Y		
241	242	243	244	245	246	247	248	249	250	251	252	253	254	255	256	257	258	259	260		
F	E	F	P	Q	P	L	P	V	C	G	D	I	K	V	E	F	F	H	K		
261	262	263	264	265	266	267	268	269	270	271	272	273	274	275	276	277	278	279	280		
Q	N	K	M	L	K	K	D	K	M	F	H	F	W	V	N	T	F	F	I		
												CBR3 loop									
281	282	283	284	285	286	287	288	289	290	291	292	293	294	295	296	297	298	299	300		
P	G	P	E	E	T	S	E	K	V	E	N	G	S	L	C	D	Q	E	I		
301	302	303	304	305	306	307	308	309	310	311	312	313	314	315	316	317	318	319	320		
D	S	I	C	S	I	E	R	A	D	N	D	K	E	Y	L	V	L	T	L		
321	322	323	324	325	326	327	328	329	330	331	332	333	334	335	336	337	338	339	340		
T	K	N	D	L	D	K	A	N	K	D	K	A	N	R	Y	F	S	P	N		
												ca2 helix									
341	342	343	344	345	346	347	348	349	350	351	352	353	354	355	356	357	358	359	360		
F	K	V	K	L	Y	F	T	K	T	V	E	E	P	S	N	P	E	A	S		
361	362	363	364	365	366	367	368	369	370	371	372	373	374	375	376	377	378	379	380		
S	S	T	S	V	T	P	D	V	S	D	N	E	P	D	H	Y	R	Y	S		
381	382	383	384	385	386	387	388	389	390	391	392	393	394	395	396	397	398	399	400		
D	T	T	D	S	D	P	E	N	E	P	F	D	E	D	Q	H	T	Q	I		
401	402	403	404	405	406	407	408	409	410	411	412	413	414	415	416	417	418	419	420		
T	K	V	K	G	N	S	A	D	I	Q	H	S	G	G	R	S	S	L	E		
PDZ binding motif																					
421	422	423	424	425	426	427	428	429	430	431	432	433	434	435	436	437	438	439	440		
G	P	R	F	E	G	K	P	I	P	N	P	L	L	G	L	D	S	T	R		
												V5 tag									
441	442	443	444	445	446	447	448														
T	G	H	H	H	H	H	H	His tag													

Key	
PIP ₂ binding domain	Grey Not identified
N-terminal domain	Black Identified
C2 domain	
C-terminal tail	
Fusion tag	

Protein Information	
No. of PTEN residue	403
No. of total residues	448
PTEN molecular weight	47 kDa
Total molecular weight	52 kDa

Abbreviations	
CL	Cytoplasmic localisation
PL	Phospholipid binding
V5	Epitope tag from simian virus
His	Histidine

References	
Lee J. et al.	1999
Campbell R. et al.	2003
Walker, S. et al.	2004
Gil, A. et al.	2006
Denning, G. et al.	2007
Hopkins B. D. et al.	2013

Figure 3.6 Representative sequence coverage of PTEN-V5-His.

Purified PTEN-V5-His was subjected to an in-gel digestion with trypsin before analysis using LC-MS/MS.

The OMFP activity assay confirmed the phosphatase activity of purified PTEN-V5-His.

To determine the specific OMFP phosphatase activity of PTEN-V5-His, the fluorescence increase was monitored and calculated by subtracting the initial fluorescence from the final fluorescence. This fluorescence increase was adjusted for the control by subtracting the fluorescence increase of OMFP in the absence of enzyme. This adjusted fluorescence increase (RFU) was converted to the amount of OMF (nmoles) using an OMF calibration curve (Figure 3.7). Figure 3.7 was analysed using simple linear regression to determine a trendline from the mean of three technical replicates from a representative data set. To calculate OMFP phosphatase activity, the amount of OMF (nmoles) produced by the sample was calculated using the equation for the trendline (Figure 3.7). The amount of OMF produced (nmoles) was then converted to specific phosphatase activity (nmoles OMF/min/mg protein) by division with the assay time (20 minutes) and the amount of enzyme assayed (0.02 mg).

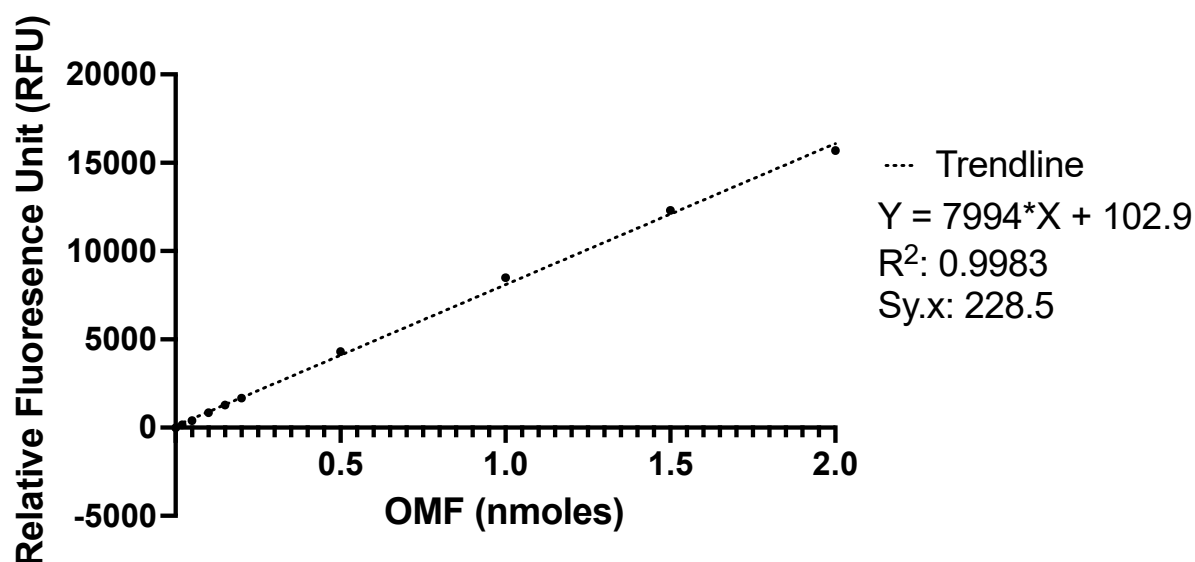


Figure 3.7 Representative OMF calibration curve.

Fluorescence at known OMF concentrations was plotted to give an OMF calibration curve. This was analysed using simple linear regression analysis. The equation shown describes the trendline (n=3; Mean \pm SEM).

Pre-incubation of PTEN eliminates initial lag and increases the linearity of the fluorescence increase during the OMFP activity assay.

During optimisation of the OMFP phosphatase assay the effect of pre-incubation on the linearity of the fluorescence increase was measured (Figure 3.8). This was done to ensure accuracy when using the fluorescence increase to quantify PTEN-V5-His OMFP phosphatase activity. In the absence of a plate pre-incubation step, initially there was a slower rate of fluorescence increase with a lag phase from 0-2 minutes (Figure 3.8), suggesting that as the plate warms to 30°C from RT the rate of activity increases. This lag is not present in the samples pre-incubated prior to the addition of OMFP, indicating that a 10-minute pre-

incubation removes the effect of temperature equilibration on the initial rate of enzyme activity. A 10-minute pre-incubation prior to the addition of the OMFP substrate increased the goodness of fit of the data in comparison to no pre-incubation. The goodness of fit was measured by the coefficient of determination, R-squared (R^2), and the standard error of the estimate ($Sy.x$) using simple linear regression analysis. Simple linear regression analysis for the fluorescence increase during the OMFP assay for the samples with a 10-minute pre-incubation step showed an R^2 of 0.9992 and an $Sy.x$ of 40.88. In comparison, in the absence of a plate pre-incubation the fluorescence increase showed a lower R^2 of 0.9894 and a higher $Sy.x$ of 105.9. The higher R^2 value and the lower $Sy.x$ value for the fluorescence increase after a 10-minute pre-incubation shows that the 10-minute pre-incubation results in a linear fluorescence increase. This demonstrates a linear conversion of OMFP to OMF by PTEN-V5-His and allows accurate phosphatase activity determination.

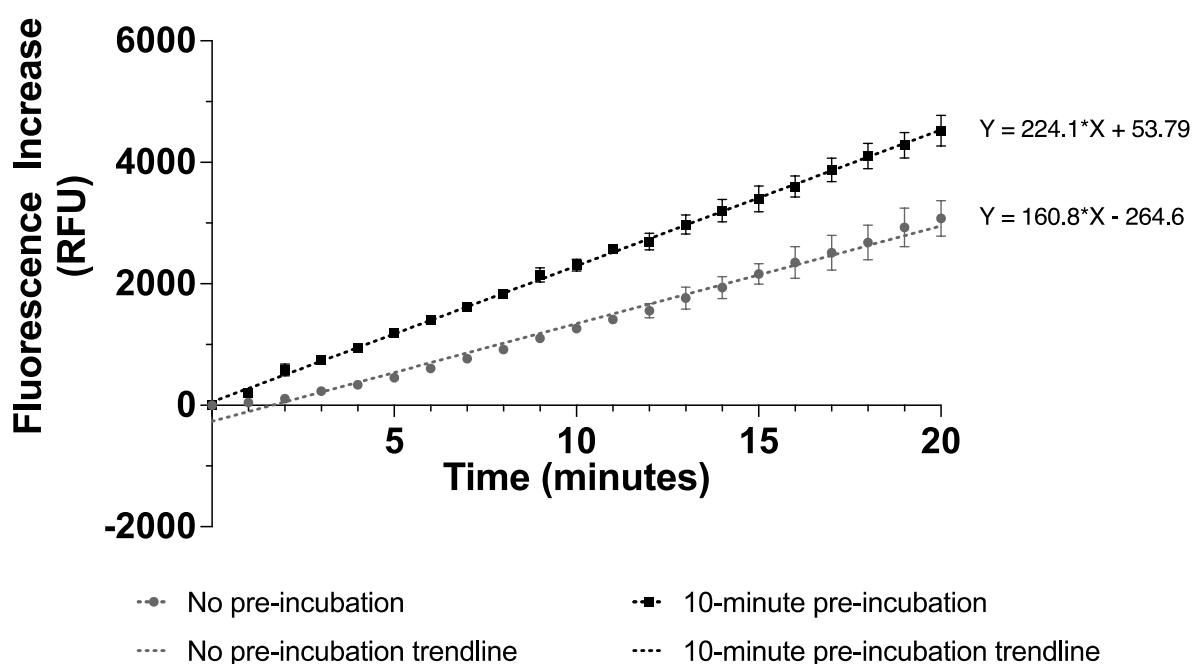


Figure 3.8 Effect of pre-incubation on the linearity of the increase in fluorescence during the OMFP phosphatase activity assay.

The fluorescence increase during the OMFP phosphatase activity analysis of PTEN-V5-His was monitored for 20 minutes with and without a 10-minute pre-incubation at 30°C (n=3; Mean \pm SEM).

Buffer exchange and concentration of purified PTEN-V5-His increased its phosphatase activity.

Phosphatase activity analysis was performed on fractions of purified, buffer exchanged and concentrated PTEN-V5-His. This ensured that there was no negative effect on the phosphatase activity of PTEN-V5-His by these final formulation steps required to buffer exchange the purified protein into an appropriate storage buffer at the desired concentration (>1 mg/ml). The OMFP phosphatase activity of purified PTEN-V5-His was assayed after

application of the protein to a PD-10 column for buffer exchange and subsequent concentration using a centrifugal concentrator. Figure 3.9 shows an increase in specific activity of purified PTEN-V5-His after buffer exchanged and concentration. Ordinary one-way ANOVA analysis of the specific activities determined the difference in activity between the purified and buffer exchanged as well as the buffer exchanged and concentrated PTEN-V5-His to be non-significant in both cases, with a P value of 0.1531 and 0.0666 respectively. However, the difference between the purified protein and the buffer exchanged and concentrated PTEN-V5-His was significant (*) with a P value of 0.0161.

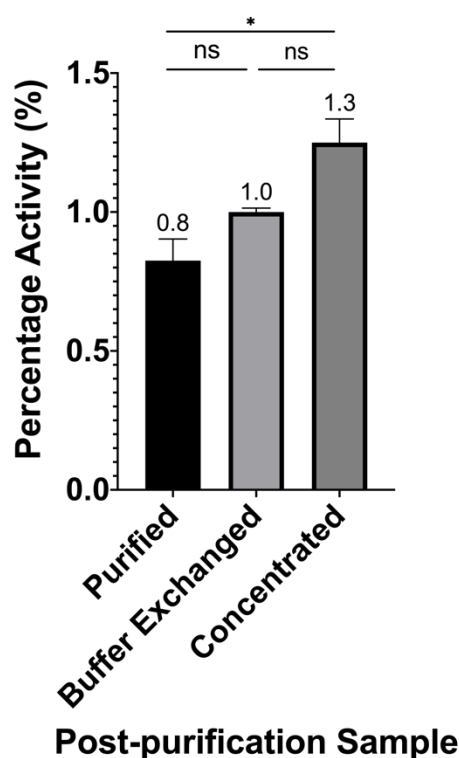


Figure 3.9 Effect of buffer exchange and concentration on the OMFP phosphatase activity of PTEN-V5-His. The OMFP activity assay was performed with purified PTEN-V5-His before and after buffer exchange and concentration (n=2; Mean \pm SEM; 0.1234 (ns), 0.0332 (*), 0.0021 (**), 0.0002 (***), <0.0001 (****)).

3.4 Discussion

To enable *in vitro* analysis of the effect of lipoxidation on PTEN's phosphatase activity and PPIs, the first aim of this project was to produce recombinant PTEN. First, PTEN-V5-His was expressed in *E. coli* before purification using immobilised metal affinity chromatography (IMAC). The purified PTEN-V5-His was then characterised using spectrophotometry, SDS-PAGE, LC-MS/MS and a phosphatase activity assay.

The first aim of this chapter was to express and purify a PTEN fusion protein for use in future *in vitro* lipoxidation studies. Soluble PTEN-V5-His was successfully expressed in the cytoplasm of *E. coli* using a low temperature expression protocol to reduce the risk of accumulation of PTEN-V5-His in inclusion bodies. As stated in section 3.1.2, successful *E. coli* expression of PTEN-His has previously been reported. This includes investigations of PTEN phosphoinositide binding, PTEN's global interactome and formation of PTEN homodimers in solution (Crockett et al., 2005, Redfern et al., 2008, Heinrich et al., 2015). Expression conditions for His-tagged PTEN have included induction with 2 mM IPTG for 8 hours at 37°C and 0.05 mM IPTG for 20-22 hours at 21°C, with the latter strategy closely matching the expression conditions described in this thesis (Crockett et al., 2005, Redfern et al., 2008). The described yields from both studies after purification was 1-2 mg/ml, however the yield per litre of culture was not specified. Previously described yields for alternative recombinant PTEN proteins, such as PTEN-GST, have included 5 mg of protein per litre of *E. coli* culture (Arora and Ghosh, 2016). The conditions reported in this chapter resulted in a lower yield than that reported yield for PTEN-GST. This difference could be explained by the use of different fusion tags. Fusion tags have the potential to increase expression by facilitating translation where the tag is introduced at the N-terminal, giving a higher yield (Jia and Jeon, 2016). Whilst the focus during the expression of recombinant proteins was once the level of protein expression, this has shifted towards the solubility of the expressed protein (Esposito and Chatterjee, 2006). Larger fusion tags, such as glutathione-S-transferase (GST) and maltose-binding protein (MBP), can increase the solubility of the target protein when combined with other factors to slow protein expression, such as reduced concentration of induction agent and reduced temperature (Rosano and Ceccarelli, 2014, Costa et al., 2014, Ki and Pack, 2020). For *E. coli* expression, increased solubility of an expressed protein decreases the likelihood of the recombinant protein accumulating in insoluble inclusion bodies (San-Miguel et al., 2013). This increase in solubility with the use of GST may explain the higher reported yield of PTEN-GST when compared to the yield of PTEN-V5-His described here. The advantages and disadvantages of the use of *E. coli* as an expression system have been extensively reviewed (Demain and Vaishnav, 2009, Rosano and Ceccarelli, 2014, Tripathi and

Shrivastava, 2019). A notable disadvantage of using a prokaryotic system such as *E. coli* as an expression system for mammalian proteins is the lack of post-translational modification machinery (Sahdev et al., 2008, Baeshen et al., 2015, Tripathi and Shrivastava, 2019). However, as described in section 3.1.2, *E. coli* has been used successfully to express recombinant PTEN previously. Notably, *E. coli* was used as the expression host for the initial landmark studies characterising the phosphatase activity and structure of PTEN (Li and Sun, 1997, Myers et al., 1997, Maehama and Dixon, 1998, Lee et al., 1999).

The choice to use the V5-His tag permitted the use of IMAC purification protocol against the his-tag and the production of a purified protein with a simple one-step process. The purification strategy is important in determining the viability of the subsequent studies reported in this thesis. Having a targeted purification against the fusion tag reduces the number of necessary purification steps, which increases the final yield of purified protein. A common fusion tag used in the expression and purification of recombinant PTEN is GST, which was used in the early landmark studies determining PTEN's crystal structure, membrane interactions and characterisation of its protein and lipid phosphatase activity (Myers et al., 1997, Maehama and Dixon, 1998, Myers et al., 1998, Lee et al., 1999). More recently, PTEN-GST has been used in a study on PTEN's ability to form homodimers and a global interactomics study into the effect of oxidation on PTEN's PPIs (Verrastro et al., 2016, Heinrich et al., 2015). Advantages of the GST tag include increased expression of soluble protein, as described above, and a robust, one-step purification strategy due to the high affinity and specificity of GST to glutathione resin. However, the large size of GST and its propensity to dimerize confers a disadvantage when using this tag for a fusion protein to be used in structural or interactomics studies. The use of a V5-His tag in this thesis is advantageous as the size of the fusion tag is reduced and this reduces its potential effects on the overall 3D structure of the recombinant PTEN protein. This is important for the work described in this thesis as it reduces the risk of the tag affecting true PTEN interactors or increasing false positive PTEN interactors. Notably, the polyhistidine (His) tag has been successfully used to express PTEN in *E. coli* for investigations into the global interactome of PTEN (Crockett et al., 2005). PTEN-His has also been used by studies into the structural effects of PTEN-phosphoinositide binding (Redfern et al., 2008). One important consideration for the use of His as a fusion tag for enzymes is its chelating properties, due to the importance of divalent cations as co-factors for some enzymes' catalytic activity. Whilst initial studies reported Mg^{2+} as a co-factor for PTEN, counterevidence was provided on elucidation of the crystal structure of PTEN, as Mg^{2+} was not found and analysis of PTEN enzymatic activity showed PTEN to be active in Mg^{2+} -free buffers (Kabuyama et al., 1996, Lee et al., 1999). The previous success in using PTEN-His to study PTEN indicates that the His tag is not detrimental to the structure, activity and PPIs of PTEN.

This is essential to meet the aims of this project, in which PTEN-V5-His was used to characterise the effect of lipoxidation on the structure, phosphatase activity and PPIs of PTEN.

To accurately characterise the physiologically relevant effects of acrolein on the structure and interactions of PTEN it was essential to confirm that the expressed and purified PTEN-V5-His was of high purity, with no cross-linking or aggregation. Wild type PTEN has a molecular weight of 47 kDa and PTEN-V5-His has a molecular weight of 50 kDa, as determined by ExPASy Protein Parameter software (Hornbeck et al., 2015, Artimo et al., 2012). Monomeric PTEN has previously been reported as appearing as a 50-55 kDa protein, higher than the theoretical molecular weight of 47 kDa (Papa et al., 2014). This would match the small molecular weight increase evident in the SDS-PAGE analysis of the purified PTEN-V5-His here, when taking into consideration the V5-His fusion tag which increases the molecular weight of PTEN protein by approximately 3 kDa. Whilst the use of reducing and non-reducing SDS-PAGE can confirm the approximate molecular weight of PTEN and whether the protein is monomeric or aggregated, it is not possible to confirm the conformation of the protein beyond this. The previous use of *E. coli* to express recombinant PTEN for both phosphatase and crystal structure studies indicates that a prokaryotic system can be used to successfully express PTEN in its correct conformation (Maehama and Dixon, 1998, Lee et al., 1999). Here, the activity of the purified PTEN-V5-His against OMFP strongly suggests that the protein is in the correct conformation. Beyond the use of x-ray crystallography, which was used to determine the original crystal structure of PTEN, examples of alternative approaches to evaluate the conformation of a protein include circular dichroism (CD) spectroscopy and attenuated total reflectance-fourier transform infrared (ATR-FTIR) spectroscopy (Lee et al., 1999, Greenfield, 2006, Glassford et al., 2013). CD spectroscopy has previously been used to characterise the secondary structure of recombinant PTEN (Arora and Ghosh, 2016).

To ensure that the PTEN-V5-His encoded human PTEN, the protein identity was confirmed using LC-MS/MS. Analysis of the resultant sequence coverage showed which residues would be detected by LC-MS/MS and likely observed in subsequent experiments. For preliminary digestions and identification of the expressed protein trypsin was used. Trypsin is the most widely used enzyme for proteomic sample preparation due to the high efficiency and specificity of its endoprotease activity. A limitation of trypsin is that its activity follows the Keil rule; specific cleavage at arginine or lysine residues at their C-terminal side except before proline (Keil, 1992). Tandem mass spectrometry confirmed that the sequence of the expressed recombinant PTEN was human, with a high sequence coverage to allow identification of key residues of interest, such as the resolving cysteine (Cys71) and the catalytic cysteine (Cys124). However, the limitations of trypsin with regards to lack of cleavage at KP sites

means that the P loop amino acids, including the catalytic cysteine, were identified within a large peptide of 41 amino acids. The length of the peptide means that detailed analysis of the MS/MS spectra is difficult due to the low intensity or absence peaks for residues in the middle of the sequence. This is an important consideration for the following chapter of this thesis, where identification and further spectral analysis of any modification of catalytic cysteine by lipid oxidation products were of particular interest. An approach to address this limitation would be to use alternative proteases to cleave at different residues and produce different peptides in regions of particular interest. The use of more than one protease during the digest increases the depth of proteomic analysis through an increase in protein sequence coverage (Wisniewski et al., 2019, Wisniewski and Mann, 2012, Li et al., 2017). This approach is detailed in Chapter 4 of this thesis during the investigation into the effect of acrolein on the structure of PTEN. Alternative digestions included the digestion of recombinant PTEN in solution, with trypsin/Lys-C and trypsin/Glu-C and in-gel, with chymotrypsin.

An integral aspect in the production of PTEN-V5-His for this thesis was the accurate quantification of OMFP phosphatase activity to enable investigation into the effect of acrolein on PTEN's activity. Ensuring a linear fluorescence increase during the OMFP assay was essential to permit the enzyme analysis to take place during the linear steady-state phase and ensure that the phosphatase activity calculated was accurate and reliable (Bisswanger, 2019). Initial assays were conducted with immediate addition of the OMFP substrate, as previously described (Verrastro et al., 2016). The resultant initial lag of fluorescence between 0 and 2 minutes was first hypothesised to be due to insufficient mixing of the substrate into the sample mix. However, increasing the initial shaking step prior to reading the absorbance from 10 seconds to 30 seconds did not improve the initial lag (data not shown). The second hypothesis was that the lag was due to temperature equilibration, despite pre-warming of the reaction buffers. The addition of a 10 minute pre-incubation step before initialisation of the assay by addition of the OMFP substrate clearly shows a vast improvement in the linearity of the fluorescence increase, with complete removal of the initial 2 minute lag (Mak and Woscholski, 2015).

The activity of PTEN-V5-His in its final formulation is higher than previous reports of the OMFP phosphatase activity of PTEN at 0.4 nmoles OMF/min/mg at RT with 1 mM DTT (Mak and Woscholski, 2015) and 0.72 nmoles OMF/min/mg at 25°C with 1 mM DTT (Verrastro et al., 2016). The lower assay temperature and lower DTT concentration of the cited studies could explain the discrepancies between the calculated and previously reported OMFP phosphatase activity. An alternative explanation is the molecular weight of the recombinant PTEN protein. The recombinant PTEN-V5-His used in this thesis has a molecular weight of approximately

50 kDa whilst the recombinant PTEN protein used in the aforementioned studies was PTEN-GST, which is approximately 70 kDa. The higher molecular weight of the GST tag in comparison to the V5-His tag means that for every 1 mg of protein, there is a lower amount of PTEN in the PTEN-GST sample than the PTEN-V5-His.

Whilst the OMFP activity assay has previously been used to quantify the phosphatase activity of PTEN, the PIP₃ assay would be a more specific and sensitive assay, as PIP₃ is PTEN's physiological substrate. Table 3.6 outlines previously published studies involving the quantification of PTEN's phosphatase activity and the substrates used. Whilst the majority of the studies in Table 3.6 used PIP₃ as a substrate, other substrates include polyGluTyr and OMFP.

Table 3.6. Enzyme Assays Used to Quantify the Phosphatase Activity of PTEN

Study	Phosphatase Assay	Substrate
Li and Sun (1997)	Protein	Phosphotyrosyl-RCML
Myers et al. (1997)	Protein	Phosphotyrosyl-RCML
		Phosphotyrosyl-MBP
		Phosphotyrosyl-polyGluTyr
		Phosphotyrosyl-EDNDYINASL
Maehama and Dixon (1998)	Lipid	PIP ₃
Myers et al. (1998)	Lipid	PIP ₃
	Protein	Phosphotyrosyl-polyGluTyr
Lee et al. (1999)	Lipid	PIP ₃ , PIP ₂ & PIP
Lee et al. (2002)	Lipid	PIP ₃
Leslie et al. (2003)	Lipid	PIP ₃
Campbell et al. (2003)	Lipid	PIP ₃
Redfern et al. (2008)	Lipid	PIP ₃
Mak et al. (2010)	Lipid	PIP ₃
	Other	OMFP
Spinelli and Leslie (2015) Mak and Woscholski (2015)	Lipid	PIP ₃
		InsP ₄ & InsP ₅
Lee et al. (2015)	Protein	Phosphotyrosyl-polyGluTyr
	Lipid	PIP ₃
Mak and Woscholski (2015)	Lipid	PIP ₃
	Lipid	InsP ₄
	Other	OMFP
	Lipid	PIP ₃
Arora and Ghosh (2016)	Other	pNPP
	Other	OMFP
Verrastro et al. (2018)	Other	OMFP

Abbreviations:

RCML: Reduced, carboxamidomethylated and maleylated lysozyme

MBP: Maltose binding protein

PIP: Phosphatidylinositol phosphate

InsP: Inositol phosphate

OMFP: 3-O-methylfluorescein phosphate

pNPP: Paranitrophenyl phosphate

Comparison of the kinetic parameters of PIP₃, IP₄ and OMFP as substrates shows that whilst PTEN has the highest affinity for PIP₃ and then IP₄, OMFP is also a suitable alternative substrate, with a K_m of 216 μM (Mak and Woscholski, 2015). Whilst pNPP has been used as a substrate, PTEN's activity against it is significantly lower (Maehama and Dixon, 1998, Maehama et al., 2001, Mak and Woscholski, 2015). The use of OMFP as a substrate for PTEN can be justified, despite the lower activity of PTEN, by the advantage that is conveyed by the continuous nature of the assay. Whilst the PIP₃ assay is highly sensitive and physiologically relevant, it is an end-point assay. The continuous monitoring that is permitted by the OMFP assay allows confirmation that the measurements used during the quantification is taking place during the linear portion of the assay, as discussed above.

In conclusion, the work in this chapter presents a strategy for the production of a soluble and active recombinant PTEN, PTEN-V5-His, that was used for subsequent *in vitro* studies. The optimisation of IMAC purification protocol permitted the production of PTEN-V5-His with few co-purified host protein impurities. The expressed recombinant PTEN was confirmed to be human PTEN with a high confidence and good sequence coverage. The phosphatase activity of PTEN-V5-His was accurately quantified after optimisation of OMFP activity assay, providing confidence that during the further work presented in this thesis, any reduction in phosphatase activity on treatment of PTEN-V5-His with acrolein would be accurately quantified. There are additional and alternative approaches to aspects of the characterisation of PTEN-V5-His detailed in this chapter. The use of CD or FTIR spectroscopy in addition to SDS-PAGE would confirm the conformation of the expressed protein and the use of PIP₃ as a substrate in the phosphatase assay would increase the confidence that the purified PTEN-V5-His is in the correct conformation with physiological activity. When the results are taken together, the data confirms the successful production of active PTEN-V5-His that meets the criteria for the *in vitro* studies into the effect of acrolein on PTEN's activity and structure that is detailed in the subsequent chapters of this thesis.

Chapter 4 – Effect of Acrolein on the Activity and Structure of Recombinant PTEN

4.1 Introduction

4.1.1 Lipoxidation of PTEN

Reactive aldehydes such as acrolein or 4-HNE can modify proteins through Michael addition of cysteine, lysine and histidine residues, or Schiff's base modification of lysine, as discussed in Section 1.1.2, and the mechanisms of which are illustrated in a review by Viedma-Poyatos et al. (2021) (LoPachin et al., 2009). The effect of acrolein adduction depends on the role of the residue affected (LoPachin et al., 2009). As discussed in section 1.2.6, PTEN is a cysteine-dependent phosphatase and its nucleophilic catalytic cysteine (Cys124) is particularly vulnerable to electrophilic attack due to its presence as a charged thiolate ion at physiological pH (Myers et al., 2011, Maehama and Dixon, 1998, Denu and Dixon, 1998). This is of particular interest when considering the effect of lipoxidation on the phosphatase activity of PTEN, where acrolein shows the highest reactivity for cysteine residues (Cai et al., 2009). It has previously been demonstrated that protein tyrosine phosphatase 1B (PTP1B), another cysteine-dependent phosphatase, is inactivated by acrolein in a time-dependent manner by covalent addition to its catalytic cysteine (Cys215) (Seiner et al., 2007). As discussed in section 1.2.6, endogenous PTEN isolated from acrolein-treated mammalian cells showed covalent modification by acrolein through western blotting, but the sites of modification were not identified (Covey et al., 2010). There was a concurrent time-dependent loss of activity shown by *in vitro* phosphatase assays with isolated endogenous PTEN and through detection of an upregulation of pAkt by western blotting, but no dose-dependency has been tested (Covey et al., 2010). Regarding 4-HNE, dose- and time-dependent inactivation of PTEN has been demonstrated using *in vitro* and *in cellulo* techniques (Shearn et al., 2011, Shearn et al., 2013). PTEN adduction by acrolein has also been demonstrated during investigations of the role of spermine oxidase (SMOX) and myeloperoxidase (MPO) in the production of acrolein (Uemura et al., 2017, Al-Salihi et al., 2015). Beyond modification of specific catalytic-dependent residues, structural changes brought by acrolein modifications across the structure of PTEN, including protein unfolding, due to an increase in carbonyl groups, and inter- or intramolecular cross-linking, due to acrolein's bifunctionality (Sayre et al., 2006, Spickett and Pitt, 2020).

4.1.2 Approaches to the Detection of Lipid Oxidation Product Adducts

Protein adducts with lipid oxidation products have been identified using both label-dependent techniques, with the use of antibodies and probes, and label-free approaches, which make use of more recent advancements with tandem mass spectrometry (Domingues et al., 2013, Afonso et al., 2018).

Traditional approaches to measuring oxidative modification of proteins involve the detection and measurement of carbonyl groups (Dalle-Donne et al., 2003). When investigating lipoxidation, there is a limitation of this approach as the formation of carbonyl groups is not exclusive to lipoxidation, as oxidation of amino acids can also produce carbonyl groups (Dalle-Donne et al., 2003, Domingues et al., 2013). In addition to being non-specific, the use of carbonyl groups to detect lipoxidation is non-inclusive as not all lipoxidation adducts have a free carbonyl group (Domingues et al., 2013). There are several ways in which oxidative modification of proteins can result in the formation of carbonyl groups. Carbonyl groups are formed on direct oxidation of lysine, arginine, proline and threonine residues and on oxidative cleavage of proteins (Berlett and Stadtman, 1997, Dalle-Donne et al., 2003). The side chains of cysteine, histidine and lysine residues can react with reactive aldehydes, such as acrolein, and reactive carbonyl derivatives, such as ketoaldehydes and ketoamines (Dalle-Donne et al., 2003). As such, the detection and measurement of carbonyl groups can be considered as a non-specific but effective approach to detect protein adducts with lipid oxidation products, when the appropriate negative controls are used.

The use of chemical probes, such as 2,4-dinitrophenylhydrazine (DNPH) and biotin hydrazide, provide a low-cost method to detect carbonyl groups that are present lipoxidised proteins and as such can be used as a marker of oxidative stress (Dalle-Donne et al., 2003, Madian and Regnier, 2010). On reaction of DNPH with carbonyl groups, dinitrophenylhydrazone is produced which can be detected using spectrophotometry due to its absorbance at 376 nm (Levine et al., 1990, Domingues et al., 2013). An alternative approach is the use of SDS-PAGE and western blotting against DNP, commonly known as oxyblotting, to detect and visualise proteins with carbonyl groups (Levine et al., 1990, Domingues et al., 2013). A quantitative approach can be taken with the use of enzyme-linked immunosorbent assay (ELISA), however this can only provide information on the relative number of carbonyl groups (Buss et al., 1997).

To provide context on sites of modification, labelled carbonyl groups can also be used as diagnostic ions for detection using mass spectrometry (Guo and Prokai, 2011, Bollineni et al., 2011). More recently, label-free mass spectrometry approaches have been developed by

identifying specific reporter ions for modified residues (Cai et al., 2009, Maeshima et al., 2012, Afonso et al., 2018).

4.1.3 Mass Spectrometry Analysis of Acrolein Protein Modifications

There are three main types of proteomics that can be used to analyse protein modification with tandem mass spectrometry: top-down, middle-down and bottom-up. Whilst top-down proteomics involves the analysis intact proteins, middle-down and bottom-up proteomics analyses peptides that are generated after restrictive or extensive proteolytic digestion, respectively (Zhang et al., 2013). Whilst intact mass analysis in top-down proteomics can provide useful information on proteoforms, bottom-up proteomics has the advantage that the modifications can be mapped to specific residues and that peptides are easier to separate and ionise than proteins, with peptides having a more predictable fragmentation patterns (Dupree et al., 2020, Rogers and Bomgarden, 2016).

The approach to post-translational modification (PTM) analysis in this thesis was bottom-up proteomics using tandem mass spectrometry, and so is the focus of this section. The mass spectrometry techniques that are commonly used in proteomics was introduced in section 3.1.3 and the advantages and disadvantages to the different approaches to bottom-up proteomics has recently been reviewed (Dupree et al., 2020). The spectra from fragmented peptides can be assigned to a protein for protein identification, by comparison to protein databases. This can be expanded to take into consideration the potential presence of post-translational modifications by taking into account the corresponding mass shift of a modified or unmodified residue (Cai et al., 2009, Steen and Mann, 2004). As discussed in section 1.1.2, acrolein can modify proteins through Michael addition at cysteine, lysine and histidine and through Schiff base formation to lysine residues. Michael addition results in a mass shift of 56 Da and Schiff base modification to residues results in a 38 Da mass shift (Cai et al., 2009).

Mascot is an example of software that can be used to search protein databases for matches to the peptide spectra, but there is a known issue of false discoveries. Whilst the resulting peptide assignments can be filtered based on the confidence of the peptide match and whether it is a unique protein assignment, it is necessary to validate the spectra for correct peak assignment. To further increase the confidence in the data, de novo sequencing can be performed. This is achieved by manual analysis of the spectra where the mass difference between neighbouring peaks can be assigned to specific amino acids, taking into account the potential for post-translational modification where applicable. This is easier when more predictive fragmentation techniques such as CID are used at the MS/MS stage, as introduced

in section 4.1.3. During CID the peptide is fragmented at the peptide bonds, and those fragments created from the C-terminus are called y ions, whilst the fragments created from the N-terminus are called b ions (Dupree et al., 2020)

4.1.4 Aims and Hypotheses

The aim of this chapter was to further characterise the effect of acrolein on the structure and phosphatase activity of PTEN. Whilst previous investigations into the effect of lipoxidation have focused on 4-HNE, there is some evidence that acrolein inactivates PTEN (Covey et al., 2010). However, *in vitro*, only a single acrolein treatment concentration was tested and no data has been collected on how PTEN is modified by acrolein and the effect the modifications have on PTEN's structure. The first objective was to analyse the effect of acrolein on PTEN's phosphatase activity by exposing recombinant PTEN *in vitro* to increasing concentrations of acrolein for increasing time points and quantifying its phosphatase activity using the OMFP activity assay. Due to the similar reactivity of acrolein to 4-HNE, it was hypothesised that acrolein would also inactivate PTEN in a time- and dose-dependent manner. The second objective was to take the acrolein-treated PTEN and visualise any changes to its structure using SDS-PAGE and map any acrolein modifications using LC-MS/MS. The ability of acrolein to cross-link proteins and cause aggregation through protein unfolding led to the second hypothesis that as the concentration of acrolein increased, higher molecular weight species would be seen by SDS-PAGE. Due to acrolein's high reactivity to thiol groups, it was hypothesised that at lower concentrations acrolein would preferentially modify cysteine residues, but as the concentration of acrolein increases lysine residues would also be modified. The vulnerability of PTEN's catalytic cysteine to electrophilic attack led to an extension of this hypothesis that Cys124 would be the most susceptible to modification and would be modified first. Previously, LC-MS/MS analysis has identified 4-HNE modifications to cysteine and lysine residues across the structure of PTEN, but acrolein's smaller size led to an additional hypothesis that less accessible residues that could also be modified.

4.2 Methods

4.2.1 Optimisation of the OMFP Activity Assay for Acrolein-Treated PTEN

Effect of Decreasing DTT Concentrations in OMFP Activity Assay Conditions

To determine the optimal DTT concentration for PTEN-V5-His phosphatase activity, the OMFP assay was performed as described in Section 3.2.3, with the following amendments; immediately prior to the assay, purified PTEN-V5-His was buffer-exchanged using a PD-10 gravity column, as per manufacturer instructions, into OMFP reaction buffer (25 mM NaPO₄ pH 8.0 with 75 mM NaCl) and the phosphatase activity was assayed in triplicate with 0, 1 or 10 mM DTT.

Effect of Sodium Borohydride Reduction on the OMFP Activity of PTEN-V5-His

To analyse the effect of sodium borohydride (NaBH₄) on the phosphatase activity of PTEN-V5-His, the OMFP assay was performed as described in Section 3.2.5, with the following amendments; immediately prior to the assay PTEN-V5-His was buffer exchanged using a PD-10 gravity column, as per manufacturer instructions, into the reaction buffer (25 mM NaPO₄ pH 7.4 with 150 mM NaCl and 10 mM DTT) before treatment with 5 mM NaBH₄ for 30 minutes at RT.

4.2.2 *In vitro* Lipoxidation of PTEN-V5-His

Buffer Exchange and Concentration into the Reaction Buffer

Immediately prior to the acrolein treatments, PTEN-V5-His was buffer exchanged using a PD-10 gravity column, as per manufacturer instructions, into the reaction buffer (25 mM NaPO₄ pH 7.4 with 150 mM NaCl). The buffer exchanged PTEN-V5-His was then concentrated to >1.5 mg/ml as described in Section 3.2.3.

Lipoxidation of PTEN-V5-His with Acrolein

100 µg of PTEN-V5-His was prepared in reaction buffer (25 mM NaPO₄ pH 7.4 with 150 mM NaCl) to a final concentration of 1 mg/ml (0.05 mM) with increasing concentrations of acrolein; 0 µM, 10 µM, 50 µM, 100 µM, 200 µM, 500 µM and 1 mM, for acrolein:PTEN ratios of 0:1, 0.2:1, 1:1, 2:1, 4:1, 10:1 and 20:1, respectively. Samples were incubated at 37°C for 10 minutes, 1 hour or 4 hours before reduction with 50 mM NaBH₄, as below.

Sodium Borohydride Reduction to Stabilise Acrolein Modifications

The first formulation trialled was in 0.2% NaOH, to provide a basic environment and prevent decomposition of NaBH₄ through its reaction with water and subsequent release of hydrogen (Minkina et al., 2012). The second formulation trialled was 50 mM NaBH₄ in reaction buffer

(25 mM NaPO₄ pH 7.4 with 150 mM NaCl) and this was prepared immediately prior to use due to the fast hydrolysis of NaBH₄ in non-basic aqueous solutions. NaBH₄ was added to each reaction to a final concentration of 5 mM before incubation for 30 minutes at RT.

4.2.3 Proteomic Analysis of the Effect of Lipoxidation on PTEN

OMFP Phosphatase Activity Analysis

After acrolein treatment and NaBH₄ reduction as above, the phosphatase activity of PTEN-V5-His was analysed using the OMFP assay as per Section 3.2.5.

SDS-PAGE Analysis

After acrolein treatment and NaBH₄ reduction as above, PTEN-V5-His was analysed by reducing SDS-PAGE on an 8% polyacrylamide gel as per Section 2.3.3. Western Blot against acrolein was conducted for acrolein-treated and untreated PTEN-V5-His as per Section 2.3.4.

Sample Preparation for LC-MS/MS Analysis

In-gel digestion of acrolein-treated PTEN was performed with trypsin or chymotrypsin, as per Section 2.4.2. In-solution digestion of acrolein-treated PTEN was performed with trypsin/Lys-C or trypsin/Glu-C, as per Section 2.4.3.

Tandem Mass Spectrometry and Analysis using Mascot

HPLC-MS/MS analysis was performed as per Section 2.4.2. Mascot searches were performed for three replicate alternative digestions for each protease with merged MS/MS data, with the settings outlined in Table 4.1. The Mascot search data was filtered to remove any peptides with an ion score less than 40 to remove any poor quality data. For the acrolein-treated PTEN digested with trypsin, the Mascot search parameters are described in Table 4.2 and the identified acrolein modifications for each replicate were validated by de novo sequencing using PeakView. For the acrolein-treated PTEN digested with chymotrypsin or trypsin/Glu-C, the MS/MS data was merged and the modifications were validated visually to confirm correct peak assignment by Mascot.

Table 4.1 Parameters used for Mascot searches for Protease Comparison

Setting	Protease			
	Trypsin	Trypsin/Lys-C	Trypsin/Glu-C	Chymotrypsin
Taxonomy	Mammalia	Mammalia	Mammalia	Mammalia
Database	SwissProt 2021_03 (565,254 sequences; 203,850,821 residues)			
Fixed Modifications	Carbamidomethyl (C)	Carbamidomethyl (C)	Carbamidomethyl (C)	Carbamidomethyl (C)
Variable Modifications	Oxidation (M)	Oxidation (M)	Oxidation (M)	Oxidation (M)
Enzyme	Trypsin	Trypsin/P	Trypsin-V8-E	Trypsin
Maximum Missed Cleavages	1	1	2	3
Peptide Charge	+2, +3, +4	+2, +3, +4	+2, +3, +4	+2, +3, +4
Peptide Tolerance	± 0.5 Da	± 0.5 Da	± 0.5 Da	± 0.5 Da
MS/MS Ions Search	✓	✓	✓	✓
Data Format	Mascot generic	Mascot generic	Mascot generic	Mascot generic
MS/MS Tolerance	± 0.5 Da	± 0.5 Da	± 0.5 Da	± 0.5 Da
Merge MS/MS?	✓	✓	✓	✓
No. of Repeat Samples (n)	3	3	3	3

Table 4.2 Parameters chosen for Mascot searches for Acrolein Modification Analysis

Setting	Parameters Chosen
Taxonomy	Mammalia
Database	SwissProt 2021_03 (565,254 sequences; 203,850,821 residues)
Fixed Modifications	None
Variable Modifications	Carbamidomethyl (C), Oxidation (M), Acrolein Michael addition (reduced) (C, K & H) and Acrolein Schiff base (reduced) (K)
Enzyme	Trypsin or Chymotrypsin or Trypsin/Glu-C
Maximum Missed Cleavages	Enzyme Dependent (See Table 4.1)
Peptide Charge	+2, +3, +4
Peptide Tolerance	± 0.5 Da
MS/MS Ions Search	✓
Data Format	Mascot generic
MS/MS Tolerance	± 0.5 Da

4.2.4 Incubation of PTEN-V5-His at 37°C with and without DTT

To visualise the effect of incubation at 37°C, PTEN-V5-His was prepared in reaction buffer, as described in Section 4.2.2, before incubation with and without 10 mM DTT for 0-4 hours. Four reaction tubes were set up with 50 µg of PTEN-V5-His at a concentration 1 mg/ml in reaction buffer (25 mM NaPO₄ pH 7.4 with 150 mM NaCl) with and without 10 mM DTT. At 0 minutes and after 10 minutes, 1 hour and 4 hours, the samples were cooled for 10 minutes to RT before alkylating with 15 mM iodoacetamide (IAM) for 30 minutes at RT in the dark to preserve the profile of oxidation by blocking any unoxidised cysteine residues from oxidation. The samples were prepared in reducing and non-reducing SDS-PAGE loading dye and analysed using an 8% polyacrylamide gel as in Section 2.3.3.

4.2.5 Statistical Analysis

Data from three experimental replicates with three or more variables was analysed using GraphPad Prism 8.0 to perform one-way ANOVA analysis, correcting for multiple comparisons using the Tukey test. Statistical significance was defined as $P < 0.05$. Data from three experimental replicates with two variables was analysed using GraphPad Prism 8.0 to perform an unpaired T-test. The P value style was as follows: 0.1234 (ns), 0.0332 (*), 0.0021 (**), 0.0002 (***), <0.0001 (****). Raw data is shown as mean values ± SEM.

4.3 Results

4.3.1 The OMFP Phosphatase Activity of Purified PTEN-V5-His Decreases with Decreasing DTT Concentration

To investigate the effect of DTT on the phosphatase activity of PTEN-V5-His, the OMFP phosphatase activity of PTEN-V5-His was assayed with increasing concentrations of DTT. The specific activity of PTEN-V5-His was assayed using the OMFP activity assay with a 10-minute pre-incubation in the presence of 0, 1 and 10 mM DTT prior to the addition of OMFP. The lowest OMFP phosphatase activity was found in the absence of DTT, with increasing activity in the presence of 1 and 10 mM DTT (Figure 4.1). Ordinary one-way ANOVA analysis found significant differences between 0 and 1 mM DTT (*), 1 and 10 mM DTT (**), and 0 and 10 mM DTT (***). The phosphatase activity of PTEN-V5-His buffer-exchanged into a buffer without DTT but subjected to a 10-minute pre-incubation with 10 mM DTT was 0.7 nmoles OMF/min/mg (Figure 4.1). This phosphatase activity is lower than the phosphatase activity of PTEN-V5-His that was maintained in the presence of 10 mM DTT, of 1.3 nmoles OMF/min/mg (Figure 3.9).

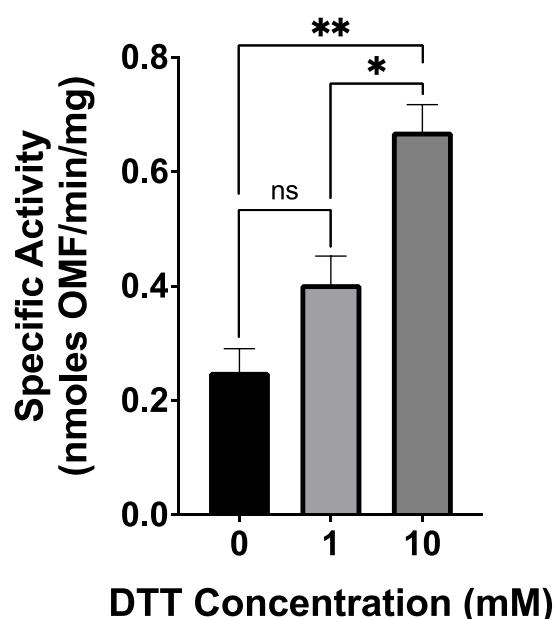


Figure 4.1 Effect of DTT on the OMFP phosphatase activity of PTEN-V5-His.

The OMFP activity assay was performed with PTEN-V5-His in the presence of 0, 1 and 10 mM DTT (n=3; Mean \pm SEM). Statistical significance was assessed by one-way ANOVA with the Geisser-Greenhouse correction, correcting for multiple comparisons using the Tukey test (p=0.1234 (ns), 0.0332 (*), 0.0021 (**), 0.0002 (***), <0.0001 (****)).

4.3.2 Sodium Borohydride Reduction Does Not Affect the OMFP Phosphatase Activity of PTEN-V5-His

Figure 4.1 demonstrated the requirement of a reducing environment for the phosphatase activity of PTEN, provided by the addition of DTT during the OMFP enzyme assay. Due to the risk of acrolein reacting with the thiol groups of DTT to form acrolein-DTT adducts, the treatment of PTEN-V5-His with acrolein was conducted in the absence of DTT and the modifications were stabilised with NaBH₄ before exposure to DTT. Although NaBH₄ shows selectivity for aldehydes and ketones, to ensure that reduction of PTEN-V5-His with NaBH₄ did not affect phosphatase activity reduced and non-reduced PTEN-V5-His was assayed for phosphatase activity using the OMFP assay (Figure 4.2) (Smith, 2017). It was important to eliminate the risk of misattribution of differences in the phosphatase activity of PTEN-V5-His to modification(s) by acrolein rather than the subsequent NaBH₄ reduction.

After reduction with NaBH₄ prepared in 0.2% NaOH, PTEN-V5-His showed no OMFP phosphatase activity (data not shown). The pH of the reaction was tested, with final concentrations of 0.85 mg/ml PTEN-V5-His, 5 mM NaBH₄ and 0.01% NaOH, using universal pH test paper. The NaBH₄ reduced PTEN-V5-His was shown to be pH 10-11, with the non-reduced PTEN-V5-His showing a pH of 7-8 (data not shown). When PTEN-V5-His was reduced with NaBH₄ prepared in OMFP reaction buffer, there was no significant difference in enzyme activity of non-reduced PTEN-V5-His (Figure 4.2)

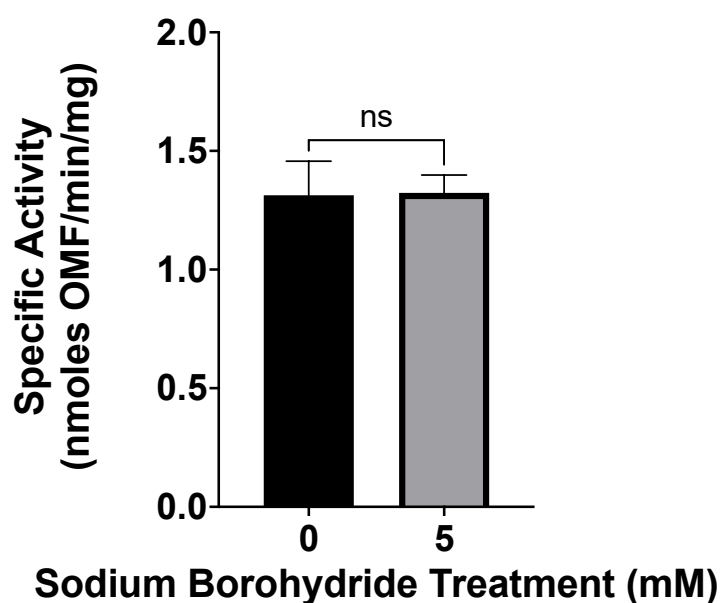


Figure 4.2 Effect of NaBH₄ reduction on the OMFP phosphatase activity of PTEN-V5-His.

The OMFP activity assay was performed with PTEN-V5-His with and without prior reduction with 5 mM NaBH₄ for 30 minutes at RT (N=3; Mean ± SEM). Statistical significance was assessed by unpaired T-test (p=0.1234 (ns), 0.0332 (*), 0.0021 (**), 0.0002 (***), <0.0001 (****)).

4.3.3 The Time-Independent Inactivation of PTEN's Phosphatase Activity by Acrolein after 10 minutes

PTEN-V5-His was treated with increasing concentrations of acrolein at a ratio of 0.2:1 (10 μ M), 1:1 (50 μ M), 2:1 (0.1 mM), 4:1 (0.2 mM), 10 :1 (0.5 mM) and 20:1 (1 mM), for 10 minutes, 1 hour and 4 hours at 37°C. Treatment with acrolein gave a decrease in specific phosphatase activity and percentage activity when compared to the untreated control, indicating inactivation of PTEN-V5-His' phosphatase activity by acrolein (Figure 4.3). Figure 4.3A shows a decrease in specific activity (nmoles OMF/min/mg) of PTEN-V5-His at each treatment concentration for each time point. In the absence of acrolein, the specific activity of PTEN-V5-His decreased with increasing incubation time. Whilst there was no significant difference between the specific activities of the 10-minute and 1-hour controls, there were significant differences between the 10-minute and 4-hour controls (**) and the 1-hour and 4-hour controls (*). This loss of activity in the absence of acrolein suggests that when PTEN is not maintained in a reducing environment it is being oxidised over time, causing a loss of phosphatase activity. Statistical significance between the specific activities of the time points is lost as the concentrations of acrolein increase, due at least in part to the large error bars and reduction of phosphatase activity (Figure 4.3A). Despite this, a trend of decreasing specific activity from the 10-minute to the 4-hour time point is clearly seen at most acrolein concentrations (Figure 4.3A). To observe the effect of acrolein on PTEN-V5-His' phosphatase activity, the data from each time point was normalised to the untreated control, set at 100%. There was no significant difference between the percentage activities of each incubation time for any acrolein treatment concentration (Figure 4.3B). On normalisation of the data, there was also a reduction in the size of the error bars indicating that whilst the specific activities varied between different treatment experiments, the degree of acrolein inhibition was consistent. Taken together, Figure 4.3 demonstrates a time-independent inhibition of the phosphatase activity of PTEN-V5-His by acrolein for time points longer than 10 minutes.

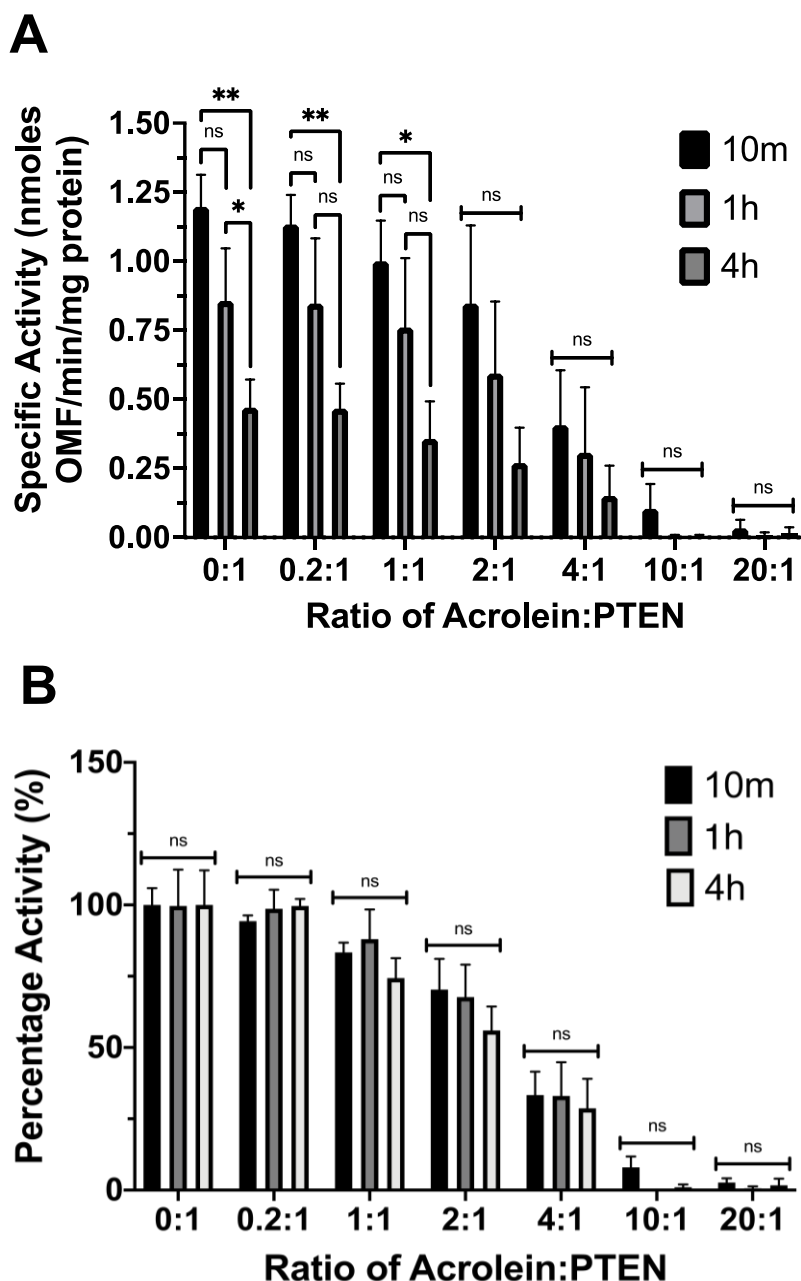


Figure 4.3 OMFP Phosphatase Activity Analysis of PTEN-V5-His Treated with Increasing Acrolein Concentrations for 10 minutes, 1 hour and 4 hours.

A) The rate of conversion of OMFP to OMF by PTEN-V5-His treated for 10 minutes, 1 hour and 4 hours with increasing concentrations of acrolein was monitored by the increase in fluorescence. The specific activity was calculated from a standard curve and expressed as nmoles OMF converted per minute per mg of PTEN-V5-His (nmoles OMF/min/mg protein) (N=3, Mean \pm SEM). B) The specific activity of PTEN-V5-His treated for 10 minutes, 1 hour and 4 hours with increasing concentrations of acrolein was expressed as a percentage of the specific activity of the control untreated PTEN-V5-His for each time point (N=3, Mean \pm SEM).

4.3.4 The Dose-Dependent Inactivation of PTEN's Phosphatase Activity by Acrolein

As described in section 4.3.3, PTEN-V5-His was treated with increasing concentrations of acrolein for 10 minutes at 37°C at a 0.2:1 (10 μ M), 1:1 (50 μ M), 2:1 (0.1 mM), 4:1 (0.2 mM), 10 :1 (0.5 mM) and 20:1 (1 mM). Further statistical analysis was performed on the percentage activities of PTEN-V5-His treated with acrolein for 10 minutes, first described in section 4.3.3,

to identify any concentration-dependent inhibition of PTEN-V5-His by acrolein. At each treatment concentration there was a decrease in percentage activity, however there wasn't a statistically significance reduction in percentage activity until 2:1 acrolein:PTEN ratio (Figure 4.4).

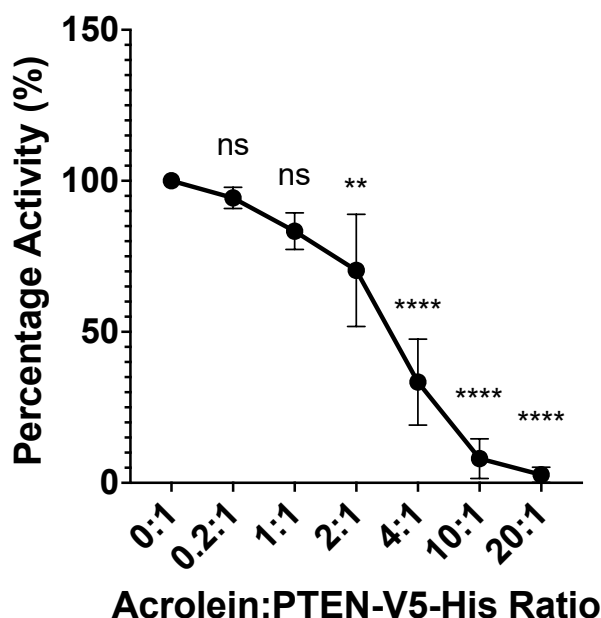


Figure 4.4 OMFP Phosphatase Activity Analysis of PTEN-V5-His Treated with Increasing Acrolein Concentrations for 10 minutes.

The rate of conversion of OMFP to OMF by PTEN-V5-His treated for 10 minutes with increasing concentrations of acrolein was monitored by the increase in fluorescence and the specific activity was calculated and expressed in nmoles OMF/min/mg. The specific activity at each concentration was calculated as a percentage of the specific activity of the control, untreated PTEN-V5-His (N=3; Mean \pm SEM). Statistical significance was assessed by one-way ANOVA with the Geisser-Greenhouse correction, correcting for multiple comparisons using the Tukey test ($p=0.1234$ (ns), 0.0332 (*), 0.0021 (**), 0.0002 (***), <0.0001 (****)).

4.3.5 The Cross-linking Effect of Acrolein on PTEN-V5-His

To determine whether acrolein caused cross-linking of PTEN, acrolein-treated and NaBH₄-reduced PTEN was visualised using reducing SDS-PAGE (Figure 4.5A-C). For each time point, densitometry analysis showed a loss of monomeric PTEN-V5-His, at approximately 60 kDa, as the treatment concentration of acrolein increased (Figure 4.5D). This correlated with the appearance of an additional lower molecular weight band between 55 kDa and 60 kDa and aggregated protein above and below the stacking gel (Figure 4.5A-C). As the incubation time increases, the concentration at which higher molecular weight aggregates appeared decreased from a 4:1 treatment ratio for the 10-minute treatment (Figure 4.5A) to a 1:1 and 0.2:1 treatment ratio for the 1-hour (Figure 4.5B) and 4-hour treatments (Figure 4.5C), respectively. Comparison of the percentage activity data (Figure 4.5B) and the percentage of intact PTEN-V5-His data (Figure 4.5D) using unpaired t-tests showed no significant differences at any acrolein treatment concentration for the 10-minute treatment, and this was

the same for the 1-hour and 4-hour treatment times (data not shown). This shows that there is a concurrent and proportional loss of monomeric PTEN-V5-His with the loss of phosphatase activity. In addition, where PTEN-V5-His is subjected to longer incubation times at 37°C in the absence of a reducing agent, the propensity of PTEN-V5-His to aggregate increases, possibly due to oxidation.

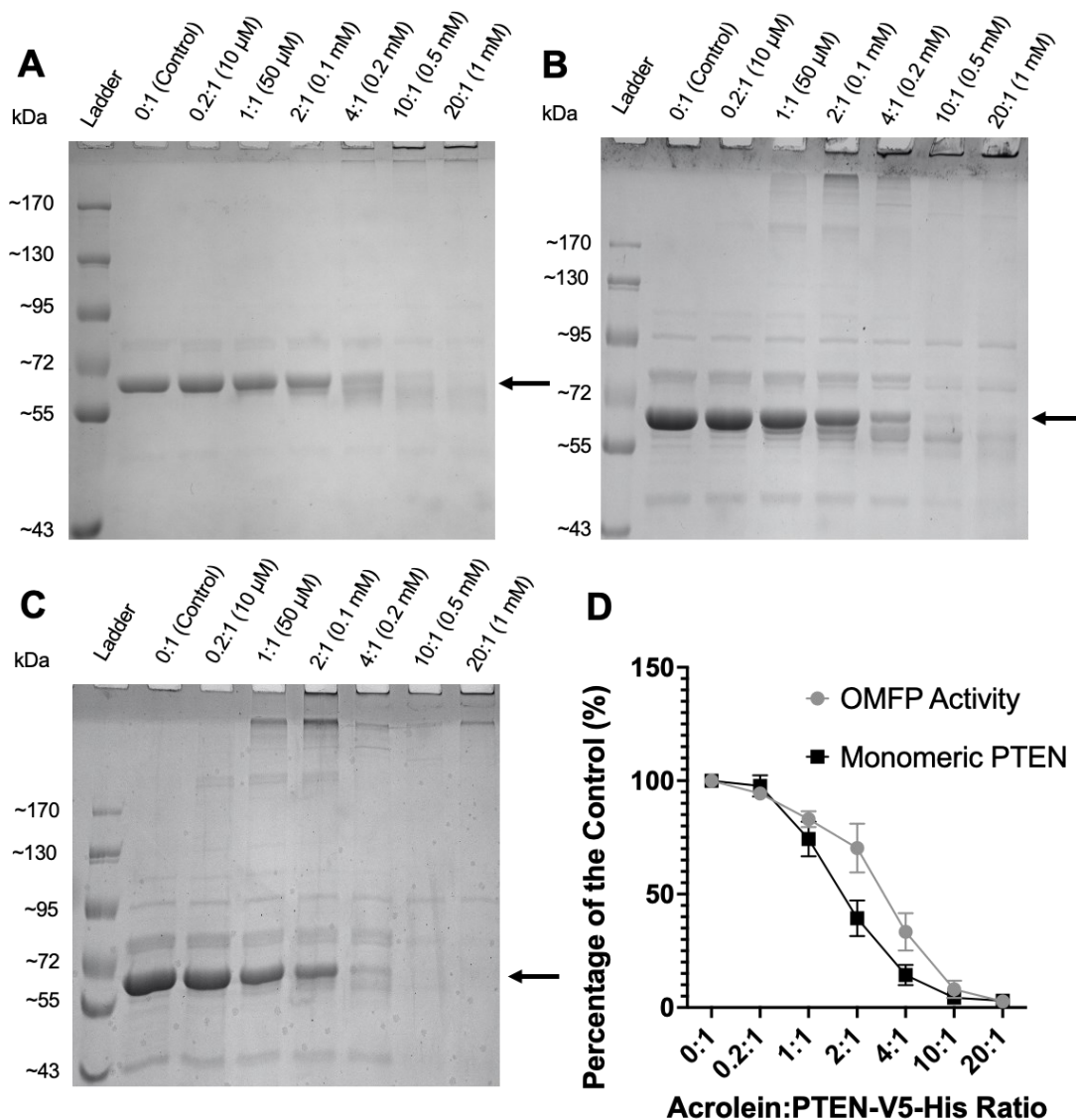


Figure 4.5 SDS-PAGE and Densitometry Analysis of PTEN-V5-His Treated with Increasing Acrolein Concentrations for 10 minutes, 1 hour and 4 hours.

PTEN-V5-His was treated with increasing concentrations of acrolein and incubated at 37°C for 10 minutes (A), 1 hour (B) and 4 hours (C) before adduct stabilisation with 5 mM NaBH₄ for 30 minutes at RT. The samples were prepared in reducing loading dye and 5 µg was analysed using an 8% polyacrylamide gel stained with Coomassie blue. Monomeric PTEN-V5-His, seen as a 60kDa band, is indicated by the black arrow. (D) The stained gel was imaged using a GBox and each treatment lane was analysed using ImageJ with the background adjusted for a light background and 50 pixels. The peak corresponding to monomeric PTEN-V5-His band (appearing at approximately 60 kDa) for each treatment lane as expressed as a percentage of the control intact band and plotted against each treatment ratio with the percentage activity for the 10-minute time point.

4.3.6 Incubation of PTEN-V5-His in the Absence of DTT Results in Oxidation and Cross-linking

The reduction in specific activity of PTEN-V5-His with increasing incubation time in the absence of acrolein treatment, as shown in Figure 4.3A, suggests another mechanism of inactivation. As the acrolein treatments of PTEN-V5-His were conducted in the absence of DTT to avoid any potential interference from the DTT's thiol groups, this could allow the PTEN-V5-His to become oxidised over the course of the treatment. SDS-PAGE has been previously used to observe oxidative modification of PTEN, due to the accompanied conformational change that occurs on disulfide bond formation between Cys71 and Cys124, as discussed in section 1.2.6, that causes the oxidised PTEN (oxPTEN) to migrate faster and appear as a slightly lower molecular weight band (Lee et al., 2002). As such, to identify whether oxidative modification was responsible for PTEN's loss of activity in the absence of acrolein (Figure 4.3), PTEN-V5-His was incubated with and without 10 mM DTT and analysed by reducing and non-reducing SDS-PAGE (Figure 4.6). PTEN-V5-His that was incubated in the absence of DTT but subsequently reduced with reducing SDS-PAGE loading dye showed no difference to the PTEN-V5-His incubated in the presence of DTT, with regards to the electrophoretic profile (Figure 4.6A). However, when the same samples were analysed under non-reducing conditions, higher molecular weight bands corresponding to aggregation or cross-linking appeared in the samples incubated for 1 hour and 4 hours without DTT (Figure 4.6A). Where PTEN-V5-His was incubated in the presence of DTT and SDS-PAGE analysis was conducted under non-reducing conditions there was also no higher molecular weight bands at any time points (Figure 4.6B). As there is no cross-linking in the presence of DTT and the cross-linking that occurred in the absence of DTT was reversed by the β -mercaptoethanol in the reducing loading dye, this indicates that the cross-linking of PTEN in the absence of acrolein is due to oxidative modification that occurs over the course of the treatment. This evidence of oxidative modification supports the hypothesis that the loss of activity of untreated PTEN-V5-His after incubation for 1 and 4 hours in the absence of DTT was due to oxidation.

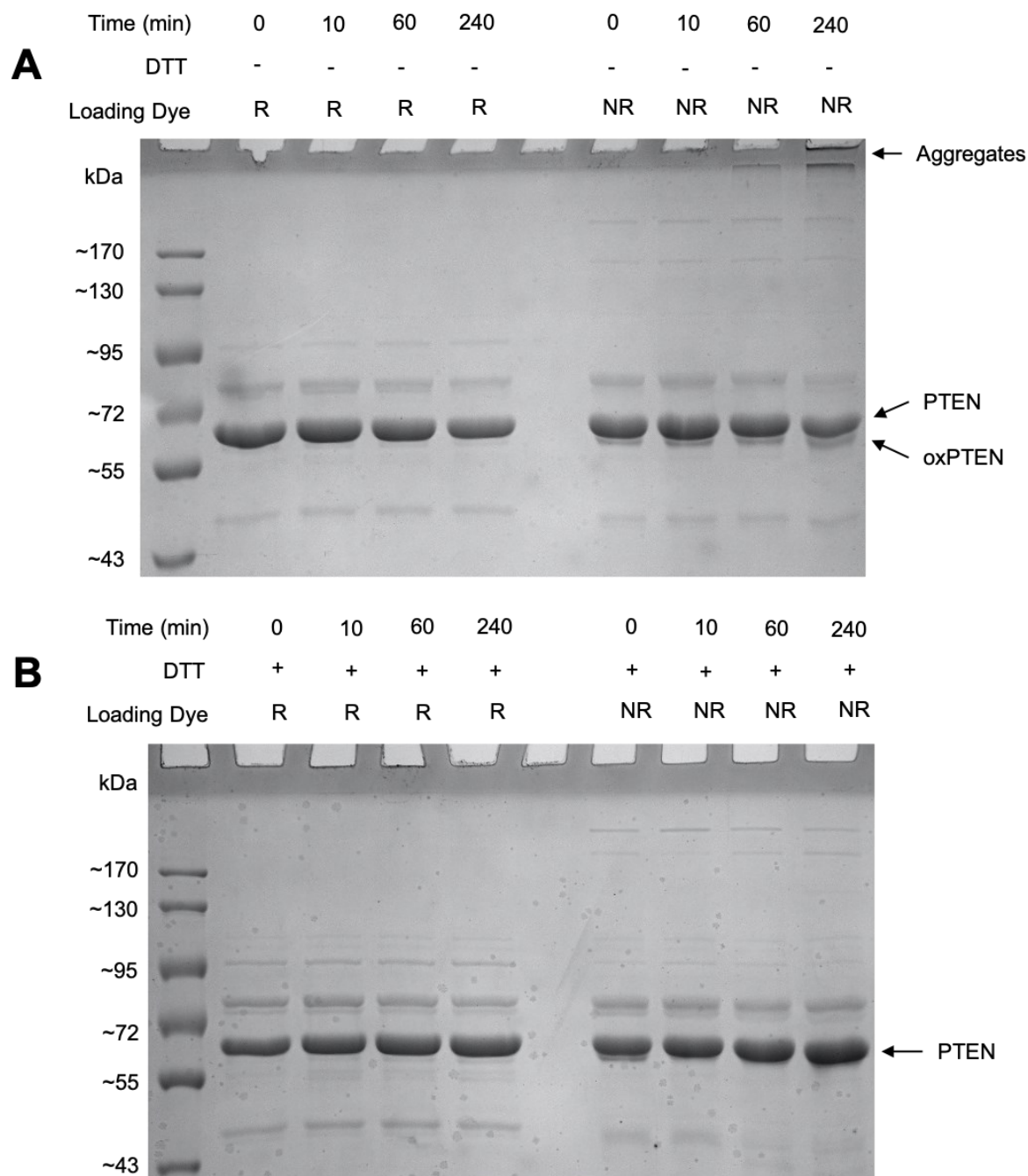


Figure 4.6 SDS-PAGE Analysis of the Effect of Incubation with and without DTT at 37°C on PTEN-V5-His. PTEN-V5-His was buffer exchanged into the reaction buffer without (A) and with (B) 10 mM DTT and incubated at 37°C before alkylation with IAM. The samples were prepared in reducing (R) and non-reducing (NR) loading dye, and 5 µg was analysed using an 8% polyacrylamide gel stained with Coomassie blue.

4.3.7 PTEN's Cysteine and Lysine Residues are the Most Susceptible to Acrolein Modification

LC-MS/MS was used to map modifications sites in PTEN-V5-His treated for 10 minutes with increasing acrolein concentrations for both the monomeric PTEN band, at approximately 60 kDa, and the aggregated PTEN bands at the top and the bottom of the stacking gel, which were analysed together (Figure 4.5A). By monitoring the appearance of modification sites as

the treatment concentration of acrolein increased, it would reveal those residues with the highest susceptibility to modification. In addition, comparison of the modifications present in the aggregated PTEN band to those present in the monomeric band may allow identification of residues that play a role in maintaining the active conformation of PTEN.

Table 4.3 shows the modifications present for each of the treatment concentrations of acrolein, and whether the modification was found in the monomeric or aggregated PTEN fraction. As the treatment concentration of acrolein increases, and therefore the ratio of acrolein:PTEN, the number of acrolein modifications also increases (Table 4.3). As expected, no true positive modifications to acrolein were found in the untreated control. However the Mascot search identified a false positive modification to Cys71, which is discussed further in section 4.3.8. The first modification site identified was an acrolein Michael addition to the resolving cysteine (Cys71), with acrolein Michael addition identified in the monomeric PTEN fraction at the lowest treatment concentration. Modification to Cys250 was detected in the monomeric band for ratios of acrolein:PTEN >1:1. At the highest ratios of acrolein:PTEN, 10:1 and 20:1, lysine modifications were found in both the monomeric and the aggregate PTEN fractions. With regard to localisation of the modification sites, there are modifications across the structure of PTEN, from the N- to the C-terminus at low and high treatment concentrations, indicating that both the phosphatase and membrane-binding domains of PTEN are susceptible to modification. Modification of the catalytic cysteine was identified during the Mascot search; however, due to the limitations of the analysis of these peptide hits due to the poor coverage of this region of PTEN when using trypsin as a protease, as discussed in section 4.3.8 and 4.3.9, it was not possible to validate this modified peptide.

Table 4.3 LC-MS/MS Identification of Acrolein Modifications of PTEN-V5-His after In-gel Digestion with Trypsin

Modified Residue [@]	Modified Peptide [£]	Intact PTEN Band						Aggregated PTEN			
		0:1	0.2:1	1:1	2:1	4:1	10:1	20:1	4:1	10:1	20:1
K6	M.TAI K EIVSR.N						✓	✓		✓	✓
C71	K.IYNL C AER.H		✓	✓	✓	✓	✓	✓	✓	✓	✓
C136	K.GRTGVM C AYLLHR.G									✓	✓
	R.TGVM C AYLLHR.G									✓	✓
K147	K.FL K AQEALDFYGRVR.T									✓	✓
K223	K.V K IYSSNSGPTR.R						✓	✓		✓	✓
C250	K.FMYFEFPQPLP V CGDIK.V			✓	✓	✓	✓	✓	✓	✓	✓
K313	R.ADND K EYLVLT L TK.N						✓	✓	✓	✓	✓

Key:

[@]: Modified amino acid residue identified by Mascot

[£]: Corresponding peptide containing the modified amino acid, with the modified residue in bold

✓: Modified Cysteine (C) residue

✓: Modified Lysine (K) residue

4.3.8 Cysteine and Lysine Residues across PTEN's Structure are Susceptible to Acrolein Modification

Manual verification of putative software-identified modifications is essential. For example, whilst verifying the acrolein-modified peptides identified in the Mascot search by de novo sequencing, several false positive modified peptide hits were identified. One relevant example is the false positive acrolein-modified peptide for Cys71 present in the untreated control PTEN monomeric band. Figure 4.7A shows the representative Mascot output for the identification for the unmodified Cys71 peptide, which shows 100% y ion coverage assigned to the most intense peaks. The high intensity of the assigned peaks increases the confidence that the peptide sequencing is correct. Figure 4.7B shows the data from an acrolein-modified peptide hit from the untreated control and this peptide identified by Mascot is a false positive hit for a Cys71 acrolein Michael addition modification. When Mascot selected the peaks (shown in red) for sequencing, an isotopic peak was selected for Cys71 (y(4)), which was carried forward to the subsequent y ions (5-7) for Leu72, Asp73 and Tyr74 (Figure 4.7B). This falsely attributed a mass difference of +161.051 between Cys71 (y(4)) ion and the preceding Ala70 (y(3)) ion and this equates to the theoretical mass difference of an acrolein Michael addition modification to the cysteine. During de novo sequencing, when selecting the monoisotopic peak for Cys71 (y(4)), the mass difference was +160.031 which equates to carbamidomethylation of cysteine. Carbamidomethylation would be the expected cysteine modification in the untreated sample due to the reduction and alkylation steps of the in-gel digestion. Figure 4.7C shows a representative example of a true positive Michael addition to Cys71, where monoisotopic peaks were picked for all y ions, after treatment with acrolein with a mass difference of +161.051 between Ala70 and Cys71.

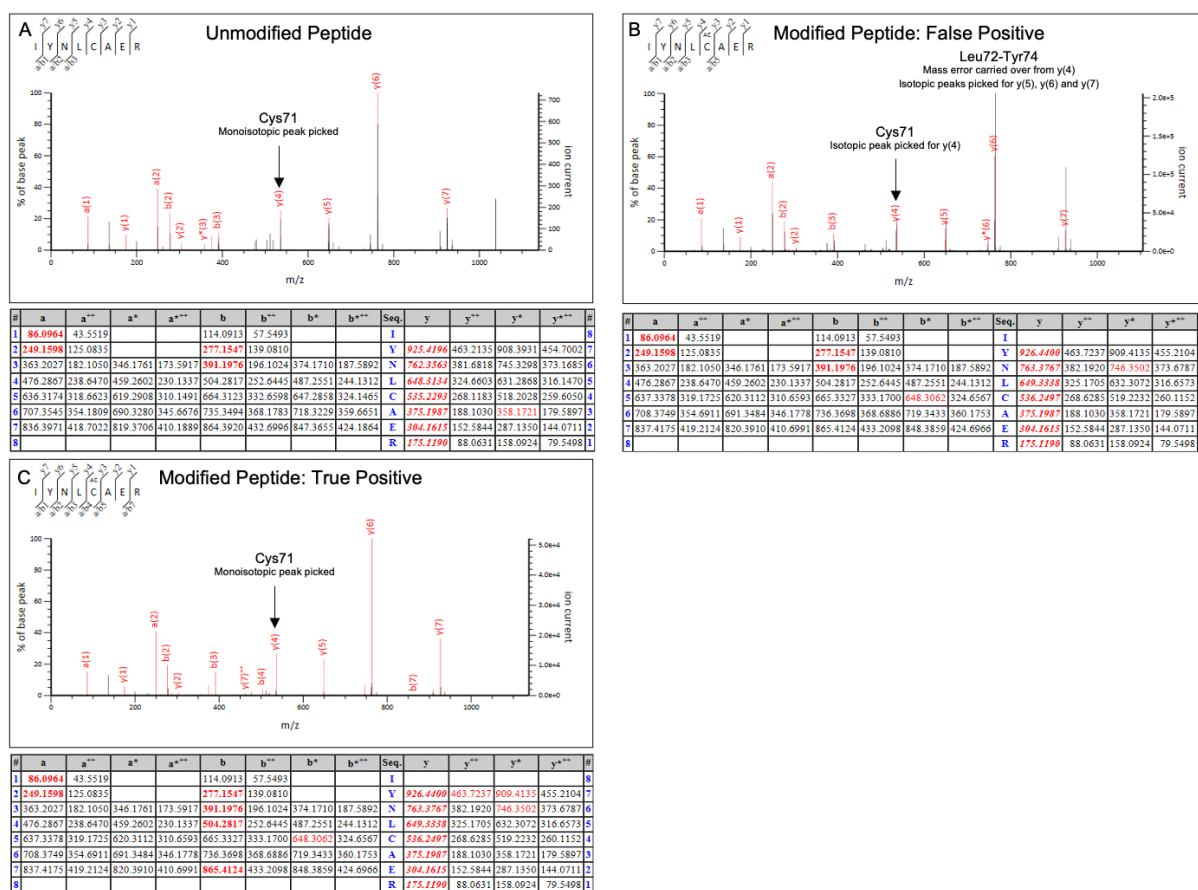


Figure 4.7 Representative Mascot Peptide Output for an Unmodified and a True and False Positive Hit for Acrolein-modified Cys71.

A Mascot search for acrolein Michael addition of PTEN-V5-His identified unmodified and modified Cys71 in the amino acid peptide 67-74, IYNLCAER. For the unmodified peptide (A) and the false (B) and true (C) positive acrolein-modified peptide hits, the upper pane shows the experimental raw data, with the picked peaks highlighted in red, and the lower table shows the Mascot matched ion coverage, where red numbers represent a match.

A Mascot search for acrolein Michael addition of acrolein-treated PTEN-V5-His identified unmodified and modified residue Cys124 in the amino acid peptide for 85-125, VAQYPFEDHNPPQLELIKPFCELDLQWLSEDDNHVAAIHCK. Whilst the peptide hits for the unmodified and acrolein-modified Cys71 residue could be confidently categorised as a false or true positive hit, the Cys124 could not be validated. Trypsin does not cleave where a lysine is followed by a proline, as per the Keil rule, meaning that there was no cleavage between Lys102/Pro103 resulting in a very large peptide. This conveys a disadvantage for MS/MS analysis, where the selection parameters would require this peptide to be highly charged in order to fall into the parameters set during data acquisition with an m/z range of 350-1250. Figure 4.8A shows that for the unmodified Cys124 peptide there was 100% y ion coverage between y(2)-y(19) but no y ion coverage between y(18)-y(40). There was some b ion coverage for these missing y ions, between b2-29. For the modified peptide hit shown in Figure 4.8C there is good sequence coverage for y ions 2-17 and b ions 13-29. Taking together the y ion and b ion coverage for both the identified unmodified and acrolein-modified peptides, it

is likely that the Cys124 peptide is present in the sample but it is not possible from these spectra to differentiate between carbamidomethylation or an acrolein Michael addition of Cys124. In order to validate the mass of Cys124, the preceding y(1) for Lys123 needs to be present to calculate the mass difference and the y(1) ion was not present in either the modified or unmodified peptide. Data cannot be confidently verified or differentiated from the unmodified peptide so the modified peptide hits so from this data as to whether Cys124 is modified by acrolein is inconclusive.

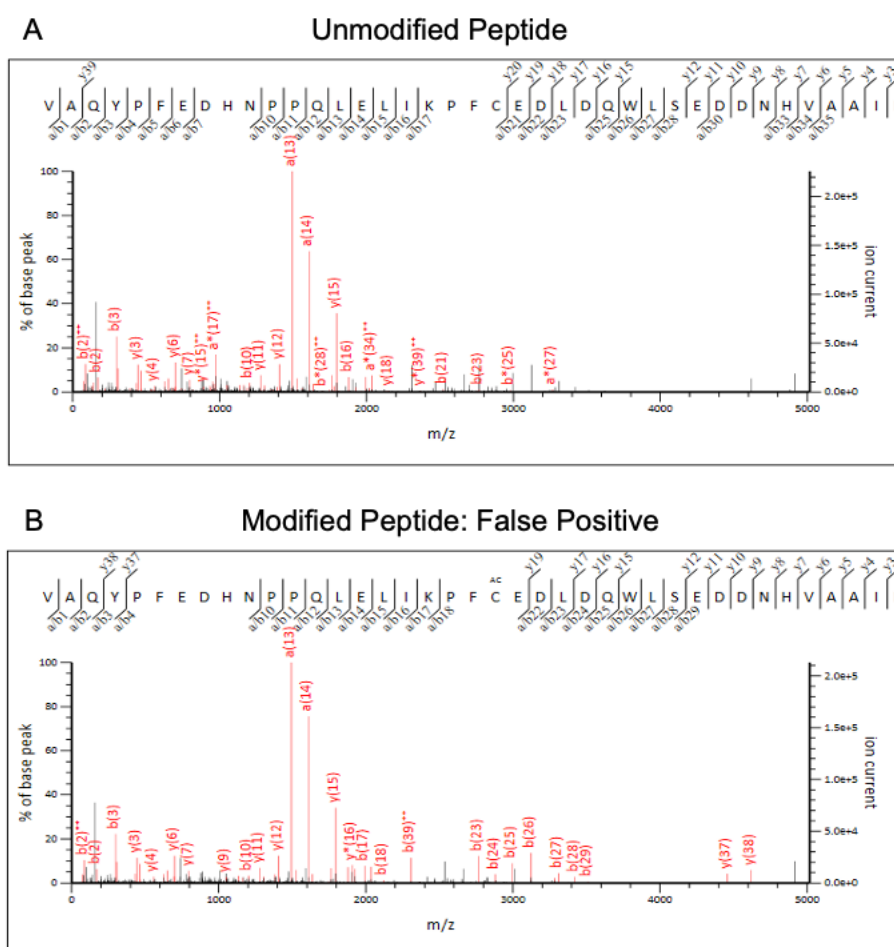


Figure 4.8 Representative Mascot Peptide Sequencing of Unmodified and Acrolein-modified Hit for the Cys124 Peptide.

Lysine residues can be modified by acrolein but are also a cleavage site for trypsin, conveying a disadvantage when using trypsin in the LC-MS/MS workflow for the identification of acrolein modifications. The specificity of trypsin means that where there is a modification at a cleavage site there will be a miss-cleave. This means that a Mascot hit for an acrolein-modified lysine residue where the lysine modification is identified at the terminus of the peptide, it is likely a false positive hit. This is demonstrated by Figure 4.9 which shows the unmodified peptide peak for Lys164 (A) and the corresponding acrolein-modified peptide (B). The Lys164 ion (b(1)) is assigned in Figure 4.9A but is missing in Figure 4.9B. As this is the b(1) ion, the corresponding

y ion is not in Mascot’s peak assignment which means that it is not possible to verify the b ion series using the y ion coverage. In addition, the b ion peaks for the modified peptide are assigned to low intensity peaks in the noise (Figure 4.9B), whereas the unmodified peptide peaks are much higher in intensity, giving further evidence to this hit being false positive (Figure 4.9A). Modified lysine residues were often identified as part of a peptide where that lysine was a missed cleavage, such as the peptide hit for Lys6 (Figure 4.9C). As the modified residue was a missed cleavage, de novo sequencing to validate the modification was easier as the lysine residue was in the middle of the sequence and often well covered by the y ion series. However, the lack of an unmodified peptide makes it difficult to quantify the susceptibility of the modification by comparison of a loss of unmodified peptide with the appearance and increase in the modified peptide hits. Whilst it was possible to validate the Lys6 modification example as shown in Figure 4.9C, it was not possible to validate the Lys164 hit.

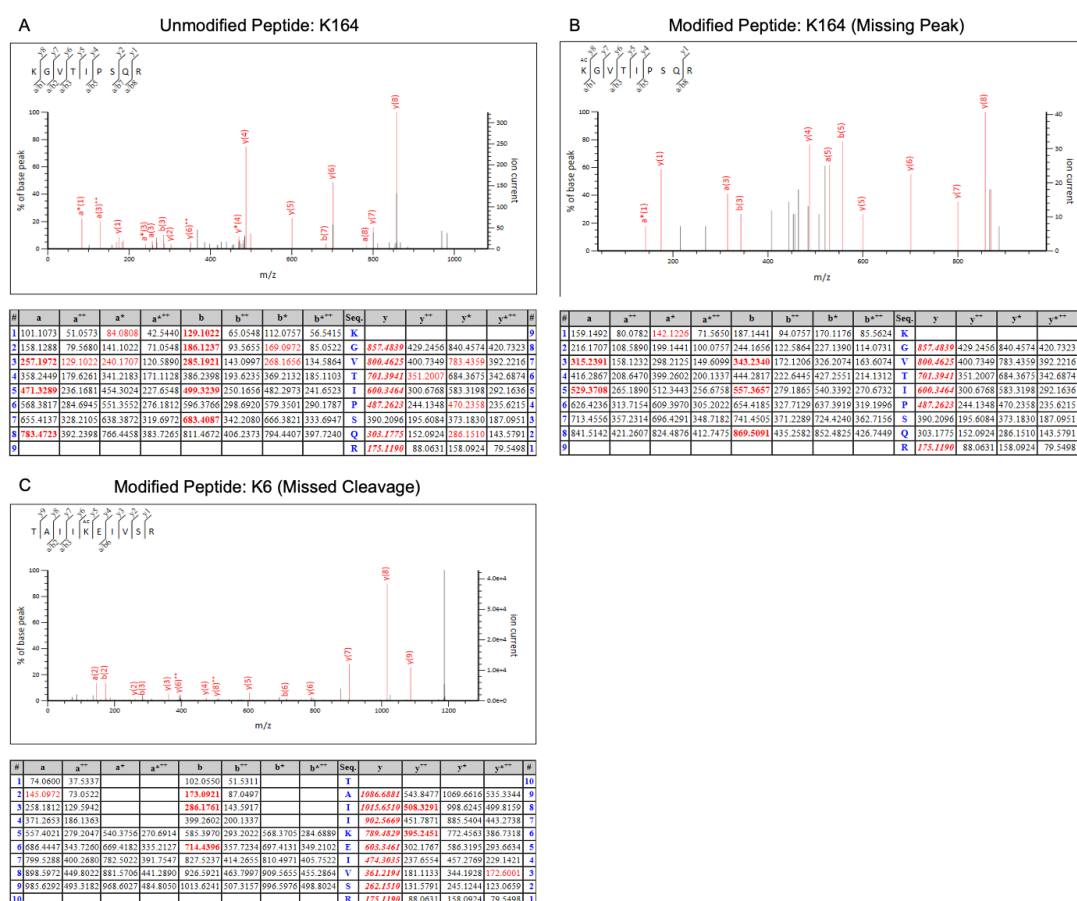


Figure 4.9 Representative Mascot Peptide Identification of Unmodified and a False Positive Hit for an Acrolein-modified Lysine Residue (Lys164) and a True Positive Hit for an Acrolein-modified Lysine Residue (Lys6).

A Mascot search for acrolein Michael addition of treated PTEN-V5-His identified potential lysine modifications, for which there is a representative experimental data and a peak assignment table for the peptide hits. The search identified unmodified and modified residues for Lys164 in the amino acid peptide 164-172, KGVTIPSPQR, and a modified residue Lys6 in the amino acid peptide 2-11, TAI|KEIVSR. Results for Lys164 identified both the unmodified

(A) and modified false positive (B), where there is a missed peak for the modified Lys164 (y(1)). Results for Lys6 identified only a modified peptide (C), resulting from a missed cleavage (y(5)).

4.3.9 Increasing the Sequence Coverage of Potential Modification Sites using Alternative Proteases

In-gel digestion of PTEN-V5-His with trypsin gave a high sequence coverage and confident identification of 7 acrolein modifications, as described in section 4.3.8. However, the sequence coverage of the catalytic cysteine is poor due to the length of the peptide (Figure 4.8) and often potential lysine modifications were identified in missed cleavage peptides or were unable to be unequivocally validated by de-novo sequencing due poor b ion coverage (Figure 4.9). To address these limitations, alternative proteases were trialled to digest PTEN-V5-His as an in-solution or an in-gel digestion, as outlined in Table 4.4. The coverage of the catalytic cysteine was important to this project to permit identification and, if present, quantification of the modified peptide as the treatment concentration of acrolein increased. To target this, in solution digestion with a combination of proteases with trypsin was tested. To improve the coverage of lysine residues, and make validation of the modification easier, an in-gel digestion with chymotrypsin was also trialled. Whilst none of the alternative digestions resulted in an improvement in sequence coverage over trypsin (Table 4.4), there were differences in the resultant peptides (Supplementary Table 1). Chymotrypsin resulted in the highest number of different peptides (Table 4.4) but due to the significantly higher missed cleavage rate, the sequence coverage remains the same as a lot of the peptides covered the same area but in a variety of peptide lengths (Supplementary Table 1). The missed cleavage rate of chymotrypsin is higher in comparison to the other proteases, which is likely due at least in part to the higher number of cleavage sites, where chymotrypsin is an endoproteinase and so as such will not cleave where the cleavage site is at the terminus of a peptide, and the effect of neighbouring residues on chymotrypsin's cleavage (Keil, 1992).

Lys-C was chosen as candidate for a double digestion with trypsin as whilst it also cleaves at Lys and Arg residues, unlike trypsin, Lys-C does not follow the Keil rule and so also cleaves where Lys is followed by Pro (Keil, 1992). The use of Lys-C in combination with trypsin was trialled to promote cleavage at the missed KP site, discussed in section 4.3.8, and shorten the length of the peptide for the catalytic cysteine from 41 residues (VAQYPFEDHNPPQLELIKPFCELDQWLSEDDNHVAAIHCK) to 23 residues (PFCELDQWLSEDDNHVAAIHCK). However, Mascot analysis of PTEN-V5-His digested with trypsin and Lys-C showed inefficient cleavage at the KP sites, with only one target peptide hit identified (Table 4.5). Glu-C is another protease that is benefits from being used with trypsin, due to the longer average length of the resultant peptides, and can cleave at Glu or

Glu and Asp depending on the digestion buffer used (Giansanti et al., 2016). To prevent over-digestion of PTEN, the digestion with trypsin and Glu-C was performed in ammonium bicarbonate buffer which promotes cleavage at Glu residues (Drapeau, 1977, Giansanti et al., 2016). Mascot analysis of the resultant peptides identified two similar peptides covering the catalytic cysteine, with 3 duplicates of the longer peptide (Table 4.5). Table 4.5 shows that double digestion of PTEN-V5-His with trypsin and Glu-C results in the best coverage of the catalytic cysteine, with the target peptide detected multiple times, increasing the reliability of the data and giving full coverage of the catalytic cysteine. Although double digestion with trypsin and Lys-C did have coverage of the catalytic cysteine, with two peptides detected, there were no duplicates, and the preceding lysine peak was not assigned or detectable meaning determining the actual mass difference between the lysine and the cysteine is not possible during de novo sequencing (Table 4.5). Taken together, orthogonal in solution digestion with both trypsin and Glu-C successfully covered the catalytic cysteine in a peptide of optimal length for MS analysis, and so was taken forward for digestion of acrolein-treated PTEN-V5-His.

Table 4.4 Mascot Analysis of PTEN-V5-His Digested with Alternative Proteases

Protease(s)	Digestion	Cleavage Sites	Aim	Sequence Coverage	Protein Sequences	Average No. of Missed Cleavages	Average Peptide Length
Trypsin	Gel	K/R, not KP	Protein Identification and acrolein modification identification	83	28	0	16
Trypsin/Lys-C	Solution	K/R, inc. KP	C124 Coverage	75	24	0	17
Trypsin/Glu-C	Solution	K/R and E/Z	C124 Coverage	61	29	1	15
Chymotrypsin	Gel	F/Y/W/L	Lysine Residue Coverage	69	48	2	19

Table 4.5 Representative Catalytic Cysteine Coverage of PTEN-V5-His Digested with Alternative Proteases

Protease(s)	Cys124 Peptide Identified?	C124 Peptide	Average No. of Peptides	No. of Residues	Cys124 Residue Peak Assigned?
Trypsin	Yes	VAQYPFEDHNPPQLELIKPFCELDQWLSEDDN HVAAIHCK	1	41	No
Trypsin/Lys-C	Yes	PFCEDLDQWLSEDDNHVAAIHCK	1	23	Yes*
		VAQYPFEDHNPPQLELIKPFCELDQWLSEDDN HVAAIHCK	1	41	Yes*
Trypsin/Glu-C	Yes	DLDQWLSEDDNHVAAIHCK	1	19	Yes
		LIKPFCELDQWLSEDDNHVAAIHCK	4	26	Yes
Chymotrypsin	No	N/A	N/A	N/A	No

Key:**C:** Cys124 residue

*: The preceding lysine (y(1)) ion is not covered in either sequence meaning verification of the mass increase for the cysteine residue is not possible during de novo sequencing.

The aim of digestion of PTEN-V5-His in-gel with chymotrypsin was to increase the coverage of lysine rich regions in PTEN, whilst also addressing the limitations of using trypsin to identify lysine modifications, as discussed above. The resulting peptides identified during the Mascot search (Supplementary Table 1) show that digestion of PTEN with chymotrypsin produces peptides with lysine residues in the middle of the sequence. The overall sequence coverage is lower for PTEN digested with chymotrypsin in comparison to trypsin (Table 4.4). Theoretical digestion using PeptideMass showed that with 0 missed cleavages, PTEN digestion with trypsin and chymotrypsin could result in similar sequence coverages of 88.1% and 78.4%, respectively (Gasteiger et al., 2005, Wilkins et al., 1997). However, as discussed above it would be expected that chymotrypsin would have a higher rate of missed cleavages due to the number of cleavage sites. It's also important to note that overall sequence coverage improvement wasn't the aim and that there was a successful improvement lysine rich regions in in the C-terminal domain, where as there are many lysine residues in close proximity, cleavage by trypsin produces peptides that would be too short to be identified by mass spectrometry (Figure 4.10)

A	Trypsin	B	Chymotrypsin
1	MTAIIKEIVS RNRKRYQEDG FLDLTYIYP NIIAMGFPAE RLEGVYRNNI	1	MTAIIKEIVS RNRKRYQEDG FLDLTYIYP NIIAMGFPAE RLEGVYRNNI
51	DDVRFRLDSK HKNHYKIYNL CAERHYDTAK FNCRVAQYFF EDHNPPQLEL	51	DDVRFRLDSK HKNHYKIYNL CAERHYDTAK FNCRVAQYFF EDHNPPQLEL
101	IKPFCELDLQ WLSEDDNHVA AIHCKAGKGR TGMICAYLL HRGKFLKAQE	101	IKPFCELDLQ WLSEDDNHVA AIHCKAGKGR TGMICAYLL HRGKFLKAQE
151	ALDFYGEVRT RDKKGVITPS QRRVYVYYSY LLKNHLDYRP VALLFHRMMF	151	ALDFYGEVRT RDKKGVITPS QRRVYVYYSY LLKNHLDYRP VALLFHRMMF
201	ETIPMFSGGT CNPQFVWQQL KVKIYSSNSG PTRREDKFMV FEFPQPLPVC	201	ETIPMFSGGT CNPQFVWQQL KVKIYSSNSG PTRREDKFMV FEFPQPLPVC
251	GDIKVEFFHK QNKMLKDKM FHPWNTFFI PGPEETSEKV ENGSLCDQEI	251	GDIKVEFFHK QNKMLKDKM FHPWNTFFI PGPEETSEKV ENGSLCDQEI
301	DSICSIERAD NDKEYLVLTLL TKNDLDKANK DKANRYFSFN FVKVLYFTKI	301	DSICSIERAD NDKEYLVLTLL TKNDLDKANK DKANRYFSFN FVKVLYFTKI
351	VEEPSNPEAS SSTSVPDPVS DNEPDHYRYS DTTDSDPENE PFDEDQHTQI	351	VEEPSNPEAS SSTSVPDPVS DNEPDHYRYS DTTDSDPENE PFDEDQHTQI
401	TKV	401	TKV

Figure 4.10 Comparison of the Sequence Coverage of PTEN-V5-His Digested with Trypsin or Chymotrypsin Mascot search showing the increase in sequence coverage in the C terminal domain region where there are several lysine residues in close proximity, highlighted by the red box, when PTEN was digested with chymotrypsin (B) in comparison to trypsin (A).

4.3.10 Digestion of Acrolein-treated PTEN with Chymotrypsin Revealed Additional Lysine Modifications at High Treatment Concentrations

Digestion of acrolein-treated PTEN-V5-His with chymotrypsin revealed additional modification sites, in addition to the Cys71 and Lys147 modifications that had previously been identified as a modified residue with a tryptic digest (Table 4.3). The additional lysine modification sites were revealed due to the increase in sequence coverage of lysine rich areas, as described in section 4.3.9. As with the pattern of residue susceptibility to modification by acrolein that was identified after digestion of acrolein-treated PTEN-V5-His, the additional cysteine modification identified was found at lower treatment concentrations than the additional lysine modifications (Table 4.6). Due to the presence of several lysine residues in the peptide TLTKNDLDKANKDKANRY, it is not possible to identify on which the lysine residue there is

acrolein modification from the available data. As with the modifications identified in Table 4.3, the distribution of the modifications are across both the N- and C-termini of PTEN.

Table 4.6 LC-MS/MS Identification of Acrolein Modifications of PTEN-V5-His after In-gel Digestion with Chymotrypsin

Modified Residue [@]	Modified Peptide [£]	Intact PTEN Band						Aggregated PTEN			
		0:1	0.2:1	1:1	2:1	4:1	10:1	20:1	4:1	10:1	20:1
C71	Y.NLCAERHY.D		✓	✓	✓	✓	✓	✓	✓	✓	✓
C83*	F.NCRVAQYPF.E				✓	✓	✓	✓	✓	✓	✓
K147	L.KAEQEALDFY.G							✓	✓		
K327 / K330*	L.TLTKNDLDKANKDKANRY.F					✓	✓	✓		✓	✓
K344*	Y.FSPNFKVKLY.F									✓	✓

Key:

[@]: Modified amino acid residue identified by Mascot Daemon

[£]: Corresponding peptide containing the modified amino acid, with the modified residue in bold

✓: Modified Cysteine (C) residue

✓: Modified Lysine (K) residue

*: New modification site

4.3.11 Digestion of Acrolein-treated PTEN with Trypsin/Glu-C Found No Modification to the Catalytic Cysteine

Two additional cysteine modifications, Cys296 and Cys304, were identified during the in-solution digestion with trypsin and Glu-C. Whilst LC-MS analysis of the peptides resulting from digestion of PTEN-V5-His in-solution with trypsin/Glu-C revealed that for both the untreated and acrolein-treated PTEN the catalytic cysteine was covered, no acrolein modification at this site was found when searching with Mascot. The raw peptide data for both the untreated control and the highest acrolein treatment ratio (20:1 acrolein:PTEN) was manually searched for peptides with an expected mass of either a carbamidomethylation or an acrolein Michael addition modification at the catalytic cysteine (Table 4.7). Peptides with an observed mass of 789.3031 and 567.5635 Da were identified in the LC-MS/MS data for acrolein-treated PTEN-V5-His, but manual de novo sequencing confirmed these were not the target peptides.

Table 4.7 Results for a Search of Acrolein-modified Cys124 Peptides with Increasing Charge States in the LC-MS Data of Acrolein-treated and Untreated PTEN-V5-His digested with Trypsin/Glu-C In-solution

Peptide [£]	Modification	Expected Peptide Mass (Da)	Peptide Charge	Expected Observed Peptide Mass (Da)	Present?
E.LIKPFC ¹ EDLDQWLSEDDNHVAAIH C ² K.A	1: Carbamidomethylation 2: Carbamidomethylation	3152.2688	4+	789.0745	✓
		3153.2966	2+	1577.6556	x
	1: Carbamidomethylation 2: Acrolein Michael (reduced)	3153.2966	3+	1052.1062	x
		3153.2966	4+	789.3314	x*
E.DLDQWLSEDDNHVAAIH C K.A	Carbamidomethylation	2264.9747	4+	567.2510	✓
		2266.0025	2+	1134.0085	x
	Acrolein Michael (reduced)	2266.0025	3+	756.3414	x
		2266.0025	4+	567.5079	x*

Key:

£: The sequence of the peptide containing the modified amino acid, with the modified residue in bold

Bold: Modified Residue

C¹: Cys104C²: Cys124

*: Peptide with an observed mass of <math>\pm 0.5\text{ Da}</math> was present but de novo sequencing suggested that it was not a match to the target peptide

To confirm that the level of acrolein-modification of the acrolein-treated PTEN-V5-His used in this analysis was at a level where acrolein modifications should be observable, the extracted ion chromatograms (XICs) for peptides identified using Mascot as containing acrolein-modified cysteine residues were extracted from the LC-MS/MS data and the area under the curve was determined and compared against that for the same peptide but with carbamidomethylation of the cysteine (i.e. the unmodified peptide). The untreated control contained 100% carbamidomethylation of the cysteine residue of each of the chosen peptides, as expected (Table 4.8). For the acrolein-treated sample, the sum of area under the curve for the XIC was taken for the carbamidomethylated and the acrolein-modified cysteine residue peptides was used to determine the percentage modification of both modifications. Each of the chosen cysteine residue peptides showed varying degrees of acrolein-modification, with Cys71 having the lowest proportion of acrolein modification and Cys250 having the highest (Table 4.8). Due to their relative proximity to each other, and so similar solvent accessibility, and the increased vulnerability of Cys124 thiol group to oxidative modification, it might be expected that Cys124 would have the potential to have a level of modification higher than that of Cys71. Taken together with the results in Table 4.7, it was concluded that there were no peptides containing acrolein Michael (reduced) modification to Cys124 identified.

To identify any intermediate crosslinking between the monomeric PTEN-V5-His band and the aggregate band (as seen in Figure 4.5), a western blot was probing for acrolein was performed against untreated and 10-minute acrolein-treated and sodium borohydride reduced PTEN-V5-His; but no bands were seen. To investigate whether it was the sodium borohydride reduction that was affecting the ability of the anti-acrolein antibody to recognise the acrolein-modified protein, BSA was treated with increasing concentrations of acrolein (0:1, 0.2:1, 2:1 and 20:1 acrolein:BSA) and left unreduced or reduced with sodium borohydride before non-reducing and reducing SDS-PAGE and western blot analysis against acrolein, but again no bands were present in any lanes. As acrolein modification was confidently identified using LC-MS/MS. this suggests that the antibody was not working under these conditions, as a BSA-acrolein conjugate was used as the example western blot by the manufacturers. However, further experiments would be required to determine the cause.

Table 4.8 Identification and Quantification of the Peptides Containing Carbamidomethylated or Acrolein Modified Cysteines from Untreated and Maximally Acrolein-treated PTEN-V5-His after In-solution Digestion with Trypsin/Glu-C

Peptide [£]	Acrolein: PTEN [%]	Modification	Modified Residue	Ion Score [^]	No. of Peptides	Mass (Expt) ^{&}	Mass Observed	Charge	Modification (%) [!]
E.IDSICSIE R.A	0:1	Carbamidomethylation	C304	56	9	1091.4974	546.7560	2+	100
	20:1			58	3	1091.4941	546.7543	2+	31
	20:1	Acrolein Michael addition (Reduced)		48	11	1092.5149	547.2647	2+	69
K.IYNLCAE R.H	0:1	Carbamidomethylation	C71	66	7	1037.4703	519.7424	2+	100
	20:1			55	3	1037.4670	519.7408	2+	65
	20:1	Acrolein Michael addition (Reduced)		53	3	1038.4907	520.2526	2+	35
E.FPQPLP VCGDIK.V	0:1	Carbamidomethylation	C250	73	3	1369.6333	685.8239	2+	100
	20:1			54	1	1369.6362	685.8254	2+	4
	20:1	Acrolein Michael addition (Reduced)		65	2	1370.6532	686.3339 800.3746	3+ 2+	96
E.LIKPFCE DLDQWLS EDDNHVA AIHCK.A	0:1	Carbamidomethylation	C124	51	3	3152.2982	789.0818	4+	100
	20:1			56	4	3152.2688	789.0745	4+	100
	20:1	Acrolein Michael addition (Reduced)		Not present					
E.DLDQWL SEDDNHV AAIHCK.A	0:1	Carbamidomethylation	C124	80	2	2264.8671	755.9630 567.2459	3+ 4+	100
	20:1			56	1	2264.9747	567.2510	4+	100
	20:1	Acrolein Michael addition (Reduced)		Not present					

Key:

£: Corresponding peptide containing the modified amino acid, with the modified residue in bold

℅: Ratio of acrolein:PTEN during treatment. 0:1 is the untreated control and 20:1 is the highest treatment level with 1 mM acrolein.

@: Modified amino acid residue identified by Mascot

^: A score given by Mascot depending on how well the experimental MS/MS data fits the theoretical MS/MS data for each peptide. The greater the ion score, the higher the confidence that the peptide is identified correctly.

&: Experimental mass of the peptide

!: Percentage modification of the cysteine taken from the sum of the modifications present

4.3.12 Lipoxidative Modification Mapping to the 3D Structure of PTEN and Solvent Accessibility Analysis

The acrolein-modified residues identified by the in-gel digestion (Table 4.3 and Table 4.6) of acrolein-treated PTEN-V5-His were mapped to the crystal structure of PTEN (Figure 4.11). Whilst the majority of the acrolein-modifications to both cysteine and lysine residues are present in the monomeric fraction (Figure 4.11A), there are two additional modifications to Cys136 and Lys344 were identified in the aggregated fraction (Figure 4.11B).

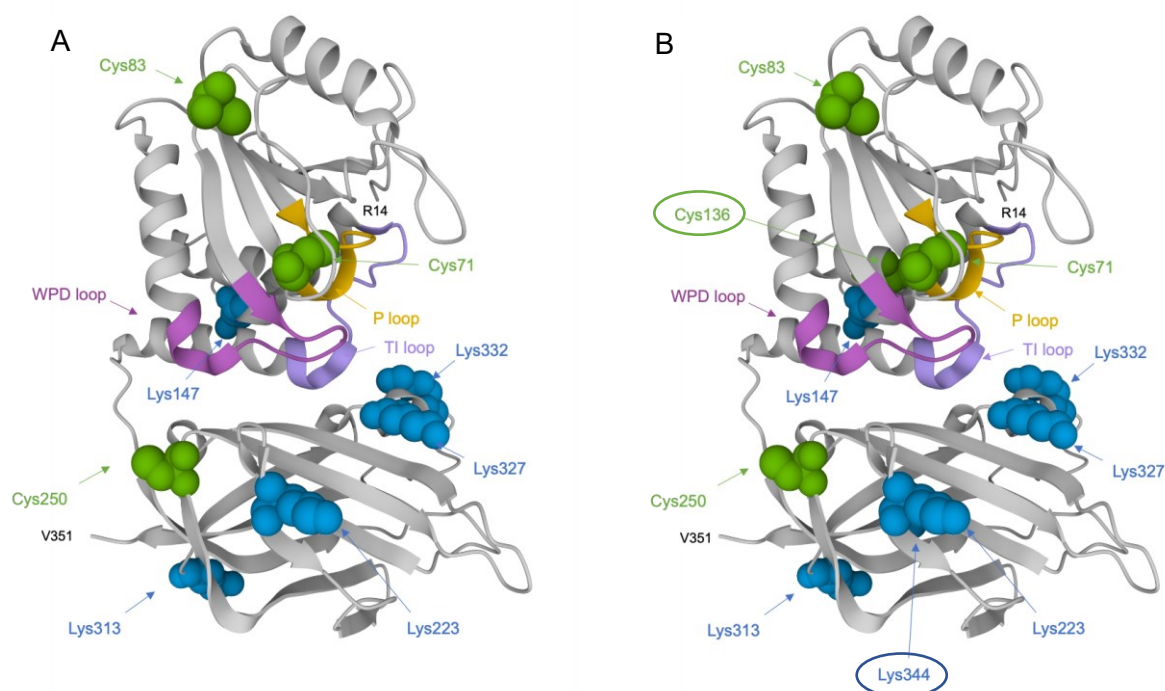


Figure 4.11 Acrolein Modified Residues Mapped to the Crystal Structure of PTEN.

The acrolein modified residues identified by in-gel digestion with trypsin and chymotrypsin were mapped to the crystal structure of PTEN (PDB: 15DR (Lee et al., 1999)) using PDB viewer (Sehna et al., 2021) for both the monomeric (A) and aggregated fractions (B). Modified cysteine residues are shown in green whilst modified lysine residues are shown in blue. Regions of interest are highlighted, with the WPD loop shown in pink, the P loop in yellow and the TI loop in purple.

To identify any correlation between the accessibility of the modified residues and their propensity to be modified, the relative solvent accessibility (RSA) and absolute solvent accessibility (ASA) were calculated using NetSurfP v2.0 (Klausen et al., 2019, Høie et al., 2022) (Table 4.9). The RSA describes the percentage of the residue that is accessible. This correlates with the ASA, where the higher the number, the more accessible the residue is. The RSA was used to categorise the modified residues into either buried or exposed, where a residue with an RSA of <0.25 denotes a buried residue. The accessible surface area (\AA^2) for each residue was calculated, with the exception of Lys6 and Cys304 which are not covered by the crystal structure. The accessibility of the modified residues is visualised in Figure 4.12

where the residues are plotted against the crystal structure of PTEN and coloured according to their accessible surface area.

The RSA, ASA and accessible surface area for cysteine residues was consistently lower than for lysine residues, where all modified lysine residues were considered 'exposed' and all modified cysteine residues were considered 'buried' due to their RSA (Table 4.9). Despite this, the cysteine residues had a higher susceptibility to modification by acrolein with modified cysteine residues being identified at all acrolein treatment concentrations used, including the lowest ratio of 0.2:1 acrolein:PTEN (Figure 4.11 and Table 4.9). The exception is Cys136, with an RSA and accessible surface area of 0. However, acrolein modification to Cys136 is only seen in the aggregated fraction of the highest treatment concentrations, which could be due to PTEN unfolding resulting in exposure of this residue. The pKa of the modified cysteine residues was determined using PropKa v2.0 (Olsson et al., 2011, Søndergaard et al., 2011) which determined that Cys71 had the lowest pKa of the modified cysteine residues of 4.15, which as discussed in section 4.1.1, could explain why modification of Cys71 is the first identified modification at the lowest treatment concentrations (Li et al., 2005). This is despite the relatively lower RSA in comparison to other modified cysteine residues, Cys83 and Cys250 with pKa's of 8.84 and 10, respectively. The properties of Cys124 and Cys71 were found to be very similar, as was hypothesised, and both residues were determined to be buried (Table 4.9). However, Cys124 had a lower solvent accessibility in terms of RSA, ASA and accessible surface area, which could lower its susceptibility to be modified despite its lower pKa (Table 4.9). However, Cys136 has the lowest accessibility of all the cysteine residues listed here but is found to be modified in the highest acrolein concentrations, although as discussed this is likely due to PTEN becoming unfolded, giving solvent accessibility that isn't available in PTEN's native form. Lysine modifications are only found at the highest treatment concentrations for both the intact and the aggregated fraction, despite their higher RSA and surface area in comparison to cysteine residues (Table 4.9).

Table 4.9 Solvent Accessibility Analysis of Acrolein-Modified PTEN-V5-His Residues

Residue [£]	RSA [@]	ASA ^{&}	Accessible Surface Area (Å ²) [^]	Accessibility [§]
K6	0.51	104.05	ND	Exposed
C71	0.11	15.11	7.17	Buried
C83	0.09	12.56	37.69	Buried
C124^U	0.03	4.00	5.77	Buried
C136	0.00	0.20	0.00	Buried
K147	0.55	112.41	128.36	Exposed
K223	0.46	95.12	148.34	Exposed
C250	0.21	29.25	44.83	Buried
C296*	0.23	32.345	ND	Buried
C304*	0.12	17.31	ND	Buried
K313	0.48	98.34	250.74	Exposed
K327	0.51	104.39	97.44	Exposed
K344	0.25	52.10	45.39	Exposed

Key:

£: Modified amino acid

@: Relative solvent accessibility

&: Actual solvent accessibility (Å)

^: Accessible surface area determined using PDB viewer (Sehnal et al., 2021) with the crystal structure of PTEN PDB: 15DR (Lee et al., 1999).

§: Residues were categorised as surface or buried residues, where an RSA of 0.25 was chosen as a cut off for buried residues

%: Fraction in which the modification was identified – monomeric or aggregated – and at which treatment ratios (acrolein:PTEN)

*: Identified during an in-solution digestion so the fraction (monomeric or aggregated) cannot be determined

ND: Not determined as these residues were not covered by the crystal structure of PTEN

U: Unmodified, included as a reference

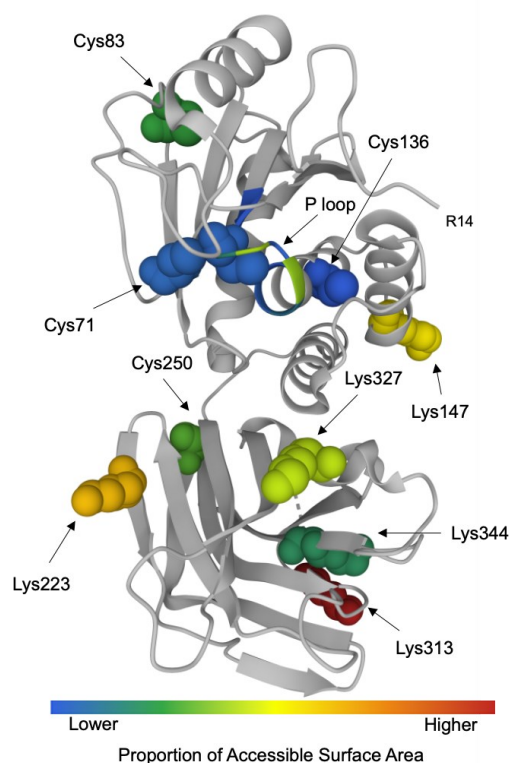


Figure 4.12 Acrolein Modified Residues Mapped to the Crystal Structure of PTEN and coloured according to their accessible surface area.

The acrolein modified residues identified by in-gel digestion with trypsin and chymotrypsin were mapped to the crystal structure of PTEN PDB: 15DR (Lee et al., 1999) using PDB viewer (Sehna et al., 2021). The highlighted residues were coloured according to the proportion of their surface area that is accessible, with blue/green residues having a lower accessible surface area and the red/orange residues having a higher accessible surface area. The P loop was also highlighted on the backbone and coloured according to the proportion of their surface area that is accessible.

4.4 Discussion

The second aim of this thesis was to further investigate the effect of lipoxidation on the activity and structure of recombinant PTEN (PTEN-V5-His) by *in vitro* treatment with increasing concentrations of acrolein for increasing incubation times. The effect of acrolein treatment on PTEN-V5-His' activity was analysed using the OMFP phosphatase assay and the effect on PTEN-V5-His' conformation was visualised using SDS-PAGE. To ensure that the experimental conditions for analysis were not subject to interference by DTT, a method of stabilising the acrolein adducts prior to analysis was validated. The treated PTEN-V5-His was analysed by LC-MS/MS using multiple digestion approaches in order to identify acrolein-modified residues and map them to the structure of PTEN.

There were several key findings, both in relation to the optimisation of monitoring the loss of phosphatase activity in the presence of acrolein as well as the effect of lipoxidation on PTEN. PTEN-V5-His' phosphatase activity was reduced in the absence of and in low concentrations of DTT but remained unaffected by NaBH₄, when NaBH₄ was prepared in reaction buffer. This provided a route to stabilise any acrolein modifications and measure PTEN's activity in a reducing environment without potential interference to the modifications by DTT. Whilst there was no additional inactivation of PTEN-V5-His with increased incubation times tested, there was a decrease in phosphatase activity with an increase in acrolein:PTEN ratio. This loss of activity was accompanied by the appearance of higher molecular weight aggregate bands, indicating that at higher concentrations, acrolein causes cross-linking and aggregation of PTEN. LC-MS/MS analysis identified PTEN's cysteine residues as the most susceptible to modification by acrolein, where its lysine residues were modified at higher acrolein treatment concentrations. Digestion of PTEN-V5-His with chymotrypsin increased the sequence coverage of lysine rich regions and led to the identification of additional acrolein-modified lysine residues. Double digestion of PTEN-V5-His with trypsin and Glu-C successfully increased the sequence coverage of PTEN to include a shorter length catalytic cysteine peptide and identified two additional cysteine modifications. Despite the vulnerability of the catalytic cysteine to electrophilic attack, and the loss of phosphatase activity of PTEN-V5-His with acrolein-treatment, no acrolein modification to Cys124 was identified.

PTEN, as all PTPs, requires a reducing environment for phosphatase activity due to the requirement of its catalytic cysteine to be in a reduced state to allow participation in catalysis (Denu and Tanner, 1998, Maehama and Dixon, 1998, Leslie et al., 2003, Spinelli and Leslie, 2015). The increase in phosphatase activity of PTEN-V5-His with increasing DTT concentrations in this study is in agreement with the landmark PTEN-PIP₃ phosphatase

activity study, which cites 10 mM DTT as the optimal concentration for PTEN's phosphatase activity (Maehama and Dixon, 1998). Consequently, the majority of the studies quantifying the phosphatase activity of PTEN have done so in the presence of 10 mM DTT (Redfern et al., 2008, Zhang et al., 2012, Lee et al., 1999, Arora and Ghosh, 2016). Some other studies have used lower concentrations of ≤ 5 mM DTT during activity analysis (Lee et al., 2015, Leslie et al., 2003, Mak et al., 2010, Mak and Woscholski, 2015, Verrastro et al., 2018). Whilst a lower specific activity was quantified for PTEN-V5-His that had previously been in the absence of DTT or ≤ 1 mM DTT in comparison to PTEN-V5-His that had always been in a stronger reducing environment (10 mM DTT), this unrecovered activity level could be explained by previous data citing lower DTT concentrations for longer incubation times (Han et al., 2017, Zhang et al., 2017) or higher concentrations of DTT (Lee et al., 2002, Verrastro et al., 2016). A limitation of this data comparison is that the studies cited for the reduction of oxidation with DTT used exogenous treatments with an oxidising agent, H_2O_2 . However, the mechanism of inactivation of PTEN on exposure to low levels of oxidants is the same regardless of whether it the source is endogenous or exogenous. A disulfide bond forms between the catalytic and resolving cysteine, and this disulfide bond can be subsequently reduced, resulting in the re-activation of PTEN. This similarity allows for comparison of the required reductant concentrations across the different data sets.

DTT contains thiol groups and, as discussed in section 4.1.1, the rate of reactivity of cysteine with acrolein is higher than reactions with other residues, such as lysine and histidine (Cai et al., 2009). Due to the requirement of a reducing environment for PTEN's phosphatase activity and the risk of DTT reaction with acrolein, stabilisation of the aldehyde modifications was required prior to the OMFP activity assay. One efficient method of stabilising acrolein adducts is the reduction of the reactive carbonyl groups through reaction with excess $NaBH_4$, commonly between 5-50 mM for 30 minutes to 1 hour at RT or 37°C, to stabilise aldehyde modifications prior to SDS-PAGE and tandem mass spectrometry analysis (Johnson and Rickborn, 1970, Fenaille et al., 2003, Afonso et al., 2018, Sousa et al., 2019, Shearn et al., 2013). Reduction with $NaBH_4$ can act in two ways: first to quench the free reactive aldehyde groups and second to stabilise the adducts, which could also act to prevent the risk of modification reversal during exposure to 10 mM DTT during the OMFP assay. When $NaBH_4$ was prepared in 0.1 M NaOH prior to addition of the PTEN-acrolein treatment, the resultant high pH could explain the lack of phosphatase activity, due to the negative effect of extreme pH levels on protein conformation and enzyme activity (Kishore et al., 2012). Preparation of $NaBH_4$ in the reaction buffer resolved this issue and gave confirmation that reduction of the acrolein-treated PTEN-V5-His with $NaBH_4$ prior to conducting the OMFP assay would provide a route to analysing the effect of aldehyde modification on the phosphatase activity of PTEN-

V5-His under optimal conditions, i.e. in the presence of 10 mM DTT, without itself affecting the phosphatase activity of PTEN. Further inspection of the literature surrounding the use of DTT in conjunction with acrolein has revealed that a high concentration of DTT (100 mM) has been used previously to reduce lysozyme prior to acrolein treatment in order to increase the accessibility of its residues and so increase the opportunity for protein modification (Afonso et al., 2018). Acrolein modifications were detected by direct infusion mass spectrometry and expansion to bottom-up analysis identified cysteine adducts to be the majority, with a small number of lysine adducts (Afonso et al., 2018). The concern here was the loss of the lysine modification data, due to acrolein's higher reactivity with thiol groups, and so the protocol developed here remains advantageous as it eliminates the risk of DTT-acrolein adduct formation. Stabilisation of the acrolein modifications prior to the activity assay meant that DTT could be re-introduced to provide the reducing environment that PTEN needs for activity during the assay.

Previous studies on the inactivation of PTEN with lipid oxidation products have utilised *in cellulo* treatments of MCF-7 cells, a human breast cancer cell line, and HepG2 cells, a human hepatocellular cell carcinoma line, in addition to *in vitro* treatments of recombinant PTEN (Covey et al., 2010, Shearn et al., 2011, Shearn et al., 2013). Treatment of MCF-7 cells with 10 μ M acrolein for 30 minutes demonstrated covalent modification of PTEN by immunoblotting for carbonylation (Covey et al., 2010). The same study demonstrated a 40% loss of phosphatase activity on treatment with 10 μ M acrolein for 30 minutes, amongst other test compounds including 4-HNE which gave 57% inactivation (Covey et al., 2010). The effect of 4-HNE has been further studied, with analysis using recombinant PTEN, cellular PTEN from HepG2 cells and a murine model (Shearn et al., 2011, Shearn et al., 2013). Previous studies involved *in vitro* treatment of recombinant PTEN with 25 nM to 10 μ M 4-HNE at a ratio of 0.1:1 to 20:1 4-HNE:PTEN for 30 minutes at RT (Shearn et al., 2011). With increasing ratio of 4-HNE:PTEN there was a decrease in PTEN activity, with a significant inactivation found at a 1:1 ratio of 4-HNE:PTEN at 25 μ M 4-HNE (Shearn et al., 2011). The data presented here demonstrates a similar profile, showing a dose-dependent inactivation of PTEN-V5-His with increasing acrolein treatments, from 0.2:1-20:1 acrolein:PTEN. However, there is not a significant reduction in the phosphatase activity of PTEN until a 2:1 ratio of acrolein:PTEN, which differs from the aforementioned 4-HNE data (Shearn et al., 2011). However, when comparing the level of inactivation of PTEN by acrolein and 4-HNE, the inactivation of PTEN *in vitro* by 10 μ M acrolein was 40% and 10 μ M 4-HNE was 57% (Covey et al., 2010). This increased inactivation of PTEN by 4-HNE in comparison to acrolein at the same treatment concentration explains the higher ratio of acrolein:PTEN required in this study to see a significant inactivation, from a 1:1 to a 2:1 ratio of lipoxidant:PTEN (Covey et al., 2010). These

observations demonstrate the importance of stating the ratios of lipoxidant:PTEN when comparing data sets. The concentrations utilised by Shearn et al. ranged from 25 pM-10 μ M 4-HNE, and Covey et al. used 10 μ M of acrolein and 4-HNE (Shearn et al., 2011, Covey et al., 2010). These are considerably lower than the 10 μ M-1 mM acrolein concentrations used in this study, but the ratios of 0.2:1-20:1 acrolein:PTEN are on a par with the previous study using 0.1-20:1 ratio of 4-HNE:PTEN (Shearn et al., 2011). Table 4.10 compares the percentage inactivation of PTEN with acrolein or 4-HNE across the previous studies and the current study, showing how the experimental conditions have resulted in lower treatment concentrations but when similar ratios of treatment to PTEN are used, comparable inactivation is seen. Whilst a 10 μ M 4-HNE treatment of PTEN, at a ratio of 20:1, has previously produced an 80% inactivation, a 10 μ M acrolein treatment at a ratio of 0.2:1 in this current study produced a 6% inactivation (Table 4.10). When the acrolein treatment concentration is increased to 1 mM to match a 20:1 ratio, the inactivation becomes comparable at 97% (Table 4.10). Taken together, the level of inactivation of PTEN-V5-His with acrolein is comparable to previously reported data on *in vitro* inactivation of recombinant PTEN. There is some disagreement between this current study and previous data indicating that the percentage activity inactivation of PTEN is higher for 4-HNE than acrolein at the same concentration (Table 4.10). At the same ratios of treatment to PTEN there is a higher inactivation of PTEN by acrolein here than previously cited for 4-HNE. However, the treatment using 4-HNE was performed for 30 minutes at RT, as opposed to 10 minutes at 37°C (Table 4.10). In addition, the phosphatase activity assays used to evaluate the inactivation of recombinant PTEN differed; the 4-HNE inactivation was measured using a PIP₃ lipid phosphatase activity assay whilst the current study measuring acrolein inactivation used the OMFP phosphatase activity assay, which is less specific (Shearn et al., 2011). In addition, the previous study used DTT to quench the excess and unreacted 4-HNE, whereas in this current study the acrolein was stabilised using NaBH₄ reduction (Shearn et al., 2011). This difference in experimental conditions might explain the inconsistency (Table 4.10). It would be interesting to validate these results from the OMFP activity assay with data using the PIP₃ phosphatase assay. A limitation in the use of the OMFP assay to quantify the effect of post-translational modifications on the activity of PTEN is that whilst the mechanism of dephosphorylation is the same, there has been a difference in the effect of residue mutation on the phosphatase activity of PTEN for protein vs lipid substrates. A Gly129Glu mutation has been reported to inhibit the recognition of PIP₃ by PTEN, with protein phosphatase activity remaining intact (Myers et al., 1998). Whilst this exact example is not relevant for any specific limitation to this study due to the inability of acrolein to modify glycine residues, it does highlight a potential consideration of the effect of non-catalytic residues for PTEN's enzyme function and differences in the effect on PTEN's catalysis of different phosphorylated substrates.

Table 4.10 Inactivation of Recombinant PTEN with Acrolein and 4-HNE

Study	Treatment	Treatment Conc.	Treatment Condition	Ratio of Treatment:PTEN	Inactivation (%)
Covey et al. (2010)	Acrolein	10 μ M	Unknown	Unknown	40
Covey et al. (2010)	4-HNE	10 μ M	Unknown	Unknown	57
Shearn et al. (2011)	4-HNE	10 μ M	30 min RT	20:1	~80
Current	Acrolein	10 μ M	10 min 37°C	0.2:1	6
Current	Acrolein	1 mM	10 min 37°C	20:1	97

Section 4.1.1 described the previous evidence for time-dependent inactivation of phosphatase enzymes by acrolein and 4-HNE. The data here appears to contradict the hypothesis that PTEN-V5-His would be inactivated by acrolein in a time-dependent manner, as PTEN is not further inactivated by acrolein after 10 minutes. However, this can be explained by the length of the acrolein treatment times used in this study as here acrolein-inactivation was investigated over a range of minutes to hours. Previous investigations demonstrating time-dependent inactivation of a cysteine-dependent phosphatase, PTP1B, used much shorter treatment times of 1, 2 and 5 minute acrolein treatments (Seiner et al., 2007). This suggests that by the first treatment time used here of 10 minutes, the time-dependency of acrolein inactivation of phosphatase activity is lost and could explain the discrepancy with previously published data on the mechanisms of acrolein inactivation being both time- and dose-dependent. The times used *in cellulo* experiments showing time-dependent inactivation of PTEN by acrolein and 4-HNE through an increase in pAkt, were over a range of minutes to hours (Covey et al., 2010, Shearn et al., 2011). But the difference in experimental conditions means that these cannot be directly compared to an *in vitro* treatment.

In addition to forming adducts, acrolein has the ability to cross-link proteins. Acrolein-induced cross-linking of PTEN has not yet been reported, but the ability of 4-HNE to cross-link PTEN has previously been investigated (Shearn et al., 2013). Treatment of recombinant PTEN 1:1 with 4-HNE produced multimeric forms of PTEN at 55-60, 120 and 180 kDa (Shearn et al., 2013). The concurrent loss of intact PTEN that occurred with the loss of phosphatase activity in this study could be explained by a loss of productive enzyme structure due to conformational changes resulting from modification of key structural residues. This has been observed during *in vitro* treatments of recombinant PTEN with hypochlorous acid (HOCl), where a strong

correlation between loss of phosphatase activity and loss of monomeric PTEN-GST was observed (Verrastro et al., 2018). At lower concentrations of acrolein, the most susceptible residues are likely to be surface or active site residues, due to their respective accessibility and reactivity. However, it has been suggested that due to the small size of acrolein it may have the ability to penetrate the structure to buried residues (Sousa et al., 2019, Spickett and Pitt, 2020). Modification of key structural residues could result in protein unfolding and subsequent aggregation due to the exposure of hydrophobic residues (Verrastro et al., 2018). There is some debate surrounding the number or proportion of residues requiring modification before protein unfolding and aggregation can occur (Spickett and Pitt, 2020). The propensity for aggregation is likely to alter for different modifications and for different proteins, but general observations include an increase in hydrophobicity due to the introduction of carbonyl groups during lipoxidation in addition to altering charge state when adducts are formed on basic residues such as lysine, arginine and histidine (Spickett and Pitt, 2020). This is a potential explanation for the complete abolishment of phosphatase activity at 10:1 and 20:1 acrolein:PTEN ratios in parallel with the loss of monomeric PTEN-V5-His and aggregate formation. At 10:1 and 20:1 acrolein:PTEN ratios, the molecules of acrolein exceed PTEN's number of cysteine residues, which increases the potential for less reactive residues such as lysine, arginine and histidine to be modified by acrolein. Alongside increasing hydrophobicity, lipoxidation of proteins has been shown to differentially alter the proportions of the secondary structure conformations α helix and β sheet, where an increase in the proportion of β sheet gave an increase in aggregation (Nieva et al., 2008, Perween et al., 2019, Spickett and Pitt, 2020).

In order to map acrolein-adducts to the structure of PTEN-V5-His, LC-MS/MS analysis was performed following digestion of treated and untreated acrolein with multiple proteases. As introduced in chapter 3, there are limitations with regards to use of trypsin where there is a proline following a lysine and sequence coverage can be increased with the use of multiple proteases. Previous studies have reported the use of Lys-C in the preparation of PTEN for mass spectrometry (Lee et al., 2002). Lys-C has an advantage over trypsin as there are no limitations by the presence of a subsequent proline (Jekel et al., 1983) and so the inclusion of Lys-C would allow lysine sites to be cleaved despite the presence of a proline. However, as Lys-C only cleaves at lysine residues, the resulting peptides are likely to be large in size, reducing the efficiency of extraction from the gel and increasing the risk of being excluded from LC-MS/MS analysis by the survey scan threshold due to the selection parameters. Therefore, the use of Lys-C in conjunction with trypsin would produce shorter peptides and allow cleavage at the KP site and the issue of the production of large peptides with Lys-C would be resolved due to additional cleavage at arginine by trypsin. However, many of the

gaps present in the sequence occur when there are lysine (K) and arginine (L) residues close together, for example Lys125 and Lys128 in the P-loop. Due to the survey scan cut off limit of 350 Da, many of these would be too small to be detected, meaning that there would only be limited sequence coverage improvement possible where a protease that cleaves at lysine residues is used. Alternative digestion enzymes include Glu-C, which cleaves at glutamic acid (E) when the digestion is performed in a basic buffer, such as ammonium bicarbonate, or chymotrypsin which mainly cleaves at phenylalanine (F), tyrosine (Y), tryptophane (W) and leucine (L). Glu-C is commonly used in a double digestion in combination with trypsin, for the same reasons discussed for Lys-C, where a single cleavage site often results in the production of long peptides that are less suited for detection by LC-MS/MS. Chymotrypsin has the opposite issue, where there are up to four potential cleavage sites, depending on the digestion buffer, increasing the risk that very small peptides could be produced that are also less suitable for detection by LC-MS/MS. However, the proteolytic efficiency of chymotrypsin is much lower than that of trypsin, often resulting in 3+ missed cleavages per peptide during time limited digestions. The results from the alternative digestions show that whilst there was some cleavage at the KP site during the trypsin/Lys-C in-solution digestion, the efficiency was low, whereas the orthogonal digestion in-solution with trypsin/Glu-C resulted in a Cys124 peptide of optimal length for LC-MS/MS. In-solution digestion is the optimal method for digestion with Glu-C, and permitted identification of modifications of the acrolein-treated PTEN as a whole sample with both the monomeric and aggregate fractions present. This has some limitations as the monomeric and aggregated PTEN are analysed together and so it is not possible to infer whether residue modifications are contributing to the cause of, or resulting from, unfolding and aggregation of PTEN after acrolein treatment, from this data. However, as the design of this double-digestion experiment was to detect the catalytic cysteine, and it was used in conjunction with the original trypsin and alternative chymotrypsin in-gel digestions where the modifications present in the monomeric and aggregate fractions were analysed separately. And so for this study this limitation is not an issue.

Analysis of the modification of PTEN by 4-HNE beyond western blotting, as described in section 1.2.6, was expanded further through the use of mass spectrometry (Shearn et al., 2011, Shearn et al., 2013). At a 5:1 ratio of 4-HNE:PTEN, MALDI-TOF MS analysis showed a mass shift of 156 Da for PTEN which corresponds to the molecular weight of 4-HNE and provides further evidence that PTEN is able to be covalently modified by 4-HNE (Shearn et al., 2011). However, as with the western blotting approach, although this method detects the adduction of 4-HNE to PTEN, it is not possible to elucidate where PTEN is modified. In addition, the authors stated that it is expected that both monomeric and multiply-modified PTEN are present but these forms are not detected due to instrument resolution at that mass

to charge ratio (Shearn et al., 2011). In a later study by the same group, this MS analysis was expanded further to permit identification of specific PTEN residues that are modified by 4-HNE (Shearn et al., 2013). LC-MS/MS analysis of PTEN treated with 4-HNE at 1:1, 5:1 and 10:1 4-HNE:PTEN, with subsequent reduction with sodium borohydride before in-gel digestion with trypsin, identified Michael addition adducts of 4-HNE with PTEN at several residues; Cys71, Cys136, Lys147, Lys223, Cys250, Lys254, Lys313, Lys327 and Lys344 (Shearn et al., 2013). The data presented in this current study corroborates this modification data for 4-HNE, where acrolein was also found to modify these residues (Table 4.11).

However, when looking at the acrolein-modification data from the current study's tryptic digest alone, two modifications, Lys327 and Lys344, were not identified whilst an additional modification site at Lys6 was (Table 4.11). Whilst Lys327 was not covered by the tryptic digestion, Lys344 was but acrolein modification of this residue could not be confidently verified using de-novo sequencing. However, acrolein-modification to Lys327 and Lys344 were identified after in-gel digestion with chymotrypsin, where acrolein-modification to lysine residues was easier to analyse due to the reduction in modification data from missed cleavages. In addition, acrolein modification to both Lys327 and Lys330 were identified after in-gel digestion with chymotrypsin but it is not possible to differentiate between modification at these two sites. Two additional modification sites are identified with acrolein in comparison to the previous study with 4-HNE at Cys296 and Cys304, which was identified after in-solution digestion with trypsin and Glu-C. Although preliminary data during digestion with trypsin did identify Cys304 as a potential modification site, this finding was discounted due to the lack of convincing data during de-novo sequencing due to missing relevant peak assignments, including the Cys304 peak and downstream residues peaks, in the LC-MS/MS data. There was only one additional acrolein-modification site to PTEN (Lys6) in comparison to 4-HNE when comparing the tryptic digestion data alone. The additional modifications to Cys83, Cys296 and Cys304 by acrolein were not confidently identified until orthogonal digestion of PTEN was carried out. Interestingly, all of the 4-HNE modifications presented in Table 4.11 were identified at a 1:1 ratio of 4-HNE:PTEN, but at the same ratio of acrolein:PTEN only Cys71 and Cys250 were identified. There were differences in the experimental conditions, where the 4-HNE treatment was conducted for 30 minutes at 37°C whilst the acrolein treatment was for 10 minutes at 37°C. The longer treatment time in the 4-HNE study in comparison to the current study could explain the presence of additional modification sites at the same lipoxidant:PTEN ratio. In order to determine whether this was the cause of the increase in modification sites at lower 4-HNE:PTEN ratios, LC-MS/MS analysis would need to be conducted on PTEN treated with acrolein for longer incubation times. The limited availability of 4-HNE at the equal molar ratio used by Shearn et al. (2013) suggests that the modifications

may be present across the pool of modified PTEN, rather than on each PTEN molecule. The use of intact mass analysis would be interesting to identify the number of modifications per protein molecule.

Table 4.11 Modification of Recombinant PTEN with Acrolein and 4-HNE Identified using LC-MS/MS

Residue	Treatment			
	4-HNE (1:1) (Shearn et al., 2013)		Acrolein (0.2:1-20:1) (Current Study)	
	Trypsin	Trypsin	Chymotrypsin	Trypsin/Glu-C
K6		X		
C71	X	X	X	X
C83			X	
C136	X	X		
K147	X	X	X	
K223	X	X		
C250	X	X		X
C296				X
C304				X
K313	X	X		
K327/330	X		X	
K344	X		X	

One limitation of the LC-MS data is that PTEN is purified and stored under reducing conditions to preserve catalytic activity. This could increase the number of free cysteine thiol groups that are able to react with acrolein (Afonso et al., 2018). Although, the PTEN was reacted with acrolein in the absence of DTT and there was identification of specific cysteine residues modified at the lower acrolein treatment concentrations, so it was possible to conclude that certain cysteine residues are more susceptible to modification by acrolein. Future analysis could include computational molecular modelling of the aldehyde-modified residues, in a similar way to that done for HNE by Shearn et al. (2013). In this study it was thought that LC-MS/MS analysis and subsequent comparison of the acrolein-modified residues of the monomeric and aggregate bands might give insight into the modified residues that could be responsible for the aggregation of PTEN-V5-His. However, there are only two additional modifications present in the monomeric fraction, Cys136 and Lys344. The lack of solvent accessibility of Cys136 suggests that the identification of this residue could be a result of the unfolding allowing access for acrolein, rather than the cause. Instead of modification to key residue sites for maintaining structure, this data set suggests that it is the proportion of modified residues, rather than modification of specific residues themselves, that caused the aggregation of PTEN-V5-His after treatment with the higher acrolein modifications. The proportion of acrolein-modification could be identified by quantification and comparison of the

proportion of unmodified to modified peptide at each treatment concentration, for example using software such as Progenesis Q1 for proteomics. A further limitation of this data set is that only the monomeric and aggregate band were taken, where it is possible that additional bands of cross-linked PTEN-V5-His could be present. Further work could include completion of the western blot analysis of the acrolein-treated PTEN-V5-His against acrolein to identify any intermediate bands, as conducted by Shearn et al. (2011) against 4-HNE and as was attempted in this chapter.

In both the previous study by Shearn et al. (2013) and this current study, no modification to the catalytic cysteine was found by 4-HNE or acrolein, respectively, despite the theoretical vulnerability of the catalytic cysteine and the confident detection of Cys124 containing peptides in this study. The explanation of the loss of phosphatase activity identified by Shearn et al. (2013) after treatment with 4-HNE was proposed to be due to steric hindrance of the active site by 4-HNE modification to Cys71 and Lys327. This provides a potential explanation for the loss of phosphatase activity of PTEN after treatment with acrolein, as both Cys71 and Lys327 were also found to be modified by acrolein. A consideration in the use of this theory to explain acrolein's inhibition of phosphatase activity is that the carbon chain of 4-HNE is longer by 5 carbons (Figure 4.13), potentially giving 4-HNE a greater effect at steric hindrance of the active site than acrolein. An alternative explanation is that the reactive aldehyde groups of both acrolein and 4-HNE are capable of forming crosslinks. Despite the differences in the carbon chain length of 4-HNE, the length of the reactive α,β -unsaturated aldehyde groups are the same, which therefore gives 4-HNE and acrolein the same range for crosslinking (Figure 4.13). The distance of neighbouring lysine residues to Cys124 was measured using Mol* (PDB). The distance between a thiol-group sulfur of a cysteine residue and the nitrogen of a lysine residue that are crosslinked by acrolein is a maximum of 5.2 Angstroms (Å), with the maximum distance between the residues respective alpha carbons being 14.2 Å. PTEN contains two active site lysine residues, Lys125 and Lys128, with distances to Cys124 of 4.89 Å and 8.48 Å, respectively, which are within a reasonable distance of each other to permit crosslinking via acrolein. These measurements were taken using the crystal structure of PTEN (PDB: 15DR (Lee et al., 1999)) with PDB viewer (Sehna et al., 2021).

Acrolein crosslinking has been previously identified in a study of the effect of acrolein on chain B of bovine insulin using SDS-PAGE and mass spectrometry (Ishii et al., 2007). The use of SDS-PAGE identified the monomeric, adduct and cross-linked forms of chain B of bovine insulin at ratios of 1:1 or 1:2 protein:acrolein (Ishii et al., 2007). Subsequent mass spectrometry analysis identified in multiple acrolein-bridges from lysine residues and the N-terminal amine of phenylalanine to other residues, such as histidine and lysine residues (Ishii et al., 2007). A

limitation of the LC-MS/MS data analysis in this chapter is that the focus was on the identification of adducts with acrolein rather than acrolein-crosslinks. Future investigation could include the use of alternative search parameters in Mascot during LC-MS/MS data analysis to include an acrolein linker could be used to search for any sites of crosslinking, with particular focus on Cys124, and molecular modelling of any potential cross-link sites. This is challenging due to the number of potential cross-linking sites. A consideration during the search for acrolein cross-links where PTEN-V5-His is used, is the possibility that the C-terminal histidine tag could participate in cross-linking with proximal lysine and histidine residues, where these crosslinked peptides would not be identified through Mascot searches without modification to the search database to include the C-terminal tag sequence. Whilst this is likely not an issue in the search for Cys124 crosslinks due to the distance between Cys124 and Val403 and the small size of the reactive aldehyde group of acrolein, it is consideration into the overall propensity for this recombinant PTEN protein to aggregate in comparison to wild type PTEN. This could be further investigated by the comparison of aggregation on treatment of tagged- and untagged-PTEN by SDS-PAGE and western blotting against acrolein.

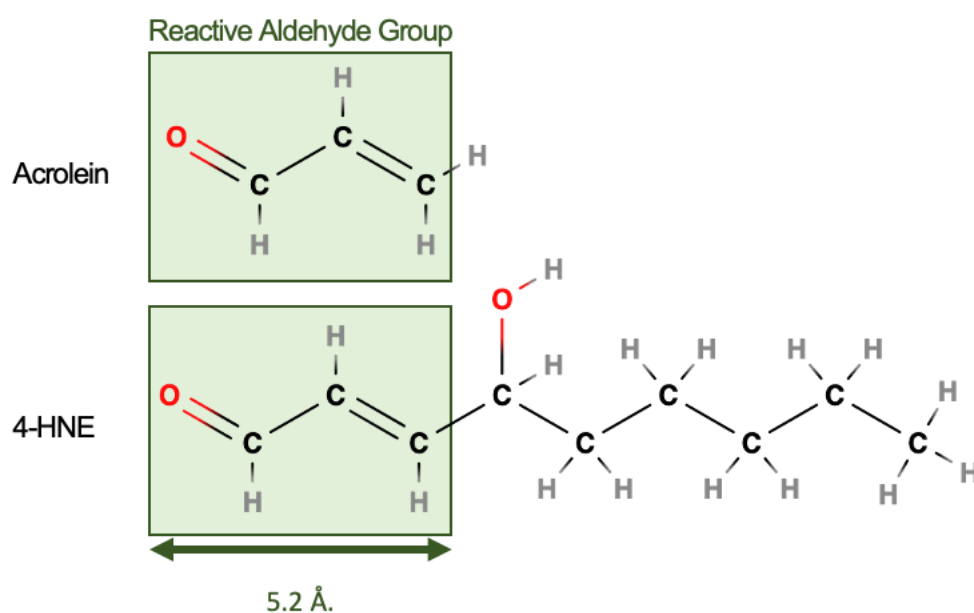


Figure 4.13 Structure of Acrolein and 4-HNE

The structure of acrolein and 4-HNE are shown with the reactive aldehyde group and its distance is highlighted in green.

In conclusion, the data presented in this study both corroborates and expands on previous investigations into the effect of lipoxidation on PTEN. Lipoxidation of PTEN-V5-His with acrolein showed a dose-dependent inactivation of phosphatase activity of PTEN-V5-His that mirrored previously-cited data for 4-HNE. Whilst previous inactivation of recombinant PTEN

with 4-HNE were shown to be time-dependent this was between 0 and 10 minutes and the results presented here only test the time-independence of acrolein inactivation of PTEN-V5-His above 10-minutes. To test any time-dependence of PTEN inactivation with acrolein, shorter treatment times of than those that were used in this study would be required. Treatment of PTEN-V5-His with higher treatment concentrations at >4:1 ratio of acrolein:PTEN induced aggregation. These aggregates appeared as higher molecular weight aggregates at the top and bottom of the stacking gel and suggest that higher ratios of acrolein:PTEN results in an increase in acrolein modifications. Digestion of acrolein-treated PTEN-V5-His and the use of tandem mass spectrometry permitted the mapping of acrolein modification sites for each treatment concentration. Modification sites closely match previous results from investigation into 4-HNE, and modification to key residues such as the resolving cysteine, Cys71, were identified. Optimisation of the digestion of PTEN-V5-His with a range of proteases, both in-gel and in-solution, increase the sequence coverage of the protein beyond what was achieved with trypsin alone. Trypsin/Glu-C in-solution digestion permitted the confident identification of the catalytic cysteine; however, no acrolein modification to the catalytic cysteine was found which could be due to accessibility. The in-gel digestion with chymotrypsin increased the proportion of lysine residues that were covered by the sequence whilst simultaneously providing peptide digest products with non-terminal lysine residues so that any modified peptide found could be more easily verified and also allowed comparison to the unmodified peptide. This chapter further characterises the effect of acrolein on the structure and phosphatase activity of PTEN-V5-His, providing the foundation of the next chapter by identifying a suitable acrolein concentration for the affinity pull down assays. The treatment concentration was chosen as 2:1 acrolein:PTEN with a treatment time of 10-minutes, as whilst it caused an inhibitory effect on the phosphatase activity and acrolein-modification to multiple residues was found, at this concentration no aggregated PTEN was identified. This permits a route to investigate whether acrolein modification to PTEN causes a change in its interactome, whilst ensuring these changes are not non-specific binding to unfolding or aggregation of the protein.

Chapter 5 – Effect of Acrolein on the Global Interactome of Recombinant PTEN

5.1 Introduction

5.1.1 Protein Interactomes and the Effect of Post-translational modification

A protein-protein interaction (PPI) is defined as the selective binding of one protein to another through specific binding domains, forming regulated networks of multi-protein complexes (De Las Rivas and Fontanillo, 2010). PPIs are dynamic and these interactions can change in response to different physiological and pathophysiological cellular states (Westermarck et al., 2013, Snider et al., 2015). A protein may come into contact with many proteins by chance, and will have an interaction with proteins that are involved in protein synthesis and quality control, and these are not considered a specific PPI (De Las Rivas and Fontanillo, 2010). A PPI is a specific and intentional interaction between two proteins that can be stable or transient in nature (De Las Rivas and Fontanillo, 2010).

Interactions between proteins can be regulated by post-translational modification (PTM), as well as mutation (Spickett et al., 2006, Li et al., 2013). PTM can alter localisation which has an indirect effect on the possible interactions of the modified protein (Yakubu et al., 2019, Wang et al., 2022). PTM can control PPIs by altering the binding affinity between proteins through modification of interaction sites, acting to directly increase or decrease binding of an interaction partner or indirectly alter binding through structural changes to the protein induced by the PTM (Seet et al., 2006, Duan and Walther, 2015, Wang et al., 2022).

5.1.2 Methods to Identify Post-translational Modification-Associated Protein-Protein Interactions

There are two main routes to study protein-protein interactions. The first is the use of low-data content methods such as co-immunoprecipitation (CoIP) and western blotting, often in hypothesis-driven investigations for a specific interaction pair. The second route is to use high-data content methods such as affinity pull down assays (APD) coupled with mass spectrometry and the yeast-2 hybrid assay (Y2H) (Smith et al., 2021). Originally, the Y2H assay was a low-throughput method used to study single interacting pairs of proteins, but this method has been scaled up to screen entire genomes (Fields and Song, 1989, Fields, 2005). The strategies that can be employed to study the effect of PTM on PPIs have previously been reviewed (Wang et al., 2022). Mass spectrometry is a useful technique for this application as it can be used to map PTM to specific residues and identify potential interacting proteins (Yakubu et al., 2019). To uncover PTM-dependent PPIs, the target PTM first needs to be

replicated under experimental conditions. Endogenous approaches include induction of the PTM under known conditions, giving uncontrolled modification at any susceptible residue, target specific delivery of an agent or the use of genetic code expansion or mutation to incorporate a mimic of the PTM at a specific site of interest (Wang et al., 2022). Exogenous approaches to introduce PTM can include the recombinant expression and purification of the protein of interest and *in vitro* treatment (Verrastro et al., 2016). Difficulties in capturing PTM-associated interactors lie in the specific induction of the desired PTM, the preparation of a homogenous pool of modified target protein and the potentially transient or non-covalent nature of the resulting PPI (Wang et al., 2022).

Whilst CoIP and APD are both chromatography-based techniques, the Y2H assay is a genetic transcription-factor based system. CoIP involves incubation of cellular lysates (prey) with an antibody against the protein of interest (bait), before enrichment of the sample for both the target protein and its interaction partners by immobilisation of the antibody-bound protein (complex) on a Protein A or G resin. Whilst there have been several developments to APD, broadly it involves the expression of a recombinant protein of interest with a tag before performing one or more chromatography steps against the tag to pull down the protein of interest and its interactors. This removes the requirement for a specific antibody against the protein of interest, as there is an extensive library of tags and complementary affinity resins available for use. The expression can be *in cellulo*, whereby the protein of interest (bait) is expressed *in situ*, and as such is exposed to potential interactors, and the APD is performed directly upon cell lysis (Herlevsen et al., 2007, Maddika et al., 2011, Ahn et al., 2008, Gunaratne et al., 2011). Alternatively, the protein of interest (bait) can be expressed in an alternative expression system before purification and exposure to cell lysates (prey) *in vitro* (Crockett et al., 2005, Verrastro et al., 2016). Once the protein of interest and any interacting proteins have been isolated, the latter needs to be identified. Liquid chromatography with tandem mass spectrometry (LC-MS/MS) allows not only identification of the interactors, but also relative quantification of their abundance. Quantification gives a route to identify potential non-specific interactors, which would be present in similar abundance in the control experiment (e.g. a tag or resin-only pull down). The advantages and disadvantages of using LC-MS/MS for identification of interactors after APD has previously been reviewed (Kaake et al., 2010, Westermarck et al., 2013). The Y2H assay makes use of a transcription factor with two functional domains that can be expressed separately on the target protein of interest (bait) and any potential protein interactors (prey), for a reporter gene (Keegan et al., 1986). Whilst there are a variety of transcription factors and reporter genes that can be applied to this technique, the most common example is the Gal4 transcription factor, consisting of a DNA-binding domain and an activator domain that can be expressed as a recombinant protein with

the bait and prey, respectively, and the reporter gene LacZ (Fields and Song, 1989, Brückner et al., 2009). When the two Gal4 transcription factor domains are brought into close proximity, if the bait and prey are interactors, there is activation of expression of LacZ resulting in an observable colour change in the presence of X-gal (Fields and Song, 1989).

With high-data content methods there is a high risk of identification of false-positive interactors and efforts have been made to reduce this risk. One strategy involves the use of additional isolation steps, either in parallel, for parallel affinity purification (PAP), or in tandem, for tandem affinity purification (TAP) (Rigaut et al., 1999, Ong et al., 2002). Whilst both techniques make use of a recombinant protein with two different tags, PAP uses two one-step purifications in parallel whilst TAP uses one two-step purification in tandem (Ong et al., 2002, Rigaut et al., 1999). By utilising two affinity isolation steps, the stringency of the binding is increased and the risk of identifying non-specific interactors that are binding to the resin support is decreased. However, as TAP requires performing two purification steps in tandem there is an increased risk of loss of weaker interactors (Berggard et al., 2007, Gunaratne et al., 2011). This decreases the risk of false-positive interactors but also increases the risk of false-negative interactors where weaker true positive interactors may be lost, and in this way TAP may be less effective than PAP. The advantages and limitations of these APD techniques have been extensively reviewed (Formosa et al., 1991, Rigaut et al., 1999, Berggard et al., 2007, Westermarck et al., 2013, Rao et al., 2014, Adelmant et al., 2019).

These high-data content techniques can produce a vast set of potential interactors but as there is a risk of false-positive identification of interactions, the use of more than one technique is recommended in the capture and validation of an interactor of interest (Berggard et al., 2007, Smith et al., 2021, Wang et al., 2022). Often, high-data content approaches are combined with low-data content approaches once potential interactors have been identified, which enables validation of the interaction. It is well documented that there is an issue with the false-positive discovery rate, as well as the lack of reproducibility, in the high-data content approaches of Y2H (von Mering et al., 2002, Mehla et al., 2017) and APD (Zhang et al., 2008, Smith et al., 2021). Recently, many efforts have been made to characterise and reduce the source of false positive identifications (Banks et al., 2015, Peng et al., 2016, Xing et al., 2016, Tian et al., 2017, Yugandhar et al., 2019, Hong et al., 2019). Beyond the aforementioned experimental techniques, 'dry' *in silico* and bioinformatic approaches have been applied to identify potential interactors by comparing expression, function and sequence homology and applying a confidence score based on the level of similarity and ranking potential interaction partners based on these parameters (Suthram et al., 2006). However, none of these techniques are a complete solution.

5.1.3 PTEN's Interactome

As an antagonist of the AKT pathway, understanding the role of PPIs in the regulation of PTEN and the subsequent effect of these interactions on the activity of PTEN is important. PTEN has additional PIP₃ phosphatase-independent functions, such as protein phosphatase-dependent regulation of cell migration and the role nuclear PTEN in genomic stability (Hopkins et al., 2014, Leslie et al., 2007, Ho et al., 2019). As such, searching for novel interactors is also of importance for the non-canonical functions of PTEN. The BioGrid identifies, at the time of writing, 476 published physical interactions for PTEN (Stark et al., 2006) (Supplementary Table 4). There are 7 previously published high-data content specifically on the analysis of PTEN's interactome using physical approaches, outlined in Table 5.1 (Gorbenko et al., 2004, Crockett et al., 2005, Herlevsen et al., 2007, Gorbenko et al., 2010, Maddika et al., 2011, Gunaratne et al., 2011, Verrastro et al., 2016). In each of these cases, APD or Y2H assays have identified between 12-400 per study, with 1-4 from each study validated with physiological functions hypothesised (Table 5.1). The validation methods varied from 'wet' techniques using surface plasmon resonance (SPR) or CoIP and western blotting, to a 'dry' technique using *in silico* data alignment (Table 5.1). Functional consequences of the interaction were further investigated by some studies, using cell migration assays and fluorescence microscopy (Table 5.1). We have recently published a review evaluating the approaches that have been used to investigate the protein interactome of PTEN (Smith et al., 2021). Figure 5.1 highlights the different routes of investigation from bait preparation to interactor validation for both Y2H and affinity pull down based investigations into PTEN's interactome (Smith et al., 2021).

Table 5.1 Summary of the Content PTEN Interactome Studies (modified from Smith et al. (2021))

Publication Date	Authors (DOI)	Condition	Isolation Method	Identification Method	Validation Method	No. of Potential Interactors	No. of Validated Interactors
2004	Gorbenko et al. (2004)	N/A	Y2H	Restriction analysis & DNA sequencing	Mating Assay	43	1
2005	Crockett et al. (2005)	N/A	APD In silico	LC-MS/MS	In vitro & in silico data alignment	In vitro: 79 In silico: 349	42
2007	Herlevsen et al. (2007)	Human Bladder Cancer	APD	LC-MS/MS	Reciprocal APD & Western Blot	400	1
2008	Ahn et al. (2008)	N/A	APD	LC-MS/MS	Co-IP, Western Blot, Fluorescence Microscopy & RT-PCR	93	1
2010	Gorbenko et al. (2010)	N/A	Y2H	Restriction analysis & DNA sequencing	Co-IP, Western Blot & SPR	12	1
2011	Gunaratne et al. (2011)	N/A	PAP-SILAC TAP	LC-MS/MS	Co-IP, Western Blot & Cell Migration Assay	100	4
2011	Maddika et al. (2011)	N/A	TAP	LC-MS/MS	Co-IP	34	1
2016	Verrastro et al. (2016)	Oxidation	APD	LC-MS/MS	Western Blot	97	4

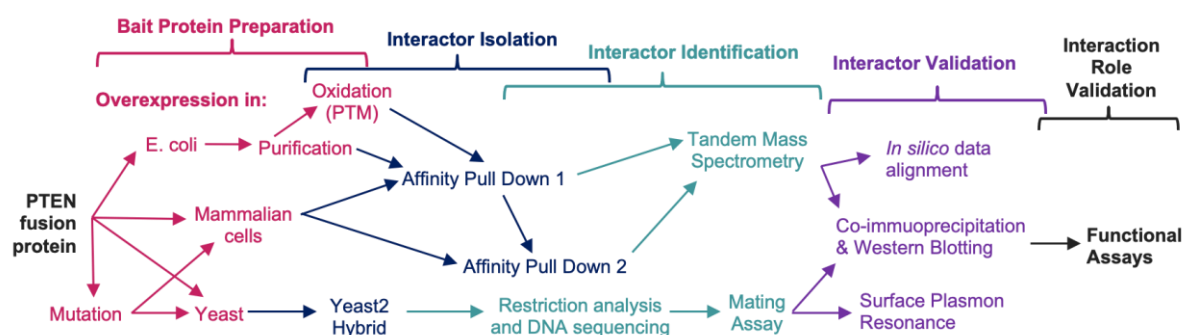


Figure 5.1 An overview of the steps involved in high-throughput investigations of the interactome of PTEN (reproduced with permission from Smith et al. (2021))

5.1.4 Redox-Sensitive Interactors of PTEN

As discussed in 1.2.6 PTEN is regulated by several post-translational modifications. Redox plays an important role in the regulation of PTEN and oxidative modification alters critical residues for conformation and catalysis. The effect of oxidative modification on PTEN's interactome has been investigated, using both low-data content and high-data content approaches.

Low-data Content PTEN Interactome Investigations

PTEN is reversibly inactivated by oxidation, with subsequent formation of an intramolecular disulfide bond between the resolving (Cys71) and catalytic (Cys124) cysteine (Lee et al., 2002). Thioredoxin, glutaredoxin, peroxiredoxin and annexin A2 are all redox regulatory proteins that have been found to have a role in reducing this disulfide bond and re-activating PTEN. Thioredoxins and peroxiredoxins are families of redox proteins with a role in maintaining a reducing cellular environment and protecting cells from oxidative damage (Lee et al., 2013, Perkins et al., 2015). The redox regulation of PTEN by thioredoxins and peroxiredoxins has previously been reviewed (Nguyen Huu et al., 2021, Zhang et al., 2020). Annexins are calcium-dependent phospholipid binding proteins that have been shown to be upregulated under conditions of oxidative stress, with a regulatory role in several diverse cellular processes (Madureira et al., 2011).

Thioredoxin-1 (Trdx-1) plays a major role in the reduction and re-activation of PTEN, and whilst both Trdx-1 and glutaredoxin co-immunoprecipitated with PTEN, Trdx-1 was found to be more efficient than glutaredoxin (Lee et al., 2002). There was a delay in reduction of oxidised PTEN on exposure to a Trdx-1 inhibitor but not a glutaredoxin inhibitor, indicating that Trdx-1 is important for PTEN reduction (Lee et al., 2002). Trdx-1 has been shown to bind to PTEN in a redox-dependent manner, where an increase in binding is seen on oxidation of Trdx-1, via an

intermolecular disulfide bond between Cys212 of PTEN and Cys32 of Trdx-1 (Meuillet et al., 2004). Further evidenced has since been obtained for the relationship between Trdx and PTEN (Schwertassek et al., 2014, Song et al., 2007, Sadeghirizi et al., 2016). Peroxiredoxin-1 (Prdx-1) has also been shown to form a complex with PTEN resulting in the protection of its phosphatase activity during mild oxidative stress (Cao et al., 2009). This protection was lost during high oxidative stress where a decrease in the interaction between Prdx-1 and PTEN was identified (Cao et al., 2009). Levels of annexin A2 (Anxa2) are upregulated on cellular exposure to H₂O₂ and co-expression studies have shown that Anxa2 binds to PTEN via its redox-sensitive cysteine (Cys8), and upregulates the phosphatase activity of PTEN (Castaldo et al., 2019). A reduction of Anxa2 resulted in a concurrent increase in Akt activation and on introduction of an alanine mutation at its Cys8, inhibition of Akt activation was lost (Castaldo et al., 2019).

High-data Content PTEN Interactome Investigations

We have recently reviewed the high-data content investigations into the interactome of PTEN (Smith et al., 2021). Of each of the 7 interactome studies, one investigated the effect of oxidation on the interactome of PTEN (Verrastro et al., 2016). This is an important investigation as key regulators of PTEN interact with PTEN in an oxidation-dependent manner (Verrastro et al., 2016). Recombinant PTEN-GST with and without prior treatment with H₂O₂ was used to isolate interacting proteins by APD (Verrastro et al., 2016). Tandem mass spectrometry was then used to identify any changes in the interactome on oxidation; 97 total potential interactors were identified with 14 found to vary with oxidation state (Verrastro et al., 2016). Four of these interactors were validated using western blot analysis. The interactions of Prdx-1, Trdx-1 and Anxa2 with PTEN were found to vary with oxidation state and all three showed an increase in binding to oxidised PTEN (Verrastro et al., 2016). DNA damage binding protein 1 (DDB1) was also validated as a novel interactor, but there was no difference in binding with redox state (Verrastro et al., 2016).

Whilst Trdx-1 had previously been shown to increase binding under oxidative conditions, as described above, an increase in binding on oxidation contradicted the previous data for Prdx-1 interaction with PTEN, as described in section above, whereby decreased binding of Prdx-1 was seen under conditions of oxidative stress (Cao et al., 2009). This conflicting data can be explained by the differences in experimental approaches. Where Cao et al. (2009) treated whole cells and subsequently performed a CoIP against PTEN, Verrastro et al. (2016) treated purified recombinant PTEN-GST and performed an APD against untreated whole cell lysates. The decrease in interaction between Prdx-1 and PTEN was hypothesised to be due to oxidation of Prdx-1 at Cys51, where oxidation of Prdx-1 would not be expected under the

experimental conditions of Verrastro et al. (2016), as only the PTEN bait protein was subjected to oxidative stress (Cao et al., 2009). The effect of oxidation was not tested as part of the low-data content investigation into Anxa2 binding to PTEN, where CoIPs were performed against PTEN overexpressing WT or mutant Anxa2 which lead to the conclusion that Anxa2 binds to PTEN through its Cys8 (Castaldo et al., 2019). As described above, the cellular levels of Anxa2 are upregulated under conditions of oxidative stress (Madureira et al., 2011). This upregulation could lead to higher levels of Anxa2 identified as binding to PTEN under conditions of oxidative stress; however, as discussed for the Prdx-1-PTEN interaction, Verrastro et al. (2016) only oxidised the PTEN bait protein while the prey lysate proteins were untreated. These experimental conditions mean that the elevation in Anxa2 levels under oxidative stress are not a consideration in the observation of increased Anxa2 binding to oxPTEN in this study (Verrastro et al., 2016).

5.1.5 Aims and Hypotheses

The previous high- and low- data content investigations provide evidence for the effect of oxidation on PPI with PTEN and highlight the relevance of studying the effect of post-translational modification on the interactome of PTEN. Whilst the effect of lipoxidation on the interactome of PTEN has not yet been studied, there is evidence to support the hypothesis that lipoxidation could also have an effect on PPI beyond the general definition of lipoxidation as a PTM. Zorrilla et al. (2019) summarise the different approaches used for various targets and lipoxidation products that have previously been used to study the effect of protein-protein interactions, amongst other areas. Targets have included the G-proteins Rho p21, H-Ras, as well as the transcription factor c-Jun, for the lipid oxidation product 4-HNE, using methods such as size exclusion chromatography (SEC) with SDS-PAGE and APD with western blotting. In addition, previous studies provide empirical evidence that lipoxidation by 4-HNE has an effect on the structure and activity of PTEN (Covey et al., 2010, Shearn et al., 2011, Shearn et al., 2013). The work described in Chapter 4 of this thesis shows that PTEN is inactivated by acrolein and there are residues across the length of the protein that are susceptible to modification by acrolein. Taken together, the previous evidence that 4-HNE has an effect on PPIs of other targets, as well as a direct effect on the structure of PTEN, in addition to the work presented in this thesis demonstrating a similar inactivation and structural modification of PTEN by acrolein, lead to the hypothesis that modification by acrolein will have an effect on the protein-protein interactors of PTEN. The first aim of this chapter was to optimise an APD protocol to allow immobilisation of PTEN, on-column treatment with acrolein, and subsequent exposure to whole cell lysate from untreated mammalian cells to capture PTEN interactors. The second aim was to apply this protocol to analyse the interactors captured by the untreated

Chapter 5 – Effect of Acrolein on the Global Interactome of Recombinant PTEN

and acrolein-treated bait PTEN using LC-MS and Mascot to identify interactors and Progenesis Q1 for proteomics to quantify the change in abundance across both.

5.2 Methods

5.2.1 Preparation of Recombinant PTEN Bait

PTEN-V5-His was expressed in BL21 (DE3) *E. coli* and purified as described in Chapter 3. PTEN-V5-His was buffer exchanged into APD binding buffer (25 mM NaPO₄ pH 8.0 with 150 mM NaCl and 1 mM DTT) using a PD-10 column, as per manufacturing instructions. If the resulting protein concentration was less than 0.5 mg/ml, PTEN-V5-His was concentrated to >0.5 mg/ml using a 10 kDa 0.5 ml VivaSpin centrifugal concentrator pre-rinsed in APD binding buffer, as per manufacturer instructions.

5.2.2 Preparation of HCT-116 Lysate Prey

HCT-116 cells were grown in complete McCoy's 5a media (McCoy's 5a with 10% (v/v) fetal bovine serum (FBS), 100 U/ml penicillin and 100 µg/ml streptomycin) in a 37°C incubator with 5% CO₂. The cells were grown to 80% confluence before harvesting as described in section 2.2.1. The harvested cells were washed twice with PBS by pelleting the cells using centrifugation at 1,000 x g for 5 minutes before re-suspension of the cell pellet in PBS. The cells were counted as described in 2.2.2 and diluted in PBS to a concentration of 5 x 10⁶ cells/ml and 1 ml aliquots were prepared for a total of 5 x 10⁶ cells per aliquot. The cells were pelleted by centrifugation at 1,000 x g for 5 minutes and the cell pellets were frozen at -20°C.

One aliquot of 5 x 10⁶ cells was thawed on ice per pull down and the pellets were resuspended in 250 µl of lysis buffer (25 mM NaPO₄ pH 7.4 with 150 mM NaCl, 1% Triton X-100, 5% glycerol and 1X cOmplete™ EDTA-free protease inhibitor cocktail (Merck, UK)). The cell suspensions were pooled and homogenised using a needle and syringe, before incubating at 4°C for 30 minutes on an end-over-end rotator. The lysate was centrifuged at 13,000 x g for 10 minutes at 4°C and the supernatant was quantified using the BCA Assay as described in section 2.3.2.

5.2.3 Pull Down Assay Optimisation

Comparison of Batch Purification and Spin Column Formats for APD

A 50% slurry of HisSelect Nickel Affinity Resin (Merck, UK) in APD binding buffer was resuspended and 40 µl was transferred to a spin column or a microcentrifuge tube, to give a final column volume (CV) of 20 µl. For the spin column format, wash steps involved resuspending the resin in each wash with gentle vortexing and centrifugation at 1,000 x g for 1 minute at 4°C to collect the fraction in the collection tube. For the batch purification format, wash steps involved resuspending the resin in each wash with gentle vortexing and centrifugation at 1,000 x g for 5 minutes at 4°C before collecting the fraction by aspiration of the supernatant. For both pull down formats the resin was washed with 3 x 5CV APD elution

buffer (25 mM NaPO₄ pH 8.0 with 150 mM NaCl and 250 mM imidazole) and 3 x 10CV APD binding buffer. The binding capacity of the resin is described as 15 mg/ml, which for 20 µl of resin gives a theoretical binding capacity of 300 µg of protein. Therefore 300 µg of PTEN-V5-His, prepared as in section 5.2.1, was added to the resin bed and the volume was made up to 600 µl with APD binding buffer. The prepared PTEN-V5-His was incubated with the resin for 2h at 4°C on an end-over-end rotator and the flow-through was collected. To wash away unbound protein, the resin was washed with 3 x 5CV APD binding buffer and the washes were collected. To elute the bound protein, the resin was incubated with 10CV of APD elution buffer for 5 minutes at RT. The fractions were quantified using the NanoDrop spectrophotometer.

Optimisation of Imidazole Concentration during Recombinant PTEN Bait Protein Immobilisation

300 µg of PTEN-V5-His was immobilised on 20 µl of HisSelect Nickel Affinity Resin in APD binding buffer as described in the section above. To minimise non-specific interactions of the HCT-116 lysate, it was necessary to include imidazole during the prey exposure step. Previous APD experiments with a recombinant PTEN-His protein included the use of 50 mM imidazole (Crockett et al., 2005), with 1 mM imidazole being used in the purification protocol described in 3.2.3. In order to test the effect of imidazole concentration on the elution of PTEN-V5-His and the resin was washed with 3 x 10CV APD binding buffer with 1 mM, 10 mM and 50 mM imidazole. The washes were collected and quantified using the NanoDrop spectrophotometer. To elute any remaining protein, the resin was incubated with 10CV of APD elution buffer for 5 minutes at RT.

Optimisation of the Imidazole Concentration during HCT-116 Lysate Protein Exposure

A 50% slurry of HisSelect Nickel Affinity Resin in APD binding buffer was resuspended and 40 µl was transferred to a spin column to give a column volume of 20 µl. The resin was washed with 3 x 5CV APD elution buffer and 3 x 10CV APD binding buffer. HCT-116 lysate was prepared as per section 5.2.2 and 800 µg was added to each spin column and the volume was made up to 600 µl with APD binding buffer with a final concentration of 0 mM, 1 mM, 10 mM or 50 mM imidazole. The lysate was incubated with the resin overnight at 4°C on an end-over-end rotator before collection of the flow through by centrifugation. The resin was washed with 3 x 10CV APD binding buffer and the bound protein was eluted by incubation with 10CV APD elution buffer at RT for 5 minutes. The eluate was quantified using the NanoDrop spectrophotometer.

5.2.4 Pull Down Assay with Untreated and Acrolein-treated Recombinant PTEN

300 µg of PTEN-V5-His was immobilised on 20 µl of HisSelect Nickel Affinity Resin in APD binding buffer as described in the section above, in a spin column format. The PTEN-V5-His was incubated with the resin for 2h at 4°C on an end-over-end rotator and the flow through was collected. To wash away unbound protein, the resin was washed with 3 x 5CV APD binding buffer. For the 2 bead-only pull downs, 600 µl APD binding buffer was added in place of the PTEN but the rest of the pull down protocol remained the same, with the inclusion of an untreated bead-only pull down and an 0.1 mM acrolein-treated bead-only pull down. To equilibrate the resin in 5 mM imidazole and remove any remaining DTT from the APD binding buffer, the resin was washed with 3 x 5CV APD wash buffer (25 mM NaPO₄ pH 8.0 with 150 mM NaCl and 5 mM imidazole). Three spin columns, two with bound PTEN-V5-His and one bead-only control, was then treated with acrolein at RT for 1h on an end-over-end rotator. The acrolein treatment was 0.1 mM acrolein in 600 µl of APD treatment buffer (25 mM NaPO₄ pH 8.0 with 150 mM NaCl), to give ratio of approximately 2:1 acrolein:PTEN. For the untreated bead-only control and the untreated PTEN, APD wash buffer was used in place of the acrolein treatment. Initially a shorter treatment time of 10 minutes was used, but LC-MS/MS analysis of the eluted PTEN-V5-His protein band suggested that the level of modification was lower than that of the *in vitro* acrolein treatments of PTEN-V5-His conducted statically at 37°C, as described in Chapter 4. One of the acrolein-treated PTEN-bound spin columns was treated with NaBH₄ to reduce and stabilise any acrolein modifications, giving a treatment-only control with no exposure to mammalian lysate. The sample was incubated with 5 mM NaBH₄ at RT on an end-over-end rotator for 30 minutes before collecting the treatment flow through, washing with 3 x 10CV APD wash buffer and eluting with 2 x 2.5CV APD elution buffer for 5 minutes at RT on a shaker. For the remaining 4 spin columns, with untreated and acrolein-treated bead-only control or immobilised PTEN, the treatment flow through was collected and excess treatment was removed by washing the resin with 3 x 10CV APD wash buffer. HCT-116 lysate was prepared as per section 5.2.2 and 800 µg was added to the 4 spin columns and the volume was made up to 600 µl with APD binding buffer with a final concentration of 5 mM imidazole. The lysate was incubated with the resin overnight at 4°C on an end-over-end rotator, before collection of the lysate flow through by centrifugation. The resin was washed with 3 x 10CV APD binding buffer and the bound protein was eluted by incubation with 10CV APD elution buffer at RT for 5 minutes. The eluate was quantified using the NanoDrop spectrophotometer.

5.2.5 Proteomic Analysis of the Effect of Lipoxidation on PTEN's interactome

SDS-PAGE Analysis of the Pull Down Fractions

The APD fractions were analysed by reducing SDS-PAGE on a 12% polyacrylamide gel as per section 2.3.3. For in-gel digestion, 15 µg of the PTEN and bead-only pull downs and 5 µg of the NaBH₄-reduced PTEN control were run at 50V for 30 minutes and 100V for 30 minutes on a 12% polyacrylamide gel, so that the samples only ran a short way into the resolving gel. For each of the pull downs the lanes were cut into 9 equal slices. For the NaBH₄-reduced PTEN-control the monomeric band and the aggregate band were also excised. The bands were frozen at -20°C for storage.

In-gel Digestion and LC-MS/MS analysis

The bands were thawed at RT for in-gel digestion with trypsin, as per section 2.4.2. The in-gel digest samples were analysed using LC-MS/MS, as per 2.4.4, where the experimental triplicates for each band were run back-to-back with a blank run between the equivalent bands from the different pull down and 2 blank runs between different bands. The pull down eluate bands were analysed using Progenesis Q1 for proteomics and the acrolein-treated PTEN treatment control bands were analysed using Mascot as per Table 5.2. The Mascot search identified peptides were filtered using an ion score of 40 to reduce the number of peptides identified with poor quality data. The peptide data with the highest ion score for each Mascot identified modification was checked visually to ensure that Mascot had assigned the correct peaks.

Table 5.2 Parameters chosen for Mascot searches for Acrolein Modification Analysis

Setting	Parameters Chosen
Taxonomy	Mammalia
Database	SwissProt
Fixed Modifications	None
Variable Modifications	Carbamidomethyl (C), Oxidation (M), Acrolein Michael addition (reduced) (C, K & H) and Acrolein Schiff base (reduced) (K)
Enzyme	Trypsin
Maximum Missed Cleavages	1
Peptide Charge	+2, +3, +4
Peptide Tolerance	± 0.5 Da
MS/MS Ions Search	✓
Data Format	Mascot generic
MS/MS Tolerance	± 0.5 Da
Merge MS/MS?	Yes

Quantitative Analysis with Progenesis Q1 for Proteomics

Each of the 9 pull down bands were analysed separately using Progenesis Q1 as per Chapter 2. The Mascot search parameters used are outlined in Table 5.3.

Table 5.3 Parameters chosen for Mascot searches for Interactor Analysis

Setting	Parameters Chosen
Taxonomy	Mammalia
Database	SwissProt 2021_03 (565,254 sequences; 203,850,821 residues)
Fixed Modifications	Carbamidomethyl (C)
Variable Modifications	Oxidation (M)
Enzyme	Trypsin
Maximum Missed Cleavages	1
Peptide Charge	+2, +3, +4
Peptide Tolerance	± 0.5 Da
MS/MS Ions Search	✓
Data Format	Mascot generic
MS/MS Tolerance	± 0.5 Da

For each band, any non-human proteins and contaminating keratin proteins were removed from the identification list. The separate band analyses for the pull downs were then recombined to give a full lane for each experiment and allow comparison between the untreated and acrolein-treated replicates for the PTEN pull downs and the bead-only controls. For the recombined samples, any proteins that did not meet the threshold criteria were filtered out. The threshold was as follows; unique peptides >2, confidence score >50 and a p value < 0.05. For the bead only control, the threshold did not include the p value of <0.05 out of caution to ensure any non-specific resin interactors were removed from the protein ID list of the pull downs. When the p value threshold was applied to the bead-only controls, only a limited number of proteins were identified due to the high variability of the proteins present in the bead-only control, likely due to the large amount of resin that is free for binding and the non-specific nature of the interactions.

Western Blot Analysis of the Pull Down Fractions

The lysate (20 µg) and elution fractions (5 µg) for each pull down were resolved by SDS-PAGE using a 10% polyacrylamide gel, as per section 2.3.3. Western blot analysis was performed as per section 2.3.4 with the following amendment: the transfer was performed at 4°C at 30 V for 16 hours. The blots were blocked in 5% Milk in TBS-T for 1 hour at RT and probed overnight at 4°C with 1:1000 dilution of Rabbit Anti-HECTD1 pAb (PA568176, Invitrogen, UK) in 5% Milk in TBS-T.

5.3 Results

5.3.1 Increasing the Concentration of Imidazole in the Affinity Pull Down Buffers Reduces Non-specific Binding to the Nickel Resin

Affinity pull downs are commonly performed using a batch purification technique or a spin column format. To reduce the volume of free resin and maximise the amount of bait immobilised onto the nickel resin support, reaching the maximum binding capacity of the resin was desired. As described above, the maximum binding capacity for HisSelect Nickel Affinity gel resin, as specified by the manufacturer, is 15 mg/ml of resin. The 20 μ l of resin used per pull down would theoretically have the capacity to bind 300 μ g of his-tagged protein. Due to the differences in binding capacity and affinity of resins to different his-tagged proteins, it would be reasonable to expect that the theoretical binding capacity might be different than the experimental binding capacity and, where the experimental binding capacity is less there could be loss of protein in the flow-through step when applying the maximal amount of protein.

To quantify the experimental binding capacity of the resin, the flow through was collected and the amount of PTEN-V5-His that did not bind quantified, before comparing this to the protein present in the eluate to determine any losses. Due to the nature of a batch purification with the low speeds at which the resin is centrifuged and the required aspiration of the fractions for each wash step, it was anticipated that the batch purification would show the highest loss of bait protein due to accidental aspiration of resin. Figure 5.2A shows a comparison of the PTEN-V5-His that was detected in the flow-through and elution fractions of the bait immobilisation performed using spin columns (SC) or microcentrifuge tubes (batch purification). Whilst the spin column showed a minimal loss of the bait protein, with >95% of the PTEN-V5-His applied to the resin detected in the flow through and eluate, the batch purification method was much less efficient, showing a loss of protein across the purification with <70% of the PTEN-V5-His applied detected in the flow through and elute (Figure 5.2A). The spin column was determined to be the most appropriate format for the affinity pull down assays, as loss of protein due to resin loss across the wash steps was prevented.

Due to the known interaction between nickel resin and histidine-rich proteins, it was necessary to find the optimal concentration of imidazole required in the loading buffer. The aim was to reduce non-specific binding of HCT-116 lysate proteins, and thereby reducing the number of false positive interactors identified, whilst retaining the PTEN-V5-His on the resin. The amount of PTEN-V5-His present in each of the washes with increasing imidazole, from 0-50 mM, was quantified to determine the effect on the retention of PTEN-V5-His. As the concentration of imidazole increased the amount of PTEN-V5-His eluted during each wash increased (Figure

5.2B). Whilst there was no additional PTEN-V5-His eluted with 1 mM imidazole in comparison to the control, there was elution of a proportion of PTEN-V5-His with 10 mM and 50 mM (Figure 5.2B). On application of 250 mM imidazole, there was further elution of PTEN-V5-His, indicating that some bait protein remained bound after the 50 mM imidazole wash (Figure 5.2B). This pattern of bait protein loss is mirrored in both the spin column and batch purification format, with a lower overall amount of protein eluted in the batch purification, matching the results shown in Figure 5.2A.

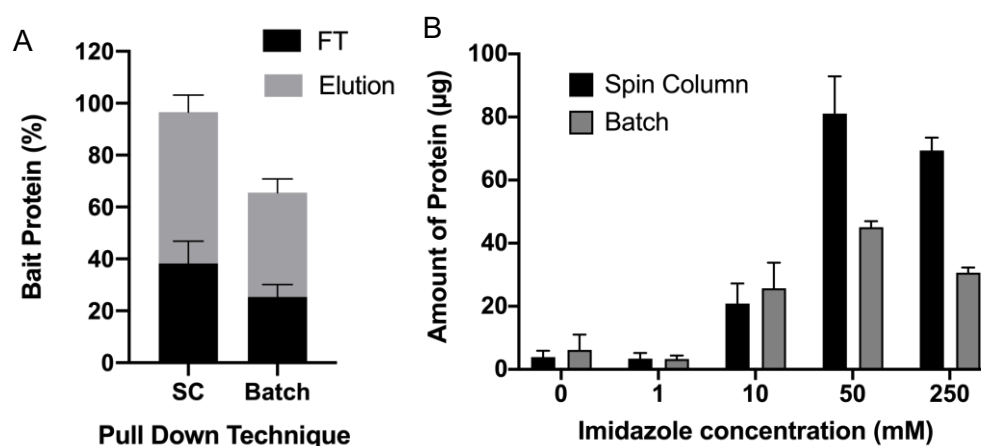


Figure 5.2 Comparison of APD Techniques and the Effect of Imidazole on PTEN-V5-His Immobilisation to Nickel Affinity Resin.

(A) 300 µg of purified PTEN-V5-His was immobilised onto 20 µl of nickel resin in a spin column and a batch purification format before eluting in the presence of a high imidazole concentration. The amount of bait protein that was found in both the flow through and the elution fraction were expressed as a percentage of the total amount applied to the resin ($n=3$; Mean \pm SEM). (B) 300 µg of purified PTEN-V5-His was immobilised onto 20 µl of nickel resin in a spin column and a batch purification format before washing with a series of wash buffers with increasing imidazole concentration and elution in the presence of 250 mM imidazole. The amount of bait protein in each fraction was quantified using the Nanodrop 2000 ($n=3$; Mean \pm SEM).

To measure the effect of increasing imidazole concentration on the non-specific binding of HCT-116 proteins to nickel resin, lysate was incubated with the resin in the presence of increasing imidazole to mimic the prey incubation step of an APD. With increasing imidazole concentration, there was a decrease in the amount of protein detected in the elution fractions due to a decrease in non-specific binding (Figure 5.3A). There was less protein detected in the elution fraction of lysate incubated with 1 mM imidazole in comparison to the 0 mM control and no detectable protein in the elution fractions of lysate incubated with 10 and 50 mM imidazole (Figure 5.3A). To visualise the prey protein binding with each imidazole concentration, the lysate, flow-through and elution fractions were analysed using SDS-PAGE (Figure 5.3B). Figure 5.3B confirms the results from Figure 5.3A and shows that whilst in the presence of 0 and 1 mM imidazole there is some non-specific protein binding to the nickel resin, no detectable protein can be seen in the presence 10 and 50 mM imidazole, showing minimal non-specific binding at these imidazole concentrations.

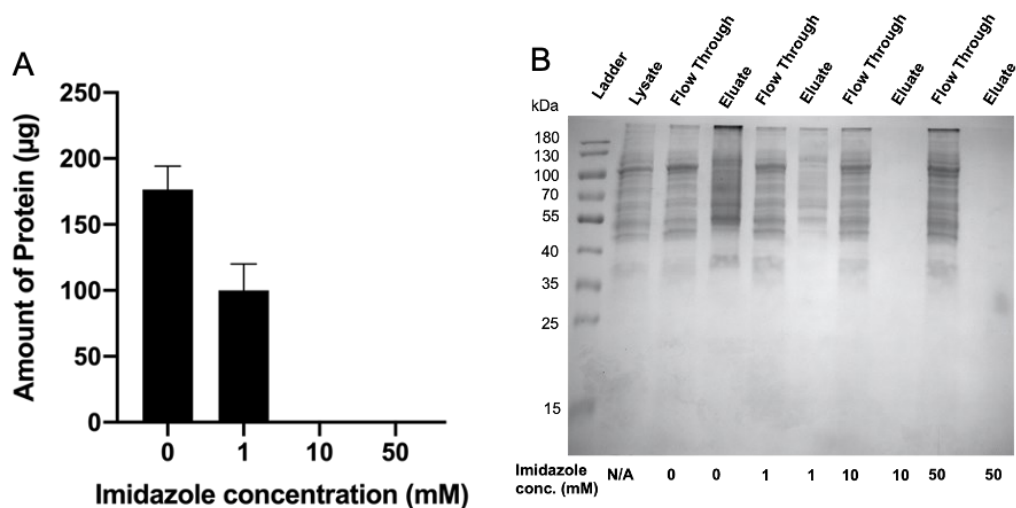


Figure 5.3 Quantification and SDS-PAGE Analysis of the Effect of Imidazole on Non-Specific Binding of HCT-116 Lysate Proteins to Nickel Resin.

(A) 900 µg of HCT-116 cell lysate was incubated with 20 µl of nickel resin in a spin column overnight at 4°C in the presence of increasing imidazole concentration before elution with 250 mM imidazole. The amount of prey protein that was in each elution fraction was quantified using the Nanodrop 2000 (n=3; Mean ± SEM). (B) A representative SDS-PAGE gel of the fractions obtained from the imidazole optimisation, where 30 µg of lysate and flow through and 30 µl eluate was resolved on a 12% polyacrylamide gel and stained with Coomassie Blue.

Figure 5.3 suggests that the most effective imidazole concentration to eliminate non-specific binding, and therefore the risk of identifying false positive PTEN interactors, is 10 mM. However, in combination with Figure 5.2, which shows the effect of increasing imidazole concentration on PTEN-V5-His retention, it appears that 10 mM imidazole is too high as there is a significant elution of PTEN-V5-His at this concentration. Due to the long overnight incubation times with the lysate during the pull down, it was important to identify concentrations that would minimise the loss of bait during this step. Whilst 1 mM imidazole did not cause a significant loss of bait protein (Figure 5.2B), there was only a small reduction in the prevention of non-specific binding by lysate proteins in comparison to 0 mM imidazole (Figure 5.3). A trial pull down was performed in the presence of 1, 2, 5 and 10 mM imidazole in order to determine whether any intermediate concentrations between 1 mM and 10 mM would provide a compromise between bait protein retention and prevention of non-specific binding of lysate proteins. There was minimal difference in the reduction of non-specific binding between 1 and 2 mM imidazole and between 5 and 10 mM imidazole (data not shown). To capitalise on the protection provided by the use of higher imidazole concentrations during the prey incubation step, whilst minimising the loss of bait, 5 mM imidazole was chosen as a suitable intermediate concentration.

5.3.2 Acrolein Treatment did not have an Adverse Effect on the Affinity Pull Down Assays

It was important to monitor the pull downs and ensure that the protein in each fraction, from bait binding, treatment, prey exposure and elution, was consistent between replicates. The pull down fractions were quantified (Table 5.4) and visualised using SDS-PAGE (Figure 5.4). Visualisation of the 'bait flow-through' lanes for the pull downs with untreated PTEN (Figure 5.4A) and acrolein-treated PTEN (Figure 5.4B) as well as the acrolein-treated PTEN treatment control (Figure 5.4E), showed that bait protein is present in the flow through and a small amount is detected in the washes, seen as a 60 kDa band. The average loss of bait protein in the flow-through and bait wash steps for the untreated, acrolein-treated pull downs and the acrolein-treated PTEN treatment control were in line with the losses of bait protein during optimisation (Table 5.4). Figure 5.2 shows that for the spin column format an average of 38% of bait was found in the flow-through, corresponding to an average of 114 µg out of the 300 µg of PTEN applied to the resin. There was minimal loss in the treatment incubation or wash steps, with a very small or no detectable band at 60 kDa in the treatment lanes (Figure 5.4A, B and E) and a very low to undetectable amount of protein in the treatment fractions (Table 5.4). Taken together the loss of bait protein in the flow-through and wash steps is acceptable, with most of the PTEN-V5-His protein binding to the resin.

In each of the pull downs, the vast majority of the lysate proteins flowed through and minimal loss of prey or bait protein in the prey wash steps, shown by no detectable bands in the prey wash lanes of Figure 5.4A, B, C and D and minimal protein quantified (Table 5.4). This confirmed that the imidazole concentration identified during the APD optimisation steps outlined in sections 5.3.1 and 5.3.2 was low enough to successfully retain the bound PTEN-V5-His. In comparison to the amount of eluted protein from the bait optimisation in section 5.3.1, there is a lower amount of protein present in the pull down assay eluates. During optimisation, an average of 58% of the bait protein was detected in the eluates, which corresponds to 174 µg of PTEN-V5-His, compared to an average of 121 µg and 104 µg for the untreated and acrolein-treated PTEN pull downs (Table 5.4). This could be due the loss during the additional treatment steps or the longer exposure to imidazole in comparison to the wash steps in Figure 5.2. However, the amount of protein eluted was consistent across the untreated and acrolein-treated pull downs and respective bead-only controls, which was the most important consideration.

Despite application of identical amounts of bait protein to the nickel resin and a comparative loss of protein in each of the bait and treatment fractions, quantification of the elution fractions

showed that there was less protein present in the acrolein-treated PTEN treatment control elution fractions in comparison to the acrolein-treated PTEN pull down assays (Table 5.4). Due to the risk of aggregation during acrolein-treatment due to protein modification, the stacking gel was retained during staining to allow detection of aggregate bands. However, whilst there were some higher molecular weight bands indicating some cross-linking, there was no aggregated protein detected in the stacking gel (Supplementary Figure 2). The lower amount of total protein eluted in the treatment control could suggest aggregation on the column, but as this is not occurring in the acrolein-treated PTEN pull downs where the same acrolein treatment was used, this was attributed to the additional NaBH₄ reduction step.

Table 5.4 Quantification of the Total Protein in the Fractions collected during the Pull Down Assays

Fraction	Total Amount of Protein (µg) (Average ± SEM (n=3))				
	Pull Down		Bead-only Control		Treatment Control
	0 µM Acrolein	100 µM Acrolein	0 µM Acrolein	100 µM Acrolein	100 µM Acrolein
Bait Flow-through	69.2 ± 11.4	80.0 ± 13.9	N/A	N/A	74.4 ± 21.0
Bait Wash	38.3 ± 1.5	37.2 ± 3.4	N/A	N/A	40.2 ± 6.0
Treatment Flow-through	8.5 ± 1.9	7.0 ± 1.2	N/A	N/A	8.5 ± 1.9
Treatment Wash	1.5 ± 0.8	1.7 ± 0.6	N/A	N/A	3.0 ± 1.7
Prey Flow-through	583.9 ± 169.8	579.1 ± 192.2	536.6 ± 181.2	585.0 ± 180.6	N/A
Prey Wash	24.0 ± 24.0	23.6 ± 23.6	23.7 ± 23.7	24.4 ± 24.4	N/A
Elution	121.3 ± 18.4	103.6 ± 9.8	15.5 ± 2.5	16.7 ± 2.9	45.8 ± 3.2

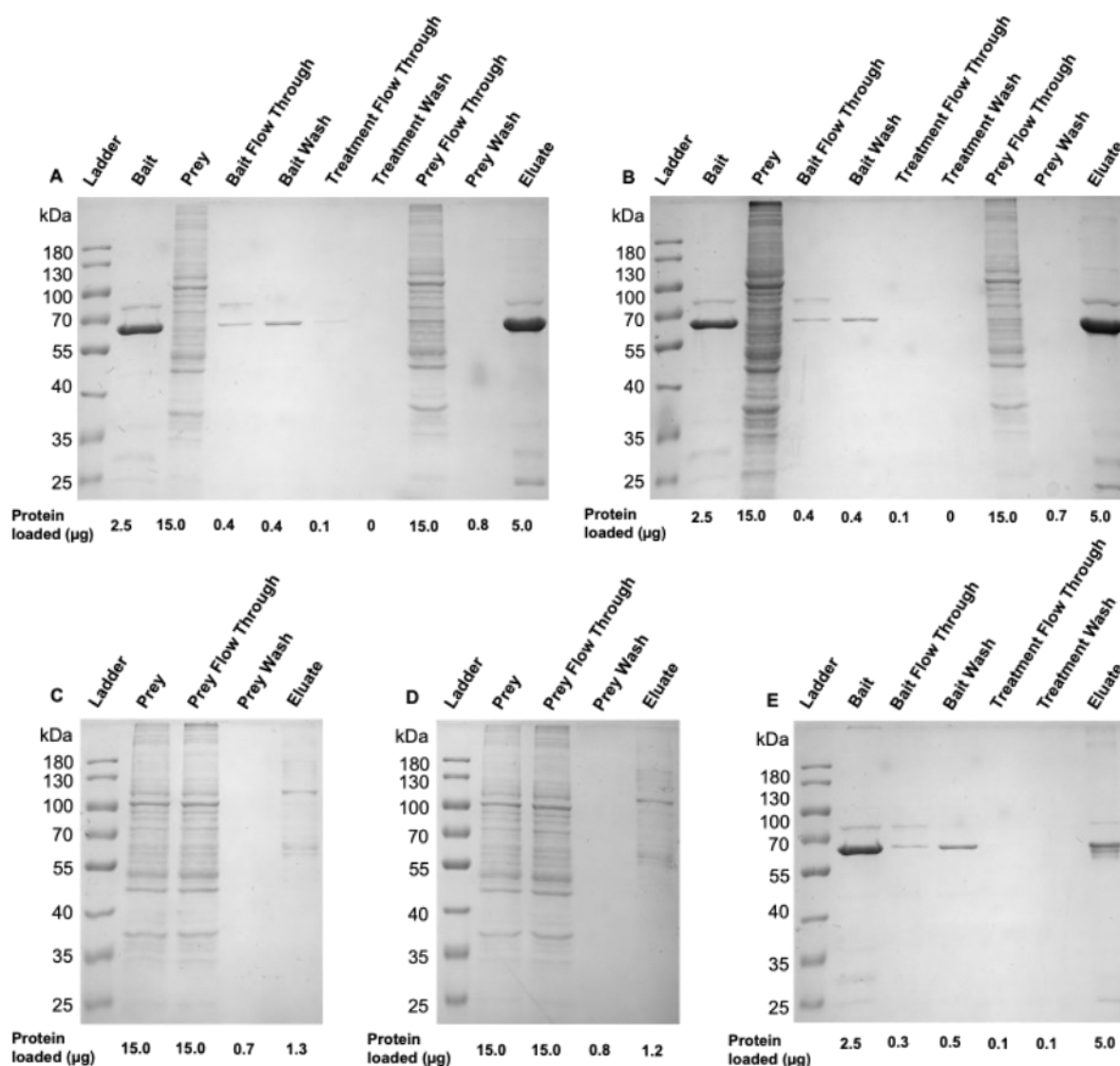


Figure 5.4 SDS-PAGE Analysis of the Fractions Obtained During Nickel Affinity Pull Down Assays with and without Acrolein Treatment of PTEN-V5-His.

The fractions obtained for the untreated PTEN pull down (A), the acrolein-treated PTEN pull down (B), the untreated bead-only pull down (C), the acrolein-treated bead-only pull down (D) and the treatment control (E) were analysed using a 12% polyacrylamide gel stained with Coomassie Blue. The bait refers to the purified PTEN-V5-His immobilised onto the nickel resin support and the prey refers to HCT-116 lysate proteins. Flow-through refers to the fractions obtained after bait exposure, treatment or prey exposure which include any proteins that did not bind or were eluted in each of these steps. The wash fractions refer to the fractions obtained during the washes performed after each incubation and treatment step, when washing away any unbound bait or prey proteins or excess acrolein, if present. The elution fraction refers to the final fraction that was eluted from the resin using a high concentration of imidazole. For (A) and (B), the elution fraction contained the PTEN-V5-His and any interacting proteins from the HCT-116 lysate. For (C) and (D), the elution fraction contained any proteins from the HCT-116 lysate that bound non-specifically to the nickel resin. For (E), the elution fraction contained only acrolein-treated PTEN-V5-His.

To increase the protein coverage during LC-MS/MS, the pull down elution fractions were resolved using SDS-PAGE prior to in-gel digestion. This gave an element of separation of the different proteins present in the sample based on their molecular weight and gel mobility. The purpose of this separation was to lower the complexity of the sample during LC-MS/MS analysis and give lower abundance proteins a better chance of being detected. If the sample

was not resolved on a gel prior to digestion, the huge amount of bait PTEN protein present in the sample pool could have caused lower abundance proteins not to be detected, as during MS/MS analysis the selection parameters for peptide fragmentation were the top 10 most abundant peptides during each scan. Figure 5.5 shows a representative SDS-PAGE image of the proteins present in each of the pull-downs. To increase the amount of protein present in each gel slice, and increase the likelihood of capturing lower abundance proteins in the interactor identification step, the amount of protein per lane was increased in comparison to Figure 5.4, where only visual comparison was desired. As expected, in the untreated and acrolein-treated pull downs the PTEN-V5-His band at 60 kDa was very strong, with some additional higher and lower molecular weight bands corresponding to both non-specific resin interactors as well as potential specific PTEN interactors. In the untreated and acrolein-treated bead-only pull downs, there was no band at 60 kD as expected as no PTEN was added as bait, but there were some higher molecular weight bands corresponding to non-specific binding of the HCT-116 lysate proteins to the resin. As expected from the quantification results in Table 5.4, visualisation of the acrolein-treatment control showed that the PTEN-V5-His band at 60 kDa was much smaller in size and the higher molecular weight (>180 kDa) aggregate bands were even more apparent.

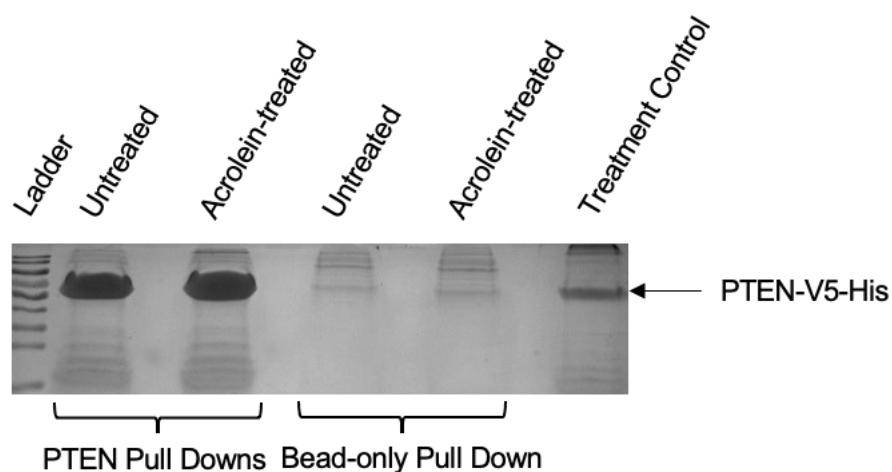


Figure 5.5 Representative SDS-PAGE Analysis of the Proteins Obtained from the Elution Fractions during the Pull Down Assay.

20 μ g of the elution fractions of the untreated and acrolein-treated pull-down assays, 2 μ g of the untreated and acrolein-treated bead-only controls and 5 μ g of the acrolein-treated PTEN treatment control were resolved on a 12% polyacrylamide gel stained with Coomassie Blue. A blank lane was left between samples to minimise any cross-over between the different samples. The PTEN pull downs and bead-only pull down lanes were excised into 9 bands, where for the treatment control only the 60 kDa PTEN band and the aggregate band at the stacking gel was excised. In-gel digestion with trypsin was performed on each band and the digests were taken forward for LC-MS/MS analysis.

5.3.3 Acrolein Treatment of Immobilised PTEN=V5-His Successfully Modified Susceptible Residues

Due to the changes in experimental format, whereby the PTEN-V5-His was immobilised onto a nickel resin support and the acrolein treatment was performed at RT on an end-over-end rotator for 1h in comparison to a static incubation at 37°C for 10 minutes, as described in section 5.2.4, an acrolein-treated PTEN treatment control was included. The treatment control involved immobilisation and acrolein treatment of PTEN with an additional NaBH₄ reduction step but there was no exposure to prey proteins and the PTEN was incubated with an equivalent wash buffer. This allowed identification of acrolein modified residues to ensure that the treatment was successful. Table 5.5 details the modifications identified for the PTEN-V5-His treatment control. In comparison to the total acrolein modifications identified in Chapter 4, all modifications identified in the treatment control were also identified in the original analyses. There were 3 acrolein modifications mapped to the 2:1 acrolein:PTEN monomeric PTEN band in Chapter 4, C71, C83 and C250. Acrolein modification to K6 was identified previously in Chapter 4, but at higher treatment concentrations of 10:1 and 20:1 acrolein:PTEN. The identification of this modification at a lower treatment concentration could be explained by the longer treatment time.

Table 5.5 Acrolein Modification of Immobilised PTEN-V5-His Identified by LC-MS/MS

Modified Residue	Modified Peptide	Modification
K6	M.TAIKEIVSR.N	Michael addition
C71	K.IYNLCAER.H	Michael addition
C83	R.HYDTAKFNCR.V	Michael addition
C250	K.FMYFEFPQPLPVCGLDIK.V	Michael addition

5.3.4 PTEN-specific Interactors were Identified from the Affinity Pull Down Assays

The PTEN-specific interactors were identified using Mascot and quantified using Progenesis Q1 for proteomics, using the thresholding parameters outlined in section 5.2.5. Figure 5.6 shows the reduction in protein hits as the thresholds are applied, giving 60 potential specific PTEN interactors that were found in both the untreated and acrolein-treated pull down assays but not in either the untreated or acrolein-treated bead-only controls. Comparison of the 60 identified proteins against the BioGRID database highlighted a high number of novel potential interactors with PTEN, where out of 60 specific PTEN interactors, only 5 proteins had previously been identified as interactors of PTEN using physical evidence in the BioGRID database (Stark et al., 2006).

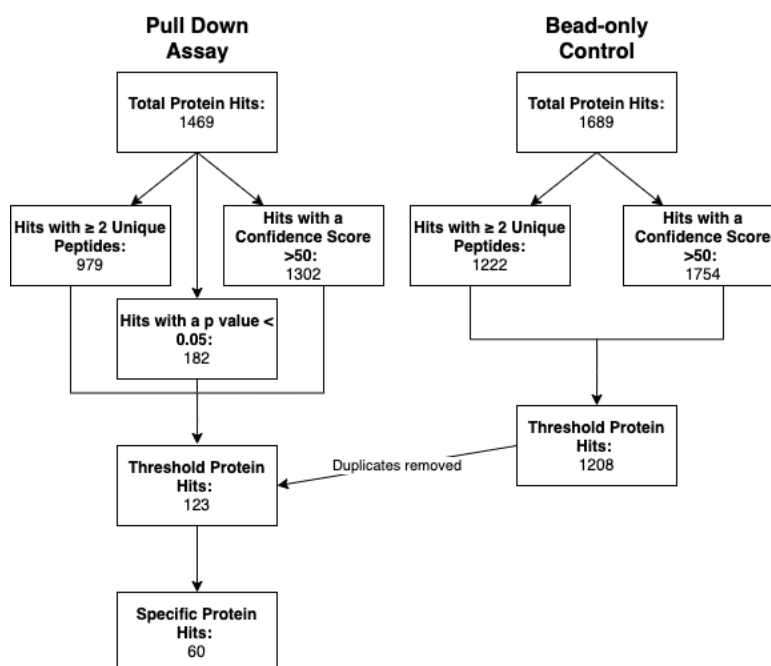


Figure 5.6 Overview of the Number of Proteins Obtained during the Pull Down Assays with and without Acrolein.

5.3.5 PTEN-specific Interactors Showed a Change in Abundance Between the Untreated and Acrolein-treated PTEN Pull Downs

Interactors were categorised as showing a difference in affinity where there was a >2-fold difference in abundance in the pull down with untreated compared to acrolein-treated PTEN. Interactors with <2-fold difference in abundance were categorised as showing no change in affinity between treatments. Previous high-data content PTEN interactome studies comparing interactors with untreated and oxidised PTEN or a wild-type and G20E mutant set this threshold >2 and >2.5-fold change in abundance (Verrastro et al., 2016, Gunaratne et al., 2011). Whilst 22 of the 60 PTEN-specific protein interactors showed no difference in abundance between the acrolein-treated and the untreated pull downs, 19 interactors showed a higher abundance in the untreated pull down and 19 showed higher abundance in the acrolein-treated pull down. Table 5.6 lists the 38 PTEN-specific interactors that showed a change in abundance, along with their threshold parameter values for unique peptides, confidence score and Anova (p), their fold change and in which pull down they showed the highest abundance. Supplementary Table 3 lists the 123 PTEN-specific interactors that were identified, including those that did not meet the threshold parameters.

Table 5.6 PTEN-Specific Interactors Identified by the Pull Down Assay that met the Threshold Parameters and Showed a Change in Abundance between the Acrolein-treated and Untreated Pull Down Assays

Accession¹	Protein Name	Unique Peptides[@]	Confidence Score[£]	Anova (p)[§]	Max. Fold Change	Highest Abundance
ACSF2_HUMAN	Medium-chain acyl-CoA ligase ACSF2, mitochondrial	7	114.47	0.0011	6.6	Control
AMOT_HUMAN*	Angiomotin	4	69.52	0.0072	5.1	Control
AN32E_HUMAN	Acidic leucine-rich nuclear phosphoprotein 32 family member E	3	175.92	0.0179	2.9	Control
BOLA2_HUMAN	BolA-like protein 2	2	116.63	0.0163	3.2	Control
BRD2_HUMAN	Bromodomain-containing protein 2	8	655.25	0.0064	2.1	Control
CADH6_HUMAN	Cadherin-6	3	79.62	0.0399	4.1	Treated
CHD3_HUMAN	Chromodomain-helicase-DNA-binding protein 3	3	152.11	0.0430	2.6	Treated
CHD7_HUMAN	Chromodomain-helicase-DNA-binding protein 7	5	276.41	0.0212	4.7	Treated
CHD9_HUMAN	Chromodomain-helicase-DNA-binding protein 9	2	335.78	0.0319	28.6	Treated
COA7_HUMAN	Cytochrome c oxidase assembly factor 7	2	155.81	0.0069	18.9	Treated
CSN2_HUMAN	COP9 signalosome complex subunit 2	4	214.29	0.0345	2.1	Control
CWC22_HUMAN	Pre-mRNA-splicing factor CWC22 homolog	24	1118.15	0.0060	2.0	Treated
EIF3I_HUMAN	Eukaryotic translation initiation factor 3 subunit I	3	161.87	0.0106	2.5	Control
FLNC_HUMAN	Filamin-C	5	214.15	0.0133	5.5	Control
HDGR2_HUMAN	Hepatoma-derived growth factor-related protein 2	4	384.18	0.0222	2.3	Control
HECD1_HUMAN	E3 ubiquitin-protein ligase HECTD1	34	1847.88	0.0372	5.1	Treated
IQEC2_HUMAN	IQ motif and SEC7 domain-containing protein 2	3	71.58	0.0038	3.1	Treated

Chapter 5 – Effect of Acrolein on the Global Interactome of Recombinant PTEN

IQGA2_HUMAN	Ras GTPase-activating-like protein IQGAP2	2	178.05	0.0189	2.4	Treated
LYSC_HUMAN	Lysozyme C	2	53.91	0.0011	6.9	Treated
PERT_HUMAN	Thyroid peroxidase	4	78.77	0.0000	16.2	Control
PPR29_HUMAN	Protein phosphatase 1 regulatory subunit	2	60.63	0.0083	2.8	Treated
RCN1_HUMAN*	Reticulocalbin-1	4	140.35	0.0033	7.5	Treated
RIC8A_HUMAN	Synembryn-A	3	72.54	0.0016	5.9	Control
RL22L_HUMAN	60S ribosomal protein L22-like 1	2	281.25	0.0077	2.7	Control
RL37A_HUMAN	60S ribosomal protein L37a	3	195.39	0.0024	7.6	Control
RM12_HUMAN	39S ribosomal protein L12, mitochondrial	2	122.66	0.0207	2.0	Treated
RS28_HUMAN	40S ribosomal protein S28	3	205.25	0.0020	19.5	Control
RS29_HUMAN	40S ribosomal protein S29	4	203.77	0.0064	21.7	Control
RT4_HUMAN	28S ribosomal protein S14, mitochondrial	3	261.1	0.0445	6.5	Control
RT24_HUMAN	28S ribosomal protein S24, mitochondrial	2	65.48	0.0001	210.5	Control
SRP09_HUMAN	Signal recognition particle 9 kDa protein	4	241.46	0.0003	7.7	Control
TBCD1_HUMAN	TBC1 domain family member 1	3	58.21	0.0065	13.5	Treated
THS7A_HUMAN	Thrombospondin type-1 domain-containing protein 7A	5	115.89	0.0093	3.0	Treated
TIM50_HUMAN	Mitochondrial import inner membrane translocase subunit TIM50	4	198.77	0.0227	2.1	Treated
TSR1_HUMAN	Pre-rRNA-processing protein TSR1 homolog	4	243.71	0.0117	2.7	Treated
UBR4_HUMAN	E3 ubiquitin-protein ligase UBR4	12	712.75	0.0077	4.4	Treated

Chapter 5 – Effect of Acrolein on the Global Interactome of Recombinant PTEN

USP9X_HUMAN*	Probable ubiquitin carboxyl-terminal hydrolase FAF-X	24	2754.68	0.0170	15.8	Control
VP13B_HUMAN	Vacuolar protein sorting-associated protein 13B	3	74.47	0.0251	15.8	Treated

Key:

!: SwissProt Protein ID

@: The number of unique peptides used for quantification

£: The protein confidence score for each protein assigned by Mascot

\$: The p-value generated by Progenesis QI for proteomics

*: Previously identified as a PTEN interactor with physical evidence in the BioGRID database (Stark et al., 2006).

There were no specific interactors that met the threshold criteria that were found only in the control or acrolein-treated pull down, where any fold changes were seen up to between 2 and 210-fold. This was to be expected as the aim during acrolein-treatment was to elicit acrolein modification of residues whilst avoiding such extensive modification that the protein becomes completely unfolded. Figure 5.7 highlights some of the interesting PTEN-specific interactors identified during the affinity pull downs. Whilst acrolein-modification to PTEN did not alter the affinity to the two signalling proteins highlighted in Figure 5.7, they are potentially novel PTEN interactors that have not previously been identified in the BioGRID database (Stark et al., 2006). Interestingly, similar isoforms of MAPK2, MAPK1, MAP2K3 and MAP2K6, have previously been identified as interactors of PTEN. Ubiquitination is an important regulatory mechanism of PTEN, as discussed in section 1.2.6, and some of the PTEN interactors with the highest number of identifications are proteins involved in ubiquitination, such as the ubiquitin protein ligases, NEDD4 and WWP2, and the ubiquitin specific peptidases, USP13 and USP7 (Stark et al., 2006). RBBP6, HECTD1 and UBR4 are ubiquitin protein ligases identified in this current study that have not previously been identified as an interactor of PTEN (Stark et al., 2006). Whilst HECTD1 and UBR4 showed a large fold-change in abundance in the acrolein-treated pull down, the abundance of RBBP6 was unchanged. An alternative isoform of RBBP6, RBBP5, has previously been reported as a PTEN interactor (Stark et al., 2006).

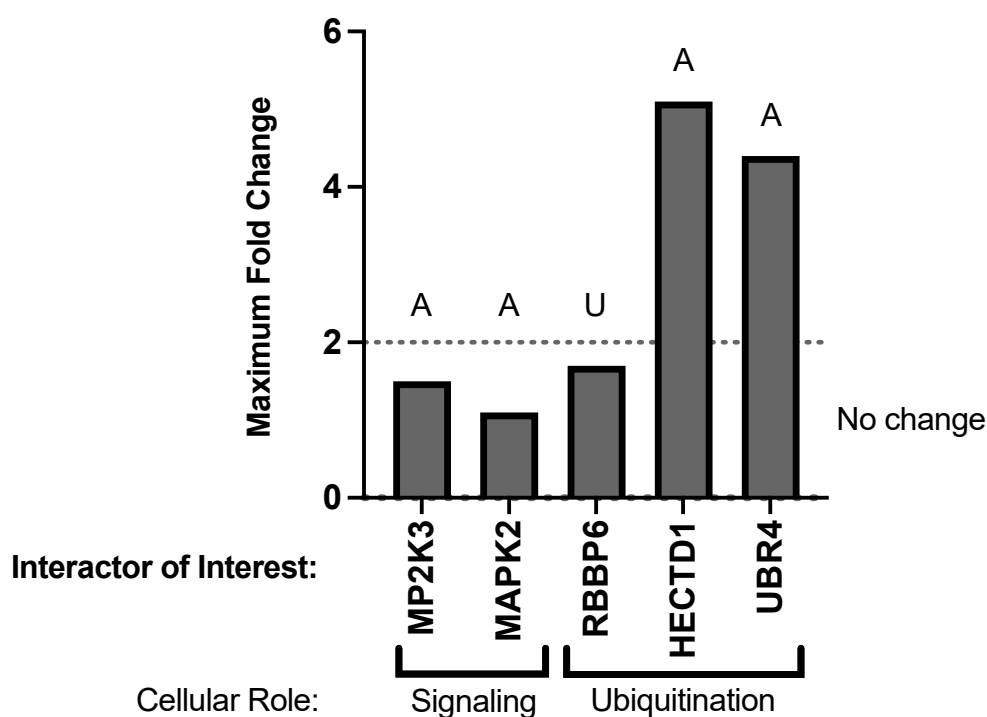


Figure 5.7 Comparison of the Maximum Fold Change in Abundance of Interactors of Interest between Control and Acrolein-treated PTEN.

A= fold change in the acrolein-treated PTEN pull down, U = fold change in the untreated PTEN pull down.

5.3.6 Validation of an Acrolein-sensitive Interactor using Western Blotting

To validate one of the specific interactors of interest, western blot analysis was performed with the elution fractions of the APDs probing for HECTD1. HECTD1 is a ubiquitin ligase involved in the regulation of protein degradation via the ubiquitination pathway. HECTD1 was chosen as an interactor of interest due to role of ubiquitination in the regulation of PTEN, and the previous evidence of other E3 ubiquitin ligases as specific interactors of PTEN with functional roles in its regulation and localisation, as described in section 1.2.6. The expected molecular weight for HECTD1 is 290 kDa. Due to the issues that can arise during the transfer of a protein of this size and to ensure that HECTD1 can be detected, a trial western blot transfer was performed. The membranes were stained with Ponceau S confirm protein transfer before probing for the target proteins (Figure 5.8A). There were clear pink bands across the length of the blot which confirmed the successful transfer of proteins <200 kDa. Strategies to improve the transfer of higher molecular weight proteins can include the use of longer transfer times or the inclusion of SDS in the transfer buffer. Trial transfers of HCT-116 lysate proteins were conducted in the presence and absence of SDS and the membrane and gel were stained with Ponceau S and Coomassie Blue, respectively, post-transfer to check for transfer of proteins from the gel to the membrane (Supplementary Figure 3). The post-transfer Coomassie stain of the gels confirmed that in the presence of SDS (Supplementary Figure 3A) higher molecular weight proteins are more efficiently eluted from the gel than in the absence of SDS (Supplementary Figure 3B) as there are fewer bands in the upper part of the gel. However, the Ponceau S staining of the membrane showed that no bands were present after transfer with SDS (Supplementary Figure 3C), whilst there were bands across the length of the membrane when transferred without SDS (Supplementary Figure 3D). This could be due to inhibition of protein binding to the membrane by SDS. A shorter transfer time at a higher voltage was also tested, which showed a similar profile of results whereby when the transfer was performed in the presence of SDS there was more efficient elution of higher molecular weight proteins from the gel but the protein did not bind to the membrane (Supplementary Figure 4).

Trial western blots were performed against HECTD1 and α/β -tubulin. The use of α/β -tubulin as a control was due to its size of 50 kDa, which is favourable for an effective transfer, and its high cellular abundance. The membrane was stained with Ponceau S to check for efficient transfer (Figure 5.8). The membrane was probed with either HECTD1 (Figure 5.8B) or α/β -tubulin (Figure 5.8C). Western blot analysis against HECTD1 in HCT-116 lysates was performed as per section 2.3.4, with no amendments due to the lack of improvement in transfer of high molecular weight proteins with the trialled changes above. Probing for HECTD1 (Figure 5.8B) gave multiple bands ranging from 80 kDa to <50 kDa. Identification of multiple bands

can be explained by non-specific binding or, as the bands are a lower molecular weight than the target protein, protein degradation during lysis and clarification. Probing for α/β -Tubulin (Figure 5.8C) gave bands at 50 kDa, which is the correct molecular weight for the protein. The same lysate was used for both blots and there are no lower molecular weight bands identified when probing for α/β -Tubulin. In addition, the lysis and clarification of the lysate was performed in the presence of protease inhibitors, which inhibits corresponding proteases, at 4°C, which drastically reduces the activity of the proteases not covered by the inhibitors in the cocktail. Taken together, this suggests that there should not have been not an issue with protein degradation during lysis and clarification. The appearance of multiple bands could be due to the relatively long exposure time of 2.5 minutes, in comparison to the exposure time for the α/β -tubulin of 12 seconds. This is likely explained by the relative abundances of both proteins, as α/β -Tubulin is routinely used as a loading control due to its high abundance in cells, whereas it could reasonably be expected that the abundance of HECTD1 would be much lower.

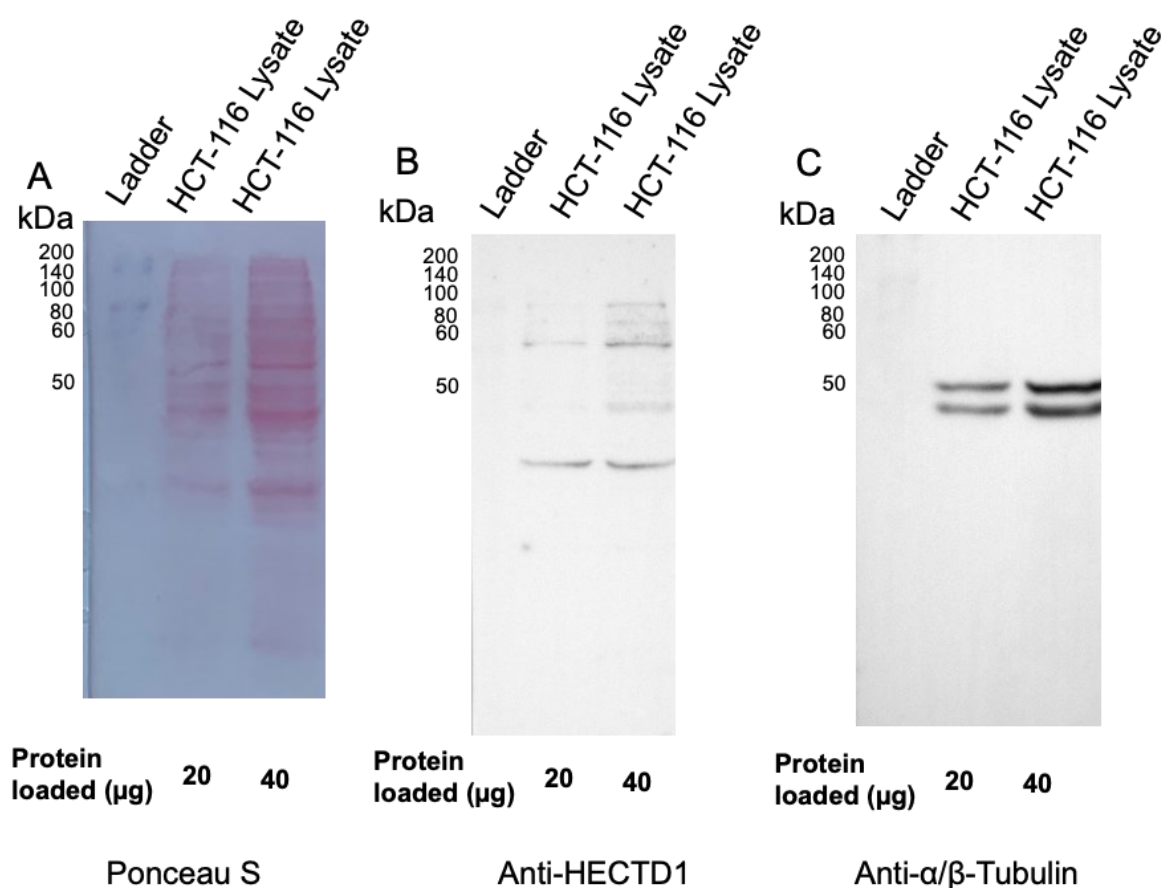


Figure 5.8 Western Blot Analysis of HCT-116 WT lysate against HECTD1 and α/β -Tubulin.

Increasing amounts of a HCT-116 lysate was analysed by Western Blot. After transfer overnight at 30V, the blots were stained with Ponceau S (A). The blots were blocked with 5% Milk/TBS-T overnight before probing for HECTD1 using a Rabbit Anti-HECTD1 polyclonal Ab (B) or α/β -Tubulin using an Anti- α/β -Tubulin polyclonal antibody (C).

As the planned use for the antibody was against the APD samples, where the sample would be enriched for PTEN and, therefore its interacting partners, it would be expected that HECTD1 would be present in these samples at comparatively higher concentrations than a whole lysate. The elution fractions from the control APD performed with untreated PTEN and acrolein-treated PTEN were analysed by western blot alongside the HCT-116 lysate used for the pull downs (Figure 5.9). Figure 5.9A confirms transfer of the lysate and APD elution fractions, with a clear band in the elution lanes for PTEN at approximately 60 kDa. There is no band for HECTD1 at 280 kDa in the HCT-116 lysate lane, which is likely due to a low abundance of the protein in whole cell lysate. There is also no band in the control APD elution lane, but there is a band at >170 kDa in the acrolein APD elution lane which matches the correct molecular weight for HECTD1 (280 kDa). Whilst the quantification results from Progenesis Q1 identified HECTD1 in both the control and acrolein-treated PTEN APDs, there was a clear increase in the abundance of HECTD1 in the acrolein APD in comparison to the control, where the maximum fold change was 5.1 (Table 5.6). This could explain why instead of seeing a band in both the control and the acrolein APD elution fractions, there is no visible band in the control APD sample and a faint band visible in the acrolein APD sample. The results from Figure 5.9B do not exactly match the quantification results from Progenesis Q1 as no HECTD1 was detected in the untreated elution. The differences could be explained by consideration to the differences in the techniques used, where on digestion there is no disadvantage conveyed by the large size of HECTD1 by LC-MS/MS but there are difficulties in analysis of large proteins by western blot. There is also a band at 60 kDa corresponding to the bait protein, PTEN-V5-His, which would not be expected due to the specificity of the anti-HECTD1 Ab and the absence of an anti-PTEN Ab. This could be due to the high concentration of PTEN in the sample in combination with the polyclonal nature of the anti-HECTD1 Ab, which could cause non-specific binding.

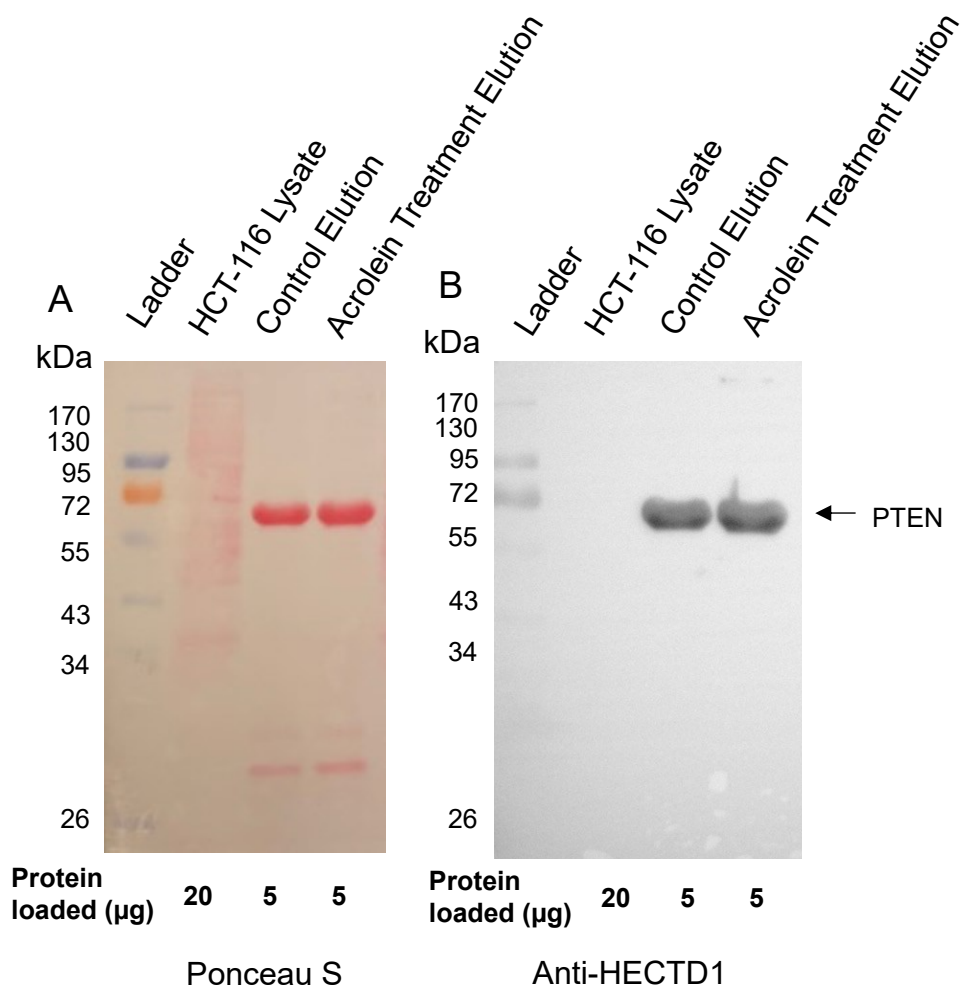


Figure 5.9 Representative Western Blot Analysis of a Potential Acrolein-Sensitive PTEN Interactor; HECTD1 20 μg of HCT-116 lysate and 5 μg of the elution fractions collected from the control and acrolein-treated APDs were analysed by Western Blot. After transfer overnight at 30V, the blots were stained with Ponceau S (A). The blots were blocked with 5% Milk/TBS-T overnight before probing for HECTD1 with a Rabbit Anti-HECTD1 polyclonal Ab (B).

5.4 Discussion

To investigate any changes in PTEN's interactome due to lipoxidative modification, the third aim of this thesis was to capture and identify interactors of untreated and acrolein-treated PTEN. To achieve this, APD conditions were identified by optimisation of the chromatography to allow immobilisation and treatment of PTEN-V5-His whilst minimising any non-specific binding on subsequent exposure to HCT-116 lysate proteins. This involved testing APD formats as well as the formulation of the chromatography buffers, where the effect of increasing imidazole concentration was characterised for both the retention of the immobilised PTEN-V5-His and the prevention of non-specific binding of HCT-116 lysate proteins. Once the optimal conditions were identified, APDs were performed using untreated and acrolein-treated PTEN-V5-His, with the inclusion of an appropriate treatment control to characterise the acrolein modification of PTEN-V5-His in this format, as well as bead-only controls to identify any non-specific interactors with the resin. Interactors were analysed using LC-MS/MS after an in-gel tryptic digest and identified using Mascot before comparison of their relative abundance across the different treatment conditions using Progenesis QI for proteomics.

The first key finding for this chapter was the conditions for the APD, where a spin-column format was identified as the most suitable for APD, with more complete washes and a reduced loss of bound protein from the practical difficulties that can occur when aspirating resin. 5 mM imidazole concentration was identified as suitable for use during prey-exposure, with a compromise on maximising PTEN-V5-His retention whilst ensuring reduction of non-specific binding. The second key finding was that, whilst there were common interactors of both untreated and acrolein-treated PTEN-V5-His that showed no change in abundance, a significant proportion of interactors showed a change in abundance across the two treatment conditions. HECTD1, an E3 ubiquitin ligase, was identified as an interactor of interest that showed an increase in abundance in the acrolein-treated APD and this interaction was validated using Western Blotting

The strategy developed in this thesis to capture of protein interactors of PTEN involved the use of a recombinant PTEN-V5-His protein, expressed in *E. coli* and purified using IMAC as described in Chapter 3, as the bait protein with subsequent exposure to prey HCT-116 lysate prey proteins *in vitro*. An alternative approach could have been a direct APD of recombinant PTEN expressed in mammalian cells. There were two main considerations during the development of the experiment: the source of PTEN and the method for introduction of acrolein modifications. The approaches to preparation of recombinant PTEN and the

execution of a pull down assay used in previous high-data content PTEN interactome studies using APD are outlined in Table 5.7 (modified from Smith et al. (2021)).

Table 5.7 Summary of APD Methods for Bait Preparation and PPI Isolation (modified from Smith et al. (2021))

Study	Assay	Fusion Protein	Tag size (amino acids)	Pull Down Conditions	
				Resin	Expression Host
Crockett et al. (2005)	In vitro APD ^A	PTEN-His ^{IU}	6	Nickel-Agarose	<i>E. coli</i> (not specified)
Herlevsen et al. (2007)	Direct APD ^B	PTEN-HA@ ^C	31	Anti-HA Agarose	Mammalian (UMUC-3)
Ahn et al. (2008)	Direct APD ^B	PTEN-HA@ ^U	31	Anti-PTEN monoclonal antibody-conjugated agarose	Murine (NIH 3T3)
Gunaratne et al. (2011)	PAP ^C -SILAC ^D	Wild type: PTEN-FLAP ^{£U}	243	Anti-FLAG or Anti-GFP	Mammalian (LN299 & U87)
	TAP ^E	Mutant: G20E PTEN-FLAP ^{£U}		Anti-GFP & Anti-S-protein	
Maddika et al. (2011)	TAP ^E	PTEN-SFB ^{\$U}	61	Streptavidin-Sepharose & Anti-S-protein Agarose	Mammalian: (293T)
Verrastro et al. (2016)	In vitro APD ^A	PTEN-GST ^{%N}	211	Glutathione Agarose	<i>E. coli</i> (DH5α)

Key:

Assay type

A: *In vitro* Affinity Pull Down (APD) – Recombinant PTEN expressed and purified from *E. coli* before exposure to mammalian cell lysates *in vitro*

B: Direct Affinity Pull Down (APD) – Recombinant PTEN expressed in mammalian cells before direct APD from the host cell lysate.

C: Parallel affinity purification (PAP)

D: Stable Isotope Labelling of Amino Acids in Cell Culture (SILAC)

E: Tandem Affinity Purification (TAP)

Tags

!: Polyhistidine tag

@: Haemagglutinin (HA) tag

£: FLAG–Green Fluorescent Protein (GFP)–S-protein (FLAP) tag

\$: S-protein–FLAG–Streptavidin-binding peptide (SFB) tag

?: Glutathione–S–Transferase (GST) tag

C: C-terminal tag

N: N-terminal tag

U: Unknown tag location

All 6 studies made use of a recombinant PTEN protein with one or more tags which gave a route to its capture using a complementary chromatography resin against the tag. This approach removes the requirement of a specific PTEN antibody, used for untagged PTEN, which gives the ability to scale more easily at a reduced cost. However, Ahn et al. (2008) used an anti-PTEN antibody conjugated resin, rather than an anti-HA resin. As discussed in Chapter 3, there are advantages and disadvantages to the use of tags as well as the choice of expression system in recombinant protein production. Briefly, whilst a tag is required for this downstream application, the size, number, and characteristics of the tag(s) and their potential effect on interactions needs to be considered. The location of the tag, whether it is on the C- or N-terminus of a protein, could also have an effect. Larger tags, such as a GST tag or a FLAP tag, have an increased risk of affecting the 3D structure of PTEN and the accessibility of any binding sites that are in its proximity. Larger tags could be expected to have an increased number of potential interactors themselves, although this limitation can be addressed by the use of a tag-only control pull down to identify specific interactors of the tag and subsequently eliminating duplicates from the list of potential interactors identified in the protein-tag pull down. Smaller tags have the advantage in that they are less likely to have an effect on the overall 3D structure of the protein. When considering the use of a tagged recombinant protein in a pull down that incorporates induction of a post-translational modification, it is important to note that the tag may also be modified if it contains vulnerable residues. This highlights the importance of selecting a tag with a suitable size and composition of a tag of the downstream applications.

Whilst all affinity tags that are used in the production of recombinant proteins and their downstream applications rely on a specific interaction between the tag and the resin, some resins have a higher specificity than others (Zhao et al., 2013). When considering the use of a His-tag, whilst the tag is small, the resin specificity is lower as there is a risk of non-specific binding by histidine rich proteins to the resin. This limitation can be reduced by the use of a bead-only control, as performed in this chapter, to identify resin interactors. The recombinant PTEN used here has a V5 tag and in addition to a his-tag. The V5 tag is a small bacteriophage epitope that is 14 amino acids long with a sequence of GKPIPPLLGLDST. Whilst the his-tag is commonly used for purification or affinity capture, the V5 tag is often used for detection (Kimple et al., 2013). Capture of the V5 tag is through a specific antibody, and there is a limitation when probing in conjunction with mammalian lysates as cross reactivity has been reported (Kimple et al., 2013). Although it was not done in this current study, the presence of both the his-tag and the V5-tag in PTEN-V5-His would provide the opportunity to use TAP or PAP. As described in section 5.1.2, TAP and PAP are developments on the original APD approach and can help to reduce false positive resin-specific interactors. Weak and transient

interactors are harder to capture using chromatography techniques, such as APD or CoIP, due the required wash steps to remove unbound protein and this is exacerbated with the use of tandem affinity purification, where two purifications are performed back-to-back. TAP reduces the overall rate of false positives but also increases the risk of false negatives, where PAP provides a compromise on this (Table 5.8).

Table 5.8 Advantages and Disadvantages of Affinity Chromatography Methods for PPI Isolation (reproduced with permission from Smith et al. (2021))

Method	Identifies:				False positives (resin bias)	False negatives (> 1 step purification)
	Direct interactors	Indirect interactors	Weak interactors	Transient interactors		
Affinity Pull Down	✓	✓	✓	✓	✓	↓
Tandem Affinity Purification	✓	✓	↓	↓	↓	↑
Parallel Affinity Purification	✓	✓	✓	✓	↓	↓

When performing small-scale chromatography, it is possible to use either a spin column, where there is an insert with a fixed filter that permits complete separation of buffer/sample from the resin during centrifugation, or a tube where separation is achieved by centrifugation and subsequent aspiration of the supernatant. The lack of manual aspiration when using a spin column not only speeds up the process but it also reduces loss of resin and achieves a better separation between different stages of the chromatography as each wash is completely removed. Although the design of these APD experiments included the use of a resin-only control, as discussed above, it was important to identify a suitable concentration of imidazole to reduce non-specific binding. The IMAC resin used here could not tolerate any imidazole in the binding buffers when used in a batch purification format, but as the PTEN-V5-His was already purified it was not necessary to include any in the binding buffer, nor use any low concentration imidazole washes as a clean-up step prior to acrolein treatment and prey exposure. This is a benefit as the purity and amount of PTEN-V5-His was identical across the different pull down conditions, reducing technical variation between the treatment conditions. A previous interactome study using PTEN-His used 50 mM imidazole in the APD binding and wash buffers, with 300 mM imidazole used in the elution buffer (Crockett et al., 2005). The use of 50 mM imidazole in the binding and wash buffers is much higher than the 1 mM imidazole used in the original purification strategy in Chapter 3, and the 5 mM imidazole determined as optimal for use during APD in this chapter. This could be explained by the differences in binding affinity for different resins, where some nickel affinity resins have a

higher tolerance for the presence of imidazole. Different recombinant proteins could also have different availability for resin binding depending on their tertiary structure.

The expression system used determines the type of APD performed, where production in *E. coli* requires purification prior to exposure to mammalian cell lysates to study mammalian PPIs, overexpression directly in the mammalian cell of interest removes this additional step. There are considerations on the effect of production of the protein of interest in a prokaryotic system instead of a eukaryotic system, due to a lack of post-translational modification machinery (Sahdev et al., 2008, Baeshen et al., 2015, Tripathi and Shrivastava, 2019). However, as mentioned previously recombinant PTEN expressed in *E. coli* has been used in a wide range of studies, including those into its structure, phosphatase activity, and interactome (Li and Sun, 1997, Myers et al., 1997, Maehama and Dixon, 1998, Lee et al., 1999, Redfern et al., 2008, Heinrich et al., 2015, Crockett et al., 2005). But, the majority of the high-throughput interactome studies have expressed PTEN in mammalian cells (Herlevsen et al., 2007, Ahn et al., 2008, Gunaratne et al., 2011, Maddika et al., 2011). Although expression of PTEN in *E. coli* produces an active protein suggesting correct conformation for catalysis, post-translational modification status is important for interactions and the disadvantage this may give would be on a protein-by-protein basis. Expressed and purified PTEN requires an *in vitro* pull down where mammalian cells are lysed separately and the bait is exposed to whole lysates *in vitro*. More physiological interactors might be expected on direct pulldown from mammalian cells where the recombinant protein is expressed *in situ*, due to the importance of localisation and spatiotemporal control of protein expression on PPIs (Westermarck et al., 2013). However, on lysis of the cells in a direct pull down, there will be also be a mix of proteins from different subcellular compartments and so binding of non-physiological interactors is remains a risk with this technique (Berggard et al., 2007).

Crucially to this thesis, a direct pull down is more suitable to interactome studies into the effect of mutation on the interactome of PTEN, as this is introduced at a genetic level, rather than post-translational modification. This approach has previously been used by Gunaratne et al. (2011) for wild type PTEN and a cancer-associated mutant, G20E. As discussed in section 5.1.2, there are several difficulties in induction of post-translational modification endogenously and the treatment of whole cells is unlikely to yield the same protein modification profile as *in vitro* treatment due to the presence of other cellular proteins. Instead of targeted modification to the protein of interest, any susceptible residue on any cellular protein could be modified and the level of modification could be hard to monitor and reproduce. This is because without the use of specialist techniques, as reviewed by Wang et al. (2022) and discussed in section 5.1.2, the target protein would not be directly modified giving a lack of control of the extent of

modification. Other cellular proteins would also be modified adding another layer of complexity in unravelling the cause behind a change in individual interactions, as both the bait and the prey would be modified. Beyond this, treatment of whole cells with acrolein has been shown to alter signal transduction by reduction of activity of key signalling proteins, such as protein kinases and phosphatases, as well as induction of oxidative stress and mitochondrial disruption (Moghe et al., 2015). Taken together, whole cell treatment and direct APD would provide a broader investigation into the effect of acrolein on whole cell interactions, rather than just the effect of acrolein-modification on PTEN's interactome. The approach of this current study, using a previously purified recombinant PTEN and treating on-column directly before the pull-down, provided a targeted investigation into the effect of acrolein-modification on PTEN's interactome. This rationale has previously been justified by Verrastro et al. (2016) in their high-data content study of the effect of oxidation on the interactome of PTEN.

The profile of residue modification and overall structural change on the *in vitro* treatment of PTEN-V5-His with acrolein from Chapter 4 allowed identification of an acrolein treatment ratio that would modify PTEN residues whilst avoiding aggregation. The threshold for this was a significant decrease in phosphatase activity and acrolein modification of residues with no significant aggregation when visualised by SDS-PAGE. This is important as the aggregation of PTEN-V5-His was seen on increasing acrolein concentration, as discussed in Chapter 4, and unfolding of proteins and exposure of buried hydrophobic regions would lead to aggregation and non-specific binding (Frutiger et al., 2021). This would prevent targeted identification of a change of binding resulting from the introduction of acrolein modifications, which is the aim of this Chapter. The modified residues identified in the treatment control identified by LC-MS/MS closely matched those presented in Chapter 4, giving confidence to the reproducibility of acrolein modification across *in vitro* formats, as well as confirming that there was successful acrolein modification to PTEN during the treatment pull down.

The aim of this thesis was to identify changes to the interactome of PTEN on exposure to acrolein, rather than profiling the complex of proteins present in the different pull downs. It is worth considering that not all proteins identified using APD will be direct interactors with the bait protein, known as binary interactors, and instead may be linked by other interactors, known as complex interactors (Teng et al., 2015). It is not possible from this LC-MS/MS data to differentiate between binary and complex interactors (Bader and Hogue, 2002, Teng et al., 2015). Computational efforts to assess interaction partner networks identified by APD and label-free LC-MS/MS experiments have recently been reviewed (Nesvizhskii, 2012, Armean et al., 2013, Tian et al., 2017). The focus of this study was the fold-change in the abundance of individual interactors for untreated and acrolein-treated PTEN. To achieve this, the relative

abundance of the identified proteins were measured using a label-free quantification approach. Alternatively, there are several labelling methods that can be used to quantify the relative or absolute abundance of interactors such as isotopic, isobaric and chemical labelling (Liu and Zhang, 2018, Bantscheff et al., 2007). These different labelling approaches have previously been reviewed (Ong and Mann, 2005, Bantscheff et al., 2007, Oeljeklaus et al., 2009). Label-free quantification uses a comparison of either signal intensity or the number of peptide spectra to determine the relative abundance of a protein between samples (Bantscheff et al., 2007). Whilst removing the requirement for labelling, label-free approaches are more prone to variation as the samples from different experiments are analysed separately, whereas the use of labels permits the mixing of different samples prior to mass spectrometry analysis (Lindemann et al., 2017). Isotope-based techniques can involve the use of isotope labelled protein or peptide standards during analysis (Ong and Mann, 2005). Alternatively, peptides of interest can be directly labelled, enzymatically, chemically or metabolically, prior to analysis to give a detectable mass shift (Ong and Mann, 2005). Stable isotope labelling by amino acids in cell culture (SILAC) involves the incorporation of unlabelled or labelled amino acids *in vivo* through supplementation of cell culture medium with a normal or heavy isotopic form of a specific amino acid that the medium was originally deficient in (Ong et al., 2002). The SILAC approach was used by one of the high-data content PTEN interactome studies introduced in section 5.1.2, where the authors sought to identify changes in the interactome of wild-type PTEN and a G20E mutant (Table 5.1) (Gunaratne et al., 2011). The ratio of the signal intensity of the peptide pairs (labelled and unlabelled) were used to compare the relative abundance of different peptides across different samples, where in the aforementioned study the control cells were grown in light medium with the normal isotope and the G20E mutant was grown in the heavy isotope medium (Gunaratne et al., 2011). A label-free approach has also been used by a previous PTEN interactome study to quantify the changes in abundance of interactors on oxidation of PTEN with H₂O₂ (Verrastro et al., 2016).

The data from this interactome study builds on previous attempts to characterise changes in PTEN's interactome under different (patho-)physiological conditions through the use of APD coupled with label-free mass spectrometry to quantify changes in abundance. It is clear that there is a change in the interactome of PTEN on acrolein modification, demonstrated by the changes in abundance of proteins between the different treatment conditions. However, it is not possible to elucidate from this data what residue modifications are responsible for changes in binding, only to infer that acrolein modification brings about these changes. The changes could be through direct modification of a residue within a binding site for an interactor, or through changes in the overall conformation brought about by the modification. Further experiments would be required to uncover the cause. One approach could be mutation of each

of the identified acrolein-modified residues, one-by-one, to an amino acid that cannot be modified by acrolein. These variants could be expressed and purified as per this study with *in vitro* pull downs alongside wild type PTEN to see if the interaction still occurs. However, this would only uncover the mechanism of binding where a single modification fell in a specific protein binding site for example, whereas general conformational changes as a result of one or more modifications would be harder to identify as a specific cause. The nature of a high-data content study is to probe for new interactors on a proteome-wide scale, and as such it is not possible within the scope of this thesis to characterise each interactor that showed a change in abundance on acrolein modification. This difficulty is highlighted by the collective data from previous high-data content interactome studies of PTEN, where >1000 proteins were identified as potential interactors but only 54 of these were validated with a second technique and only 3 had a functional role proposed (Figure 5.10) (Smith et al., 2021).

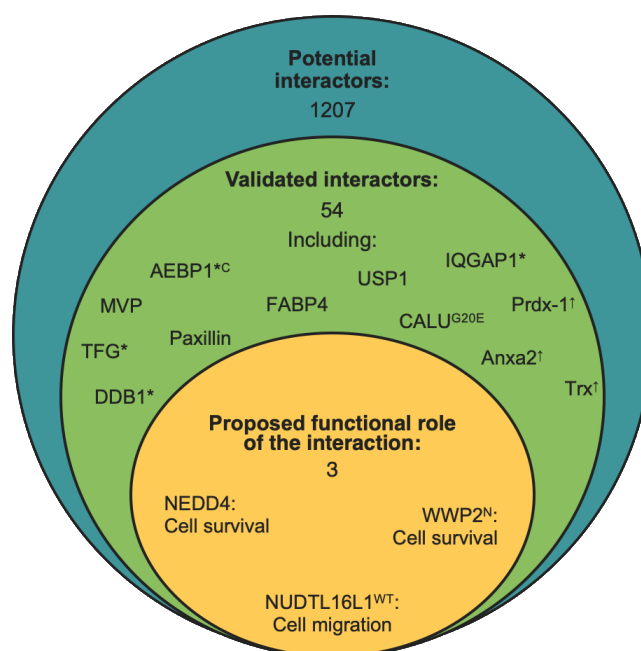


Figure 5.10 The number of potential PTEN interactors, validated PTEN interactors and interactors with a proposed functional role for the interaction with PTEN.

Key: *: a novel PTEN interactor; †: an interactor with increased binding to oxidised PTEN; C: an interactor shown to bind to PTEN's C-terminal domain; N: an interactor shown to bind to PTEN's N-terminal domain; G20E: an interactor specific for the G20E PTEN mutant; WT: an interactor specific for wild-type PTEN, not the G20E mutant. (Reproduced with permission Figure from Smith et al. (2021)).

Whilst the results from the APD with untreated and acrolein-treated PTEN showed a low number of interactors that have previously been identified as PTEN interactors using physical high-data content approaches, the percentage is comparable to the level of single evidence interactors on BioGRID (Stark et al., 2006). Supplementary Table 4 lists the previous interactors of PTEN that have been identified as physical interactors in high-data content studies and out of the 476 total interactors, only 42 have more than one identification, with

only 2 interactors having >2 identifications. This has a single interactor evidence rate of 91%, closely matching the single interactor hit in this pull-down study of 90%. Of the 476 interactors listed on BioGRID, 30 of these have also been identified using low-data content studies and, of these, 15 have >1 piece of evidence and 9 have >2 pieces of evidence. This highlights the low rate of reproducibility of high-data content studies with the same protein, which is a well-recognised issue with high-data content, proteome-wide interactome studies, as discussed in section 5.1.2. False positive discovery rate of APD is estimated to be between 10-40%, which can be measured by the application of computational validation, and the reproducibility rate is between 60-85%, measured by the percentage similarity of biological replicates (Gavin et al., 2011). Computational methods that can be used to assess the reliability of a PPI are based on topological information, as introduced in section 5.1.2, and proteins are ranked according to similarities in gene ontology (GO) and other protein properties (Dong and Provar, 2018). Regarding the reproducibility of the APDs performed in this current study, when considering proteins that were identified in 2/3 replicates the rate of reproducibility was 65%-71%, which dropped to 38-52% when considering proteins present in all 3 replicates.

A key aspect of proteome-wide high-data content studies is the validation of potential interactors. Due to the high number of potential interactors that can be identified by APD and Y2H assays, it is not possible to validate each one. Instead, interactors of interest can be taken forward for further binding analysis and functional studies. Ubiquitination has a key role in the regulation of PTEN. Polyubiquitination has been shown to target PTEN for proteasomal degradation (Wang et al., 2007) and monoubiquitination plays a role in PTEN's localisation (Trotman et al., 2007). At the time of writing, NEDD4 and WWP2, two E3 ubiquitin ligases, have the highest number of interactor identification out of the 549 published physical interactions for PTEN, with identification in 17 and 16 independent studies, respectively (Stark et al., 2006). Although there is little overlap between the previous and current study in terms of E3 ligase identification (Figure 5.11), this is representative of the issue in reproducibility for high-data content interactome studies as discussed above. Although there is extensive evidence of the PTEN/NEDD4 and PTEN/WWP1 interactions, most of these studies were low-data content, and the other E3 ligases have been cited to a much lower extent (Figure 5.11).

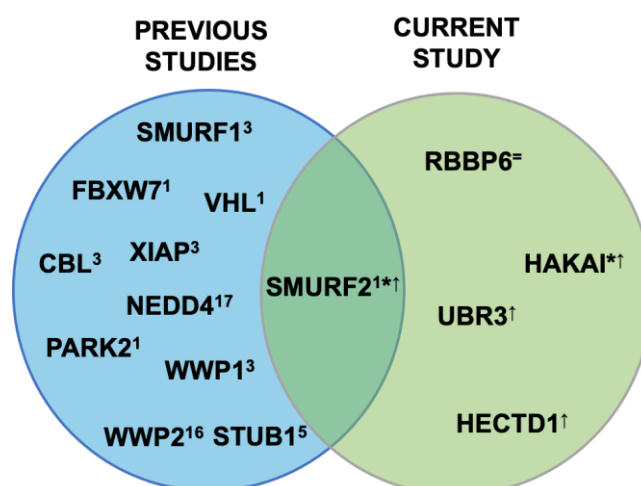


Figure 5.11 A diagram showing the E3 ubiquitin ligases that have been identified as potential interactors of PTEN, in previous high- and low-data content studies (blue) and the current study (green).

Key: Number: Number of previous identifications, *: Present in the current study's beadome, †: Increased abundance in the acrolein-treated sample, =: Equal abundance across both treatments.

In conclusion, APD with untreated and acrolein-treated PTEN identified a number of interactors that had a change in abundance between the treatments. HECTD1 is a novel E3 ubiquitin ligase that has showed a higher abundance in the acrolein-treated PTEN sample. A limitation of the data presented in this chapter is only evidence of an *in vitro* interaction between PTEN and HECTD1, where no functional analysis was attempted. This reinforces the role of high data-content studies in opening new lines of investigation. For the PTEN/HECTD1 interaction it would be key to first demonstrate this in the cell, as was attempted in Chapter 6 with the CoIP experiment, before moving to any functional assays. There are several techniques that can be employed to validate and characterise an interaction and this is explored in more detail in the next chapter. CoIP, SPR and functional studies, such as the cell migration assay, have been employed in previous PTEN interactome studies (Table 5.1). The work described in the next chapter sought to use CoIP as a secondary validation technique to confirm this interaction *in cellulo*. In order to further characterise the effect of acrolein on the interactome of PTEN, further pull downs could be performed with acrolein-treated prey or acrolein-treated bait and prey. The (patho-)physiological context of a cell has a drastic effect on PPI and so does PTM. By separating these investigations it is intended to provide a more comprehensive understanding of why changes in interactions occur during lipoxidation.

Chapter 6 – Effects of Acrolein on the Function of PTEN *In Cellulo*

6.1 Introduction

6.1.1 Approaches to Assessment of Cell Viability

There are several molecular mechanisms through which acrolein can exert a toxic effect on mammalian cells, including apoptosis (Moghe et al., 2015). There are various approaches to monitoring cell viability, from dye-exclusion staining to spectrophotometry-based assays, and these techniques have previously been reviewed (Adan et al., 2016, Kamiloglu et al., 2020). Dye-exclusion staining relies on the uptake of a dye, such as trypan blue, by dead cells whereas the dye is excluded from living cells (Kamiloglu et al., 2020). This technique requires membrane damage, meaning intermediate cytotoxicity and sublethal treatment concentrations cannot be detected, as well as being a low-throughput technique requiring cell counting (Kamiloglu et al., 2020). Colourimetric assays, including the 3-(4,5-dimethylthiazol-2-yl)-2,5-diphenyl tetrazolium bromide (MTT) and 2,3-bis-(2-methoxy-4-nitro-5-sulfophenyl)-2H-tetrazolium-5-carboxanilide (XTT) assays, are simple to perform, high-throughput and widely accessible (Kamiloglu et al., 2020). These tetrazolium-based assays rely on the metabolic activity of cells to convert a substrate into a detectable product that is then measured by absorbance at a particular wavelength by spectrophotometry, and this substrate-product conversion is proportional to the number of viable cells present (Aslantürk, 2018). Sensitivity can be improved through the use of fluorometric assays, such as the resazurin assay and, where real-time viability assessment is required, luminometric assays can be used (Kamiloglu et al., 2020). Beyond access to the required equipment and the desired sensitivity, the most important consideration when attempting to characterise the loss of cell viability on endogenous treatment, is that the assay does not interfere with the treatment compound or vice versa (Aslantürk, 2018).

Developed in 1983 to measure cytotoxicity, cell proliferation or activation, the basis of the MTT assay is the reduction of MTT to formazan, an insoluble purple crystal, which is solubilised by the addition of an organic solvent before detection (Mosmann, 1983, Berridge et al., 2005). However, the ability of the MTT assay to assess proliferation accurately has been contested, due to the measurement of cellular metabolism rather than specific markers of proliferation (Riss et al., 2013). The most accepted explanation of the uptake of MTT by cells is the facilitation of its transfer across the cell membrane by its amphiphilic and lipophilic nature and the positive charge of its tetrazole ring (Berridge et al., 2005, Stockert et al., 2018). However, endocytosis of MTT has also been proposed (Lü et al., 2012, Liu et al., 1997). Whilst original

studies attributed the reduction of MTT at the mitochondria by mitochondrial dehydrogenases, formazan has since been localised to the endoplasmic reticulum, cytosol and plasma membranes (Stockert et al., 2018, Ghasemi et al., 2021). The primary location of MTT reduction is now thought to be at the endoplasmic reticulum by NAD(P)H-dependent oxidoreductase enzymes and dehydrogenases associated with the glycolytic pathway (Berridge et al., 2005, Stockert et al., 2018). MTT can also be reduced non-enzymatically by reductants such as ascorbic acid, cysteine and glutathione (Stockert et al., 2018). Formazan is lipophilic and forms intracellular granules that are localised to cell membranes, lipid droplets and, through exocytosis, presents as needle-like aggregates at the cell surface (Liu et al., 1997, Diaz et al., 2007, Lü et al., 2012, Stockert et al., 2018). Whilst there are several considerations to the use of MTT as a cell viability assay, with remaining questions on the exact mechanisms of MTT internalisation and reduction, the MTT assay has previously been used to successfully measure cytotoxicity of acrolein for several different cell lines (Table 6.1).

Table 6.1 Previous Studies Utilising the MTT Assay to Test Acrolein Cytotoxicity on Mammalian Cell Lines

Study	Cell Line	Acrolein Conc. (μM)	Treatment Time (hours)
Luo et al. (2005)	PC12	1-100	24
Mohammad et al. (2012)	HepG2	2.5-100	24
Shah et al. (2015)	HepG2	40-120	24
Wang et al. (2016)	HeLa A549	25-250	24
Chen et al. (2016a)	H4IIEC	30	24
Luo et al. (2018)	EAhy926	25-400	24
Yin et al. (2020a)	LO2	10-100	24
Gupta et al. (2021)	hCSFs	10-150	4
Tsai et al. (2021)	SW480 HCT-116	0-100	24

6.1.2 Effect of Oxidation and Lipoxidation on PTEN's Regulation of the Akt Signalling Pathway

Oxidative stress has multiple effects on the PI3K/Akt signalling pathway and this has recently been reviewed in the context of cancer (Koundouros and Poulogiannis, 2018). Specific reviews have previously been conducted on effect of redox regulation of the PI3K/Akt signalling pathway through inactivation of PTEN (Leslie, 2006, Zhang et al., 2020). Due to the focus of this thesis on PTEN, the direct effect of oxidative modification to PTEN on the PI3K/Akt signalling pathway will be expanded further here. The effect of oxidative stress on the regulation of the PI3K/Akt signalling pathway by PTEN has been demonstrated by observable increases in the cellular levels of the second messenger PIP₃, PTEN's physiological substrate, or phosphorylated Akt (pAkt), a serine/threonine kinase that is activated on binding by PIP₃ (Georgescu, 2010).

Insulin can stimulate the activation of the PI3K/Akt signalling pathway and on stimulation of HEK293 cells with insulin an increase in PIP₃ was seen, but on concurrent overexpression of PTEN these levels decreased (Maehama and Dixon, 1998, Manning and Cantley, 2007). Even without insulin stimulation, transfection with the phosphatase-inactive Cys124Ser PTEN mutant resulted in an increase in PIP₃ (Maehama and Dixon, 1998). This was supported by an additional study where transfection of HEK293 cells with wild type PTEN showed a decrease in the amount of PIP₃, but an increase in PIP₃ was seen on transfection with a Cys124Ser PTEN mutant (Myers et al., 1998). These observations were the cornerstone of the identification of PIP₃ as the physiological substrate of PTEN and highlight the dependence of PTEN on Cys124 for its PIP₃ phosphatase activity and subsequent negative regulation of the PI3K/Akt signalling pathway, and as such the levels of PIP₃ and pAkt (Maehama and Dixon, 1998). As discussed in section 1.2.6, PTEN's Cys124 is vulnerable to oxidative modification and H₂O₂-oxidation reversibly inactivates PTEN by formation of a disulfide bond between Cys124 and Cys71 (Lee et al., 2002). Both exogenous treatment with H₂O₂ and stimulation of endogenous oxidant production by peptide growth factors resulted in a reduction of PTEN's phosphatase activity with an increase in PIP₃ and pAkt (Leslie et al., 2003, Kwon et al., 2004). As introduced in section 1.2.6 and explored further in Chapter 4, PTEN is also vulnerable to modification by lipid oxidation products and both acrolein and 4-HNE have been shown to modify and inactivate PTEN (Covey et al., 2010, Shearn et al., 2011, Shearn et al., 2013). Exogenous treatment of several mammalian cell lines (MCF7, HEK293 and HepG2) cells with 4-HNE and acrolein showed an accompanying increase in pAKT with the inactivation of PTEN (Covey et al., 2010, Shearn et al., 2011). Endogenous production of acrolein, as a by-product of spermine oxidase and myeloperoxidase catalyses, has replicated this effect, resulting in acrolein modification of PTEN with a concurrent increase in pAKT (Al-Salihi et al., 2015, Uemura et al., 2017).

6.1.3 Protein-Protein Interaction (PPI) Validation

There are several methods that can be used to validate PPIs, such as visualisation of co-localisation, spectroscopy, quantitative binding studies or secondary identification using CoIP with western blotting (Berggard et al., 2007). Approaches to visualising co-localisation with microscopy have previously been reviewed as a method of PPI validation (Yakubu et al., 2019). Immunofluorescence can be visualised with microscopy to determine the subcellular location of the two interactors with the use of fluorophore-conjugated antibodies against primary antibodies that directly bind to the proteins of interest, if a specific antibody or a tag are available (Miyashita, 2015, Yakubu et al., 2019). This provides evidence for the validity of a proposed PPI, as for two proteins to interact they would require similarities in subcellular localisation (Snider et al., 2015, Yakubu et al., 2019). There is a risk when choosing to probe

for recombinant versions of the proteins of interest, as the presence of a tag can affect the localisation of the protein and cause differences in subcellular distribution in comparison to its endogenous counterpart, resulting in exposure to potentially non-physiological protein interactors (Berggard et al., 2007, Yakubu et al., 2019). Fluorescence resonance energy transfer (FRET) allows visualisation of protein-protein interactions with microscopy, through the use of donor- and acceptor-fluorophore conjugation to respective binding partners (Yakubu et al., 2019). The emission spectrum of the donor-fluorophore is selected to overlap with the absorption spectrum of the acceptor-fluorophore, such that fluorescence is seen on excitation of the donor-fluorophore when it is within close proximity to the acceptor-fluorophore, for example during a PPI (Ma et al., 2014, Yakubu et al., 2019). In combination with fluorescence and confocal microscopy, PPIs can be detected and monitored *in vivo* and in real-time with FRET (Yakubu et al., 2019). A similar but related approach relies on the use of bioluminescence, for bioluminescence resonance energy transfer (BRET), where a luciferase protein is the donor and a fluorescent protein is the acceptor (Yakubu et al., 2019). Other approaches to fluorescence microscopy, including but not limited to fluorescence lifetime imaging microscopy (FLIM) and fluorescence correlation spectroscopy, can also be used to visualise PPI *in cellulo* (Hink et al., 2002).

Spectroscopy can be used to validate an interaction and one interaction partner can be titrated against a fixed concentration of the other to estimate binding kinetics (Berggard et al., 2007). Circular dichroism (CD) spectroscopy uses absorbance at far or near ultraviolet (UV) and visible light regions to analyse protein conformation in solution (Greenfield, 2006). The resultant change in absorption that accompanies the change in protein conformation on PPI can be monitored to quantify the interaction (Zhou et al., 2016). Whilst CD spectra in the far UV regions, between 190-250 nm, result from the protein backbone amides and as such are sensitive to changes in secondary structure, spectra in the near UV and visible light regions result from aromatic residues and disulfide bonds and are sensitive to a proteins tertiary structure (Greenfield, 2006, Zhou et al., 2016). Resolution can be improved to an atomic level with the use of nuclear magnetic resonance (NMR) to elucidate binding interfaces, binding kinetics and conformational changes on protein-protein interaction (Purslow et al., 2020). The frequency of electromagnetic radiation absorption, on orientation of the NMR-active nuclei of an isotopically labelled protein by a strong magnetic field, is sensitive to changes in the local environment, for example, on introduction of another nuclei on interaction with a protein or ligand (Purslow et al., 2020, O'Connell et al., 2009). This is known as chemical shift perturbation (CSP) and whilst this NMR technique can identify intermolecular binding interfaces between proteins, it does not reveal their relative orientation (O'Connell et al., 2009).

Other NMR techniques can be applied to elucidate structural changes and binding interfaces, which have been reviewed recently by Purslow et al. (2020).

Binding studies can measure affinity as well as the association and dissociation rates of two interacting proteins, which is useful for validating a direct interaction as well as characterising the transient or stable nature of the interaction (Berggard et al., 2007). SPR involves immobilisation of one binding partner, the ligand, through covalent coupling to a surface and the rate of binding of its proposed interaction partner, the analyte, is measured by monitoring changes to the refractive index at the surface medium (Douzi, 2017, Drescher et al., 2018). Whilst no tag is required, removing any risk of introduction of changes to the ligand's structure, the proteins are binding in a non-physiological context where one is immobilised, rather than both being free in solution (Berggard et al., 2007). Similar in concept to APD, CoIP involves the binding of the target of interest with a complementary antibody and subsequent capture on a protein A or G resin before identification of interaction partners using mass spectrometry or western blotting (Yakubu et al., 2019).

6.1.4 Aims and Hypotheses

The aim of this chapter was to investigate the effect of acrolein on PTEN's activity and interactions *in cellulo*. The ability of acrolein to inactivate PTEN *in cellulo* and upregulate the levels of pAkt has been previously documented, as introduced above (Al-Salihi et al., 2015, Uemura et al., 2017, Covey et al., 2010, Shearn et al., 2011). To ensure that PTEN-V5-His would be sufficiently modified without becoming completely unfolded, it was necessary here to determine sublethal acrolein concentrations. Once sublethal concentrations of acrolein were identified, these treatments could then be applied exogenously and any increase in pAKT could be monitored to characterise any upregulation of the Akt pathway and to infer a loss of PTEN activity *in cellulo*. Chapter 5 demonstrated a change in PTEN's interactome on acrolein modification of PTEN, with an E3 ubiquitin ligase, HECTD1, identified as a novel interactor of PTEN. The HECTD1-PTEN interaction was preliminarily validated with western blotting as a protein interactor that increased in abundance for acrolein-treated PTEN. But, it is well established that interactions identified *in vitro* need to be corroborated with further evidence and this can be achieved by validation of the interaction using CoIP, among other methods as described above.

The first aim of this chapter was to validate the optimal MTT assay conditions to monitor loss of cell viability for HCT-116 cells and apply this to quantify the loss of cell viability with exposure to increasing concentrations of acrolein. The second aim of this chapter was to treat HCT-116

cells with increasing, sublethal concentrations of acrolein and probe the lysates for Akt and pAkt, using α/β -tubulin as a loading control, to identify if, and at what acrolein concentration, there is an upregulation of activated Akt, pAkt, that correlates with a loss of PTEN activity. The third aim of this chapter was to use lysates from acrolein-treated HCT-116 cells for CoIP against PTEN, to validate the novel PTEN-HECTD1 interaction using western blotting as well as confirm the increase in binding under lipoxidative modification. Several hypotheses are associated with these aims. Firstly, it was hypothesised that with increasing concentrations of acrolein there will be a decrease in the cell viability of HCT-116 cells and that on treatment of HCT-116 cells with sub-lethal concentrations of acrolein there will be an increase in pAKT. Secondly, it was hypothesised that CoIP using untreated and acrolein-treated HCT-116 cells would show an increase in HECTD1 in the treated sample.

6.2 Methods

6.2.1 MTT Assay and Optimisation

HCT-116 cells were grown to 70-80% confluence before harvesting with trypsin as described in section 2.2.3. Cells were pelleted by centrifugation at 1000 x g for 10 minutes at RT. The cell pellet was resuspended in complete McCoy's 5a Media and cells were counted using trypan blue. Cells were diluted to 5×10^6 cells/ml or 5×10^5 cells/ml for the two standard curves and 1×10^5 cells/ml for the treatment wells. Standard curves were prepared with 1:2 serial dilution with 100 μ l 5×10^6 cells/ml or 5×10^5 cells/ml with 100 μ l media to produce standard curves starting with 5×10^5 cells/well and 5×10^4 cells/well, respectively. Treatment wells were seeded with 100 μ l 1×10^5 cells/ml to give 1×10^4 cells/well. The plate was covered and incubated for 24 hours at 37°C and 5% CO₂. Old media was aspirated and 100 μ l of fresh complete McCoy's 5a media was added to the standard curves whilst 90 μ l of fresh complete McCoy's 5a media and 10 μ l of fresh 10X acrolein treatments prepared in PBS was added to treatment wells. Acrolein treatment concentrations were as follows; 0 μ M, 5 μ M, 10 μ M, 50 μ M, 100 μ M, 200 μ M, 500 μ M and 1000 μ M. The plate was swirled for 10 seconds to mix before incubation at 37°C and 5% CO₂ for 1h or 24h. The treatments and media were aspirated and each well was washed with 100 μ l of PBS. 90 μ l of McCoy's 5a media (Phenol, Antibiotic and Serum-free) (Cytiva, UK) and 10 μ l of sterile filtered 5 mg/ml MTT in PBS was added to each well and the plate was incubated for 3 hours at 37°C and 5% CO₂. Initially, the MTT was solubilised by addition of 100 μ l of acidified SDS (10% SDS in 10 mM HCl) and incubation overnight at 37°C and 5% CO₂. The plate was shaken for 5 seconds and the absorbance was read at 570 nm. Low absorbance values for even the highest cell concentrations in combination with the observation of a plateauing standard curve suggested that the MTT was not fully solubilised. The solubilisation protocol was changed to incorporate the use of an alcohol based MTT solubilisation solution and a physical resuspension step. 100 μ l of acidified IPA with detergent (10% SDS and 40 mM HCl in isopropanol) was added to each well and the cells were resuspended using a multichannel pipette before incubation for 30min at RT on a shaker and the absorbance was read at 570 nm.

6.2.2 Trial Immunoprecipitation of PTEN and α,β -tubulin from HCT-116 and MCF-7 cells

HCT-116 WT, HCT-116 PTEN null (-/-) and MCF-7 cells were grown to 70-80% confluence before harvesting with trypsin. Cells were pelleted by centrifugation at 1000 x g at RT for 10 minutes. The pellet was washed twice in PBS before resuspension in PBS. The cells were counted with a trypan blue exclusion before dilution to 2×10^5 cells/ml in PBS. The cells were

aliquoted into 1 ml aliquots and centrifuged at 1,000 x g at 4°C for 10 minutes before aspiration of the supernatant. The pellets were frozen at -20°C for later use.

The pellets of 2×10^7 cells were thawed on ice before addition of 1 ml ice-cold lysis buffer (25 mM NaPO₄ pH 7.4 with 150 mM NaCl, 1% Triton X-100, 5% glycerol, 1 mM DTT, 2 mM EDTA, 1X cComplete™ EDTA-free protease inhibitor cocktail (Merck, UK) and 1X PhosSTOP™ phosphatase inhibitor cocktail (Roche, UK)). The pellet was homogenised in the lysis buffer with a needle and a syringe, and the lysates were incubated on an end-over-end rotator for 30 minutes at 4°C. The lysates were centrifuged at 16,000 x g for 20 minutes at 4°C and the supernatants were transferred to a new tube. The lysates were quantified using the BCA assay to quantify an average protein concentration from a 1:5 and a 1:10 dilution, as per section 2.3.2.

Immunoprecipitation (IP) was performed by diluting 200 µg of lysate to 200 µl in lysis buffer for a final protein concentration of 1 mg/ml in a spin column. Initial IPs were conducted either with 1:100 or 1:200 Rabbit Anti-PTEN polyclonal Ab (#9552, Cell Signaling Technology, USA) and one IP with no Ab added as a bead-only control. The IPs, with and without Ab, were incubated on an end-over-end rotator at 4°C for 18h before addition of 40 µl of a Protein A Sepharose (Cytiva, UK) prepared as a 50 % slurry in lysis buffer (20 µl resin in total). The IPs were incubated on an end-over-end rotator at 4°C for 3 hours before centrifugation at 1,500 x g for 5 minutes at 4°C. The flow through was collected and the resin was washed 3 times with 10 column volumes (CV) of lysis buffer before centrifugation at 1,500 x g for 5 minutes at 4°C and the washes were collected. The resin was resuspended in 2 x 25 µl 1X Laemelli Buffer per 20 µl resin and the resin was incubated on a shaker for 10 min at RT. The eluate was collected by centrifugation at 1,500 x g for 5 minutes. 20 µl of eluate from each IP was analysed using Western Blotting as per section 2.3.4. The blot was performed against PTEN by initially probing with Rabbit Anti-PTEN polyclonal Ab (#9552, Cell Signaling Technology, USA) and a Mouse Anti-Rabbit IgG (Conformation Specific)-HRP conjugated monoclonal secondary antibody so that only the native antibody using during Western Blot analysis is recognised, and not the antibody present in the IP sample. This was to ensure that any band observed was specifically PTEN, as the molecular weight for both PTEN and an IgG heavy chain is approximately 50 kDa and enable confirmation that the IP was precipitating endogenous PTEN. The blot was washed, exposed and imaged as described previously. The blot was then stripped with a mild stripping buffer (0.2 M glycine pH 2.2 with 0.1% SDS and 1% Tween 20) at RT for 3 x 10 minutes before equilibration with PBS for 2 x 10 minutes and TBS-T for 2 x 5 minutes. The blot was re-blocked in 5% Milk/TBS-T for 1h at RT before re-probing with Goat Anti-Rabbit IgG-HRP polyclonal secondary antibody 1:1000 in 5% Milk/TBS-T for 1 hour at RT

to recognise the antibody present in the CoIP sample. This analysis enabled confirmation that the antibody was being captured by the Protein A Sepharose, in the case that no PTEN band was detected.

The first trial IP used HCT-116 WT lysates with and without a 1:100 dilution of 1:100 Rabbit Anti-PTEN polyclonal Ab (#9552, Cell Signaling Technology, USA). Due to difficulty in detecting PTEN in the IP samples, subsequent experiments included IPs against PTEN and α/β -Tubulin. Lysates alone from several cell types were also analysed using Western Blot analysis for PTEN and α/β -tubulin. The following improvements were also made to the Western Blot analysis procedure to improve detection of low abundance proteins: the transfer step was performed overnight at 30V when more than 1 blot was transferred at one time, the use of Thick Blot Filter Paper (BioRad, USA) and the use of freshly purchased Clarity™ HRP Substrate (BioRad, USA).

6.2.3 Co-immunoprecipitation of Endogenous PTEN and HECTD1 from Untreated and Acrolein-treated HCT-116 Cells

HCT-116 cells were grown to 70-80% confluency before harvesting with trypsin. Cells were pelleted by centrifugation at 1,000 x g at RT for 10 minutes. The pellet was resuspended in complete McCoy's 5a media and cells were counted. Cells were diluted to 5×10^5 cells/ml in complete McCoy's 5a media. Two 150 mm cell culture plates were seeded with 10 ml cells and 20 ml complete McCoy's 5a media, to give 5×10^6 cells/plate in 30 ml of media and the plate was incubated for 48h at 37°C with 5% CO₂. Old media was aspirated and 27 ml of complete McCoy's 5a media and 3 ml of PBS or 1 mM acrolein in PBS, to give a final concentration of 100 μ M acrolein, was added to the plate. The plate was incubated for 1 hour at 37°C with 5% CO₂. The treatments were removed and each well was washed with 5 ml of ice-cold PBS three times. 1.5 ml of ice-cold lysis buffer (25 mM NaPO₄ pH 7.4 with 150 mM NaCl, 1% Triton X-100, 5% glycerol, 1 mM DTT, 2 mM EDTA and 1X cOmplete™ EDTA-free protease inhibitor cocktail (Merck, UK)) was added to each plate on ice. The plates were scraped and the lysate was transferred to pre-cooled microcentrifuge tubes. The lysates were incubated on an end-over-end rotator for 30 minutes at 4 °C. The lysates were centrifuged at 16,000 x g for 20 minutes at 4°C and the supernatants were transferred to a new tube. The lysates were quantified using the BCA assay at a 1:5 dilution.

Two CoIPs were prepared for the untreated and acrolein-treated lysate samples. The CoIPs were performed as in section 6.2.2 but scaled up to 500 μ g of lysate. In addition to this, a pre-clearing step was included prior to the addition of antibody by incubating 600 μ g lysate in 600

µl lysis buffer with 120 µl of Protein A Sepharose (Cytiva, UK) prepared as a 50% slurry in lysis buffer (60 µl resin in total) for 30 minutes at 4°C on an end over end rotator in a microcentrifuge tube. The samples were centrifuged at 12,000 x g for 5 minutes to pellet the resin and 500 µl of supernatant was transferred to a spin column. Once the lysates had been pre-cleared, to one of the CoIPs for each lysate either no Ab was used as a bead-only control or 1:100 Rabbit Anti-PTEN polyclonal Ab (#9552, Cell Signaling Technology, USA) was added. The remaining steps of the CoIP were performed as per section 6.2.2 and 3 x 15 µl of eluate from each CoIP was analysed using Western Blotting as above, probing for PTEN using Rabbit Anti-PTEN polyclonal Ab (#9552, Cell Signaling Technology, USA), Rabbit IgG using a Goat Anti-Rabbit IgG-HRP polyclonal antibody (ThermoScientific, UK) and HECTD1 using Rabbit Anti-HECTD1 pAb (PA568176, Invitrogen, UK).

6.2.4 Mammalian Cell Lysis Optimisation for Western Blotting

HCT-116 cells were grown to 70-80% confluency before harvesting with trypsin. Cells were pelleted by centrifugation at 1,000 x g at RT for 10 minutes. The pellet was resuspended in complete McCoy's 5a media and cells were counted. Cells were diluted to 5×10^5 cells/ml in complete McCoy's 5a media. Each well of a 6-well plate was seeded with 0.5 ml cells and 2.5 ml complete McCoy's 5a media, to give 2.5×10^5 cells/well and the plate was incubated for 48 hours at 37 °C with 5% CO₂. Each well was washed with 500 µl of ice-cold PBS three times. 100 µl of ice-cold 1X Laemelli Buffer or ice-cold lysis buffer (25 mM NaPO₄ pH 7.4 with 150 mM NaCl, 1% Triton X-100, 5% glycerol, 1 mM DTT, 2 mM EDTA, 1X cComplete™ EDTA-free protease inhibitor cocktail (Merck, UK) and 1X PhosSTOP™ phosphatase inhibitor cocktail (Roche, UK)) was added to each well on ice. The wells were scraped and the lysate was transferred to pre-cooled microcentrifuge tubes. The lysates in 1X Laemelli Buffer were sonicated on ice using a handheld sonicator and an MSF-1 probe at 50% amplitude for 3 x 5 second bursts with a 10 second rest in between. The lysates in lysis buffer were incubated on an end-over-end rotator for 30 minutes at 4 °C. The lysates were centrifuged at 16,000 x g for 20 minutes at 4 °C and the supernatants were transferred to a new tube.

The lysates in lysis buffer were quantified using the BCA assay at a 1:5 dilution. SDS-PAGE analysis was performed by loading 20 µl of lysates in 1X Laemelli buffer and 20 µg of lysate in lysis buffer and resolving on a 10% polyacrylamide gel at 50V for 30 minutes and 100V for 1 hour 15 minutes. Western Blot analysis was performed as above. The blot was incubated overnight on a shaker at 4°C with Rabbit Anti-PTEN polyclonal antibody (Ab) (#9552, Cell Signaling Technology, USA) prepared 1:1000 in 5% Milk/TBS-T before washing and subsequent incubation with Goat Anti-Rabbit IgG-HRP (ThermoScientific, UK) 1:1000 in 5%

Milk/TBS-T for 1 hour at RT on a shaker. The blot was washed then exposed and imaged. The blot was then stripped with a mild stripping buffer (0.2 M glycine pH 2.2 with 0.1% SDS and 1% Tween 20) at RT for 3 x 10 minutes before equilibration with PBS for 2 x 10 minutes and TBS-T for 2 x 5 minutes. The blot was re-blocked in 5% Milk/TBS-T for 1h at RT before re-probing overnight at 4°C with Rabbit Anti- α/β -Tubulin Ab (#2148, Cell Signaling Technology, USA) prepared 1:1000 in 5% Milk/TBS-T. The blot was washed in TBS-T and incubated with Goat Anti-Rabbit IgG-HRP (ThermoScientific, UK) 1:1000 in 5% Milk/TBS-T for 1 hour at RT on a shaker before subsequent washing and exposure.

6.2.5 Acrolein Treatment of HCT-116 Cells for Western Blot Analysis

A 6-well plate was seeded with HCT-116 cells at 2.5×10^5 cells/well as above in section 6.2.4 and incubated at 37°C with 5% CO₂ for 48 hours. Old media was aspirated and 2.7 ml of fresh complete McCoy's 5a media and 300 μ l of fresh 10X acrolein treatments prepared in PBS was added to each well. Acrolein treatment concentrations were chosen based on the results from the MTT cell viability assay. The acrolein treatment concentrations that didn't have an observable effect on cell viability were taken forward and were as follows; 0 μ M, 5 μ M, 50 μ M, 100 μ M and 200 μ M acrolein. The plate was incubated for 1 hour at 37°C with 5% CO₂. The treatments were removed and each well was washed with 500 μ l of ice-cold PBS three times. 100 μ l ice-cold lysis buffer (25 mM NaPO₄ pH 7.4 with 150 mM NaCl, 1% Triton X-100, 5% glycerol, 1 mM DTT, 2 mM EDTA, 1X cOmplete™ EDTA-free protease inhibitor cocktail (Merck, UK) and 1X PhosSTOP™ phosphatase inhibitor cocktail (Roche, UK)) was added to each well on ice. The wells were scraped and the lysate was transferred to pre-cooled microcentrifuge tubes. The lysates were incubated on an end-over-end rotator for 30 minutes at 4°C. The lysates were centrifuged at 16,000 x g for 20 minutes at 4°C and the supernatants were transferred to a new tube.

The lysates in lysis buffer were quantified using the BCA assay at a 1:5 dilution. SDS-PAGE analysis was performed with 20 μ g of lysate from each treatment concentration on 4 x 10% polyacrylamide gel. Western Blot analysis was performed as above, with the following amendments. Where 4 blots were transferred at once the transfer was performed at 4 °C at 30V for 16h. The blots were blocked in 5% BSA in TBS-T for 1 hour at RT and probed overnight with one of the following antibodies prepared 1:1000 in 5% BSA in TBS-T; Rabbit Anti-Akt (pan) Ab (#4691, Cell Signaling Technology, USA), Rabbit Anti-Akt (phosSer403) Ab (#9271, Cell Signaling Technology, USA) or Rabbit Anti- α/β -Tubulin Ab (#2148, Cell Signaling Technology, USA).

6.2.6 Statistical Analysis

Data from three experimental replicates with three variables was analysed using GraphPad Prism 8.0 to perform one-way ANOVA analysis with the Geisser-Greenhouse correction, correcting for multiple comparisons using the Tukey test. Data from three experimental replicates with two variables was analysed using GraphPad Prism 8.0 to perform a paired T-test with a confidence level of 95 % with statistical significance defined as $P < 0.05$. The P value style was as follows: 0.1234 (ns), 0.0332 (*), 0.0021 (**), 0.0002 (***), <0.0001 (****). Raw data is shown as mean values \pm SEM.

6.3 Results

6.3.1 The Use of Acidified IPA as an MTT Solubilisation Solution Increases the Absorbance in Comparison to the use of Acidified SDS

A standard curve was performed at two cell densities to model the effect of a loss of cell viability. It is important to seed the plate with an appropriate cell density that after incubation with MTT and subsequent solubilisation of formazan the absorbance falls within the linear range and the error bars are small to allow differences in cell viability to be detected. The initial strategy of using acidified SDS resulted in a very low absorbance for both of the serial dilutions performed, 5×10^5 and 5×10^4 cells/well (Figure 6.1A). Changing to an acidified IPA solubilisation with a physical resuspension step increased the absorbance dramatically (Figure 6.1A). For both solubilisation agents the two serial dilution densities showed a similar profile of increasing absorbance, where for the 5×10^5 cells/well serial dilution there was a steep increase between $0-1 \times 10^5$ cells/well, with a plateau at cell densities greater than 1×10^5 cells/well (Figure 6.1A). The error bars are large for the 5×10^5 cells/well serial dilution solubilised in acidified IPA, indicating that the cell concentration is too high and it would not be possible to detect the differences in cell density accurately, making it unsuitable to detect small changes in cell viability. The 5×10^4 cells/well serial dilution was the most suitable standard curve concentration, where the absorbance was between 0.1 and 1 mAU and the error bars are very small before the plateau for $>1 \times 10^4$ cells/well indicating that small changes in cell number, and therefore cell viability, would be detected. Therefore, the absorbances for $\leq 1.25 \times 10^4$ cells/well were plotted separately to assess the linearity of the data (Figure 6.1B). Whilst there was a slight plateau effect between 0.63×10^4 cells/well and 1.25×10^4 cells/well, linear regression analysis using Prism 9 calculated the R^2 value was 0.9729 and so the seeding density for the acrolein treatments was chosen as 1×10^4 cells/well (Figure 6.1B).

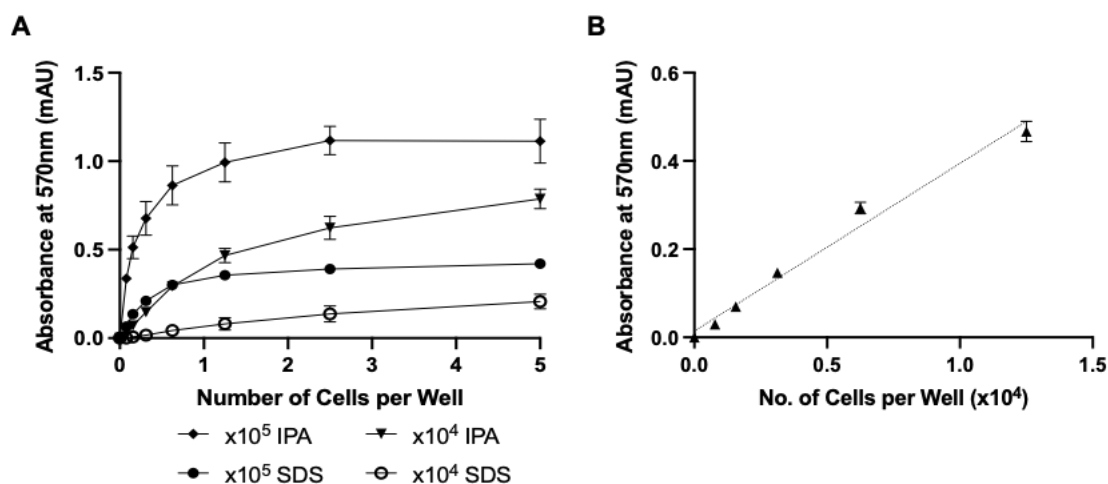


Figure 6.1 Effect of Acidified IPA vs Acidified SDS in the Solubilisation of MTT when Assaying for Cell Viability

A) MTT assay standard curves were produced from a serial dilution of two different HCT-116 cell concentrations of 5×10^5 cells/well and 5×10^4 cells/well and the MTT solubilisation was performed with acidified IPA or acidified SDS. B) A smaller range of the standard curve from a starting concentration of 5×10^4 cells/well and solubilised with acidified IPA was identified as below 1.25×10^4 cells/well to test for linearity. The absorbance values were plotted against each cell concentration and a trendline was plotted. ($n=3$, Mean \pm SEM)

6.3.2 Acrolein Treatment has a Dose- and Time-dependent Effect on Cell Viability

The effect of increasing acrolein concentration on the cell viability of HCT-116 cells after a 1- and 24-hour treatment was analysed using the MTT assay. For the 1-hour treatment, there wasn't a significant decrease in cell viability until 0.5 mM acrolein (Figure 6.2A), where for the 24-hour treatment there was a significant decrease in cell viability from 50 μ M acrolein (Figure 6.2A). Interestingly, after a 1-hour treatment with 5 and 10 μ M acrolein there appeared to be a slight increase in cell viability but it was not statistically significant. A 1-hour treatment with 100 μ M was chosen as a suitable acrolein concentration for the subsequent co-immunoprecipitation experiments to validate HECTD1 as an interactor of PTEN, where there was no significant decrease in cell viability after 1 hour and it matches the treatment concentration used by previous PTEN-lipoxidation studies, where cells were treated with 100 μ M 4-HNE was used to treat HepG2 cells (Shearn et al., 2011).

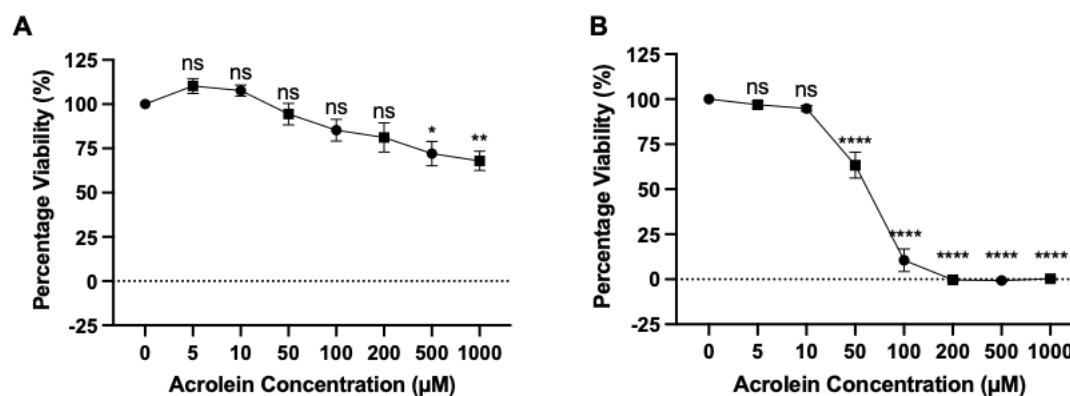


Figure 6.2 Effect of Acrolein Treatment on the Cell Viability of HCT-116 cells after 1 and 24 hours
An MTT assay was performed for 1×10^4 cells/well treated with increasing acrolein concentrations for 1 hour (A) and 24 hours (B), before solubilisation with acidified IPA. (n=3, Mean \pm SEM)

6.3.3 Immunoprecipitation of Endogenous PTEN from HCT-116 cells

Once a suitable acrolein treatment concentration was identified using the MTT assay, it was necessary to test the immunoprecipitation (IP) of PTEN from the HCT-116 cells prior to IP from untreated and acrolein-treated HCT-116 cells as a validation step for the data presented in Chapter 5. As a control, an IP against PTEN was performed with both HCT-116 wild type (WT) and PTEN knockout (-/-) cells. Lysates from HCT-116 WT and -/- cells were incubated with increasing concentrations of rabbit anti-PTEN polyclonal Ab and the PTEN/Ab complex was captured with protein A sepharose resin. A control IP was performed without the addition of Ab to detect any non-specific binding to the resin. The samples were analysed using western blot and probing for PTEN, to assess the successful binding of the anti-PTEN Ab to endogenous PTEN, and for rabbit Ab, to assess for successful capture of the rabbit anti-PTEN. Purified PTEN-GST was used as a positive control for the western blot detection of PTEN. A band at approximately 80 kDa, corresponding to PTEN-GST, was seen in the control lane which confirmed the successful transfer and detection of PTEN. Whilst no band for endogenous PTEN, at approximately 60 kDa, would be expected in the HCT-116 -/- lysate or IP eluates, due to the knockout of PTEN in the cell line, or the HCT-116 WT lysate or the IPs using the anti-PTEN Ab (Figure 6.3A). Figure 6.3B shows a band at approximately 50 kDa which corresponds to the heavy chain of the anti-PTEN antibody and demonstrates successful capture, and subsequent elution, of the antibody from the lysates by the protein A resin. The successful detection of the PTEN-GST control on the western blot probing for PTEN suggests that there is no issue with the recognition of PTEN with the antibody, as the same primary antibody was used for both the western blots and the IP.

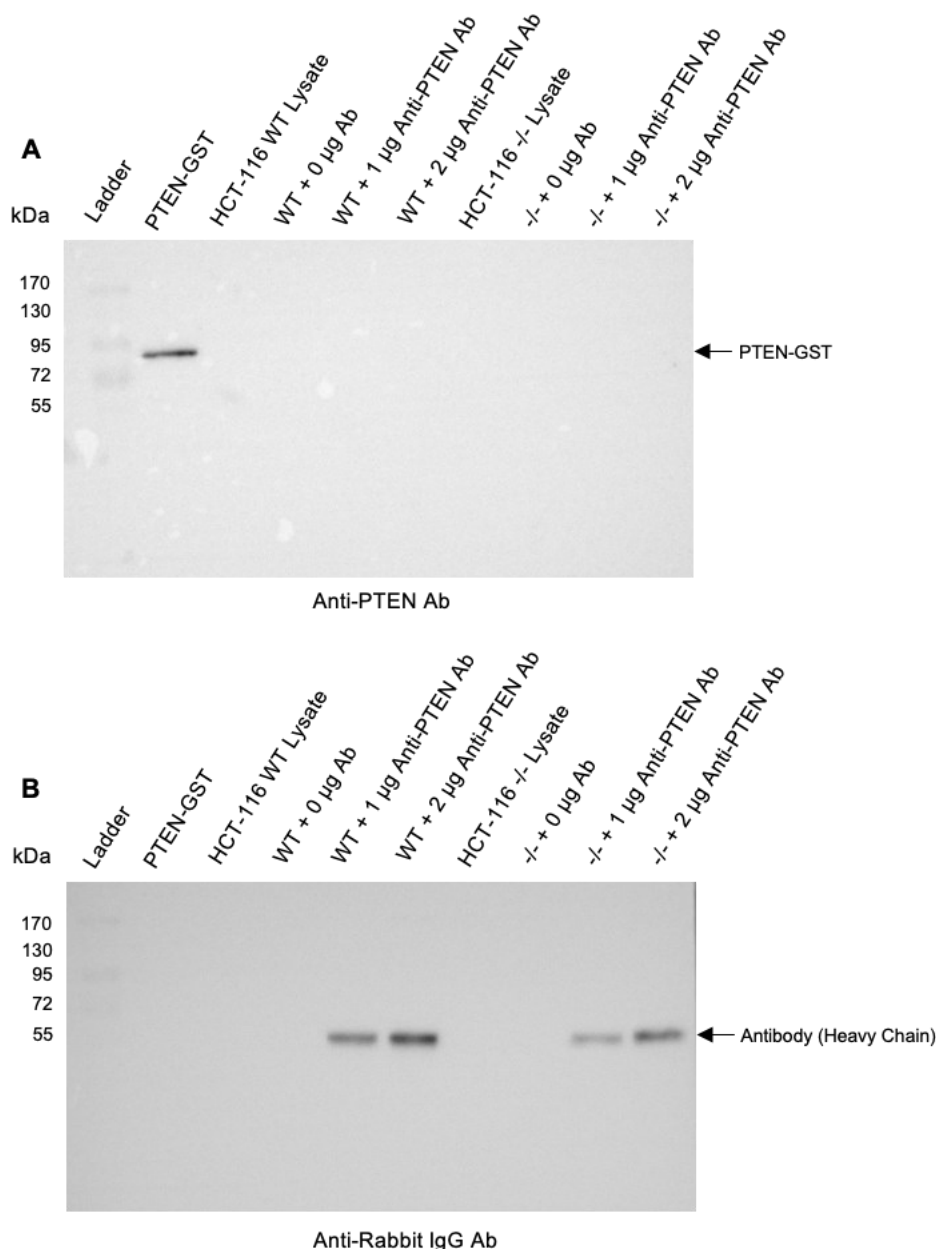


Figure 6.3 Initial IP of PTEN showed successful binding of the anti-PTEN Ab to the Protein A resin but no observable detection of PTEN.

IP against PTEN was performed with an overnight incubation of 1:100 dilution of Rabbit Anti-PTEN polyclonal Ab in 200 µl of HCT-116 WT and -/- lysate at 1 mg/ml in 200 µl, with bead-only controls included where no antibody was added to the lysates. A) Western Blot analysis was performed for PTEN using a Rabbit Anti-PTEN polyclonal primary antibody and a Mouse Anti-Rabbit IgG (Conformation Specific)-HRP monoclonal secondary antibody to detect only native IgG. B) After stripping and re-blocking, the blot was re-probed for Rabbit IgG using a Goat Anti-Rabbit-HRP conjugate polyclonal secondary antibody to detect the denatured IgG in the CoIP samples.

To ensure that the IP protocol was suitable for the capture of a target protein by its corresponding Ab to allow subsequent isolation of the protein/Ab complex using protein A chromatography, the IP was repeated for PTEN but an additional IP was performed against α/β -tubulin in parallel. Whilst the abundance of PTEN varies between cell lines (Ghandi et al., 2019), α/β -tubulin is routinely used as loading control for western blotting due to its relatively

high cellular abundance. This was performed for both HCT-116 WT and -/- cells, where a successful α/β -tubulin IP would be expected for both cell lines but PTEN should only be detected in the IP using HCT-116 WT cells. Fractions from the IPs were visualised using SDS-PAGE (Figure 6.4). Most of the proteins from the lysates did not bind to the protein A Sepharose and are detected in the flow-through, as expected, and unbound protein was successfully washed away during the wash steps (Figure 6.4A and B). There is non-specific binding to the protein A Sepharose resin as there are bands detected in the eluate of the control IP with no Ab (Figure 6.4A and B). Due to the non-specific binding of lysate proteins, the low amount of protein present and the similar size of each of the target bands, where the Ab heavy chain, endogenous PTEN and α/β -tubulin are all approximately 50 kDa, it was necessary to perform western blot analysis against the target proteins to determine successful capture by the Ab.

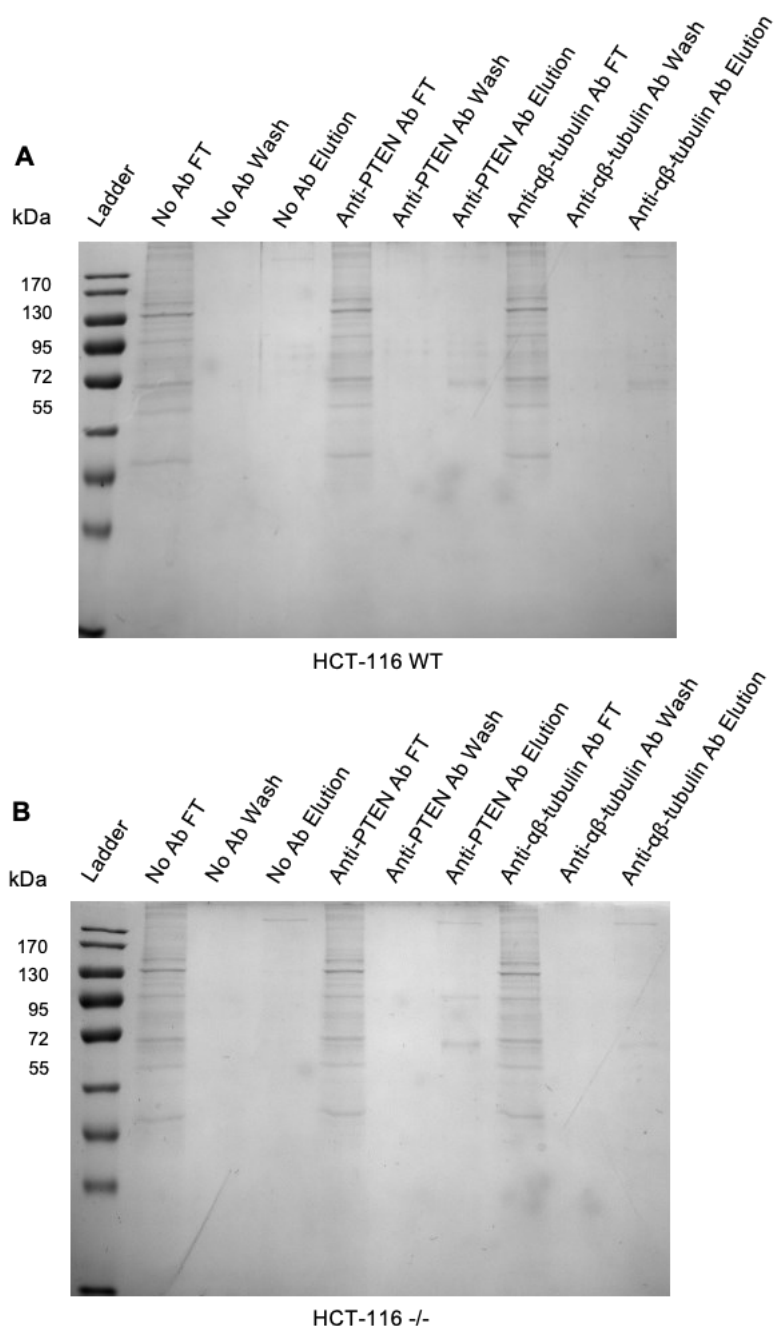


Figure 6.4 SDS-PAGE Analysis of the PTEN and α/β -Tubulin IP Fractions

IPs against PTEN were performed with an overnight incubation of 1:100 dilution of Rabbit Anti-PTEN polyclonal Ab or 1:100 dilution of Rabbit Anti- α/β -Tubulin polyclonal Ab in 200 μ l of HCT-116 WT lysate or HCT-116 -/- lysate at 1 mg/ml, with bead-only controls where no antibody was added to the lysates. Fractions collected during the IPs were analysed by SDS-PAGE for both the HCT-116 WT IPs (A) and the HCT-116 -/- IPs (B).

When probing for PTEN, western blot analysis of the eluates from the IPs performed with HCT-116 WT and -/- cells against PTEN and α/β -tubulin, no bands for PTEN were detected other than the control band for PTEN-GST (Figure 6.5A). Whilst no band for PTEN would be expected in the HCT-116 -/- lysate or the IP eluates for WT and -/- against α/β -tubulin, a band at 50 kDa for endogenous PTEN would be expected in the HCT-116 WT lysate and the eluate from the WT IP against PTEN. Probing for α/β -tubulin showed a strong band at 50 kDa in the

HCT-116 WT and *-/-* lysates, with a stronger band in the anti- α/β -tubulin IP eluates, indicating successful isolation of α/β -tubulin during the IP. There was a weak band present in the anti-PTEN IP eluates, as well as in one of the control IPs with no Ab, which could be explained by non-specific binding of α/β -tubulin to the protein A Sepharose resin. Taken together with the results from Figure 6.3, where the heavy chain of the anti-PTEN Ab was detected but there was no observable detection of PTEN, the IP protocol successfully isolates a target protein. This could be explained by a low endogenous level of PTEN in the WT cells and/or poor detection of PTEN during western blotting, as although there was a band corresponding to the purified PTEN-GST, 0.5 μ g was loaded which is a relatively large amount of protein for western blot detection.

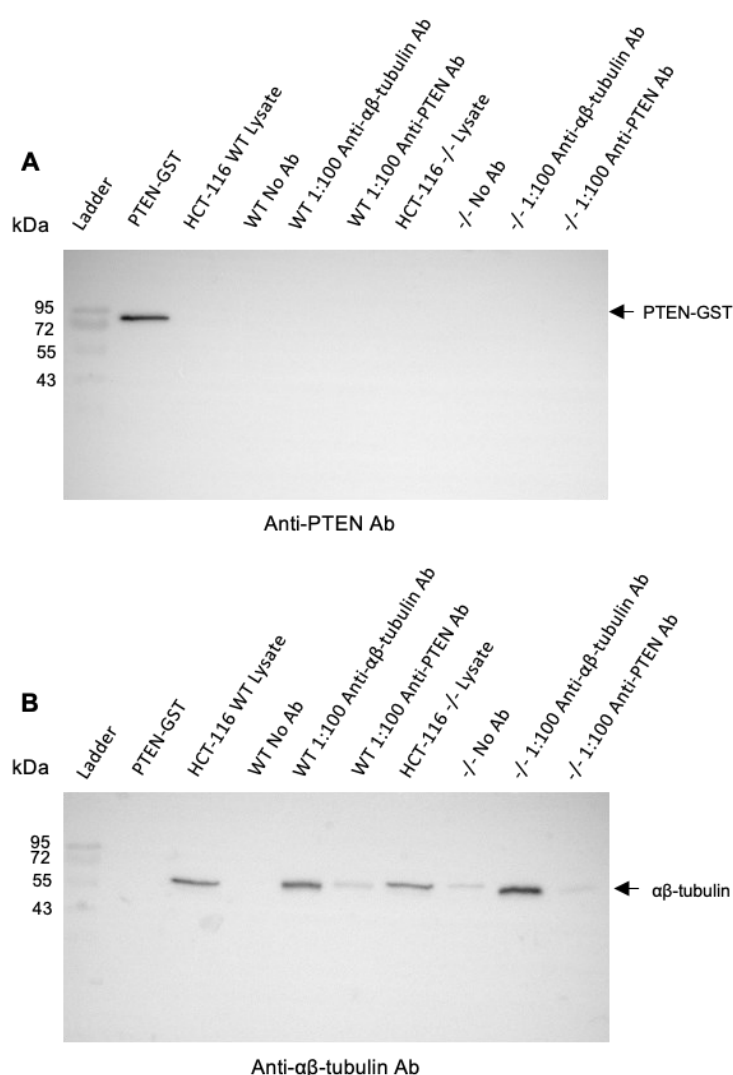


Figure 6.5 Western Blot Analysis of the PTEN and α/β -Tubulin CoIP Elution Fractions

CoIP against PTEN was performed with an overnight incubation of 1:100 dilution of Rabbit Anti-PTEN polyclonal Ab or 1:100 dilution of Rabbit Anti- α/β -Tubulin polyclonal Ab in HCT-116 WT or *-/-* lysate at 1 mg/ml in 200 μ l, with bead-only controls included where no antibody was added to the lysates. Elution fractions were analysed by Western Blot. A) Western Blot analysis was performed for PTEN using a Rabbit Anti-PTEN polyclonal primary antibody and a Mouse Anti-Rabbit IgG (Conformation Specific)-HRP monoclonal secondary antibody to detect only native IgG. B) After stripping and re-blocking, the blot was re-probed for α/β -Tubulin using a Rabbit Anti- α/β -Tubulin polyclonal Ab

and a Mouse Anti-Rabbit IgG (Conformation Specific)-HRP monoclonal secondary antibody to detect only native IgG.

6.3.4 Detection of Endogenous PTEN in HCT-116 Lysate and Optimisation of Lysis for Western Blot Analysis

After improvements were made to the western blot protocol, as described in section 6.2.3, detection of PTEN and α/β -tubulin in mammalian cell lysates was tested. Two lysis buffers, 1X reducing SDS-PAGE loading dye and a mammalian lysis buffer, were tested in parallel to determine the optimal lysis conditions for western blot detection. Figure 6.6A shows a strong band at 80 kDa, corresponding to PTEN-GST, in the western blot positive control. There is a weak band at 50 kDa corresponding to endogenous PTEN for both the MCF-7 and HCT-116 WT lysates, whilst no band was detected in the HCT-116 -/- lysate (Figure 6.6A). The intensity of the band was slightly higher for the cells lysed in lysis buffer, indicating a more efficient lysis (Figure 6.6A). There was also a slight increase in intensity of the endogenous PTEN band in the MCF-7 lanes in comparison to the HCT-116 WT lanes, indicating a slightly higher abundance of PTEN in MCF-7 cells. The blot was stripped and re-blocked before probing for α/β -tubulin (Figure 6.6B). There was a band at 80 kDa in the PTEN-GST control lane, which can be explained by insufficient stripping of the anti-PTEN antibody prior to incubation with α/β -tubulin and re-exposure (Figure 6.6B). There was a band at 50 kDa in all lysate lanes, across all three cell lines, with a slight increase in band intensity for the lysates in lysis buffer, mirroring the results from Figure 6.6A.

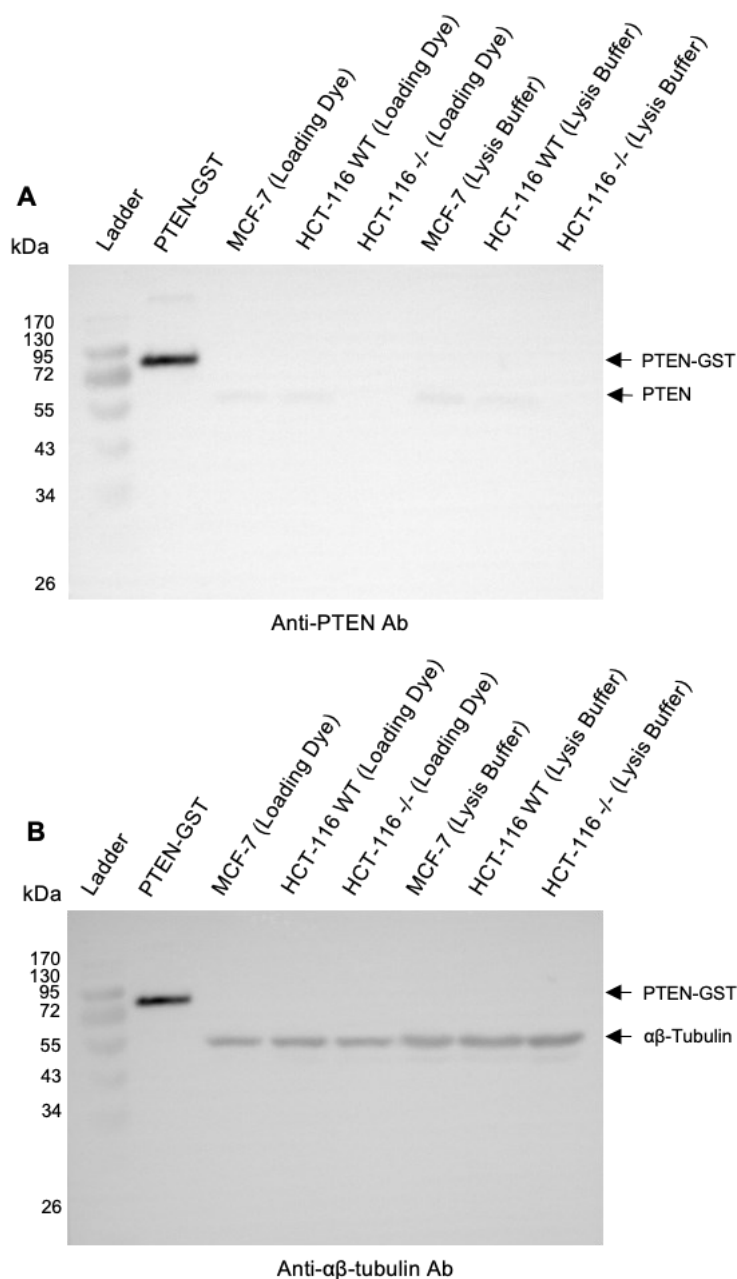


Figure 6.6 Western Blot Analysis of the Detection of PTEN and α/β -Tubulin Under Different Lysis Conditions
 Two wells of a 6-well plate were seeded with 2.5×10^5 cells/well of HCT-116 WT, ^{-/-} or MCF-7 cells and the plate was incubated for 48 hours at 37°C and 5% CO₂ before lysis with either 1X Laemmli Buffer or lysis buffer. Western Blot analysis was performed with 20 μ l of lysates in 1X Laemmli Buffer and 20 μ g of lysates. A) Western Blot analysis was performed for PTEN using a Rabbit Anti-PTEN polyclonal primary antibody. B) After stripping and re-blocking, the blot was re-probed for α/β -Tubulin using a Rabbit Anti- α/β -Tubulin polyclonal Ab.

6.3.5 Repeat IP of Endogenous PTEN from HCT-116 WT and MCF-7 Cells

Figure 6.6 showed successful detection of endogenous PTEN, confirming the expression of PTEN in HCT-116 WT cells, as would be expected, and a clear improvement in the detection of PTEN during western blot analysis was seen. IP of PTEN was performed for MCF-7 and HCT-116 WT cells, with a control IP without Ab, and the eluates were analysed by western blot for PTEN and Rabbit IgG (Figure 6.7). A clear band at 80 kDa was seen in the PTEN

positive control, corresponding to PTEN-GST (Figure 6.7A). Whilst there was a faint band at 60 kDa corresponding to endogenous PTEN in the MCF-7 lysate, no band was observed in the HCT-116 WT lysate (Figure 6.7A). The absence of observable endogenous PTEN in the HCT-116 WT lysate contradicts the results in Figure 6.6A, where endogenous PTEN is detected in both HCT-116 WT and MCF-7 lysates, despite equal loading of 30 µg of lysate. Despite this, a 60 kDa band is visible in the IP eluates from both MCF-7 cells and HCT-116 WT cells, demonstrating the presence of endogenous PTEN in both cell lysates and successful capture and isolation during the IP (Figure 6.7A). The membrane was stripped, re-blocked and probed for Rabbit IgG as validation for capture of the Ab and an additional band at 50 kDa is observed in both eluates, corresponding to the heavy chain of the Ab used in the IP (Figure 6.7B). Despite stripping the membrane after the first exposure, the PTEN bands are still visible, indicating insufficient stripping of the PTEN antibody.

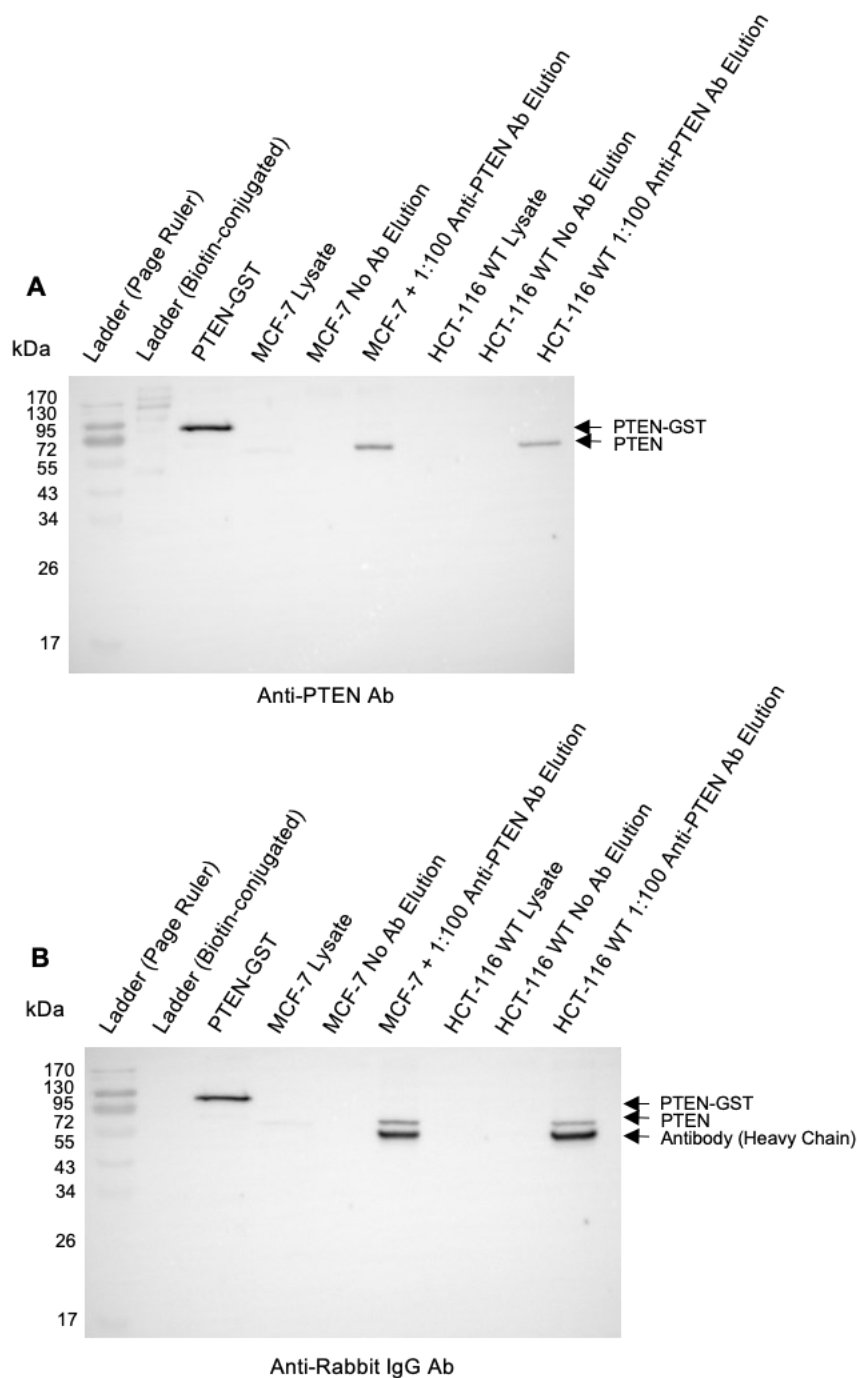


Figure 6.7 Western Blot Analysis of PTEN IP from HCT-116 WT and MCF-7 Cells

IP against PTEN was performed with an overnight incubation of 1:100 dilution of Rabbit Anti-PTEN polyclonal Ab in 200 μ l of HCT-116 WT lysate or MCF-7 lysate at 1 mg/ml, with bead-only controls included where no antibody was added to the lysates. Elution fractions were analysed by Western Blot. A) Western Blot analysis was performed for PTEN using a Rabbit Anti-PTEN polyclonal primary antibody and a Mouse Anti-Rabbit IgG (Conformation Specific)-HRP monoclonal secondary antibody to detect only native IgG. B) After stripping and re-blocking, the blot was re-probed for Rabbit IgG using a Goat Anti-Rabbit-HRP conjugate polyclonal secondary antibody to detect the denatured IgG in the IP samples.

6.3.6 CoIP of Endogenous PTEN from Untreated and Acrolein-treated HCT-116 Cells

As endogenous PTEN could now be detected in the lysate and the IP eluates, coIP was performed on untreated cells and cells treated with 100 μ M acrolein. Due to the non-specific binding demonstrated by SDS-PAGE analysis of the control IP where no Ab was used in Figure 6.4, a pre-clearing step was added to the protocol to remove any proteins with non-specific binding to the resin. There was no observable protein detected in the eluates of the control IPs, where no Ab was added to the lysates, for both the untreated and acrolein-treated cells indicating that the pre-clearing step was successful in reducing non-specific binding (Figure 6.8A and B). The eluates for the PTEN IPs showed a clear band at approximately 50 kDa, which is likely to be the heavy chain of the PTEN Ab, but very little other protein (Figure 6.8A and B). An additional elution step was performed to confirm that all protein was eluted, but minimal extra protein was detected in this fraction (Figure 6.8A and B). The first elution fraction was taken forward for western blot analysis for PTEN, Rabbit IgG and HECTD1 (Figure 6.9).

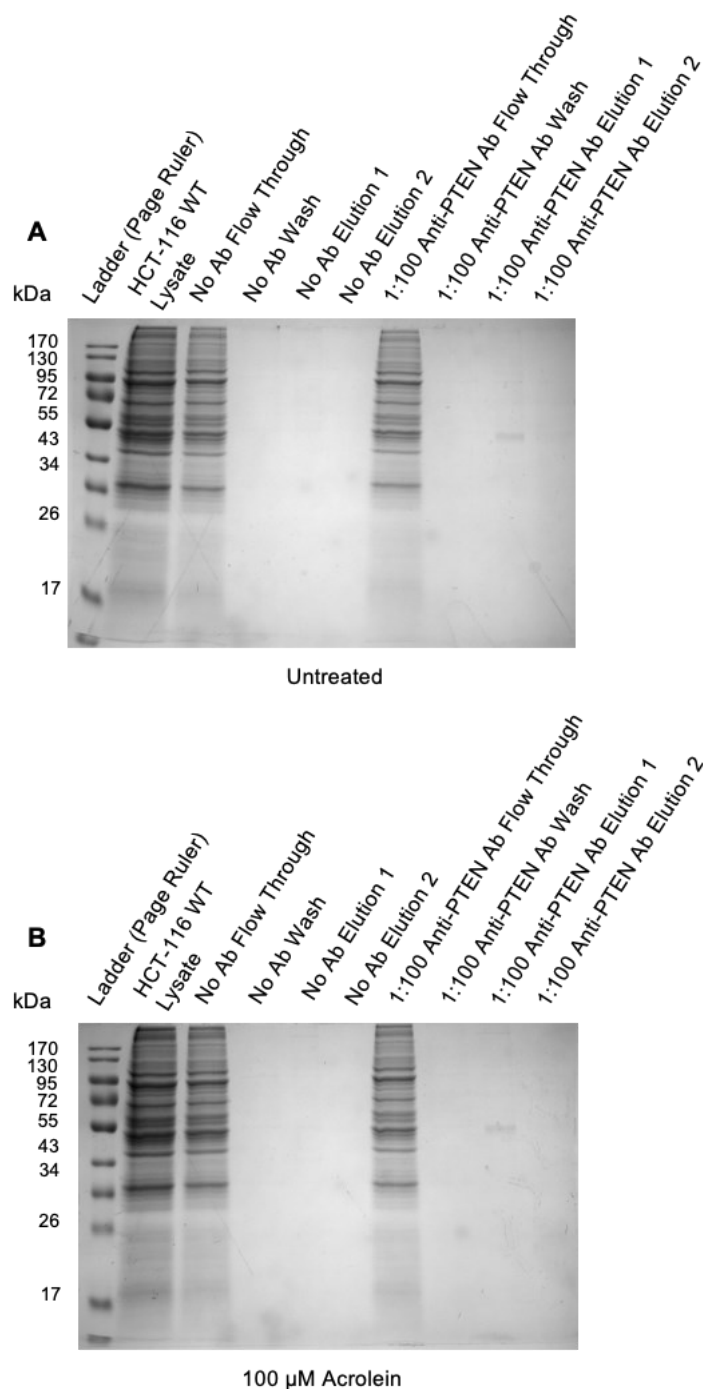


Figure 6.8 SDS-PAGE Analysis of the PTEN CoIP Fractions from Untreated and Acrolein-Treated HCT-116 Lysates

Two 150 mm cell culture plates were seeded with 5×10^5 cells/plate of HCT-116 WT cells and the plate was incubated for 48 hours at 37 °C and 5% CO₂. Plates were untreated or treated with 100 μM acrolein for 1 hour before lysis. CoIPs for PTEN was performed with an overnight incubation of 1:100 dilution of Rabbit Anti-PTEN polyclonal Ab in 500 μl of HCT-116 WT lysate at 1 mg/ml, with bead-only controls included where no antibody was added to the lysates. Fractions collected during the CoIPs were analysed by SDS-PAGE for both the HCT-116 WT untreated CoIP (A) and the HCT-116 WT 100 μM acrolein-treated CoIP (B).

The lysates from the untreated and acrolein-treated cells used for the CoIPs were analysed by Western Blot for PTEN and Rabbit IgG to confirm successful IP of PTEN and HECTD1 to assess the CoIP of HECTD1 (Figure 6.9A). The western blot for PTEN confirmed the presence of endogenous PTEN in the lysates from the untreated and acrolein-treated cells, where there appeared to be a slight increase in intensity on acrolein-treatment of cells (Figure 6.9A: Anti-PTEN). As expected, there was no band with anti-Rabbit IgG as this is not expressed endogenously in human cells (Figure 6.9A: Anti-Rabbit IgG). There was no observable band at 290 kDa, the expected molecular weight of HECTD1, with anti-HECTD1 Ab in either the untreated or treated cell lysates (Figure 6.9A: Anti-HECTD1). This could be due to a low endogenous expression of HECTD1, as HECTD1 was successfully detected in Chapter 5 during the APD using recombinant PTEN and HCT-116 cell lysates, where the concentration of HECTD1 would be higher than in the original lysate. There were no bands present in either of the elution fractions from the bead-only control, where the CoIP was performed with the omission of the PTEN Ab, demonstrating no detectable non-specific binding to the resin of PTEN or HECTD1 (Figure 6.9B: Anti-PTEN, Anti-Rabbit IgG and Anti-HECTD1).

The CoIP elution fractions from the untreated and acrolein-treated cells did not show a clear band for endogenous PTEN when probing with the anti-PTEN Ab (Figure 6.9C: Anti-PTEN). There was some higher molecular weight bands and a band at around 40 kDa in the acrolein-CoIP, which could be non-specific binding of the anti-PTEN Ab during the western blot process in combination with overexposure of the membrane, where there are visible white patches due to drying out of the membrane (Figure 6.9C: Anti-PTEN). The heavy chain of the anti-PTEN Rabbit Ab is detected in both the elution fractions, indicating the successful capture of the antibody (Figure 6.9C: Anti-Rabbit IgG). There was also no detection of HECTD1 in either of the elution fractions, which could be explained by an issue during the CoIP as PTEN was also not detected (Figure 6.9C: Anti-HECTD1). The CoIP with untreated and acrolein-treated cells was only performed once due to time restraints and so no firm conclusion can be drawn from this set of results as to the validity of the PTEN-HECTD1 interaction and its potential upregulation on acrolein exposure.

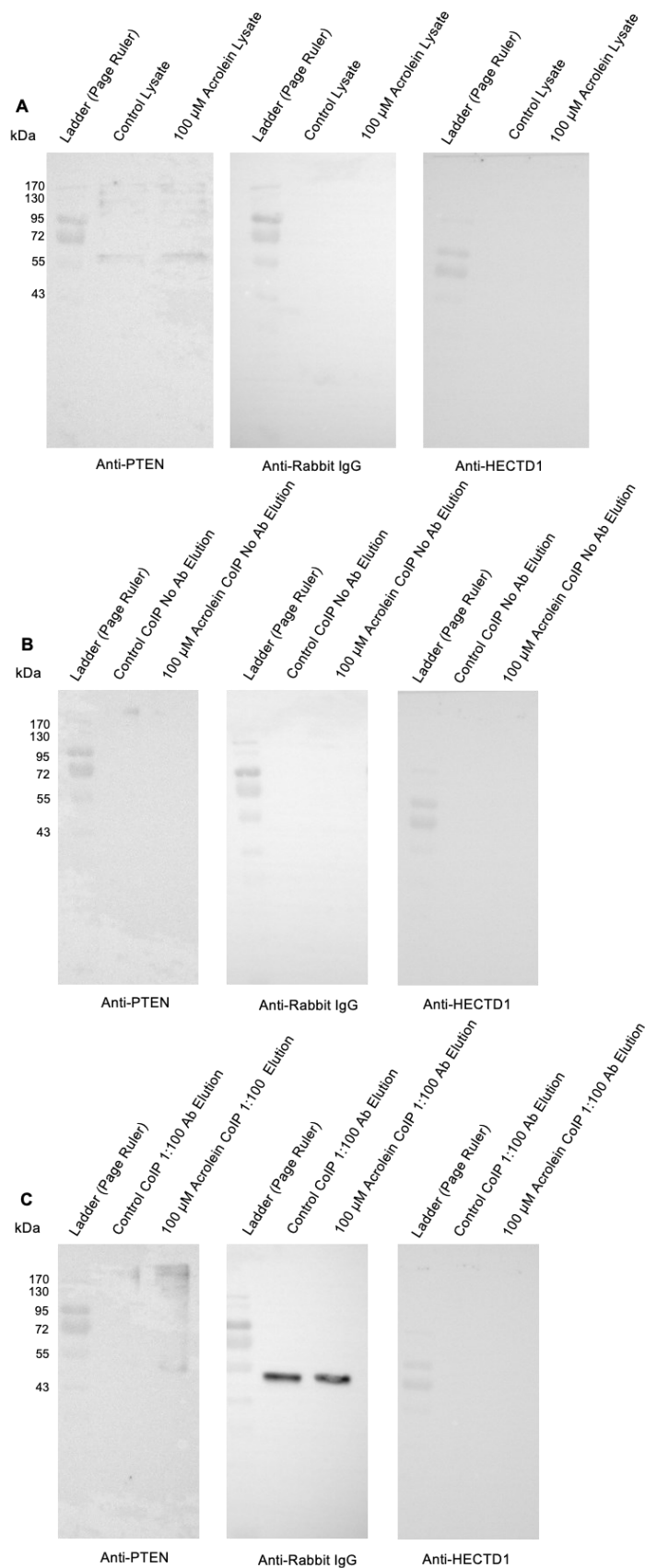


Figure 6.9 Western Blot Analysis of PTEN CoIP from HCT-116 WT and MCF-7 cells

Two 150 mm cell culture plates were seeded with 5×10^5 cells/plate of HCT-116 WT cells and the plate was incubated for 48 hours at 37 °C and 5% CO₂. Plates were left untreated or treated with 100 μ M acrolein for 1 hour before lysis. CoIPs against PTEN was performed with an overnight incubation of 1:100 dilution of Rabbit Anti-PTEN

polyclonal Ab or 1:100 dilution of Rabbit Anti- α/β -Tubulin polyclonal Ab in 500 μ l of HCT-116 WT lysate at 1 mg/ml in 500 μ l, with bead-only controls included where no antibody was added to the lysates. Fractions collected during the ColPs were analysed by Western Blot using Rabbit Anti-PTEN polyclonal Ab, Rabbit Anti- α/β -Tubulin polyclonal Ab, Rabbit Anti-HECTD1 polyclonal Ab for the HCT-116 WT untreated and 100 μ M acrolein-treated lysates (A) and untreated and 100 μ M acrolein-treated bead-only ColP control (B) and PTEN ColPs (C).

6.3.7 Acrolein Treatment Increases the Level of pAkt whilst levels of total Akt Remain Stable

Due to the observation of a loss of PTEN activity on exposure to acrolein in Chapter 4, to analyse the *in cellulo* effect of acrolein on the Akt pathway, the amount of active pAKT was analysed using Western Blot. Using the results from the MTT assay in Figure 6.2, HCT-116 cells were treated with increasing acrolein concentrations below the level at which there was a significant decrease in cell viability for 1 hour. The lysates from the treated cells were probed for panAKT, AKT phosphorylated on Ser403 and α/β -tubulin was used as a loading control (Figure 6.10A). Whilst there was no observable change in the levels of panAKT on increasing acrolein concentration (Figure 6.10A: AKT (pan)), there was an observable increase in the levels of phosphorylated AKT (Figure 6.10A: AKT (pSer403)). There was also no observable change in the levels of α/β -tubulin, which confirmed equal loading across each of the treatment concentrations, attributing the increase in acrolein concentration to the cause of an increase in pAkt levels, rather than unequal sample loading. Densitometry analysis was performed and the intensity of the AKT and pAKT bands were normalised to the α/β -tubulin control (Figure 6.10B). Normalisation confirmed that whilst there was a minimal change in the levels of AKT or α/β -tubulin, there was an increase in pAKT as the acrolein concentration increases, where there is a large difference between 5 and 50 μ M acrolein, this plateaus between 50 and 200 μ M acrolein (Figure 6.10B).

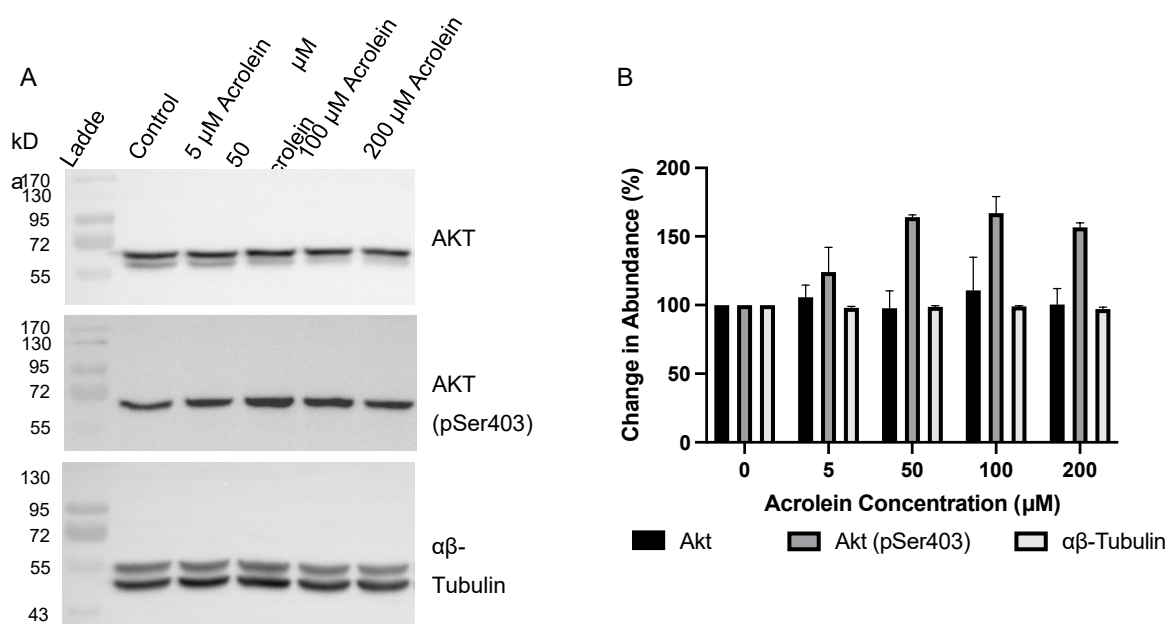


Figure 6.10 Western Blot Analysis of the Detection of Akt, phosphoAkt (Ser403) and αβ-Tubulin with Increasing Acrolein Treatment Concentration

A 6-well plate was seeded with 2.5×10^5 cells/well of HCT-116 WT and the plate was incubated for 48 hours at 37°C and 5% CO₂ before treatment with increasing concentrations of acrolein for 1 hour at 37°C. The cells were washed in PBS and lysed before quantification with the BCA assay. 20 μg of lysates was resolved by SDS-PAGE and western blot analysis was performed using Rabbit Anti-Akt polyclonal Ab, Rabbit phosphoAkt (Ser403) polyclonal Ab and Rabbit αβ-Tubulin polyclonal Ab (A). The bands were analysed by densitometry using ImageJ and the band abundance was normalised to the αβ-Tubulin control bands. The change in abundance of Akt, phosphoAkt (Ser403) and αβ-Tubulin at increasing acrolein concentrations was calculated by expressing the abundance as a percentage of the untreated control for each blot (n=3; Mean ± SEM).

6.4 Discussion

The work presented in this thesis preceding this chapter characterised the effect of acrolein on PTEN's activity, structure, and interactions *in vitro*. The aim of this final chapter was to investigate the *in cellulo* effects of acrolein. The effect of whole cell exposure to acrolein on PTEN's activity was investigated indirectly through analysis of the PI3K/Akt signalling pathway and the effect on PTEN's interactome was attempted directly by trialled investigation of the HECTD1-PTEN interaction using CoIP. To achieve this, the effect of acrolein on the cell viability of HCT-116 cells was quantified using the MTT assay and sublethal acrolein concentrations were taken forward to treat HCT-116 cells to analyse the effect on the levels of activate pAkt by western blotting and densitometry analysis. CoIP of PTEN from both HCT-116 cells and MCF-7 cells was trialled to test the successful IP of endogenous PTEN before attempting to incorporate a whole cell sublethal acrolein treatment, determined from the cell viability data. CoIP was performed on untreated and acrolein-treated HCT-116 cells to attempt to validate the HECTD1-PTEN interaction *in cellulo* and identify any changes in the abundance of this interaction on exposure to acrolein. However, this CoIP was unsuccessful in precipitating endogenous PTEN from both the untreated and acrolein-treated cells, meaning that no conclusions could be drawn from this data set.

The first key finding for this chapter was the optimal protocol for the MTT assay, by finding the appropriate HCT-116 cell seeding density and an effective formazan solubilisation solution strategy. The identified MTT protocol was then used to quantify any loss of cell viability on treatment with acrolein for 1 and 24 hours. A loss of cell viability on increasing acrolein concentration was seen at both time points, but there was an increased loss of cell viability at lower acrolein concentrations at the longer time point, indicating a greater loss of cell viability with increasing length of exposure. The second key finding was that on treatment of HCT-116 cells with sublethal acrolein concentrations, there was an increased abundance of pAkt whilst the levels of inactive Akt remained stable, indicating an upregulation of the PI3K/Akt signalling pathway.

As introduced in section 6.1.1, the principle of the MTT assay is that metabolism of viable cells is proportional to cell viability and as such, the assay relies on the ability to detect a decrease/increase in metabolism with a decrease/increase in the number of viable cells present (Aslantürk, 2018). Despite there being several studies using the MTT assay to assess the cytotoxicity of a range of compounds for HCT-116 cells, it was still necessary to confirm the appropriate seeding density under these laboratory conditions. The plateau effect that occurs for increasing numbers of cells per well has been reported as a result of over-

confluence which can cause changes in the local environment due to media exhaustion which can affect cellular metabolism (Carreño et al., 2021). The linear range of three different cancer cell lines, GL21, U87 and SHSY5Y, have previously been tested and the maximal cell numbers of the linear range was determined as between 1.2 and 3.0×10^4 cells/well (Carreño et al., 2021). A narrow range of seeding densities, between 0.1 and 2.5×10^4 cells/well, have previously been cited for HCT-116 cells, and the seeding density used here of 1×10^4 cells/well fits within this range (Grbović et al., 2013, El Khoury et al., 2016, Liu et al., 2017, Oliveira et al., 2020, Kim and Park, 2020, Yaacoub et al., 2021, Fu et al., 2021, Tsai et al., 2021). As performed in this current study, each of the aforementioned studies included a 24-hour incubation step prior to the MTT assay. This step was included here for practical reasons, to give the cells time to adhere to the plate and allow the well washes and media changes to be completed with manual aspiration. This removes the requirement for centrifugation which minimises the risk of cell loss during washes and allows the assay to proceed quickly. This 24-hour incubation step also gives the cells time to recover from the harvest and seeding preparation steps. In addition to falling within the linear range of absorbance, the importance of performing this assay during the log phase of cell proliferation has been raised (van Meerloo et al., 2011). This could have been verified by performing a growth curve, where the MTT assay is performed at different time points from the point of cell seeding (van Meerloo et al., 2011).

There are several adaptations that can be made to the MTT protocol depending on the application. The concentration of MTT and the MTT incubation time can vary, from between 0.1 - 0.5 mg/ml and 2-4 hours. The effect of increasing MTT concentration and incubation time on the final absorbance has previously been tested, where a plateau was reached with both increases (Ghasemi et al., 2021). Whilst the MTT incubation time has varied from 1-4 hours for previous studies using HCT-116 cells, the final concentration of MTT was consistent at 0.5 mg/ml (El Khoury et al., 2016, Grbović et al., 2013, Liu et al., 2017, Kim and Park, 2020). Here, the acrolein treatment was removed and the cells were washed with PBS prior to the addition of MTT. This was done to ensure that there was no interference of continued acrolein exposure during incubation with and reduction of MTT and, as such, the viability data could be correlated to a specific treatment time that could be taken forward for further experiments. The excess MTT was not removed prior to the addition of the solubilisation reagent, as unreduced MTT does not interfere with the absorption, and this absence of an MTT wash step follows the original protocol developed by Mosmann (1983) (Ghasemi et al., 2021). One consideration for the inclusion of a wash step prior to formazan solubilisation is the potential for organic solvents to precipitate serum proteins in media (Young et al., 2005). However, here a serum- and phenol-red free media was used during the MTT incubation step, and the inclusion of the PBS

wash step post-acrolein treatment would have removed any excess serum-containing media before addition of the MTT. Another consideration is that the presence of extracellular formazan crystals has previously been proposed as a potential route for the overestimation of cell viability where MTT has been reported to be reduced by cell culture media (Young et al., 2005) and as such could introduce a source of false positive data (Stockert et al., 2018). This is easily mitigated by the inclusion of 'blank' wells, as was done here, where MTT is incubated with media in the absence of any cells and this background absorbance can then be subtracted from the absorbance of the wells containing cells. Importantly, there are several other hypotheses for the appearance of extracellular formazan: release of intracellular formazan by exocytosis (Liu et al., 1997), damage to the cell membrane by the crystals (Bernas and Dobrucki, 2004) or as a result of other molecular interactions (Diaz et al., 2007). The loss of this exported formazan during a post-MTT incubation wash step could result in an underestimation of cell viability and, where there may be damage to cellular membranes after cytotoxic treatments, this effect could be exacerbated at higher treatment concentrations or longer treatment times. By excluding a wash step prior to solubilisation, both the intracellular and extracellular formazan will be solubilised and will contribute to the absorption values and estimation of cell viability (Ghasemi et al., 2021).

With regard to the formazan solubilisation strategy, as introduced above there is a consideration in the use of organic solvents in the presence of serum proteins, due to their propensity to precipitate and the potential interference of these precipitates on absorption (Young et al., 2005) and the use of a mildly acidic solution in the presence of phenol red, which without pH adjustment would interfere with the absorption due to its absorption at 570 nm (Mosmann, 1983). As described above, the media used here during the MTT incubation step was serum- and phenol-red free, this was not a consideration for this study. However, both HCl and SDS were included in both solubilisation solutions trialled in this study, and so could have minimised the risk of absorbance interference by the presence of phenol red and serum. As the MTT incubation step was always performed in the absence of serum, the effect of the lack of serum on metabolism during the MTT incubation step was not assessed here. However, as this was constant across all treatment concentrations, it would not have affected the percentage loss of cell viability calculated here. The key considerations during solubilisation were to ensure that the formazan was sufficiently solubilised, to minimise well-to-well variation that may occur on uneven solubilisation, and ensure that the absorbance was in a detectable range. The lipophilic nature of formazan renders it insoluble in aqueous solutions (Riss et al., 2013). The original MTT protocol used acidified isopropanol (Mosmann, 1983), and other early strategies made use of other organic solvents, such as DMSO and dimethylformamide (DMF), often in combination with HCl or SDS, however more recent

studies have cited the successful use of aqueous buffers, such as acidified SDS (Lü et al., 2012). The studies cited here applying the MTT assay to HCT-116 cells have used both acidified IPA and DMSO as the solubilisation solutions (El Khoury et al., 2016, Grbović et al., 2013, Liu et al., 2017, Kim and Park, 2020, Tsai et al., 2021). Due to formazan's insolubility in aqueous solutions, solubilisation in acidified isopropanol would be expected to yield a higher absorbance, which was mirrored by the results in this current study where the absorbance for the highest cell number was over 2-fold higher when solubilised in acidified isopropanol in comparison to acidified SDS. Although there was an additional practical change, where the cells were manual resuspended with acidified isopropanol, where in SDS the wells were only mixed by shaking and then incubated statically overnight, which likely would have also increased the absorbance. Alternative tetrazolium-based colourimetric assays include the MTS and XTT assays, which have benefits over the MTT assay as the formazan produced is soluble in aqueous solutions (Adan et al., 2016), and these different approaches are reviewed by Kamiloglu et al. (2020).

The data presented in this thesis describes a dose- and time-dependent loss of cell viability for HCT-116 cells. This dose-dependent loss of cell viability on exposure to acrolein is confirmed by previous MTT assays performed for a variety of cell lines. To allow comparison, the previously cited cell viabilities for a defined acrolein concentration of 100 µM and a defined time point of 24 hours was chosen and the data is presented in Table 6.2. With the exception of Luo et al. (2018) for EAhy926 cells, the loss of cell viability was <55%, with the majority of cell lines cited as having <25% cell viability after a 24 hour treatment with acrolein (Table 6.2). This severe loss of cell viability seen by 5/6 of the studies is mirrored by the results of this current study, where a 24-hour treatment with 100 µM acrolein resulted in a cell viability of 11%. Minor differences in cell viability for the same treatment conditions could be explained by differences in the cell line, or practical variations in seeding density and confluency of the cells. However, the previous cell viability of HCT-116 cells after treatment for 24 hours with 0-100 µM acrolein is much higher than reported here, between 45-55% cell viability for 100 µM acrolein (Tsai et al., 2021). The only experimental difference is the seeding density, which was 10x lower at 1×10^3 cells/well. The opposite phenomena might be expected, where there could be a greater effect of acrolein when treating lower cell densities due to a comparatively higher acrolein concentration per cell. Interestingly, the profile of cell viability for the 24 hour treatment conducted by Tsai et al. (2021) more closely matches the profile for the 1 hour treatment conducted in this current study, where there is an initial increase in cell viability at low levels of acrolein between 0-10 µM, before decreasing to and beyond the cell viability of the control as the acrolein concentration increases. However, cell viability after a 1-hour treatment with 100 µM acrolein in this current study is much higher at 85%, where for the cited study is

between 45-55%, which would be expected due to the longer treatment time (Tsai et al., 2021). Other studies have evaluated the cytotoxicity of acrolein-derived compounds, such as cinnamaldehyde-analogues, on HCT-116 cells, using the MTT assay (Chew et al., 2010, Omar et al., 2020).

Table 6.2 Previous Cell Viability for Different Cell Lines after Treatment with 100 μ M Acrolein for 24 hours using the MTT Assay

Study	Cell Line	Cell Viability (%)
Luo et al. (2005)	PC12	8
Mohammad et al. (2012)	HepG2	10-20*
Wang et al. (2016)	HeLa	15-25*
	A549	15-25*
Luo et al. (2018)	EAh926	>90
Yin et al. (2020b)	HBE	10-20*
	Caco-2	25-35*
Yin et al. (2020a)	LO2	29
Tsai et al. (2021)	HCT-116	45-55*
Current	HCT-116	11

Key:
*: Approximation of cell viability from the graphical figure from each study, where the cell viability for 100 μ M acrolein treatment was not specifically stated

Whilst the effect of acrolein on the cell viability of HCT-116 cells in this study was analysed to determine sub-lethal concentrations of acrolein for further experiments, it would have been interesting to further characterise the mechanisms through which acrolein caused cell death. As the MTT assay relies on the cell metabolism to infer the number of viable cells and acrolein is known to cause mitochondrial dysfunction (Moghe et al., 2015), in future work it would be beneficial to assess cell death through a mitochondria-independent experiment alongside the cell viability assay. Previous efforts to characterise further the mechanism through which acrolein induces cell death have included determination of the type of cell death, necrosis or apoptosis, by probing for apoptosis markers. Markers of apoptosis assessed by the studies in Table 6.2 include DNA fragmentation, upregulation of caspases and exposure of annexin V at the cell surface (Mohammad et al., 2012, Yin et al., 2020b). DNA fragmentation has been identified using ELISA, staining with propidium iodide and visualisation with microscopy or quantification using flow cytometry (Luo et al., 2005, Mohammad et al., 2012, Yin et al., 2020b). Upregulation of caspases has been identified by western blotting for inactive pro-caspases and active cleaved caspases (Mohammad et al., 2012, Wang et al., 2016, Luo et al., 2018, Yin et al., 2020b, Yin et al., 2020a). Exposure of annexin V has been quantified using flow cytometry (Yin et al., 2020a, Yin et al., 2020b). Acrolein has been identified to induce cell death by both apoptosis and necrosis; Luo et al. (2005) and Mohammad et al. (2012) identified necrosis as the main mechanism of cell death whereas Wang et al. (2016)

identified apoptosis as the main mechanism of cell death. Luo et al. (2018), Yin et al. (2020a) and Yin et al. (2020b) did not seek to identify necrosis but identified induction of apoptosis by acrolein. Tsai et al. (2021) focused on the oncogenic transformation induced by acrolein, rather than characterisation of a loss of cell viability. Further characterisation of the effect of acrolein on cells has included quantification of ROS generation to determine induction of oxidative stress, assessment of mitochondrial dysfunction by quantification of membrane potential and assessment of the downstream signalling effects by western blotting for cell signalling proteins (Luo et al., 2005, Mohammad et al., 2012, Wang et al., 2016, Luo et al., 2018, Yin et al., 2020a, Yin et al., 2020b).

With regard to the *in cellulo* effect of acrolein on PTEN's activity, this has been inferred by the levels of the phosphorylated active form of Akt (pAkt), as discussed in section 6.1.2, and this can be measured by western blot analysis probing for Akt and pAkt alongside a loading control. Outside of the context of PTEN, activation of the MAPK pathway by acrolein has been analysed by western blot analysis of HCT-116 cells treated with 5 μ M acrolein for 3-24 hours, and 2.5-10 μ M acrolein for 24 hours. This has included analysis of Akt and pAkt, alongside other signalling proteins involved in the MAPK pathway. The levels of Akt remained stable with increasing treatment time with 5 μ M acrolein, and, whilst there was no increase in the levels of pAkt after a 3-hour treatment, an increase was seen at 8 hours and 24 hours acrolein treatment (Tsai et al., 2021). An increase in pAkt was seen for lower acrolein concentrations (<5 μ M) after a longer treatment of 24 hours, however this was accompanied by an increase in AKT and would require normalisation to confirm activation of AKT (Tsai et al., 2021). All acrolein concentrations used in the previous study were sublethal and this was determined by the MTT assay (Tsai et al., 2021). The correlation of pAkt with alkylation or inactivation of PTEN has previously been reported after treatment with acrolein (Covey et al., 2010), 4-HNE (Shearn et al., 2011, Covey et al., 2010), an α/β -enone, Δ 12PGJ₂ (Covey et al., 2010) and spermine oxidase, which induces endogenous acrolein production (Uemura et al., 2017). This supports the correlation of the *in vitro* results from Chapter 4, which showed modification and inhibition of PTEN's phosphatase activity, with the activation of the Akt pathway identified in this current Chapter, and strengthens the hypothesis that acrolein inhibits PTEN's ability to modulate the Akt pathway. The detection of acrolein-modified PTEN from cell lysates, in addition to probing for Akt and pAkt, would have further strengthened this data set and this has previously been achieved by tagging alkylated PTEN by a biotin-conjugated tagging method and detecting by western blot (Covey et al., 2010, Uemura et al., 2017) or through biotin-labelling of alkylated PTEN and subsequent pull down with streptavidin (Shearn et al., 2011). This could be taken one step further by the investigation of endogenous PTEN's

phosphatase activity, through pulldown of PTEN from treated cells and subsequent measurement of phosphatase activity of the immunoprecipitates (Spinelli and Leslie, 2016).

There are several approaches to the validation of protein-protein interactions identified *in vitro* by affinity pull down assay, as introduced in section 6.1.3. Co-immunoprecipitation involves the use of a specific antibody and Protein A or G resin to capture a target protein and any interacting proteins, including direct and indirect interactors (Lin and Lai, 2017). Co-immunoprecipitation is a common affinity method for both the identification and validation of protein-protein interactions and this approach has been used to validate PTEN interactors by 4 of the 7 previous high data content PTEN interactome studies detailed in Table 5.1. There are several different variations of coimmunoprecipitation, where the bait can be endogenous or overexpressed and the specific antibody can be against a target protein or a tag, when the bait is a fusion protein. The antibody can be applied to whole lysates for capture *in cellulo* or to purified protein for capture *in vitro* and there is an option to immobilise the antibody to Protein A or G resin prior to bait exposure, or apply a separate resin binding step once the antibody has been exposed to the bait. The approaches to coimmunoprecipitation of the previous PTEN interactome studies are detailed in Table 6.3.

Table 6.3 Methods for Coimmunoprecipitation of PTEN from Mammalian Cell Lines from Previous PTEN Interactome Studies

Study	Bait	Bait Source	Prey	Prey Source
Ahn et al. (2008)	Wild Type PTEN	Endogenous	HeLa proteins	Endogenous
Gorbenko et al. (2010)	Purified GST-FABP4	Exogenous (Overexpressed in <i>E. coli</i>)	Purified PTEN-His	Exogenous (Overexpressed in <i>E. coli</i>)
Gunaratne et al. (2011)	PTEN-FLAP	Endogenous	U87MG proteins	Endogenous
Maddika et al. (2011)	Wild Type PTEN PTEN-FLAP	Endogenous	293T proteins	Endogenous

Whilst these studies utilised co-immunoprecipitation as a validation technique for specific potential interactors that were identified by other biochemical means, such as affinity pull down, there were differences in the source of PTEN and prey proteins. Whilst Ahn et al. (2008), Gunaratne et al. (2011) and Maddika et al. (2011) performed the co-immunoprecipitation from whole cell lysates containing both the bait and prey proteins with subsequent capture of the bait/prey complexes by binding with specific antibodies and precipitating with specific resin, Gorbenko et al. (2010) performed the co-immunoprecipitation with purified fusion proteins of both PTEN and the potential interactor, FABP4. Whilst the use of purified protein allows a specific and targeted investigation to confirm the capability of FABP4 to interact with PTEN,

this does not validate this interaction in a physiological context and there is consideration to the effect of a tag, as has been previously discussed in Chapter 3 and 5. This is also a consideration for the co-immunoprecipitation approach used by Gunaratne et al. (2011), where although the co-immunoprecipitation was performed with whole cell lysates, this was from a mammalian cell line (U87MG) stably expressing PTEN-FLAP. Briefly, the inclusion of a tag may influence proteins subcellular localisation and conformation as well as accessibility of native binding sites and the potential introduction of new binding sites on the tag itself. Overexpression has the advantage in that there will be a higher yield of target protein and, as not all cell lines express PTEN with equal abundance (Ghandi et al., 2019), this may improve detection of low abundance interactors. Due to the difficulties described in this chapter in the detection of the PTEN precipitated from HCT-116 cells with an anti-PTEN antibody, transient transfection of a PTEN fusion protein could have solved this practical issue. However, increasing the amount of target protein above native levels may lead to the detection of interactions at a non-physiological level. This is highlighted by a discrepancy in the results from two of the high data content PTEN interactome studies. Initially NEDD4-1 was identified as a ubiquitin ligase for PTEN (Ahn et al., 2008) but it was later found that ubiquitination of PTEN was unaffected in cells with a NEDD4-1 deficiency and WWP2 was the lead ubiquitin ligase for PTEN (Maddika et al., 2011). This difference in experimental findings was suggested to be due to the use of overexpression of NEDD4-1 by Ahn et al. (2008), where Maddika et al. (2011) utilised physiological levels of NEDD4-1, causing an initial exaggeration of the relationship of NEDD4-1 and its requirement to regulate PTEN (Fouladkou et al., 2008). The role of NEDD4-1 and WWP2 in the ubiquitination of PTEN has more recently been directly compared, identifying both as ubiquitin ligases of PTEN and confirming the previous exaggeration of the reliance of PTEN ubiquitination and NEDD4-1 as WWP2 was identified as more active in terms of PTEN ubiquitination (Chen et al., 2016b). At the time of writing, there has been 14 identifications of NEDD4-1 and 13 identifications of WWP2 as interactors of PTEN (Stark et al., 2006).

Whilst on improvement of western blot detection, PTEN was detected after trial immunoprecipitations from HCT-116 and MCF-7 cells with the anti-PTEN antibody, and the studies outlined in Table 6.3 demonstrate that endogenous PTEN can be successfully precipitated from several other mammalian cell lines, the final immunoprecipitation of endogenous PTEN from lysates of untreated and acrolein-treated HCT-116 cells was unsuccessful as PTEN was undetectable in the eluates. Therefore, the novel PTEN-HECTD1 interaction could not be validated from these results. Due to time constraints, this experiment could not be repeated, and so whilst this does not provide any evidence against the PTEN-

HECTD1 interaction, there is no additional *in cellulo* evidence for this interaction or any upregulation of it on acrolein treatment from this experimental data.

Future work to validate the proposed novel interaction between HECTD1 and PTEN would involve successful co-immunoprecipitation of HECTD1 with PTEN to confirm the interaction *in cellulo*. To overcome the issues with detection of PTEN, as mentioned above, transient expression of recombinant PTEN could be used to increase the amount of PTEN in the cell, with consideration to the potential interference of overexpression discussed above. Future work could also involve SPR to quantify the binding kinetics and it would be interesting to compare this to other proven E3 ligase interactors to add strength to proposition of HECTD1 as a specific interactor of PTEN. It would also be important to demonstrate co-localisation, to confirm whether this interaction is likely to take place under physiological conditions, as SPR would only provide evidence that the proteins can interact. As described in section 6.1.3, co-localisation could be achieved by fluorescence microscopy of endogenous HECTD1 and PTEN. Beyond proof of a physical interaction, a functional role of the interaction needs to be investigated. Previous efforts to demonstrate a functional interaction of NEDD4 and PTEN have included an *in vitro* ubiquitination assay by performing a western blot for a tagged ubiquitin with isolated PTEN from wildtype and NEDD4 knockout strains (Fouladkou et al., 2008). Another approach was a biochemical assay involving the incubation of recombinant PTEN with two recombinant enzyme components of the ubiquitination system, the E1 activating enzyme and the E2 conjugating enzyme, and mammalian cell lysate to provide the E3 ligase enzyme, before pull down of the PTEN and western blot for ubiquitin (Wang et al., 2007). This could be adapted for future experiments with HECTD1, by replacing the mammalian lysate for a specific recombinant HECTD1 E3 ligase, to demonstrate a specific functional interaction *in vitro*. These potential future experiments could be performed alongside other known PTEN E3 ubiquitin ligases as a positive control, in the event that the PTEN-HECTD1 interaction is validated. This would also help to establish the importance of HECTD1 amongst the other E3 ubiquitin ligases that have been shown to have a functional interaction with PTEN.

Once the PTEN-HECTD1 interaction has been validated, there needs to be comparison with acrolein-treated PTEN to investigate the new hypothesis that the HECTD1 interaction increases with acrolein-modified PTEN as a method of clearance. First a difference in interaction needs to be demonstrated, and this investigation could take the form of the *in vitro* binding kinetics analysis, such as SPR, of purified PTEN and HECTD1 to establish whether acrolein-treatment of PTEN alters this. As for a functional change, it would be important to conduct the *in vitro* ubiquitination experiments for the two conditions. The polyubiquitination

of PTEN could be compared between PTEN isolated from untreated and acrolein-treated cells using the *in vitro* ubiquitination assay described above. To determine whether HECTD1 specifically has a role in this, comparison could be with wild type or HECTD1 knockout cells, mirroring the approach by Fouladkou et al. (2008) for NEDD4, or overexpression of HECT1 and a catalytic mutant, mirroring the approach by Maddika et al. (2011) for WWP2. Alternatively, the polyubiquitination levels of untreated and acrolein-treated recombinant PTEN could be compared using an adapted version of the biochemical assay developed by Wang et al. (2007), as described above. The *in vitro* polyubiquitination assays could be performed in combination with western blotting for PTEN in whole cell lysates to establish whether this has a functional effect in downregulating the amount of PTEN. This would give insight into whether the HECTD1 interaction targets PTEN for proteosomal degradation, as has been shown for NEDD4 (Wang et al., 2007), and whether this is increased on acrolein exposure. If the interaction between HECTD1 and PTEN is upregulated when PTEN is modified by acrolein, this could suggest a mechanism of clearance of acrolein-modified PTEN by the cell. However, as is discussed further in Chapter 7, there is a limited amount of data for the role of the ubiquitin-dependent pathway on degradation of oxidatively modified proteins, where the majority of the degradation is through the ubiquitin-independent pathway (Jung et al., 2014). The downregulation of PTEN by proteosomal degradation would cause an upregulation of the Akt pathway, which has wide implications for cell survival and metabolism, as discussed in section 1.2.3.

In conclusion, the final experimental chapter of this thesis provides further evidence of the detrimental effect of acrolein on HCT-116 cell viability and the application of sublethal acrolein treatments provided further evidence of the upregulation of the PI3K signalling pathway by reactive aldehydes.

Chapter 7 – General Discussion

7.1 Knowledge Gap and Key Findings

The role of reactive oxygen species and protein oxidation in the regulation of signal transduction is a key area of interest, with well-established mechanisms of activation and inactivation of signalling proteins, known as redox signalling. The role of redox reactions in the regulation of PTEN is well established, with extensive characterisation of the effect of reactive oxygen species, such as H₂O₂, on its activity and structure (Zhang et al., 2020). Beyond this, there have been investigations into the effect of oxidation on PTEN's interactome, with changes in its interactions with key reducing proteins, such as thioredoxin and peroxiredoxin, during conditions of oxidative stress (Meuillet et al., 2004, Cao et al., 2009, Verrastro et al., 2016). Reactive oxygen species can modify both proteins and lipids, including cell membrane unsaturated fatty acids (Schopfer et al., 2011). As described in 1.1.2, oxidation of lipids initiates the production of primary and secondary lipid oxidation products that can covalently modify proteins, in a process called lipoxidation. With consideration to the localisation of PTEN, where its primary function takes place at the cell membrane, and the vulnerability of its catalytic cysteine for attack by electrophilic species such as reactive carbonyls, there is potential for lipoxidation to be an alternative regulatory mechanism. An early study challenged PTEN with several electrophilic species, from reactive aldehydes and ketones to α,β -enones, and provided evidence of the inactivation of PTEN on modification by these species (Covey et al., 2010). Later studies focused on the effect of 4-HNE, with characterisation of the profile of modification and the extent of inactivation *in vitro* and *in vivo* in mouse models (Shearn et al., 2011, Shearn et al., 2013). Whilst evidence of PTEN adduction and inactivation by acrolein have been published, the mechanism of inactivation and the effect on PTEN's structure and interactions had not yet been investigated (Covey et al., 2010, Al-Salihi et al., 2015, Uemura et al., 2017).

Underpinning all the *in vitro* experiments was the use of purified recombinant PTEN, PTEN-V5-His, the production of which is presented in Chapter 3. The first research aim of this thesis was to characterise the effect of acrolein on PTEN's phosphatase activity. The two objectives to meet this were to use an *in vitro* phosphatase assay, presented in Chapter 4, and western blotting for *in cellulo* analysis of the Akt pathway, presented in Chapter 6. Monitoring the effect of increasing acrolein treatment ratios and treatment time on PTEN's catalytic activity using the OMFP phosphatase assay quantified the dose-dependent inactivation of PTEN by acrolein. Visualisation of the amount of pAkt in comparison to Akt on cellular exposure to increasing concentrations of acrolein was used to monitor any upregulation of the Akt pathway

to infer a loss of activity of endogenous PTEN. The second research aim was to characterise the structural changes that occurred to PTEN on exposure to acrolein. The objectives for this were to use two biochemical techniques, SDS-PAGE, to first visualise any structural changes such as cross-linking and aggregation, and then LC-MS/MS to map any acrolein modifications to PTEN's structure, presented in Chapter 4. By characterising the structural changes that occurred at each treatment ratio, these changes could be correlated to any inactivation of phosphatase activity. It was also necessary to characterise the extent of modification, cross-linking and aggregation to ensure that the appropriate conditions could be taken forward to meet the third and final aim, which was to investigate whether acrolein modification to PTEN would affect its interactions. Use of the APD format gave the opportunity to incorporate a targeted treatment step after the PTEN bait was immobilised, prior to cell lysate exposure, but it was important to avoid using treatment ratios that could cause significant unfolding as this could cause non-specific interactions. LC-MS/MS was used to identify the interactors present in each treatment condition and the use of label-free quantification identified a significant proportion of interactors that varied in abundance, presented in Chapter 5. A novel interactor with increased abundance in the pull down with acrolein-treated PTEN, HECTD1, was taken forward for validation *in cellulo* using coimmunoprecipitation from untreated and acrolein-treated HCT-116 cells, presented in Chapter 6. This first required quantification of the any change in cell viability on exposure of HCT-116 cells, so that sublethal concentrations could be used for the cell treatment. There were practical difficulties in the detection of PTEN in the IP samples, and so there was no further evidence for the PTEN-HECTD1 interaction from this attempted experiment.

7.2 Inactivation of PTEN by Acrolein *In Vitro* and *In Cellulo*

One of the major findings in this thesis was the dose-dependent inactivation and aggregation of PTEN by acrolein. This was achieved by taking forward the recombinant PTEN (PTEN-V5-His), produced in Chapter 3, for *in vitro* treatment with acrolein. The key findings from Chapter 4 were the inactivation and aggregation of PTEN by acrolein in a dose-dependent manner and the identification of acrolein modifications across the structure of PTEN. With confidence that NaBH₄ reduction did not affect PTEN's phosphatase activity, the acrolein modifications could be stabilised by reduction and the enzyme activity could be analysed under optimal conditions in the presence of DTT. PTEN-V5-His treated with increasing concentrations of acrolein for 10 minutes, 1 hour and 4 hours was assayed for phosphatase activity using OMFP as a substrate. The raw data showed that with increasing time and increasing treatment ratios, PTEN's activity was reduced, which matched the original hypothesis that acrolein would cause a time- and dose-dependent inactivation of PTEN. Closer examination revealed that with

increasing time there was also a loss of activity of the control, indicating that the treatment conditions alone were also causing a reduction in activity. This was due to the absence of DTT during the treatment resulting in inactivation of PTEN by oxidation that was not reversed by the short DTT exposure prior to the initialisation of the activity assay.

Normalisation of the specific activity to each treatment control, known as the percentage activity, revealed that whilst there was a dose-dependent loss of activity, there was no significant difference in activity of PTEN with increasing exposure time to acrolein. This did not match the original hypothesis which was based on previously published data showing further inactivation of PTEN by 4-HNE as the time increased over a range of 5 minutes to 2 hours (Shearn et al., 2011). On reflection, the time-dependent loss of activity for 4-HNE was demonstrated *in cellulo* by monitoring Akt/pAkt levels and this is a vastly different approach to an *in vitro* study with a one-on-one treatment and a direct enzyme assay for activity, as performed here (Shearn et al., 2011). Even if there had been expansion of the other work presented by Shearn et al. (2011), where endogenous PTEN was isolated from treated cells and assayed directly for activity, the indirect nature of the treatment means that differences in the time to inactivate would again be reasonably expected. A limitation of this current data set is that the shortest treatment time is 10 minutes, where previous *in vitro* functional studies for recombinant PTP1B, another cysteine-dependent phosphatase, used much shorter acrolein treatment times from 1-5 minutes (Seiner et al., 2007). Future work could involve expanding the activity analysis to shorter treatment times to capture the data for time-dependent inactivation of PTEN by acrolein. As the more electrophilic aldehyde, acrolein has highest reactivity and it has been reported that acrolein reacts between 110-150 times faster with GSH than 4-HNE (Esterbauer et al., 1975, Esterbauer et al., 1991). With this, the original hypothesis stands in that acrolein will inactivate PTEN in a time-dependent manner, but this could be defined to a time-dependency over seconds-minutes rather than minutes-hours.

Statistical analysis revealed that a 10-minute treatment with acrolein significantly inactivated PTEN at a 2:1 ratio of acrolein:PTEN, with a complete inactivation of activity at >10:1 acrolein:PTEN. This dose-dependent loss of activity matches the original hypothesis and comparison to previous literature identified a similar level of inactivation for equivalent treatments, whilst also highlighting the importance of reporting the ratios of protein:aldehyde in order to allow accurate comparison across different data sets (Shearn et al., 2011). This loss of activity was mirrored *in cellulo* for sublethal concentrations of acrolein, where there was an increase in pAkt, with the levels of Akt remaining the same. Future work could involve monitoring the levels of pAkt for shorter exposure times, to identify how quickly this upregulation of the Akt pathway is seen. A limitation of this is that the effect on acrolein on

PTEN's activity was not measured directly, but as described before an increase in pAkt over Akt has been cited several times previously for this use (Maehama and Dixon, 1998, Leslie et al., 2003, Kwon et al., 2004, Covey et al., 2010, Shearn et al., 2011). As PTEN's physiological substrate, measurement of cellular levels of PIP₃ would be a more targeted analysis of the effect of acrolein treatment on PTEN's activity, and this approach has also been used (Maehama and Dixon, 1998, Myers et al., 1998). The most targeted analysis would be the precipitation of endogenous PTEN and measurement of its activity *in vitro*, as done by Spinelli and Leslie (2016). Future visualisation of any changes in the localisation and levels of PTEN using fluorescence microscopy and western blotting would also be interesting, as post-translational modification has been shown to play a key role in both.

Further analysis of the *in vitro* acrolein-treated PTEN focused on the two distinct fractions visualised by SDS-PAGE, the monomeric fraction and the aggregate fraction, but intermediate cross-linking was not monitored or further analysed. The aggregation of PTEN is in-line with the original hypothesis that acrolein would cause protein cross-linking, however it was expected that there would be a higher proportion of intermediate cross-linked protein bands in comparison to the high molecular weight aggregate band. Inspection of the intermediate molecular weight range between the 60 kDa monomeric PTEN band and the aggregate bands of the stacking gel did reveal faint bands at around 120 and 180 kDa. However, further characterisation by western blot or mass spectrometry would be required for confident identification of any cross-linked PTEN, due to the presence of co-purified *E. coli* proteins which would also be expected to cross-link on exposure to acrolein. A limitation of using SDS-PAGE to analyse protein conformation is that only large changes that affect size or protein mobility can be detected. Identification of smaller changes in structure and conformation would have required techniques such as circular dichroism (CD) or fourier transform IR (FTIR) spectroscopy.

The initial LC-MS/MS analysis of PTEN in Chapter 3 provided a baseline of sequence coverage that could be expected during future experiments when attempting to map acrolein modifications to the structure of PTEN. Despite difficulties in getting full coverage of PTEN's active site due to the lack of cleavage at Lys102/Pro103 when digesting with trypsin, digestion with trypsin gave a high sequence coverage of 81% which was sufficient to confirm PTEN's identity and validate the actual protein sequence of the expressed PTEN against the theoretical protein sequence. Experimental procedures used to identify sites of oxidative and lipoxidative modification have included the use of various proteases. Lys-C was used in the original paper establishing the mechanism of inactivation of PTEN by oxidation through the formation of a disulfide bond between Cys71 and Cys124 (Lee et al., 2002). Trypsin alone as

well as trypsin with chymotrypsin was used the previous lipoxidation study to map PTEN 4-HNE modifications, and trypsin with Lys-C was used in a later paper mapping PTEN HOCl modifications (Shearn et al., 2013, Verrastro et al., 2018). Both Shearn et al. (2013) and Verrastro et al. (2018) described difficulty in getting complete sequence coverage of the catalytic site, even where an orthogonal digestion was used. The advantage conveyed by the approach used in this thesis is that as different proteases were used to target different residues and so the total sequence coverage for the acrolein-treated PTEN was very high. Chymotrypsin digestion increased the coverage of lysine rich areas and uncovered two additional lysine modifications, where double digestion with Trypsin/Glu-C in solution increased the coverage of the catalytic site.

Due to acrolein's highest reactivity with the thiol groups of cysteine residues, as discussed in section 1.1.2, it was hypothesised that acrolein would modify PTEN's cysteine residues first, with lysine residues being modified at increased treatment ratios. At the lowest treatment concentrations Cys71, Cys83 and Cys250 were identified across the different proteolytic digestions, with additional cysteine residues and lysine residue modifications found at >4:1 acrolein:PTEN. Due to the susceptibility of the catalytic cysteine of cysteine-dependent phosphatase, such as PTEN, to oxidative and lipoxidative modification, as discussed in section 1.2.6, it was hypothesised that the loss of activity would be accompanied by an increase in acrolein modification to Cys124. However, despite the successful effort to increase the sequence coverage at the catalytic site, there was no evidence of modification to Cys124 by acrolein in Chapter 4. It was concluded that the loss of activity could be due to the loss of PTEN in a productive enzyme conformation, which is supported by correlation of the percentage loss of monomeric PTEN with the percentage loss of activity in Chapter 4, or due to cross-linking of Cys124 with proximal lysine residues, the determination of which would require further inspection of the LC-MS/MS data for acrolein cross-links.

The aggregation of acrolein-treated PTEN-V5-His could be caused by protein unfolding due to modification of key structural residues or due to the extent of modification, where increased hydrophobicity from an increased number of acyl groups on acrolein adduction, could cause proteins to unfold (Spickett and Pitt, 2020). Both would result in a loss of a productive enzyme conformation and so the formation of aggregates would be accompanied by a reduction in activity. This study involved the identification of modified residues, but no quantification was attempted which may have allowed further insight into the cause of the aggregation. It would be interesting to apply the use of Progenesis Q1 for proteomics to the modified peptides and analyse the level of modification between the monomeric and aggregate bands and between the different treatment ratios. In combination with the required future work mentioned above

to search the LC-MS/MS data for cross-links and identify changes in conformation using more sensitive techniques. With this, the mechanism of inactivation of PTEN by acrolein could be more confidently proposed.

7.3 Acrolein-treated PTEN showed Changes in its Interactome

Previous PTEN interactome studies have utilised different approaches to affinity pull down assays (Table 5.1). Out of the 6 studies, two used an *in vitro* pull down approach here whereby purified recombinant PTEN was used as bait (Crockett et al., 2005, Verrastro et al., 2016), while the remaining 4 used a direct affinity pull down where the recombinant PTEN was immobilised from cell lysate (Herlevsen et al., 2007, Ahn et al., 2008, Gunaratne et al., 2011, Maddika et al., 2011). The advantage of using purified and characterised PTEN-V5-His as bait in an APD is that differences between the baits across different pull downs were minimised so that the only difference was the treatment. This minimises any changes in interactor abundance due to differences in the bait, for example a different profile of co-purified impurities, or amount of protein. This is less of a consideration when the aim of the study is to identify potential novel interactors without any comparison between two pull down conditions, or where more stringent resins/pull-down conditions are used, such as parallel or tandem affinity purification, which reduce the amount of non-specific resin interactors (Ahn et al., 2008, Gunaratne et al., 2011, Maddika et al., 2011).

The primary aim of the pull-down assay was to identify interactors that demonstrated a difference in abundance for untreated and acrolein-treated PTEN samples, but there was the potential for novel interactors that showed no change to be identified. Even though non-specific resin interactors would be expected to be the same for both conditions, it was necessary to optimise the pull-down chromatography conditions to minimise non-specific prey binding to increase the confidence in the identified interactors. The bead-only control identified interactors that were present in the absence of the PTEN bait protein, and as such are likely to be non-specific resin interactors. This is important for resins with a higher risk of non-specific binding, such as IMAC and nickel resin, but remains important for all interactome studies where the identification of false positives remains one of the biggest disadvantages.

The structural data from Chapter 4 provided insight on the effect of increasing acrolein treatment ratios on the structure PTEN, in terms of modification. This gave confidence that there would be potential for a change in interactions and also provided the opportunity to select a treatment ratio that would modify residues but minimise the risk of unfolding and aggregation to keep the acrolein-treated PTEN in a monomeric, monomeric format. Chapter 5 revealed

that whilst there were several common interactors between untreated PTEN and acrolein-treated PTEN, a significant proportion of the identified interactors showed a change in abundance across the two conditions. There were no specific interactors that met the threshold parameters that were only present in the untreated or acrolein-treated PTEN pull-downs, which was expected due to the design of the experiment where PTEN was only moderately modified and the threshold for a change in abundance was 2-fold increase or decrease in abundance. By setting a threshold for the specific interactors that are identified in the PTEN pull-down, the risk of taking forward false positive interactors is reduced. The change in interactor abundance across the treatment conditions met the original hypothesis that acrolein modification would cause changes in PTEN's interactome, although the scope of this hypothesis was very broad. Previously, PTEN mutations that change the size or property of the residue have been identified as a cause of changes in interactor binding (Smith and Briggs, 2016), and this theory can be extended to post-translational modifications. It was hypothesised that acrolein modification of PTEN would cause changes in its interactome as lipoxidative modifications change residue properties by increasing their hydrophobicity through the introduction of a carbonyl group and through changes in charge state on adduction to basic Lys, Arg and His residues or the thiolate form of Cys (de Graff et al., 2016, Spickett and Pitt, 2020). However, the biggest limitation of this study is that it is not possible to infer from this data the cause of a change in interaction, whether it is due to modification at a binding site or a change in PTEN's conformation due to the acrolein modifications. Future work could include *in silico* modelling of the binding interface between PTEN and a potential interactor to help elucidate whether individual modified residues are the cause of the change in binding, but this is only viable to do for a small subset of the identified proteins.

Inspection of the list of interactors highlighted several E3 ubiquitin ligases as having a higher abundance in the acrolein-treated PTEN pull-down, with HECTD1 showing the highest fold change. As discussed in Chapter 6, beyond the successful validation of an interaction *in cellulo*, future demonstration of the functional nature of this interaction using additional techniques to quantify the binding kinetics, visualise any co-localisation and validate the ability of HECTD1 to ligate ubiquitin to PTEN. The evidence of an increase in binding of HECTD1 with acrolein-treated PTEN created a new hypothesis that this interaction could be a potential adaptive response of the cell to remove acrolein-modified PTEN under conditions of oxidative stress. However, previous literature describes the majority of the degradation of oxidatively damaged proteins as being ubiquitin-independent through the 20S proteasome, with evidence that conditions of oxidative stress inhibit the 26S proteasome, the ubiquitin-dependent system (Jung et al., 2014, Raynes et al., 2016). At low to moderate levels of oxidative modification, proteins may have a reduction or inactivation of activity accompanied by low level protein

unfolding that exposes hydrophobic regions, facilitating the proteins proteasomal degradation by the 20S proteasome (Jung et al., 2014). More extensive oxidative modification causes a protein to become completely unfolded which facilitates protein aggregation, with or without covalent crosslinking, and these aggregates are more resistance to proteasomal degradation (Jung et al., 2014). Removal of mildly/moderately oxidised proteins is an adaptive response that prevents further modification and the formation of aggregates, which acts as a protection against their accumulation (Jung et al., 2014). However, there has been some evidence that the ubiquitin-dependent pathway does play a role in the degradation of 4-HNE-modified proteins (Botzen and Grune, 2007), so a similar role could be true for acrolein-modified proteins. Due to this literature surrounding the inactivity of ubiquitin-dependent proteasome in the degradation of oxidised proteins, it could also be interesting in the future to compare this HECTD1 interaction with several modification states, from unmodified to extensively modified PTEN. The downregulation of PTEN by proteasomal degradation would cause an upregulation of the Akt pathway, providing a second mechanism beyond the direct inactivation of PTEN's phosphatase activity. This correlates with the *in cellulo* data presented in Chapter 6 which saw an increase in pAkt on acrolein exposure to cells, which was used in combination with the data in Chapter 4 to infer a loss of activity of PTEN. But, as discussed previously, this was an indirect measurement and so there could be a number of reasons to this upregulation, including a reduction in cellular PTEN. The further characterisation of the nature and function of the potential PTEN/HECTD1 interaction fits with the future work previously proposed to investigate whether acrolein treatment affects the amount of endogenous PTEN present in the cell and whether acrolein-modification of PTEN can be seen exposure of whole cells to acrolein.

7.4 Conclusion and Future Directions

The work presented in this thesis provides further characterisation of the effect of acrolein on PTEN's activity, structure, and interaction. As such, the three research aims of this thesis were met, with demonstration of the inactivation, aggregation and modification of PTEN by acrolein exposure, in addition to changes in its interactome. The inactivation of PTEN by acrolein in a dose-dependent manner was demonstrated *in vitro* and *in cellulo*, building upon previously limited evidence of the effect of acrolein on PTEN. However, further work needs to be done to characterise any time-dependency of this inactivation and this could be achieved by testing shorter time points. Acrolein modifications were demonstrated *in vitro* across the structure of PTEN, with induction of aggregation at higher treatment concentrations. This *in vitro* analysis provided a foundation of evidence for the modification of PTEN by acrolein and a profile of the most vulnerable residues, but this should be expanded *in cellulo* to demonstrate adduction of

PTEN in mammalian cells. The modification data presented here matches previous evidence for 4-HNE, highlighting a similar profile of inactivation of reactive aldehydes, despite their difference in size. Future modelling of the modified residues could help to elucidate the mechanism of inactivation, in combination with higher resolution structural analysis for the conformational changes. Acrolein modification resulted in changes in PTEN's interactome and particular interest was taken in the upregulation of the interaction between PTEN and the E3 ubiquitin ligase, HECTD1. Further validation is required to confidently state HECTD1 as an interactor of PTEN, and this could include completing the attempted CoIP of PTEN with HECTD1, along with more functional analysis, such as ubiquitination assays.

In conclusion, there are several routes to exposure to acrolein, including oxidative stress, and several mechanisms through which acrolein exerts its cellular toxicity (Moghe et al., 2015), Acrolein exposure is implicated across several pathophysiological conditions, including those related to tumourigenesis. This includes recently published data implicating diet-associated acrolein in the activation of the Akt pathway in colorectal cancer (Tsai et al., 2021). Changes in the activity, structure and interactome of key signalling molecules, such as PTEN, by acrolein has wide implications for cell survival and metabolism. Further elucidation of the molecular mechanisms through which acrolein can affect these key signalling proteins is important in providing an understanding of how and why these observable cellular effects occur.

References

- ADAM WHALEY-CONNELL, P. A. M., JAMES R. SOWERS 2011. The Role of Oxidative Stress in the Metabolic Syndrome. *Reviews in Cardiovascular Medicine*, 12, 21-29.
- ADAN, A., KIRAZ, Y. & BARAN, Y. 2016. Cell Proliferation and Cytotoxicity Assays. *Curr Pharm Biotechnol*, 17, 1213-1221.
- ADELMANT, G., GARG, B. K., TAVARES, M., CARD, J. D. & MARTO, J. A. 2019. Tandem Affinity Purification and Mass Spectrometry (TAP-MS) for the Analysis of Protein Complexes. *Curr Protoc Protein Sci*, 96, e84.
- AEBERSOLD, R. & MANN, M. 2003. Mass spectrometry-based proteomics. *Nature*, 422, 198-207.
- AFONSO, C. B., SOUSA, B. C., PITT, A. R. & SPICKETT, C. M. 2018. A mass spectrometry approach for the identification and localization of small aldehyde modifications of proteins. *Archives of Biochemistry and Biophysics*, 646, 38-45.
- AHN, Y., HWANG, CHAE Y., LEE, S.-R., KWON, K.-S. & LEE, C. 2008. The tumour suppressor PTEN mediates a negative regulation of the E3 ubiquitin-protein ligase Nedd4. *Biochemical Journal*, 412, 331-338.
- AL-SALIHI, M., REICHERT, E. & FITZPATRICK, F. A. 2015. Influence of myeloperoxidase on colon tumor occurrence in inflamed versus non-inflamed colons of ApcMin/+ mice. *Redox Biology*, 6, 218-225.
- ALTOMARE, D. A. & KHALED, A. R. 2012. Homeostasis and the Importance for a Balance Between AKT/mTOR Activity and Intracellular Signaling. *Current Medicinal Chemistry*, 19, 3748-3762.
- ANNESLEY, T. M. 2003. Ion suppression in mass spectrometry. *Clinical chemistry*, 49, 1041-1044.
- ARMEAN, I. M., LILLEY, K. S. & TROTTER, M. W. 2013. Popular computational methods to assess multiprotein complexes derived from label-free affinity purification and mass spectrometry (AP-MS) experiments. *Mol Cell Proteomics*, 12, 1-13.
- ARORA, N. & GHOSH, S. S. 2016. Functional characterizations of interactive recombinant PTEN-silica nanoparticles for potential biomedical applications. *RSC Advances*, 6, 114944-114954.
- ARTIMO, P., JONNALAGEDDA, M., ARNOLD, K., BARATIN, D., CSARDI, G., DE CASTRO, E., DUVAUD, S., FLEGEL, V., FORTIER, A., GASTEIGER, E., GROSDIDIER, A., HERNANDEZ, C., IOANNIDIS, V., KUZNETSOV, D., LIECHTI, R., MORETTI, S., MOSTAGUIR, K., REDASCHI, N., ROSSIER, G., XENARIOS, I. & STOCKINGER, H. 2012. ExPASy: SIB bioinformatics resource portal. *Nucleic Acids Research*, 40, W597-W603.
- ASLANTÜRK, Ö. 2018. In Vitro Cytotoxicity and Cell Viability Assays: Principles, Advantages, and Disadvantages.
- AYALA, A., MUÑOZ, M. F. & ARGÜELLES, S. 2014. Lipid peroxidation: production, metabolism, and signaling mechanisms of malondialdehyde and 4-hydroxy-2-nonenal. *Oxidative medicine and cellular longevity*, 2014, 360438-360438.
- BADER, G. D. & HOGUE, C. W. 2002. Analyzing yeast protein-protein interaction data obtained from different sources. *Nat Biotechnol*, 20, 991-7.
- BAESHEN, M., AL-HEJIN, A., BORA, R., AHMED, M., RAMADAN, H., SAINI, K., BAESHEN, N. & REDWAN, E. 2015. Production of Biopharmaceuticals in E. coli: Current Scenario and Future Perspectives. *Journal of microbiology and biotechnology*, 25.

References

- BANERJEE, S. & MAZUMDAR, S. 2012. Electrospray ionization mass spectrometry: a technique to access the information beyond the molecular weight of the analyte. *Int J Anal Chem*, 2012, 282574.
- BANKS, C. A. S., BOANCA, G., LEE, Z. T., FLORENS, L. & WASHBURN, M. P. 2015. Proteins interacting with cloning scars: a source of false positive protein-protein interactions. *Scientific reports*, 5, 8530-8530.
- BANTSCHIEFF, M., SCHIRLE, M., SWEETMAN, G., RICK, J. & KUSTER, B. 2007. Quantitative mass spectrometry in proteomics: a critical review. *Anal Bioanal Chem*, 389, 1017-31.
- BARFORD, D., DAS, A. K. & EGLOFF, M. P. 1998. The structure and mechanism of protein phosphatases: insights into catalysis and regulation. *Annu Rev Biophys Biomol Struct*, 27, 133-64.
- BARFORD, D., FLINT, A. J. & TONKS, N. K. 1994. Crystal structure of human protein tyrosine phosphatase 1B. *Science*, 263, 1397.
- BASSI, C., HO, J., SRIKUMAR, T., DOWLING, R. J. O., GORRINI, C., MILLER, S. J., MAK, T. W., NEEL, B. G., RAUGHT, B. & STAMBOLIC, V. 2013. Nuclear PTEN Controls DNA Repair and Sensitivity to Genotoxic Stress. *Science*, 341, 395.
- BATEMAN, N. W., GOULDING, S. P., SHULMAN, N. J., GADOK, A. K., SZUMLINSKI, K. K., MACCOSS, M. J. & WU, C. C. 2014. Maximizing Peptide Identification Events in Proteomic Workflows Using Data-Dependent Acquisition (DDA)*. *Molecular & Cellular Proteomics*, 13, 329-338.
- BELL, M. R., ENGLEKA, M. J., MALIK, A. & STRICKLER, J. E. 2013. To fuse or not to fuse: what is your purpose? *Protein science : a publication of the Protein Society*, 22, 1466-1477.
- BERGGARD, T., LINSE, S. & JAMES, P. 2007. Methods for the detection and analysis of protein-protein interactions. *Proteomics*, 7, 2833-42.
- BERLETT, B. S. & STADTMAN, E. R. 1997. Protein Oxidation in Aging, Disease, and Oxidative Stress*. *Journal of Biological Chemistry*, 272, 20313-20316.
- BERNAS, T. & DOBRUCKI, J. W. 2004. Backscattered light confocal imaging of intracellular MTT-formazan crystals. *Microsc Res Tech*, 64, 126-34.
- BERNIER, S. C., CANTIN, L. & SALESSE, C. 2018. Systematic analysis of the expression, solubility and purification of a passenger protein in fusion with different tags. *Protein Expression and Purification*, 152, 92-106.
- BERRIDGE, M., HERST, P. & TAN, A. 2005. Tetrazolium dyes as tools in cell biology: New insights into their cellular reduction. *Biotechnology annual review*, 11, 127-52.
- BEUREL, E., GRIECO, S. F. & JOPE, R. S. 2015. Glycogen synthase kinase-3 (GSK3): Regulation, actions, and diseases. *Pharmacology & Therapeutics*, 148, 114-131.
- BIRBEN, E., SAHINER, U. M., SACKESSEN, C., ERZURUM, S. & KALAYCI, O. 2012. Oxidative Stress and Antioxidant Defense. *World Allergy Organization Journal*, 5, 9-19.
- BISSWANGER, H. 2019. *Practical Enzymology*, Wiley.
- BOLDUC, D., RAHDAR, M., TU-SEKINE, B., SIVAKUMAREN, S. C., RABEN, D., AMZEL, L. M., DEVREOTES, P., GABELLI, S. B. & COLE, P. 2013. Phosphorylation-mediated PTEN conformational closure and deactivation revealed with protein semisynthesis. *eLife*, 2, e00691.
- BOLLINENI, R. C., HOFFMANN, R. & FEDOROVA, M. 2011. Identification of protein carbonylation sites by two-dimensional liquid chromatography in combination with MALDI- and ESI-MS. *Journal of Proteomics*, 74, 2338-2350.
- BONONI, A., BONORA, M., MARCHI, S., MISSIROLI, S., POLETTI, F., GIORGI, C., PANDOLFI, P. P. & PINTON, P. 2013. Identification of PTEN at the ER and MAMs and

References

- its regulation of Ca²⁺ signaling and apoptosis in a protein phosphatase-dependent manner. *Cell Death & Differentiation*, 20, 1631-1643.
- BONONI, A. & PINTON, P. 2015. Study of PTEN subcellular localization. *Methods*, 77-78, 92-103.
- BOTZEN, D. & GRUNE, T. 2007. Degradation of HNE-modified proteins – possible role of ubiquitin. *Redox Report*, 12, 63-67.
- BRÜCKNER, A., POLGE, C., LENTZE, N., AUERBACH, D. & SCHLATTNER, U. 2009. Yeast two-hybrid, a powerful tool for systems biology. *Int J Mol Sci*, 10, 2763-88.
- BRUINS, A. P. 1998. Mechanistic aspects of electrospray ionization. *Journal of Chromatography A*, 794, 345-357.
- BRUNET, A., BONNI, A., ZIGMOND, M. J., LIN, M. Z., JUO, P., HU, L. S., ANDERSON, M. J., ARDEN, K. C., BLENIS, J. & GREENBERG, M. E. 1999. Akt Promotes Cell Survival by Phosphorylating and Inhibiting a Forkhead Transcription Factor. *Cell*, 96, 857-868.
- BURCHAM, P. C., RASO, A., THOMPSON, C. & TAN, D. 2007. Intermolecular Protein Cross-Linking During Acrolein Toxicity: Efficacy of Carbonyl Scavengers as Inhibitors of Heat Shock Protein-90 Cross-Linking in A549 Cells. *Chemical Research in Toxicology*, 20, 1629-1637.
- BUSS, H., CHAN, T. P., SLUIS, K. B., DOMIGAN, N. M. & WINTERBOURN, C. C. 1997. Protein Carbonyl Measurement by a Sensitive ELISA Method. *Free Radical Biology and Medicine*, 23, 361-366.
- CAI, J., BHATNAGAR, A. & PIERCE, W. 2009. Protein Modification by Acrolein: Formation and Stability of Cysteine Adducts. *Chemical research in toxicology*, 22, 708-16.
- CALLIS, J. 2014. The ubiquitination machinery of the ubiquitin system. *The arabidopsis book*, 12, e0174-e0174.
- CAMPBELL, R. B., LIU, F. & ROSS, A. H. 2003. Allosteric activation of PTEN phosphatase by phosphatidylinositol 4,5-bisphosphate. *J Biol Chem*, 278, 33617-20.
- CAO, J., SCHULTE, J., KNIGHT, A., LESLIE, N. R., ZAGOZDZON, A., BRONSON, R., MANEVICH, Y., BEESON, C. & NEUMANN, C. A. 2009. Prdx1 inhibits tumorigenesis via regulating PTEN/AKT activity. *Embo j*, 28, 1505-17.
- CARON, A., RICHARD, D. & LAPLANTE, M. 2015. The Roles of mTOR Complexes in Lipid Metabolism. *Annual Review of Nutrition*, 35, 321-348.
- CARREÑO, E. A., ALBERTO, A. V. P., DE SOUZA, C. A. M., DE MELLO, H. L., HENRIQUES-PONS, A. & ANASTACIO ALVES, L. 2021. Considerations and Technical Pitfalls in the Employment of the MTT Assay to Evaluate Photosensitizers for Photodynamic Therapy. *Applied Sciences*, 11, 2603.
- CASTALDO, S. A., AJIME, T., SERRÃO, G., ANASTÁCIO, F., ROSA, J. T., GIACOMANTONIO, C. A., HOWARTH, A., HILL, R. & MADUREIRA, P. A. 2019. Annexin A2 Regulates AKT Upon H₂O₂-Dependent Signaling Activation in Cancer Cells. *Cancers*, 11.
- CHALHOUB, N. & BAKER, S. J. 2009. PTEN and the PI3-Kinase Pathway in Cancer. *Annual Review of Pathology: Mechanisms of Disease*, 4, 127-150.
- CHALLEN, B. & CRAMER, R. 2022. Advances in ionisation techniques for mass spectrometry-based omics research. *PROTEOMICS*, 22, 2100394.
- CHEN, C. Y., CHEN, J. Y., HE, L. N. & STILES, B. L. 2018. PTEN: Tumor Suppressor and Metabolic Regulator. *Frontiers in Endocrinology*, 9.
- CHEN, R. 2012. Bacterial expression systems for recombinant protein production: E. coli and beyond. *Biotechnology Advances*, 30, 1102-1107.
- CHEN, W.-Y., ZHANG, J., GHARE, S., BARVE, S., MCCLAIN, C. & JOSHI-BARVE, S. 2016a. Acrolein Is a Pathogenic Mediator of Alcoholic Liver Disease and the Scavenger

References

- Hydralazine Is Protective in Mice. *Cellular and Molecular Gastroenterology and Hepatology*, 2, 685-700.
- CHEN, Z., THOMAS, S. N., BOLDUC, D. M., JIANG, X., ZHANG, X., WOLBERGER, C. & COLE, P. A. 2016b. Enzymatic Analysis of PTEN Ubiquitylation by WWP2 and NEDD4-1 E3 Ligases. *Biochemistry*, 55, 3658-66.
- CHEW, E.-H., NAGLE, A. A., ZHANG, Y., SCARMAGNANI, S., PALANIAPPAN, P., BRADSHAW, T. D., HOLMGREN, A. & WESTWELL, A. D. 2010. Cinnamaldehydes inhibit thioredoxin reductase and induce Nrf2: potential candidates for cancer therapy and chemoprevention. *Free Radical Biology and Medicine*, 48, 98-111.
- CHIA, J. Y., GAJEWSKI, J. E., XIAO, Y., ZHU, H. J. & CHENG, H. C. 2010. Unique biochemical properties of the protein tyrosine phosphatase activity of PTEN—demonstration of different active site structural requirements for phosphopeptide and phospholipid phosphatase activities of PTEN. *Biochim Biophys Acta*, 1804, 1785-95.
- CORCORAN, A. & COTTER, T. G. 2013. Redox regulation of protein kinases. *The FEBS Journal*, 280, 1944-1965.
- COSTA, S., ALMEIDA, A., CASTRO, A. & DOMINGUES, L. 2014. Fusion tags for protein solubility, purification and immunogenicity in *Escherichia coli*: the novel Fh8 system. *Frontiers in Microbiology*, 5.
- COVEY, T. M., EDES, K., COOMBS, G. S., VIRSHUP, D. M. & FITZPATRICK, F. A. 2010. Alkylation of the tumor suppressor PTEN activates Akt and β -catenin signaling: a mechanism linking inflammation and oxidative stress with cancer. *PloS one*, 5, e13545-e13545.
- CROCKETT, D. K., FILLMORE, G. C., ELENITOBA-JOHNSON, K. S. & LIM, M. S. 2005. Analysis of phosphatase and tensin homolog tumor suppressor interacting proteins by in vitro and in silico proteomics. *Proteomics*, 5, 1250-62.
- CROSS, D. A. E., ALESSI, D. R., COHEN, P., ANDJELKOVICH, M. & HEMMING, B. A. 1995. Inhibition of glycogen synthase kinase-3 by insulin mediated by protein kinase B. *Nature*, 378, 785-789.
- DALLE-DONNE, I., ROSSI, R., GIUSTARINI, D., MILZANI, A. & COLOMBO, R. 2003. Protein carbonyl groups as biomarkers of oxidative stress. *Clinica Chimica Acta*, 329, 23-38.
- DAS, S., DIXON, J. E. & CHO, W. 2003. Membrane-binding and activation mechanism of PTEN. *Proceedings of the National Academy of Sciences*, 100, 7491.
- DAVIES, MICHAEL J. 2016. Protein oxidation and peroxidation. *Biochemical Journal*, 473, 805-825.
- DE GRAFF, ADAM M. R., HAZOGLOU, MICHAEL J. & DILL, KEN A. 2016. Highly Charged Proteins: The Achilles' Heel of Aging Proteomes. *Structure*, 24, 329-336.
- DE LAS RIVAS, J. & FONTANILLO, C. 2010. Protein–Protein Interactions Essentials: Key Concepts to Building and Analyzing Interactome Networks. *PLOS Computational Biology*, 6, e1000807.
- DEMAIN, A. L. & VAISHNAV, P. 2009. Production of recombinant proteins by microbes and higher organisms. *Biotechnology Advances*, 27, 297-306.
- DEMPSEY, D. R. & COLE, P. A. 2018. Protein Chemical Approaches to Understanding PTEN Lipid Phosphatase Regulation. *Methods in enzymology*, 607, 405-422.
- DENU, J. M. & DIXON, J. E. 1998. Protein tyrosine phosphatases: mechanisms of catalysis and regulation. *Curr Opin Chem Biol*, 2, 633-41.
- DENU, J. M. & TANNER, K. G. 1998. Specific and reversible inactivation of protein tyrosine phosphatases by hydrogen peroxide: evidence for a sulfenic acid intermediate and implications for redox regulation. *Biochemistry*, 37, 5633-42.

References

- DIAZ, G., MELIS, M., MUSIN, A., PILUDU, M., PIRAS, M. & FALCHI, A. M. 2007. Localization of MTT formazan in lipid droplets. An alternative hypothesis about the nature of formazan granules and aggregates. *Eur J Histochem*, 51, 213-8.
- DOMINGUES, R. M., DOMINGUES, P., MELO, T., PEREZ-SALA, D., REIS, A. & SPICKETT, C. M. 2013. Lipoxidation adducts with peptides and proteins: deleterious modifications or signaling mechanisms? *J Proteomics*, 92, 110-31.
- DONG, S. & PROVART, N. J. 2018. Analyses of Protein Interaction Networks Using Computational Tools. *Methods Mol Biol*, 1794, 97-117.
- DOUZI, B. 2017. Protein-Protein Interactions: Surface Plasmon Resonance. In: JOURNET, L. & CASCALES, E. (eds.) *Bacterial Protein Secretion Systems: Methods and Protocols*. New York, NY: Springer New York.
- DRAPEAU, G. R. 1977. [21] Cleavage at glutamic acid with staphylococcal protease. *Methods in Enzymology*. Academic Press.
- DRESCHER, D. G., SELVAKUMAR, D. & DRESCHER, M. J. 2018. Analysis of Protein Interactions by Surface Plasmon Resonance. *Adv Protein Chem Struct Biol*, 110, 1-30.
- DUAN, G. & WALTHER, D. 2015. The Roles of Post-translational Modifications in the Context of Protein Interaction Networks. *PLOS Computational Biology*, 11, e1004049.
- DUPREE, E. J., JAYATHIRTHA, M., YORKEY, H., MIHASAN, M., PETRE, B. A. & DARIE, C. C. 2020. A Critical Review of Bottom-Up Proteomics: The Good, the Bad, and the Future of This Field. *Proteomes*, 8, 14.
- DÜVEL, K., YECIES, J. L., MENON, S., RAMAN, P., LIPOVSKY, A. I., SOUZA, A. L., TRIANTAFELLOW, E., MA, Q., GORSKI, R., CLEAVER, S., VANDER HEIDEN, M. G., MACKEIGAN, J. P., FINAN, P. M., CLISH, C. B., MURPHY, L. O. & MANNING, B. D. 2010. Activation of a Metabolic Gene Regulatory Network Downstream of mTOR Complex 1. *Molecular Cell*, 39, 171-183.
- EL KHOURY, F., CORCOS, L., DURAND, S., BRIGITTE, S. & LE JOSSIC-CORCOS, C. 2016. Acquisition of anticancer drug resistance is partially associated with cancer stemness in human colon cancer cells. *International Journal of Oncology*, 49, 2558-2568.
- ENG, C. 2003. PTEN: one gene, many syndromes. *Hum Mutat*, 22, 183-98.
- ESPOSITO, D. & CHATTERJEE, D. K. 2006. Enhancement of soluble protein expression through the use of fusion tags. *Current Opinion in Biotechnology*, 17, 353-358.
- ESTERBAUER, H., SCHAUR, R. J. & ZOLLNER, H. 1991. Chemistry and biochemistry of 4-hydroxynonenal, malonaldehyde and related aldehydes. *Free Radic Biol Med*, 11, 81-128.
- ESTERBAUER, H., ZÖLLNER, H. & SCHOLZ, N. 1975. Reaction of Glutathione with Conjugated Carbonyls. *Zeitschrift für Naturforschung C*, 30, 466-473.
- EVANGELISTI, C., CHIARINI, F., PAGANELLI, F., MARMIROLI, S. & MARTELLI, A. M. 2020. Crosstalks of GSK3 signaling with the mTOR network and effects on targeted therapy of cancer. *Biochimica et Biophysica Acta (BBA) - Molecular Cell Research*, 1867, 118635.
- FANNING, A. S. & ANDERSON, J. M. 1999. PDZ domains: fundamental building blocks in the organization of protein complexes at the plasma membrane. *The Journal of Clinical Investigation*, 103, 767-772.
- FEIDER, C. L., KRIEGER, A., DEHOOG, R. J. & EBERLIN, L. S. 2019. Ambient Ionization Mass Spectrometry: Recent Developments and Applications. *Analytical Chemistry*, 91, 4266-4290.
- FENAILLE, F., GUY, P. A. & TABEL, J.-C. 2003. Study of protein modification by 4-hydroxy-2-nonenal and other short chain aldehydes analyzed by electrospray ionization tandem

References

- mass spectrometry. *Journal of the American Society for Mass Spectrometry*, 14, 215-226.
- FIELDS, S. 2005. High-throughput two-hybrid analysis. *The FEBS Journal*, 272, 5391-5399.
- FIELDS, S. & SONG, O. 1989. A novel genetic system to detect protein-protein interactions. *Nature*, 340, 245-6.
- FORMAN, H. J., FUKUTO, J. M. & TORRES, M. 2004. Redox signaling: thiol chemistry defines which reactive oxygen and nitrogen species can act as second messengers. *American Journal of Physiology-Cell Physiology*, 287, C246-C256.
- FORMAN, H. J. & TORRES, M. 2002. Reactive Oxygen Species and Cell Signaling. *American Journal of Respiratory and Critical Care Medicine*, 166, S4-S8.
- FORMOSA, T., BARRY, J., ALBERTS, B. M. & GREENBLATT, J. 1991. Using protein affinity chromatography to probe structure of protein machines. *Methods Enzymol*, 208, 24-45.
- FOULADKOU, F., LANDRY, T., KAWABE, H., NEEB, A., LU, C., BROSE, N., STAMBOLIC, V. & ROTIN, D. 2008. The ubiquitin ligase Nedd4-1 is dispensable for the regulation of PTEN stability and localization. *Proceedings of the National Academy of Sciences*, 105, 8585.
- FRUTIGER, A., TANNO, A., HWU, S., TIEFENAUER, R. F., VÖRÖS, J. & NAKATSUKA, N. 2021. Nonspecific Binding—Fundamental Concepts and Consequences for Biosensing Applications. *Chemical Reviews*, 121, 8095-8160.
- FU, X., ZHAO, W., LI, K., ZHOU, J. & CHEN, X. 2021. Cryptotanshinone Inhibits the Growth of HCT116 Colorectal Cancer Cells Through Endoplasmic Reticulum Stress-Mediated Autophagy. *Frontiers in Pharmacology*, 12.
- FUCHS, B. & SCHILLER, J. 2016. Mass Spectrometry of Biological Molecules. *Encyclopedia of Analytical Chemistry*.
- FURUHATA, A., ISHII, T., KUMAZAWA, S., YAMADA, T., NAKAYAMA, T. & UCHIDA, K. 2003. N(epsilon)-(3-methylpyridinium)lysine, a major antigenic adduct generated in acrolein-modified protein. *J Biol Chem*, 278, 48658-65.
- GAJEWSKI, J. E., BIRD, M. J., CROWHURST, M. O., SIO-SENG LIO, D., LIU, J., WETTENHALL, R. E., ZHU, H. J. & CHENG, H. C. 2007. Expression, generation, and purification of unphosphorylated and phospho-Ser-380/Thr-382/Thr-383 form of recombinant PTEN phosphatase. *Protein Expr Purif*, 55, 334-42.
- GASTEIGER, E., HOOGLAND, C., GATTIKER, A., DUVAUD, S. E., WILKINS, M. R., APPEL, R. D. & BAIROCH, A. 2005. Protein Identification and Analysis Tools on the ExPASy Server. In: WALKER, J. M. (ed.) *The Proteomics Protocols Handbook*. Totowa, NJ: Humana Press.
- GAVIN, A. C., MAEDA, K. & KÜHNER, S. 2011. Recent advances in charting protein-protein interaction: mass spectrometry-based approaches. *Curr Opin Biotechnol*, 22, 42-9.
- GEORGESCU, M.-M., KIRSCH, K. H., AKAGI, T., SHISHIDO, T. & HANAFUSA, H. 1999. The tumor-suppressor activity of PTEN is regulated by its carboxyl-terminal region. *Proceedings of the National Academy of Sciences*, 96, 10182.
- GEORGESCU, M. M. 2010. PTEN Tumor Suppressor Network in PI3K-Akt Pathway Control. *Genes Cancer*, 1, 1170-7.
- GEORGESCU, M. M., KIRSCH, K. H., KALOUDIS, P., YANG, H., PAVLETICH, N. P. & HANAFUSA, H. 2000. Stabilization and productive positioning roles of the C2 domain of PTEN tumor suppressor. *Cancer Res*, 60, 7033-8.
- GHANDI, M., HUANG, F. W., JANÉ-VALBUENA, J., KRYUKOV, G. V., LO, C. C., MCDONALD, E. R., 3RD, BARRETINA, J., GELFAND, E. T., BIELSKI, C. M., LI, H., HU, K., ANDREEV-DRAKHLIN, A. Y., KIM, J., HESS, J. M., HAAS, B. J., AGUET, F., WEIR, B. A., ROTHBERG, M. V., PAOLELLA, B. R., LAWRENCE, M. S., AKBANI, R., LU, Y., TIV, H. L., GOKHALE, P. C., DE WECK, A., MANSOUR, A. A., OH, C., SHIH,

References

- J., HADI, K., ROSEN, Y., BISTLINE, J., VENKATESAN, K., REDDY, A., SONKIN, D., LIU, M., LEHAR, J., KORN, J. M., PORTER, D. A., JONES, M. D., GOLJI, J., CAPONIGRO, G., TAYLOR, J. E., DUNNING, C. M., CREECH, A. L., WARREN, A. C., MCFARLAND, J. M., ZAMANIGHOMI, M., KAUFFMANN, A., STRANSKY, N., IMIELINSKI, M., MARUVKA, Y. E., CHERNIACK, A. D., TSHERNIAK, A., VAZQUEZ, F., JAFFE, J. D., LANE, A. A., WEINSTOCK, D. M., JOHANNESSEN, C. M., MORRISSEY, M. P., STEGMEIER, F., SCHLEGEL, R., HAHN, W. C., GETZ, G., MILLS, G. B., BOEHM, J. S., GOLUB, T. R., GARRAWAY, L. A. & SELLERS, W. R. 2019. Next-generation characterization of the Cancer Cell Line Encyclopedia. *Nature*, 569, 503-508.
- GHASEMI, M., TURNBULL, T., SEBASTIAN, S. & KEMPSON, I. 2021. The MTT Assay: Utility, Limitations, Pitfalls, and Interpretation in Bulk and Single-Cell Analysis. *Int J Mol Sci*, 22.
- GIANSANTI, P., TSIATSIANI, L., LOW, T. Y. & HECK, A. J. R. 2016. Six alternative proteases for mass spectrometry-based proteomics beyond trypsin. *Nature Protocols*, 11, 993-1006.
- GLASSFORD, S. E., BYRNE, B. & KAZARIAN, S. G. 2013. Recent applications of ATR FTIR spectroscopy and imaging to proteins. *Biochimica et Biophysica Acta (BBA) - Proteins and Proteomics*, 1834, 2849-2858.
- GONZÁLEZ-SANTAMARÍA, J., CAMPAGNA, M., ORTEGA-MOLINA, A., MARCOS-VILLAR, L., DE LA CRUZ-HERRERA, C. F., GONZÁLEZ, D., GALLEGO, P., LOPITZ-OTSOA, F., ESTEBAN, M., RODRÍGUEZ, M. S., SERRANO, M. & RIVAS, C. 2012. Regulation of the tumor suppressor PTEN by SUMO. *Cell Death & Disease*, 3, e393-e393.
- GORBENKO, O., KUZNETSOV, V., KUKHARENKO, O., ZHYVOLOUP, A., PANASYUK, G., NEMAZANYI, I., FILONENKO, V. & GOUT, I. 2004. Identification of a novel binding partners for tumor suppressor PTEN by a yeast two-hybrid approach. *Eksp Onkol*, 26, 15-9.
- GORBENKO, O., PANAYOTOU, G., ZHYVOLOUP, A., VOLKOVA, D., GOUT, I. & FILONENKO, V. 2010. Identification of novel PTEN-binding partners: PTEN interaction with fatty acid binding protein FABP4. *Mol Cell Biochem*, 337, 299-305.
- GRBOVIĆ, F., STANKOVIĆ, M. S., ČURČIĆ, M., ĐORĐEVIĆ, N., ŠEKLIĆ, D., TOPUZOVIĆ, M. & MARKOVIĆ, S. 2013. In Vitro Cytotoxic Activity of *Origanum vulgare* L. on HCT-116 and MDA-MB-231 Cell Lines. *Plants (Basel)*, 2, 371-8.
- GREENFIELD, N. J. 2006. Using circular dichroism spectra to estimate protein secondary structure. *Nature protocols*, 1, 2876-2890.
- GUÉRAUD, F., ATALAY, M., BRESGEN, N., CIPAK, A., ECKL, P. M., HUC, L., JOUANIN, I., SIEMS, W. & UCHIDA, K. 2010. Chemistry and biochemistry of lipid peroxidation products. *Free Radical Research*, 44, 1098-1124.
- GUNARATNE, J., GOH, M. X., SWA, H. L., LEE, F. Y., SANFORD, E., WONG, L. M., HOGUE, K. A., BLACKSTOCK, W. P. & OKUMURA, K. 2011. Protein interactions of phosphatase and tensin homologue (PTEN) and its cancer-associated G20E mutant compared by using stable isotope labeling by amino acids in cell culture-based parallel affinity purification. *J Biol Chem*, 286, 18093-103.
- GUO, J. & PROKAI, L. 2011. To tag or not to tag: A comparative evaluation of immunoaffinity-labeling and tandem mass spectrometry for the identification and localization of posttranslational protein carbonylation by 4-hydroxy-2-nonenal, an end-product of lipid peroxidation. *Journal of Proteomics*, 74, 2360-2369.
- GUPTA, A. & LESLIE, N. R. 2016. Controlling PTEN (Phosphatase and Tensin Homolog) Stability: A DOMINANT ROLE FOR LYSINE 66. *Journal of Biological Chemistry*, 291, 18465-18473.

References

- GUPTA, S., KAMIL, S., SINHA, P. R., RODIER, J. T., CHAURASIA, S. S. & MOHAN, R. R. 2021. Glutathione is a potential therapeutic target for acrolein toxicity in the cornea. *Toxicology Letters*, 340, 33-42.
- HAN, S. J., ZHANG, Y., KIM, I., CHAY, K. O., YOON, H. J., JANG, D. I., YANG, S. Y., PARK, J., WOO, H. A., PARK, I. & LEE, S. R. 2017. Redox regulation of the tumor suppressor PTEN by the thioredoxin system and cumene hydroperoxide. *Free Radic Biol Med*, 112, 277-286.
- HAN, S. Y., KATO, H., KATO, S., SUZUKI, T., SHIBATA, H., ISHII, S., SHIIBA, K., MATSUNO, S., KANAMARU, R. & ISHIOKA, C. 2000. Functional evaluation of PTEN missense mutations using in vitro phosphoinositide phosphatase assay. *Cancer Res*, 60, 3147-51.
- HEINRICH, F., CHAKRAVARTHY, S., NANDA, H., PAPA, A., PANDOLFI, P., ROSS, ALONZO H., HARISHCHANDRA, RAKESH K., GERICKE, A. & LÖSCHE, M. 2015. The PTEN Tumor Suppressor Forms Homodimers in Solution. *Structure*, 23, 1952-1957.
- HEMMINGS, B. A. & RESTUCCIA, D. F. 2012. PI3K-PKB/Akt pathway. *Cold Spring Harb Perspect Biol*, 4, a011189.
- HERLEVSEN, M., OXFORD, G., PTAK, C., SHABANOWITZ, J., HUNT, D. F., CONAWAY, M. & THEODORESCU, D. 2007. A novel model to identify interaction partners of the PTEN tumor suppressor gene in human bladder cancer. *Biochemical and Biophysical Research Communications*, 352, 549-555.
- HERSHKO, A. & CIECHANOVER, A. 1998. THE UBIQUITIN SYSTEM. *Annual Review of Biochemistry*, 67, 425-479.
- HINK, M. A., BISSELIN, T. & VISSER, A. J. 2002. Imaging protein-protein interactions in living cells. *Plant Mol Biol*, 50, 871-83.
- HO, C. S., LAM, C. W., CHAN, M. H., CHEUNG, R. C., LAW, L. K., LIT, L. C., NG, K. F., SUEN, M. W. & TAI, H. L. 2003. Electrospray ionisation mass spectrometry: principles and clinical applications. *Clin Biochem Rev*, 24, 3-12.
- HO, J., CRUISE, E. S., DOWLING, R. J. O. & STAMBOLIC, V. 2019. PTEN Nuclear Functions. *Cold Spring Harbor Perspectives in Medicine*.
- HØIE, M. H., KIEHL, E. N., PETERSEN, B., NIELSEN, M., WINTHER, O., NIELSEN, H., HALLGREN, J. & MARCATILI, P. 2022. NetSurfP-3.0: accurate and fast prediction of protein structural features by protein language models and deep learning. *Nucleic Acids Research*, 50, W510-W515.
- HONG, J., LUO, Y., ZHANG, Y., YING, J., XUE, W., XIE, T., TAO, L. & ZHU, F. 2019. Protein functional annotation of simultaneously improved stability, accuracy and false discovery rate achieved by a sequence-based deep learning. *Briefings in Bioinformatics*, 21, 1437-1447.
- HOPKINS, B. D., FINE, B., STEINBACH, N., DENDY, M., RAPP, Z., SHAW, J., PAPPAS, K., YU, J. S., HODAKOSKI, C., MENSE, S., KLEIN, J., PEGNO, S., SULIS, M.-L., GOLDSTEIN, H., AMENDOLARA, B., LEI, L., MAURER, M., BRUCE, J., CANOLL, P., HIBSHOOSH, H. & PARSONS, R. 2013. A Secreted PTEN Phosphatase That Enters Cells to Alter Signaling and Survival. *Science*, 341, 399.
- HOPKINS, B. D., HODAKOSKI, C., BARROWS, D., MENSE, S. M. & PARSONS, R. E. 2014. PTEN function: the long and the short of it. *Trends in Biochemical Sciences*, 39, 183-190.
- HORNBECK, P. V., ZHANG, B., MURRAY, B., KORNHAUSER, J. M., LATHAM, V. & SKRZYPEK, E. 2015. PhosphoSitePlus, 2014: mutations, PTMs and recalibrations. *Nucleic Acids Res*, 43, D512-20.

References

- HUANG, J., YAN, J., ZHANG, J., ZHU, S., WANG, Y., SHI, T., ZHU, C., CHEN, C., LIU, X., CHENG, J., MUSTELIN, T., FENG, G.-S., CHEN, G. & YU, J. 2012. SUMO1 modification of PTEN regulates tumorigenesis by controlling its association with the plasma membrane. *Nature Communications*, 3, 911.
- HUNTER, D. J. B., BHUMKAR, A., GILES, N., SIERECKI, E. & GAMBIN, Y. 2018. Unexpected instabilities explain batch-to-batch variability in cell-free protein expression systems. *Biotechnol Bioeng*, 115, 1904-1914.
- INOKI, K., LI, Y., ZHU, T., WU, J. & GUAN, K.-L. 2002. TSC2 is phosphorylated and inhibited by Akt and suppresses mTOR signalling. *Nature Cell Biology*, 4, 648-657.
- ISHII, T., YAMADA, T., MORI, T., KUMAZAWA, S., UCHIDA, K. & NAKAYAMA, T. 2007. Characterization of acrolein-induced protein cross-links. *Free Radical Research*, 41, 1253-1260.
- ISRAR, M. Z., BERNIEH, D., SALZANO, A., CASSAMBAI, S., YAZAKI, Y. & SUZUKI, T. 2020. Matrix-assisted laser desorption ionisation (MALDI) mass spectrometry (MS): Basics and clinical applications. *Clinical Chemistry and Laboratory Medicine (CCLM)*, 58, 883-896.
- JIA, B. & JEON, C. O. 2016. High-throughput recombinant protein expression in *Escherichia coli*: current status and future perspectives. *Open Biology*, 6, 160196.
- JOHNSON, M. R. & RICKBORN, B. 1970. Sodium borohydride reduction of conjugated aldehydes and ketones. *The Journal of Organic Chemistry*, 35, 1041-1045.
- JUNG, T., HÖHN, A. & GRUNE, T. 2014. The proteasome and the degradation of oxidized proteins: Part II – protein oxidation and proteasomal degradation. *Redox Biology*, 2, 99-104.
- KAAKE, R. M., WANG, X. & HUANG, L. 2010. Profiling of Protein Interaction Networks of Protein Complexes Using Affinity Purification and Quantitative Mass Spectrometry. *Molecular & Cellular Proteomics*, 9, 1650.
- KABUYAMA, Y., NAKATSU, N., HOMMA, Y. & FUKUI, Y. 1996. Purification and Characterization of the phosphatidylinositol-3,4,5-trisphosphate Phosphatase in Bovine Thymus. *European Journal of Biochemistry*, 238, 350-356.
- KAIDANOVICH-BEILIN, O. & WOODGETT, J. R. 2011. GSK-3: Functional Insights from Cell Biology and Animal Models. *Front Mol Neurosci*, 4, 40.
- KAMILOGLU, S., SARI, G., OZDAL, T. & CAPANOGLU, E. 2020. Guidelines for cell viability assays. *Food Frontiers*, 1, 332-349.
- KEEGAN, L., GILL, G. & PTASHNE, M. 1986. Separation of DNA binding from the transcription-activating function of a eukaryotic regulatory protein. *Science*, 231, 699.
- KEIL, P. D. B. Specificity of Proteolysis. Springer Berlin Heidelberg, 1992.
- KI, M.-R. & PACK, S. P. 2020. Fusion tags to enhance heterologous protein expression. *Applied Microbiology and Biotechnology*, 104, 2411-2425.
- KIM, E. T. & PARK, D.-G. 2020. YM155, specific survivin inhibitor, can enhance artesunate-induced cytotoxicity in HCT116 colon cancer cells. *Korean J Clin Oncol*, 16, 131-137.
- KIM, J., KUNDU, M., VIOLLET, B. & GUAN, K.-L. 2011. AMPK and mTOR regulate autophagy through direct phosphorylation of Ulk1. *Nature Cell Biology*, 13, 132-141.
- KIM, J. R., YOON, H. W., KWON, K. S., LEE, S. R. & RHEE, S. G. 2000a. Identification of proteins containing cysteine residues that are sensitive to oxidation by hydrogen peroxide at neutral pH. *Anal Biochem*, 283, 214-21.
- KIM, S., JUNG, Y., KIM, D., KOH, H. & CHUNG, J. 2000b. Extracellular Zinc Activates p70 S6 Kinase through the Phosphatidylinositol 3-Kinase Signaling Pathway *. *Journal of Biological Chemistry*, 275, 25979-25984.
- KIMPLE, M. E., BRILL, A. L. & PASKER, R. L. 2013. Overview of affinity tags for protein purification. *Current protocols in protein science*, 73, 9.9.1-9.9.23.

References

- KISHORE, D., KUNDU, S. & KAYASTHA, A. M. 2012. Thermal, chemical and pH induced denaturation of a multimeric β -galactosidase reveals multiple unfolding pathways. *PLoS One*, 7, e50380.
- KLAUSEN, M. S., JESPERSEN, M. C., NIELSEN, H., JENSEN, K. K., JURTZ, V. I., SØNDERBY, C. K., SOMMER, M. O. A., WINTHER, O., NIELSEN, M., PETERSEN, B. & MARCATILI, P. 2019. NetSurfP-2.0: Improved prediction of protein structural features by integrated deep learning. *Proteins*, 87, 520-527.
- KOUNDOUROS, N. & POULOGIANNIS, G. 2018. Phosphoinositide 3-Kinase/Akt Signaling and Redox Metabolism in Cancer. *Front Oncol*, 8, 160.
- KWAK, Y.-D., MA, T., DIAO, S., ZHANG, X., CHEN, Y., HSU, J., LIPTON, S. A., MASLIAH, E., XU, H. & LIAO, F.-F. 2010. NO signaling and S-nitrosylation regulate PTEN inhibition in neurodegeneration. *Molecular Neurodegeneration*, 5, 49.
- KWON, J., LEE, S.-R., YANG, K.-S., AHN, Y., KIM, Y. J., STADTMAN, E. R. & RHEE, S. G. 2004. Reversible oxidation and inactivation of the tumor suppressor PTEN in cells stimulated with peptide growth factors. *Proceedings of the National Academy of Sciences of the United States of America*, 101, 16419-16424.
- LEE, C.-U., HAHNE, G., HANSKE, J., BANGE, T., BIER, D., RADEMACHER, C., HENNIG, S. & GROSSMANN, T. N. 2015. Redox Modulation of PTEN Phosphatase Activity by Hydrogen Peroxide and Bisperoxidovanadium Complexes. *Angewandte Chemie International Edition*, 54, 13796-13800.
- LEE, H.-J. & ZHENG, J. J. 2010. PDZ domains and their binding partners: structure, specificity, and modification. *Cell Communication and Signaling*, 8, 8.
- LEE, J. O., YANG, H., GEORGESCU, M. M., DI CRISTOFANO, A., MAEHAMA, T., SHI, Y., DIXON, J. E., PANDOLFI, P. & PAVLETICH, N. P. 1999. Crystal structure of the PTEN tumor suppressor: implications for its phosphoinositide phosphatase activity and membrane association. *Cell*, 99, 323-34.
- LEE, S., KIM, S. M. & LEE, R. T. 2013. Thioredoxin and thioredoxin target proteins: from molecular mechanisms to functional significance. *Antioxidants & redox signaling*, 18, 1165-1207.
- LEE, S. R., YANG, K. S., KWON, J., LEE, C., JEONG, W. & RHEE, S. G. 2002. Reversible inactivation of the tumor suppressor PTEN by H₂O₂. *Journal of Biological Chemistry*, 277, 20336-20342.
- LEE, Y. R., CHEN, M. & PANDOLFI, P. P. 2018. The functions and regulation of the PTEN tumour suppressor: new modes and prospects. *Nature Reviews Molecular Cell Biology*, 19, 547-562.
- LEITNER, M. G., HOBIGER, K., MAVRANTONI, A., FEUER, A., OBERWINKLER, J., OLIVER, D. & HALASZOVICH, C. R. 2018. A126 in the active site and T1167/168 in the TI loop are essential determinants of the substrate specificity of PTEN. *Cellular and Molecular Life Sciences*, 75, 4235-4250.
- LESLIE, N. R. 2006. The redox regulation of PI 3-kinase-dependent signaling. *Antioxid Redox Signal*, 8, 1765-74.
- LESLIE, N. R., BENNETT, D., LINDSAY, Y. E., STEWART, H., GRAY, A. & DOWNES, C. P. 2003. Redox regulation of PI 3-kinase signalling via inactivation of PTEN. *Embo j*, 22, 5501-10.
- LESLIE, N. R., YANG, X., DOWNES, C. P. & WEIJER, C. J. 2007. PtdIns(3,4,5)P(3)-dependent and -independent roles for PTEN in the control of cell migration. *Curr Biol*, 17, 115-25.
- LEVINE, R. L., GARLAND, D., OLIVER, C. N., AMICI, A., CLIMENT, I., LENZ, A.-G., AHN, B.-W., SHALTIEL, S. & STADTMAN, E. R. 1990. [49] Determination of carbonyl content in oxidatively modified proteins. *Methods in enzymology*, 186, 464-478.

References

- LI, D.-X., GAN, L., BRONJA, A. & SCHMITZ, O. J. 2015. Gas chromatography coupled to atmospheric pressure ionization mass spectrometry (GC-API-MS): Review. *Analytica Chimica Acta*, 891, 43-61.
- LI, D. M. & SUN, H. 1997. TEP1, encoded by a candidate tumor suppressor locus, is a novel protein tyrosine phosphatase regulated by transforming growth factor beta. *Cancer Res*, 57, 2124-9.
- LI, H., ROBERTSON, A. D. & JENSEN, J. H. 2005. Very fast empirical prediction and rationalization of protein pKa values. *Proteins*, 61, 704-21.
- LI, J., YEN, C., LIAW, D., PODSYPANINA, K., BOSE, S., WANG, S. I., PUC, J., MILIARESIS, C., RODGERS, L., MCCOMBIE, R., BIGNER, S. H., GIOVANELLA, B. C., ITTMANN, M., TYCKO, B., HIBSHOOSH, H., WIGLER, M. H. & PARSONS, R. 1997. PTEN, a putative protein tyrosine phosphatase gene mutated in human brain, breast, and prostate cancer. *Science*, 275, 1943-1947.
- LI, P., WANG, D., LI, H., YU, Z., CHEN, X. & FANG, J. 2014. Identification of nucleolus-localized PTEN and its function in regulating ribosome biogenesis. *Molecular Biology Reports*, 41, 6383-6390.
- LI, Q., FENG, Y., TAN, M.-J. & ZHAI, L.-H. 2017. Evaluation of Endoproteinase Lys-C/Trypsin Sequential Digestion Used in Proteomics Sample Preparation. *Chinese Journal of Analytical Chemistry*, 45, 316-321.
- LI, X., FOLEY, E. A., KAWASHIMA, S. A., MOLLOY, K. R., LI, Y., CHAIT, B. T. & KAPOOR, T. M. 2013. Examining post-translational modification-mediated protein-protein interactions using a chemical proteomics approach. *Protein Sci*, 22, 287-95.
- LIAN, Z. & DI CRISTOFANO, A. 2005. Class reunion: PTEN joins the nuclear crew. *Oncogene*, 24, 7394-400.
- LIANG, H., CHEN, X., YIN, Q., RUAN, D., ZHAO, X., ZHANG, C., MCNUTT, M. A. & YIN, Y. 2017. PTEN β is an alternatively translated isoform of PTEN that regulates rDNA transcription. *Nature Communications*, 8, 14771.
- LIANG, H., HE, S., YANG, J., JIA, X., WANG, P., CHEN, X., ZHANG, Z., ZOU, X., MCNUTT, MICHAEL A., SHEN, WEN H. & YIN, Y. 2014. PTEN β , a PTEN Isoform Translated through Alternative Initiation, Regulates Mitochondrial Function and Energy Metabolism. *Cell Metabolism*, 19, 836-848.
- LIANG, H. & YIN, Y. 2019. Multiple roles of PTEN isoforms PTEN α and PTEN β in cellular activities and tumor development. *Science China Life Sciences*, 62, 1722-1724.
- LIM, J. C., CHOI, H. I., PARK, Y. S., NAM, H. W., WOO, H. A., KWON, K. S., KIM, Y. S., RHEE, S. G., KIM, K. & CHAE, H. Z. 2008. Irreversible oxidation of the active-site cysteine of peroxiredoxin to cysteine sulfonic acid for enhanced molecular chaperone activity. *J Biol Chem*, 283, 28873-80.
- LIN, J. S. & LAI, E. M. 2017. Protein-Protein Interactions: Co-Immunoprecipitation. *Methods Mol Biol*, 1615, 211-219.
- LINDEMANN, C., THOMANEK, N., HUNDT, F., LERARI, T., MEYER, H. E., WOLTERS, D. & MARCUS, K. 2017. Strategies in relative and absolute quantitative mass spectrometry based proteomics. *Biological Chemistry*, 398, 687-699.
- LIU, C. W. & ZHANG, Q. 2018. Isobaric Labeling-Based LC-MS/MS Strategy for Comprehensive Profiling of Human Pancreatic Tissue Proteome. *Methods Mol Biol*, 1788, 215-224.
- LIU, F., WAGNER, S., CAMPBELL, R. B., NICKERSON, J. A., SCHIFFER, C. A. & ROSS, A. H. 2005. PTEN enters the nucleus by diffusion. *Journal of Cellular Biochemistry*, 96, 221-234.
- LIU, L., GAO, H., WANG, H., ZHANG, Y., XU, W., LIN, S., WANG, H., WU, Q. & GUO, J. 2017. Catalpol promotes cellular apoptosis in human HCT116 colorectal cancer cells via

References

- microRNA-200 and the downregulation of PI3K-Akt signaling pathway. *Oncol Lett*, 14, 3741-3747.
- LIU, T., WANG, Y., WANG, Y. & CHAN, A. M. 2019. Multifaceted Regulation of PTEN Subcellular Distributions and Biological Functions. *Cancers (Basel)*, 11.
- LIU, Y., PETERSON, D. A., KIMURA, H. & SCHUBERT, D. 1997. Mechanism of cellular 3-(4,5-dimethylthiazol-2-yl)-2,5-diphenyltetrazolium bromide (MTT) reduction. *J Neurochem*, 69, 581-93.
- LIU, Z., TYO, K. E. J., MARTÍNEZ, J. L., PETRANOVIC, D. & NIELSEN, J. 2012. Different expression systems for production of recombinant proteins in *Saccharomyces cerevisiae*. *Biotechnology and Bioengineering*, 109, 1259-1268.
- LOPACHIN, R. M., GAVIN, T., PETERSEN, D. R. & BARBER, D. S. 2009. Molecular mechanisms of 4-hydroxy-2-nonenal and acrolein toxicity: nucleophilic targets and adduct formation. *Chemical research in toxicology*, 22, 1499-1508.
- LOUCHE, A., SALCEDO, S. P. & BIGOT, S. 2017. Protein-Protein Interactions: Pull-Down Assays. *Methods Mol Biol*, 1615, 247-255.
- LÜ, L., ZHANG, L., WAI, M., YEW, D. & XU, J. 2012. Exocytosis of MTT formazan could exacerbate cell injury. *Toxicology in vitro : an international journal published in association with BIBRA*, 26, 636-44.
- LUO, J., ROBINSON, J. P. & SHI, R. 2005. Acrolein-induced cell death in PC12 cells: role of mitochondria-mediated oxidative stress. *Neurochem Int*, 47, 449-57.
- LUO, S., JIANG, L., LI, Q., SUN, X., LIU, T., PEI, F., ZHANG, T., LIU, T., DONG, L., LIU, X. & JIANG, L. 2018. Acrolein-induced autophagy-dependent apoptosis via activation of the lysosomal-mitochondrial pathway in EAhy926 cells. *Toxicology in Vitro*, 52, 146-153.
- MA, L., YANG, F. & ZHENG, J. 2014. Application of fluorescence resonance energy transfer in protein studies. *J Mol Struct*, 1077, 87-100.
- MADDIKA, S., KAVELA, S., RANI, N., PALICHARLA, V. R., POKORNY, J. L., SARKARIA, J. N. & CHEN, J. 2011. WWP2 is an E3 ubiquitin ligase for PTEN. *Nat Cell Biol*, 13, 728-33.
- MADIAN, A. G. & REGNIER, F. E. 2010. Proteomic Identification of Carbonylated Proteins and Their Oxidation Sites. *Journal of Proteome Research*, 9, 3766-3780.
- MADUREIRA, P. A., HILL, R., MILLER, V. A., GIACOMANTONIO, C., LEE, P. W. & WAISMAN, D. M. 2011. Annexin A2 is a novel cellular redox regulatory protein involved in tumorigenesis. *Oncotarget*, 2, 1075-93.
- MAEHAMA, T. & DIXON, J. E. 1998. The tumor suppressor, PTEN/MMAC1, dephosphorylates the lipid second messenger, phosphatidylinositol 3,4,5-trisphosphate. *Journal of Biological Chemistry*, 273, 13375-13378.
- MAEHAMA, T., TAYLOR, G. S. & DIXON, J. E. 2001. PTEN and Myotubularin: Novel Phosphoinositide Phosphatases. *Annual Review of Biochemistry*, 70, 247-279.
- MAESHIMA, T., HONDA, K., CHIKAZAWA, M., SHIBATA, T., KAWAI, Y., AKAGAWA, M. & UCHIDA, K. 2012. Quantitative Analysis of Acrolein-Specific Adducts Generated during Lipid Peroxidation-Modification of Proteins in Vitro: Identification of N^ε-(3-Propanal)histidine as the Major Adduct. *Chemical Research in Toxicology*, 25, 1384-1392.
- MAK, L. H., VILAR, R. & WOSCHOLSKI, R. 2010. Characterisation of the PTEN inhibitor VO-OHpic. *Journal of chemical biology*, 3, 157-63.
- MAK, L. H. & WOSCHOLSKI, R. 2015. Targeting PTEN using small molecule inhibitors. *Methods*, 77-78, 63-8.
- MALANEY, P., PATHAK, R. R., XUE, B., UVERSKY, V. N. & DAVÉ, V. 2013. Intrinsic Disorder in PTEN and its Interactome Confers Structural Plasticity and Functional Versatility. *Scientific Reports*, 3, 2035.

References

- MANNING, B. D. & CANTLEY, L. C. 2007. AKT/PKB signaling: navigating downstream. *Cell*, 129, 1261-74.
- MANNING, B. D. & TOKER, A. 2017. AKT/PKB Signaling: Navigating the Network. *Cell*, 169, 381-405.
- MCKENZIE, E. A. & ABBOTT, W. M. 2018. Expression of recombinant proteins in insect and mammalian cells. *Methods*, 147, 40-49.
- MEHLA, J., CAUFIELD, J. H., SAKHAWALKAR, N. & UETZ, P. 2017. Chapter Seventeen - A Comparison of Two-Hybrid Approaches for Detecting Protein-Protein Interactions. In: SHUKLA, A. K. (ed.) *Methods in Enzymology*. Academic Press.
- MEUILLET, E. J., MAHADEVAN, D., BERGGREN, M., COON, A. & POWIS, G. 2004. Thioredoxin-1 binds to the C2 domain of PTEN inhibiting PTEN's lipid phosphatase activity and membrane binding: a mechanism for the functional loss of PTEN's tumor suppressor activity. *Archives of Biochemistry and Biophysics*, 429, 123-133.
- MINKINA, V. G., SHABUNYA, S. I., KALININ, V. I., MARTYNENKO, V. V. & SMIRNOVA, A. L. 2012. Stability of alkaline aqueous solutions of sodium borohydride. *International Journal of Hydrogen Energy*, 37, 3313-3318.
- MIYASHITA, T. 2015. Confocal microscopy for intracellular co-localization of proteins. *Methods Mol Biol*, 1278, 515-26.
- MOGHE, A., GHARE, S., LAMOREAU, B., MOHAMMAD, M., BARVE, S., MCCLAIN, C. & JOSHI-BARVE, S. 2015. Molecular Mechanisms of Acrolein Toxicity: Relevance to Human Disease. *Toxicological Sciences*, 143, 242-255.
- MOHAMMAD, M. K., AVILA, D., ZHANG, J., BARVE, S., ARTEEL, G., MCCLAIN, C. & JOSHI-BARVE, S. 2012. Acrolein cytotoxicity in hepatocytes involves endoplasmic reticulum stress, mitochondrial dysfunction and oxidative stress. *Toxicol Appl Pharmacol*, 265, 73-82.
- MOSMANN, T. 1983. Rapid colorimetric assay for cellular growth and survival: application to proliferation and cytotoxicity assays. *J Immunol Methods*, 65, 55-63.
- MYERS, C. R., MYERS, J. M., KUFAHL, T. D., FORBES, R. & SZADKOWSKI, A. 2011. The effects of acrolein on the thioredoxin system: implications for redox-sensitive signaling. *Molecular nutrition & food research*, 55, 1361-1374.
- MYERS, M. P., PASS, I., BATTY, I. H., VAN DER KAAJ, J., STOLAROV, J. P., HEMMINGS, B. A., WIGLER, M. H., DOWNES, C. P. & TONKS, N. K. 1998. The lipid phosphatase activity of PTEN is critical for its tumor suppressor function. *Proc Natl Acad Sci U S A*, 95, 13513-8.
- MYERS, M. P., STOLAROV, J. P., ENG, C., LI, J., WANG, S. I., WIGLER, M. H., PARSONS, R. & TONKS, N. K. 1997. P-TEN, the tumor suppressor from human chromosome 10q23, is a dual-specificity phosphatase. *Proc Natl Acad Sci U S A*, 94, 9052-7.
- NAGUIB, A., BENCZE, G., CHO, H., ZHENG, W., TOCILJ, A., ELKAYAM, E., FAEHNLE, C. R., JABER, N., PRATT, C. P., CHEN, M., ZONG, W. X., MARKS, M. S., JOSHUA-TOR, L., PAPPIN, D. J. & TROTMAN, L. C. 2015. PTEN functions by recruitment to cytoplasmic vesicles. *Mol Cell*, 58, 255-68.
- NALEFSKI, E. A. & FALKE, J. J. 1996. The C2 domain calcium-binding motif: Structural and functional diversity. *Protein Science*, 5, 2375-2390.
- NESVIZHSHKII, A. I. 2012. Computational and informatics strategies for identification of specific protein interaction partners in affinity purification mass spectrometry experiments. *Proteomics*, 12, 1639-55.
- NGUYEN HUU, T., PARK, J., ZHANG, Y., PARK, I., YOON, H. J., WOO, H. A. & LEE, S.-R. 2021. Redox Regulation of PTEN by Peroxiredoxins. *Antioxidants (Basel, Switzerland)*, 10, 302.

References

- NIEVA, J., SHAFTON, A., ALTOBELL, L. J., 3RD, TRIPURANENI, S., ROGEL, J. K., WENTWORTH, A. D., LERNER, R. A. & WENTWORTH, P., JR. 2008. Lipid-derived aldehydes accelerate light chain amyloid and amorphous aggregation. *Biochemistry*, 47, 7695-705.
- NIKI, E., YOSHIDA, Y., SAITO, Y. & NOGUCHI, N. 2005. Lipid peroxidation: Mechanisms, inhibition, and biological effects. *Biochemical and Biophysical Research Communications*, 338, 668-676.
- O'CONNELL, M. R., GAMSJAEGER, R. & MACKAY, J. P. 2009. The structural analysis of protein-protein interactions by NMR spectroscopy. *PROTEOMICS*, 9, 5224-5232.
- OELJEKLAUS, S., MEYER, H. E. & WARSCHEID, B. 2009. New dimensions in the study of protein complexes using quantitative mass spectrometry. *FEBS Letters*, 583, 1674-1683.
- OGAWARA, Y., KISHISHITA, S., OBATA, T., ISAZAWA, Y., SUZUKI, T., TANAKA, K., MASUYAMA, N. & GOTOH, Y. 2002. Akt Enhances Mdm2-mediated Ubiquitination and Degradation of p53. *Journal of Biological Chemistry*, 277, 21843-21850.
- OLIVEIRA, A. P. A., FREITAS, J. T. J., DINIZ, R., PESSOA, C., MARANHÃO, S. S., RIBEIRO, J. M., SOUZA-FAGUNDES, E. M. & BERALDO, H. 2020. Triethylphosphinegold(I) Complexes with Secnidazole-Derived Thiosemicarbazones: Cytotoxic Activity against HCT-116 Colorectal Cancer Cells under Hypoxia Conditions. *ACS Omega*, 5, 2939-2946.
- OLSSON, M. H., SØNDERGAARD, C. R., ROSTKOWSKI, M. & JENSEN, J. H. 2011. PROPKA3: Consistent Treatment of Internal and Surface Residues in Empirical pKa Predictions. *J Chem Theory Comput*, 7, 525-37.
- OMAR, A. M., EL-ARABY, M. E., ABDELGHANY, T. M., SAFO, M. K., AHMED, M. H., BOOTHELLO, R., PATEL, B. B., ABDEL-BAKKY, M. S., MALEBARI, A. M., AHMED, H. E. A. & ELHAGGAR, R. S. 2020. Introducing of potent cytotoxic novel 2-(aroylamino)cinnamamide derivatives against colon cancer mediated by dual apoptotic signal activation and oxidative stress. *Bioorganic Chemistry*, 101, 103953.
- ONG, S.-E. & MANN, M. 2005. Mass spectrometry-based proteomics turns quantitative. *Nature Chemical Biology*, 1, 252-262.
- ONG, S. E., BLAGOEV, B., KRATCHMAROVA, I., KRISTENSEN, D. B., STEEN, H., PANDEY, A. & MANN, M. 2002. Stable isotope labeling by amino acids in cell culture, SILAC, as a simple and accurate approach to expression proteomics. *Mol Cell Proteomics*, 1, 376-86.
- PAPA, A., WAN, L., BONORA, M., SALMENA, L., SONG, MIN S., HOBBS, ROBIN M., LUNARDI, A., WEBSTER, K., NG, C., NEWTON, RYAN H., KNOBLAUCH, N., GUARNERIO, J., ITO, K., TURKA, LAURENCE A., BECK, ANDY H., PINTON, P., BRONSON, RODERICK T., WEI, W. & PANDOLFI, PIER P. 2014. Cancer-Associated PTEN Mutants Act in a Dominant-Negative Manner to Suppress PTEN Protein Function. *Cell*, 157, 595-610.
- PENG, X., WANG, J., PENG, W., WU, F.-X. & PAN, Y. 2016. Protein-protein interactions: detection, reliability assessment and applications. *Briefings in Bioinformatics*, 18, 798-819.
- PERKINS, A., NELSON, K. J., PARSONAGE, D., POOLE, L. B. & KARPLUS, P. A. 2015. Peroxiredoxins: guardians against oxidative stress and modulators of peroxide signaling. *Trends in biochemical sciences*, 40, 435-445.
- PERWEEN, S., ABIDI, M., FAIZY, A. F. & MOINUDDIN 2019. Post-translational modifications on glycated plasma fibrinogen: A physicochemical insight. *Int J Biol Macromol*, 126, 1201-1212.

References

- PIZZIMENTI, S., CIAMPORCERO, E., DAGA, M., PETTAZZONI, P., ARCARO, A., CETRANGOLO, G., MINELLI, R., DIANZANI, C., LEPORE, A., GENTILE, F. & BARRERA, G. 2013. Interaction of aldehydes derived from lipid peroxidation and membrane proteins. *Front Physiol*, 4, 242.
- POOLE, L. B. 2015. The basics of thiols and cysteines in redox biology and chemistry. *Free radical biology & medicine*, 80, 148-157.
- PORSTMANN, T., SANTOS, C. R., GRIFFITHS, B., CULLY, M., WU, M., LEEVERS, S., GRIFFITHS, J. R., CHUNG, Y.-L. & SCHULZE, A. 2008. SREBP Activity Is Regulated by mTORC1 and Contributes to Akt-Dependent Cell Growth. *Cell Metabolism*, 8, 224-236.
- PORTER, N. A., CALDWELL, S. E. & MILLS, K. A. 1995. Mechanisms of free radical oxidation of unsaturated lipids. *Lipids*, 30, 277-90.
- PURSLOW, J. A., KHATIWADA, B., BAYRO, M. J. & VENDITTI, V. 2020. NMR Methods for Structural Characterization of Protein-Protein Complexes. *Frontiers in Molecular Biosciences*, 7.
- PUTZ, U., HOWITT, J., DOAN, A., GOH, C. P., LOW, L. H., SILKE, J. & TAN, S. S. 2012. The tumor suppressor PTEN is exported in exosomes and has phosphatase activity in recipient cells. *Sci Signal*, 5, ra70.
- RAFTOPOULOU, M., ETIENNE-MANNEVILLE, S., SELF, A., NICHOLLS, S. & HALL, A. 2004. Regulation of Cell Migration by the C2 Domain of the Tumor Suppressor PTEN. *Science*, 303, 1179.
- RAO, V. S., SRINIVAS, K., SUJINI, G. N. & KUMAR, G. N. 2014. Protein-protein interaction detection: methods and analysis. *Int J Proteomics*, 2014, 147648.
- RAYNES, R., POMATTO, L. C. & DAVIES, K. J. 2016. Degradation of oxidized proteins by the proteasome: Distinguishing between the 20S, 26S, and immunoproteasome proteolytic pathways. *Mol Aspects Med*, 50, 41-55.
- RECHSTEINER, M. & ROGERS, S. W. 1996. PEST sequences and regulation by proteolysis. *Trends in Biochemical Sciences*, 21, 267-271.
- REDFERN, R. E., REDFERN, D., FURGASON, M. L., MUNSON, M., ROSS, A. H. & GERICKE, A. 2008. PTEN phosphatase selectively binds phosphoinositides and undergoes structural changes. *Biochemistry*, 47, 2162-71.
- REIS, A. & SPICKETT, C. M. 2012. Chemistry of phospholipid oxidation. *Biochim Biophys Acta*, 1818, 2374-87.
- REQUENA, J. R., FU, M. X., AHMED, M. U., JENKINS, A. J., LYONS, T. J. & THORPE, S. R. 1996. Lipoxidation products as biomarkers of oxidative damage to proteins during lipid peroxidation reactions. *Nephrol Dial Transplant*, 11 Suppl 5, 48-53.
- RIGAUT, G., SHEVCHENKO, A., RUTZ, B., WILM, M., MANN, M. & SERAPHIN, B. 1999. A generic protein purification method for protein complex characterization and proteome exploration. *Nat Biotechnol*, 17, 1030-2.
- RISS, T., MORAVEC, R., NILES, A. & BENINK, H. 2013. Cell viability assays. *Assay Guid. Man.*
- RIZO, J. & SÜDHOF, T. C. 1998. C2-domains, Structure and Function of a Universal Ca²⁺-binding Domain. *Journal of Biological Chemistry*, 273, 15879-15882.
- RODRIGUEZ, M. S., DARGEMONT, C. & HAY, R. T. 2001. SUMO-1 Conjugation in Vivo Requires Both a Consensus Modification Motif and Nuclear Targeting*. *Journal of Biological Chemistry*, 276, 12654-12659.
- ROGERS, J. C. & BOMGARDEN, R. D. 2016. Sample Preparation for Mass Spectrometry-Based Proteomics; from Proteomes to Peptides. *Adv Exp Med Biol*, 919, 43-62.
- ROOS, G., FOLOPPE, N. & MESSENS, J. 2012. Understanding the pK_a of Redox Cysteines: The Key Role of Hydrogen Bonding. *Antioxidants & redox signaling*, 18.

References

- ROSANO, G. L. & CECCARELLI, E. A. 2014. Recombinant protein expression in *Escherichia coli*: advances and challenges. *Frontiers in Microbiology*, 5.
- SADEGHIRIZI, A., YAZDANPARAST, R. & AGHAZADEH, S. 2016. Combating trastuzumab resistance by targeting thioredoxin-1/PTEN interaction. *Tumor Biology*, 37, 6737-6747.
- SAHDEV, S., KHATTAR, S. K. & SAINI, K. S. 2008. Production of active eukaryotic proteins through bacterial expression systems: a review of the existing biotechnology strategies. *Molecular and Cellular Biochemistry*, 307, 249-264.
- SAN-MIGUEL, T., PÉREZ-BERMÚDEZ, P. & GAVIDIA, I. 2013. Production of soluble eukaryotic recombinant proteins in *E. coli* is favoured in early log-phase cultures induced at low temperature. *Springerplus*, 2, 89.
- SAXTON, R. A. & SABATINI, D. M. 2017. mTOR Signaling in Growth, Metabolism, and Disease. *Cell*, 168, 960-976.
- SAYRE, L. M., LIN, D., YUAN, Q., ZHU, X. & TANG, X. 2006. Protein adducts generated from products of lipid oxidation: focus on HNE and one. *Drug Metab Rev*, 38, 651-75.
- SCHILLBERG, S., RAVEN, N., SPIEGEL, H., RASCHE, S. & BUNTRU, M. 2019. Critical Analysis of the Commercial Potential of Plants for the Production of Recombinant Proteins. *Frontiers in Plant Science*, 10.
- SCHOPFER, F. J., CIPOLLINA, C. & FREEMAN, B. A. 2011. Formation and Signaling Actions of Electrophilic Lipids. *Chemical Reviews*, 111, 5997-6021.
- SCHWERTASSEK, U., HAQUE, A., KRISHNAN, N., GREINER, R., WEINGARTEN, L., DICK, T. P. & TONKS, N. K. 2014. Reactivation of oxidized PTP1B and PTEN by thioredoxin 1. *The FEBS Journal*, 281, 3545-3558.
- SEET, B. T., DIKIC, I., ZHOU, M.-M. & PAWSON, T. 2006. Reading protein modifications with interaction domains. *Nature Reviews Molecular Cell Biology*, 7, 473-483.
- SEHNAL, D., BITTRICH, S., DESHPANDE, M., SVOBODOVÁ, R., BERKA, K., BAZGIER, V., VELANKAR, S., BURLEY, S. K., KOČA, J. & ROSE, A. S. 2021. Mol* Viewer: modern web app for 3D visualization and analysis of large biomolecular structures. *Nucleic Acids Research*, 49, W431-W437.
- SEINER, D. R., LABUTTI, J. N. & GATES, K. S. 2007. Kinetics and mechanism of protein tyrosine phosphatase 1B inactivation by acrolein. *Chemical research in toxicology*, 20, 1315-1320.
- SHAH, H., SPEEN, A. M., SAUNDERS, C., BROOKE, E. A., NALLASAMY, P., ZHU, H., LI, Y. R. & JIA, Z. 2015. Protection of HepG2 cells against acrolein toxicity by 2-cyano-3,12-dioxooleana-1,9-dien-28-imidazolide via glutathione-mediated mechanism. *Exp Biol Med (Maywood)*, 240, 1340-51.
- SHEARN, C. T., SMATHERS, R. L., BACKOS, D. S., REIGAN, P., ORLICKY, D. J. & PETERSEN, D. R. 2013. Increased carbonylation of the lipid phosphatase PTEN contributes to Akt2 activation in a murine model of early alcohol-induced steatosis. *Free Radical Biology & Medicine*, 65, 680-692.
- SHEARN, C. T., SMATHERS, R. L., STEWART, B. J., FRITZ, K. S., GALLIGAN, J. J., HAIL, N., JR. & PETERSEN, D. R. 2011. Phosphatase and tensin homolog deleted on chromosome 10 (PTEN) inhibition by 4-hydroxynonenal leads to increased Akt activation in hepatocytes. *Mol Pharmacol*, 79, 941-52.
- SHEN, S.-M., ZHANG, C., GE, M.-K., DONG, S.-S., XIA, L., HE, P., ZHANG, N., JI, Y., YANG, S., YU, Y., ZHENG, J.-K., YU, J.-X., XIA, Q. & CHEN, G.-Q. 2019. PTEN α and PTEN β promote carcinogenesis through WDR5 and H3K4 trimethylation. *Nature Cell Biology*, 21, 1436-1448.
- SIES, H., BERNDT, C. & JONES, D. P. 2017. Oxidative Stress. *Annual Review of Biochemistry*, 86, 715-748.

References

- SMITH, I. N. & BRIGGS, J. M. 2016. Structural mutation analysis of PTEN and its genotype-phenotype correlations in endometriosis and cancer. *Proteins*, 84, 1625-1643.
- SMITH, M. B. 2017. Chapter 7 - Functional Group Exchange Reactions: Reductions. *In*: SMITH, M. B. (ed.) *Organic Synthesis (Fourth Edition)*. Boston: Academic Press.
- SMITH, S. L., PITT, A. R. & SPICKETT, C. M. 2021. Approaches to Investigating the Protein Interactome of PTEN. *Journal of Proteome Research*, 20, 60-77.
- SNIDER, J., KOTLYAR, M., SARAON, P., YAO, Z., JURISICA, I. & STAGLJAR, I. 2015. Fundamentals of protein interaction network mapping. *Molecular Systems Biology*, 11, 848.
- SØNDERGAARD, C. R., OLSSON, M. H., ROSTKOWSKI, M. & JENSEN, J. H. 2011. Improved Treatment of Ligands and Coupling Effects in Empirical Calculation and Rationalization of pKa Values. *J Chem Theory Comput*, 7, 2284-95.
- SONG, M. S., SALMENA, L. & PANDOLFI, P. P. 2012. The functions and regulation of the PTEN tumour suppressor. *Nature Reviews Molecular Cell Biology*, 13, 283-296.
- SONG, Z., SAGHAFI, N., GOKHALE, V., BRABANT, M. & MEUILLET, E. J. 2007. Regulation of the activity of the tumor suppressor PTEN by thioredoxin in *Drosophila melanogaster*. *Experimental Cell Research*, 313, 1161-1171.
- SOUSA, B. C., AHMED, T., DANN, W. L., ASHMAN, J., GUY, A., DURAND, T., PITT, A. R. & SPICKETT, C. M. 2019. Short-chain lipid peroxidation products form covalent adducts with pyruvate kinase and inhibit its activity in vitro and in breast cancer cells. *Free Radical Biology and Medicine*, 144, 223-233.
- SOUSA, B. C., PITT, A. R. & SPICKETT, C. M. 2017. Chemistry and analysis of HNE and other prominent carbonyl-containing lipid oxidation compounds. *Free Radic Biol Med*, 111, 294-308.
- SPICKETT, C. M. & PITT, A. R. 2020. Modification of proteins by reactive lipid oxidation products and biochemical effects of lipoxidation. *Essays Biochem*, 64, 19-31.
- SPICKETT, C. M., PITT, A. R., MORRICE, N. & KOLCH, W. 2006. Proteomic analysis of phosphorylation, oxidation and nitrosylation in signal transduction. *Biochimica et Biophysica Acta (BBA) - Proteins and Proteomics*, 1764, 1823-1841.
- SPINELLI, L. & LESLIE, N. R. 2015. Assaying PTEN catalysis in vitro. *Methods*, 77-78, 51-57.
- SPINELLI, L. & LESLIE, N. R. 2016. Assays to Measure PTEN Lipid Phosphatase Activity In Vitro from Purified Enzyme or Immunoprecipitates. *In*: PULIDO, R. (ed.) *Protein Tyrosine Phosphatases: Methods and Protocols*. New York, NY: Springer New York.
- STARK, C., BREITKREUTZ, B. J., REGULY, T., BOUCHER, L., BREITKREUTZ, A. & TYERS, M. 2006. BioGRID: a general repository for interaction datasets. *Nucleic Acids Res*, 34, D535-9.
- STECK, P. A., PERSHOUSE, M. A., JASSER, S. A., YUNG, W. K., LIN, H., LIGON, A. H., LANGFORD, L. A., BAUMGARD, M. L., HATTIER, T., DAVIS, T., FRYE, C., HU, R., SWEDLUND, B., TENG, D. H. & TAVTIGIAN, S. V. 1997. Identification of a candidate tumour suppressor gene, MMAC1, at chromosome 10q23.3 that is mutated in multiple advanced cancers. *Nat Genet*, 15, 356-62.
- STEEN, H. & MANN, M. 2004. The ABC's (and XYZ's) of peptide sequencing. *Nat Rev Mol Cell Biol*, 5, 699-711.
- STEVENS, J. F. & MAIER, C. S. 2008. Acrolein: sources, metabolism, and biomolecular interactions relevant to human health and disease. *Molecular nutrition & food research*, 52, 7-25.
- STOCKERT, J. C., HOROBIN, R. W., COLOMBO, L. L. & BLÁZQUEZ-CASTRO, A. 2018. Tetrazolium salts and formazan products in Cell Biology: Viability assessment, fluorescence imaging, and labeling perspectives. *Acta Histochemica*, 120, 159-167.

References

- STUCKEY, J. A., SCHUBERT, H. L., FAUMAN, E. B., ZHANG, Z. Y., DIXON, J. E. & SAPER, M. A. 1994. Crystal structure of Yersinia protein tyrosine phosphatase at 2.5 Å and the complex with tungstate. *Nature*, 370, 571-5.
- SUN, Y., LU, D., YIN, Y., SONG, J., LIU, Y., HAO, W., QI, F., ZHANG, G., ZHANG, X., LIU, L., LIN, Z., LIANG, H., ZHAO, X., JIN, Y. & YIN, Y. 2021. PTEN α functions as an immune suppressor and promotes immune resistance in PTEN-mutant cancer. *Nature Communications*, 12, 5147.
- SUTHERLAND, C., LEIGHTON, I. A. & COHEN, P. 1993. Inactivation of glycogen synthase kinase-3 β by phosphorylation: new kinase connections in insulin and growth-factor signalling. *Biochemical Journal*, 296, 15-19.
- SUTHRAM, S., SHLOMI, T., RUPPIN, E., SHARAN, R. & IDEKER, T. 2006. A direct comparison of protein interaction confidence assignment schemes. *BMC Bioinformatics*, 7, 360.
- TENG, B., ZHAO, C., LIU, X. & HE, Z. 2015. Network inference from AP-MS data: computational challenges and solutions. *Brief Bioinform*, 16, 658-74.
- TENG, D. H. F., HU, R., LIN, H., DAVIS, T., ILIEV, D., FRYE, C., SWEDLUND, B., HANSEN, K. L., VINSON, V. L., GUMPPER, K. L., ELLIS, L., EL-NAGGAR, A., FRAZIER, M., JASSER, S., LANGFORD, L. A., LEE, J., MILLS, G. B., PERSHOUSE, M. A., POLLACK, R. E., TORNOS, C., TRONCOSO, P., ALFRED YUNG, W. K., FUJII, G., BERSON, A., BOOKSTEIN, R., BOLEN, J. B., TAVTIGIAN, S. V. & STECK, P. A. 1997. MMAC1/PTEN Mutations in Primary Tumor Specimens and Tumor Cell Lines. *Cancer Research*, 57, 5221.
- TIAN, B., ZHAO, C., GU, F. & HE, Z. 2017. A two-step framework for inferring direct protein-protein interaction network from AP-MS data. *BMC Systems Biology*, 11, 82.
- TORRES, J. & PULIDO, R. 2001. The tumor suppressor PTEN is phosphorylated by the protein kinase CK2 at its C terminus - Implications for PTEN stability to proteasome-mediated degradation. *Journal of Biological Chemistry*, 276, 993-998.
- TRIPATHI, N. K. & SHRIVASTAVA, A. 2019. Recent Developments in Bioprocessing of Recombinant Proteins: Expression Hosts and Process Development. *Frontiers in Bioengineering and Biotechnology*, 7.
- TROTMAN, L. C., WANG, X., ALIMONTI, A., CHEN, Z., TERUYA-FELDSTEIN, J., YANG, H., PAVLETICH, N. P., CARVER, B. S., CORDON-CARDO, C., ERDJUMENT-BROMAGE, H., TEMPST, P., CHI, S.-G., KIM, H.-J., MISTELI, T., JIANG, X. & PANDOLFI, P. P. 2007. Ubiquitination Regulates PTEN Nuclear Import and Tumor Suppression. *Cell*, 128, 141-156.
- TSAI, H.-C., TSOU, H.-H., LIN, C.-C., CHEN, S.-C., CHENG, H.-W., LIU, T.-Y., CHEN, W.-S., JIANG, J.-K., YANG, S.-H., CHANG, S.-C., TENG, H.-W. & WANG, H.-T. 2021. Acrolein contributes to human colorectal tumorigenesis through the activation of RAS-MAPK pathway. *Scientific Reports*, 11, 12590.
- TSIATSIANI, L. & HECK, A. J. 2015. Proteomics beyond trypsin. *Febs j*, 282, 2612-26.
- UCHIDA, K., KANEMATSU, M., MORIMITSU, Y., OSAWA, T., NOGUCHI, N. & NIKI, E. 1998. Acrolein is a product of lipid peroxidation reaction. Formation of free acrolein and its conjugate with lysine residues in oxidized low density lipoproteins. *J Biol Chem*, 273, 16058-66.
- UEMURA, T., TAKASAKA, T., IGARASHI, K. & IKEGAYA, H. 2017. Spermine oxidase promotes bile canalicular lumen formation through acrolein production. *Scientific Reports*, 7, 14841.
- VAN DER VOS, K. E. & COFFER, P. J. 2010. The Extending Network of FOXO Transcriptional Target Genes. *Antioxidants & Redox Signaling*, 14, 579-592.

References

- VAN MEERLOO, J., KASPERS, G. J. L. & CLOOS, J. 2011. Cell Sensitivity Assays: The MTT Assay. In: CREE, I. A. (ed.) *Cancer Cell Culture: Methods and Protocols*. Totowa, NJ: Humana Press.
- VAZQUEZ, F., GROSSMAN, S. R., TAKAHASHI, Y., ROKAS, M. V., NAKAMURA, N. & SELLERS, W. R. 2001. Phosphorylation of the PTEN Tail Acts as an Inhibitory Switch by Preventing Its Recruitment into a Protein Complex. *Journal of Biological Chemistry*, 276, 48627-48630.
- VAZQUEZ, F., RAMASWAMY, S., NAKAMURA, N. & SELLERS, W. R. 2000. Phosphorylation of the PTEN tail regulates protein stability and function. *Molecular and cellular biology*, 20, 5010-5018.
- VERRASTRO, I., TVEEN-JENSEN, K., SPICKETT, C. M. & PITT, A. R. 2018. The effect of HOCl-induced modifications on phosphatase and tensin homologue (PTEN) structure and function. *Free Radic Res*, 52, 232-247.
- VERRASTRO, I., TVEEN-JENSEN, K., WOSCHOLSKI, R., SPICKETT, C. M. & PITT, A. R. 2016. Reversible oxidation of phosphatase and tensin homolog (PTEN) alters its interactions with signaling and regulatory proteins. *Free Radic Biol Med*, 90, 24-34.
- VIEDMA-POYATOS, Á., GONZÁLEZ-JIMÉNEZ, P., LANGLOIS, O., COMPANY-MARIN, I., SPICKETT, C. M. & PÉREZ-SALA, D. 2021. Protein Lipoxidation: Basic Concepts and Emerging Roles. *Antioxidants*, 10, 295.
- VON MERING, C., KRAUSE, R., SNEL, B., CORNELL, M., OLIVER, S. G., FIELDS, S. & BORK, P. 2002. Comparative assessment of large-scale data sets of protein–protein interactions. *Nature*, 417, 399-403.
- WAITE, K. A. & ENG, C. 2002. Protean PTEN: form and function. *American journal of human genetics*, 70, 829-844.
- WANG, H. T., CHEN, T. Y., WENG, C. W., YANG, C. H. & TANG, M. S. 2016. Acrolein preferentially damages nucleolus eliciting ribosomal stress and apoptosis in human cancer cells. *Oncotarget*, 7, 80450-80464.
- WANG, L., CHO, Y.-L., TANG, Y., WANG, J., PARK, J.-E., WU, Y., WANG, C., TONG, Y., CHAWLA, R., ZHANG, J., SHI, Y., DENG, S., LU, G., WU, Y., TAN, H. W.-S., PAWIJIT, P., LIM, G. G.-Y., CHAN, H.-Y., ZHANG, J., FANG, L., YU, H., LIOU, Y.-C., KARTHIK, M., BAY, B.-H., LIM, K.-L., SZE, S.-K., YAP, C. T. & SHEN, H.-M. 2018. PTEN-L is a novel protein phosphatase for ubiquitin dephosphorylation to inhibit PINK1–Parkin-mediated mitophagy. *Cell Research*, 28, 787-802.
- WANG, S., OSGOOD, A. O. & CHATTERJEE, A. 2022. Uncovering post-translational modification-associated protein–protein interactions. *Current Opinion in Structural Biology*, 74, 102352.
- WANG, X., TROTMAN, L. C., KOPPIE, T., ALIMONTI, A., CHEN, Z., GAO, Z., WANG, J., ERDJUMENT-BROMAGE, H., TEMPST, P., CORDON-CARDO, C., PANDOLFI, P. P. & JIANG, X. 2007. NEDD4-1 Is a Proto-Oncogenic Ubiquitin Ligase for PTEN. *Cell*, 128, 129-139.
- WESTERMARCK, J., IVASKA, J. & CORTHALS, G. L. 2013. Identification of protein interactions involved in cellular signaling. *Mol Cell Proteomics*, 12, 1752-63.
- WILKINS, M. R., LINDSKOG, I., GASTEIGER, E., BAIROCH, A., SANCHEZ, J. C., HOCHSTRASSER, D. F. & APPEL, R. D. 1997. Detailed peptide characterization using PEPTIDEMASS—a World-Wide-Web-accessible tool. *Electrophoresis*, 18, 403-8.
- WINTERBOURN, C. C. & HAMPTON, M. B. 2008. Thiol chemistry and specificity in redox signaling. *Free Radical Biology and Medicine*, 45, 549-561.

References

- WISNIEWSKI, J. R. & MANN, M. 2012. Consecutive proteolytic digestion in an enzyme reactor increases depth of proteomic and phosphoproteomic analysis. *Anal Chem*, 84, 2631-7.
- WISNIEWSKI, J. R., WEGLER, C. & ARTURSSON, P. 2019. Multiple-Enzyme-Digestion Strategy Improves Accuracy and Sensitivity of Label- and Standard-Free Absolute Quantification to a Level That Is Achievable by Analysis with Stable Isotope-Labeled Standard Spiking. *J Proteome Res*, 18, 217-224.
- WU, W., WANG, X., ZHANG, W., REED, W., SAMET, J. M., WHANG, Y. E. & GHIO, A. J. 2003. Zinc-induced PTEN Protein Degradation through the Proteasome Pathway in Human Airway Epithelial Cells. *Journal of Biological Chemistry*, 278, 28258-28263.
- XIAO, Y., YEONG CHIT CHIA, J., GAJEWSKI, J. E., SIO SENG LIO, D., MULHERN, T. D., ZHU, H.-J., NANDURKAR, H. & CHENG, H.-C. 2007. PTEN catalysis of phospholipid dephosphorylation reaction follows a two-step mechanism in which the conserved aspartate-92 does not function as the general acid — Mechanistic analysis of a familial Cowden disease-associated PTEN mutation. *Cellular Signalling*, 19, 1434-1445.
- XING, S., WALLMEROOTH, N., BERENDZEN, K. W. & GREFEN, C. 2016. Techniques for the Analysis of Protein-Protein Interactions in Vivo. *Plant Physiology*, 171, 727.
- YAACOUB, C., RIFI, M., DANY, E., MAWLAWI, H., SABATIER, J.-M., COUTARD, B. & FAJLOUN, Z. 2021. The Cytotoxic Effect of Apis mellifera Venom with a Synergistic Potential of Its Two Main Components-Melittin and PLA2-On Colon Cancer HCT116 Cell Lines. *Molecules*, 26, 2264.
- YAKUBU, R. R., NIEVES, E. & WEISS, L. M. 2019. The Methods Employed in Mass Spectrometric Analysis of Posttranslational Modifications (PTMs) and Protein-Protein Interactions (PPIs). In: WOODS, A. G. & DARIE, C. C. (eds.) *Advancements of Mass Spectrometry in Biomedical Research*. Cham: Springer International Publishing.
- YAMAMOTO, S. 1992. Mammalian lipoxygenases: molecular structures and functions. *Biochimica et Biophysica Acta (BBA) - Lipids and Lipid Metabolism*, 1128, 117-131.
- YANG, M., SCHIAPPARELLI, P., NGUYEN, H. N., IGARASHI, A., ZHANG, Q., ABBADI, S., AMZEL, L. M., SESAKI, H., QUINONES-HINOJOSA, A. & IJIMA, M. 2017. Characterization of PTEN mutations in brain cancer reveals that pten mono-ubiquitination promotes protein stability and nuclear localization. *Oncogene*, 36, 3673-3685.
- YEE, K. S. & VOUSDEN, K. H. 2005. Complicating the complexity of p53. *Carcinogenesis*, 26, 1317-1322.
- YIN, Z., GUO, H., JIANG, K., OU, J., WANG, M., HUANG, C., LIU, F., BAI, W., ZHENG, J. & OU, S. 2020a. Morin decreases acrolein-induced cell injury in normal human hepatocyte cell line LO2. *Journal of Functional Foods*, 75, 104234.
- YIN, Z., JIANG, K., SHI, L., FEI, J., ZHENG, J., OU, S. & OU, J. 2020b. Formation of di-cysteine acrolein adduct decreases cytotoxicity of acrolein by ROS alleviation and apoptosis intervention. *Journal of Hazardous Materials*, 387, 121686.
- YOUNG, C. L., BRITTON, Z. T. & ROBINSON, A. S. 2012. Recombinant protein expression and purification: A comprehensive review of affinity tags and microbial applications. *Biotechnology Journal*, 7, 620-634.
- YOUNG, F. M., PHUNGTAMDET, W. & SANDERSON, B. J. S. 2005. Modification of MTT assay conditions to examine the cytotoxic effects of amitraz on the human lymphoblastoid cell line, WIL2NS. *Toxicology in Vitro*, 19, 1051-1059.
- YU, C.-X., LI, S. & WHORTON, A. R. 2005. Redox Regulation of PTEN by S-Nitrosothiols. *Molecular Pharmacology*, 68, 847.

References

- YUGANDHAR, K., GUPTA, S. & YU, H. 2019. Inferring Protein-Protein Interaction Networks From Mass Spectrometry-Based Proteomic Approaches: A Mini-Review. *Computational and Structural Biotechnology Journal*, 17, 805-811.
- YUVANIYAMA, J., DENU, J. M., DIXON, J. E. & SAPER, M. A. 1996. Crystal structure of the dual specificity protein phosphatase VHR. *Science*, 272, 1328-31.
- ZHANG, B., PARK, B.-H., KARPINETS, T. & SAMATOVA, N. F. 2008. From pull-down data to protein interaction networks and complexes with biological relevance. *Bioinformatics*, 24, 979-986.
- ZHANG, X. C., PICCINI, A., MYERS, M. P., VAN AELST, L. & TONKS, N. K. 2012. Functional analysis of the protein phosphatase activity of PTEN. *Biochem J*, 444, 457-64.
- ZHANG, Y., FONSLow, B. R., SHAN, B., BAEK, M. C. & YATES, J. R., 3RD 2013. Protein analysis by shotgun/bottom-up proteomics. *Chem Rev*, 113, 2343-94.
- ZHANG, Y., HAN, S.-J., PARK, I., KIM, I., CHAY, K.-O., KIM, M. S., JANG, I. D., LEE, T.-H. & LEE, S.-R. 2017. Redox Regulation of the Tumor Suppressor PTEN by Hydrogen Peroxide and Tert-Butyl Hydroperoxide. *International Journal of Molecular Sciences*, 18.
- ZHANG, Y., NICHOLATOS, J., DREIER, J. R., RICOULT, S. J. H., WIDENMAIER, S. B., HOTAMISLIGIL, G. S., KWIATKOWSKI, D. J. & MANNING, B. D. 2014. Coordinated regulation of protein synthesis and degradation by mTORC1. *Nature*, 513, 440-443.
- ZHANG, Y., PARK, J., HAN, S.-J., YANG, S. Y., YOON, H. J., PARK, I., WOO, H. A. & LEE, S.-R. 2020. Redox regulation of tumor suppressor PTEN in cell signaling. *Redox Biology*, 34, 101553.
- ZHANG, Z.-Y. 2003. Chemical and Mechanistic Approaches to the Study of Protein Tyrosine Phosphatases. *Accounts of Chemical Research*, 36, 385-392.
- ZHAO, J., ZHAI, B., GYGI, S. P. & GOLDBERG, A. L. 2015. mTOR inhibition activates overall protein degradation by the ubiquitin proteasome system as well as by autophagy. *Proceedings of the National Academy of Sciences*, 112, 15790.
- ZHAO, X., LI, G. & LIANG, S. 2013. Several Affinity Tags Commonly Used in Chromatographic Purification. *Journal of Analytical Methods in Chemistry*, 2013, 581093.
- ZHOU, M., LI, Q. & WANG, R. 2016. Current Experimental Methods for Characterizing Protein-Protein Interactions. *ChemMedChem*, 11, 738-56.
- ZHU, Y., HOELL, P., AHLEMEYER, B. & KRIEGLSTEIN, J. 2006. PTEN: A crucial mediator of mitochondria-dependent apoptosis. *Apoptosis*, 11, 197-207.
- ZILFOU, J. T. & LOWE, S. W. 2009. Tumor Suppressive Functions of p53. *Cold Spring Harbor Perspectives in Biology*, 1.
- ZORRILLA, S., MÓNICO, A., DUARTE, S., RIVAS, G., PÉREZ-SALA, D. & PAJARES, M. A. 2019. Integrated approaches to unravel the impact of protein lipoxidation on macromolecular interactions. *Free Radical Biology and Medicine*, 144, 203-217.

Appendices

AGGAGGTAAAACATATGACCGCGATTATCAAAGAGATCGTGTCCCGTAACAAGCGCCG
 TTATCAAGAAGATGGCTTTGACCTGGACCTGACCTACATCTACCCGAACATTATCGCGA
 TGGGTTTTCCAGCCGAGCGCCTGGAGGGCGTCTACCGTAATAACATCGATGATGTGGT
 TCGTTTTCTGGACAGCAAACATAAGAACCATTACAAGATCTATAATCTGTGCGCCGAGC
 GTCATTATGACACCGCGAAATTCAATTGCCGTGTTGCGCAGTACCCGTTGAGGACCA
 CAATCCGCCGCAACTGGAAGTATTAAACCGTTCTGCGAGGACCTGGATCAGTGGCTG
 TCCGAGGACGACAACCACGTGGCCGCGATTCACTGTAAGGCCGGCAAAGGTCGTACC
 GCGTCATGATCTGCGCGTACCTGCTGCACCGCGGTAAGTTTCTGAAGGCGCAAGAAG
 CGCTGGACTTTTACGGCGAGGTGCGTACCCGCGACAAAAGGGTGTACCATCCCGA
 GCCAACGCCGCTATGTTTACTACTACAGCTATTTGCTGAAAAACACCTGGATTATCGT
 CCTGTCGCCCTGTTGTTTACAAGATGATGTTTGAACGATTCCGATGTTTCAGCGGCGG
 TACCTGTAATCCGCAGTTCGTCGTTTGTGAGCTGAAGGTGAAGATCTACAGCTCTAATA
 GCGGTCCGACCCGTCGCGAAGATAAGTTTATGTATTTTCAATTCCCGCAGCCGCTGCC
 GGTTTGTGGTGACATCAAGGTGGAGTTCTTCCATAAACAAAACAAGATGTTGAAGAAAG
 ATAAGATGTTCCATTTTTGGGTCAACACTTTCTTTATTCCGGGTCCGGAGGAGACTAGC
 GAGAAAGTTGAGAACGGTAGCCTGTGCGATCAAGAAATCGATAGCATTTCAGCATCG
 AACGTGCGGATAATGACAAAGAATATCTGGTCTTGACCCTGACGAAAAACGACCTGGAC
 AAAGCGAACAAAGATAAAGCGAATCGCTATTTAGCCCGAATTTCAAAGTTAAGCTGTA
 CTTTACCAAACACTGTGGAGGAACCGAGCAATCCGGAGGCGTCTAGCTCTACCAGCGTG
 ACCCCGGACGTCAGCGACAATGAGCCGGACCACTATCGTTACAGCGACACGACCGAC
 AGCGATCCTGAAAATGAACCGTTTGACGAAGATCAACATACGCAGATTACCAAGGTGAA
 AGGCAACAGCGCGGATATTCAGCATTCTGGTGGCCGTAGCAGCTTGGAAGGCCCTCG
 CTTGAGGGTAAGCCGATTCCGAATCCGCTGCTGGGTCTGGATAGCACGCGCACGGG
 TCACCACCACCATCACCACTAACTCGAG

Supplementary Figure 1 JpExpress404 PTEN-V5-His Plasmid Insert Sequence

JpExpress404 PTEN was a gift from Ramon Parsons (Addgene plasmid # 49420 ; <http://n2t.net/addgene:49420> ; RRID:Addgene_49420) (Hopkins et al., 2013).

Supplementary Table 1 Resultant Peptides of PTEN-V5-His Digestion with Different Proteases

Peptide	No. of Residues	N-terminal Cleavage Site
<i>Trypsin</i>		
YFSPNFK	7	R
NNIDDVVR	8	R
KGVTIPSQR	9	K
IYNLCAER	8	K
EYLVLTGTK	9	K
IYSSNSGPTR	10	K

Appendices

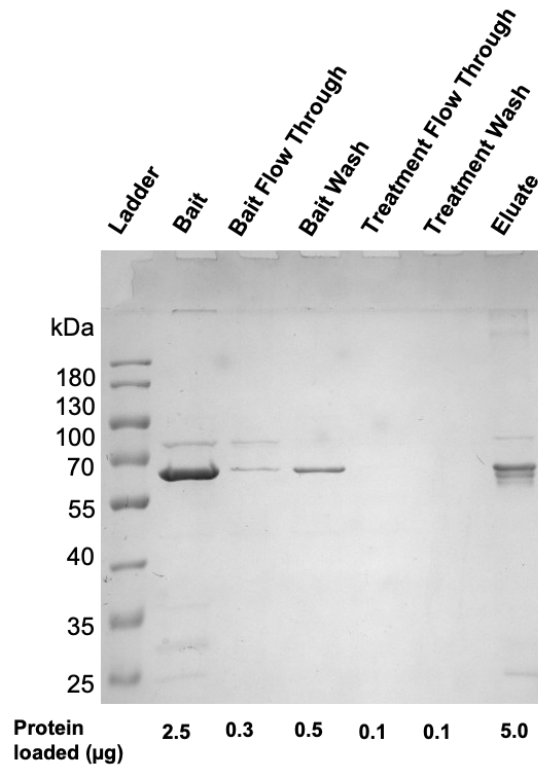
TAIKEIVSR	10	M
VKIYSSNSGPTR	12	K
YVYYYSYLLK	10	R
AQEALDFYGEVR	12	K
TGVMICAYLLHR	12	R
RYVYYYSYLLK	11	R
NHYKIYNLCAER	12	K
ADNDKEYLVLTCLK	14	R
GRTGVMICAYLLHR	14	K
NHLDYRPVALLFHK	14	K
FLKAQEALDFYGEVR	15	K
FMYFEFPQPLPVCGLIK	17	K
VENGSLCDQEIDSICSIER	19	K
MFHFVWNTFFIPGPEETSEK	20	K
EDKFMFEPQPLPVCGLIK	20	R
DKMFHFVWNTFFIPGPEETSEK	22	K
YSDTTDSDPENEPFDEDQHTQITK	24	R
MMFETIPMFSGGTCNPQFVVCQLK	24	K
FMYFEFPQPLPVCGLIKVEFFHK	23	K
YQEDGFDLDTYIYPNIIAMGFPAER	26	R
TVEEPSNPEASSSTSVTPDVSDNEPDHYR	29	K
VAQYPFEDHNPQLELIKPFCELDQWLSEDDN HVAIHCK	41	R
<i>Trypsin/Lys-C</i>		
NNIDDVVR	8	R
KGVTIPSQR	9	K
IYNLCAER	8	K
EYLVLTCLK	9	K
IYSSNSGPTR	10	K
TAIKEIVSR	10	M
YVYYYSYLLK	10	R
AQEALDFYGEVR	12	K
TGVMICAYLLHR	12	R
RYVYYYSYLLK	11	R
ADNDKEYLVLTCLK	14	R
GRTGVMICAYLLHR	14	K
LEGVYRNNIDDVVR	14	R
FMYFEFPQPLPVCGLIK	17	K
VENGSLCDQEIDSICSIER	19	K
MFHFVWNTFFIPGPEETSEK	20	K
EDKFMFEPQPLPVCGLIK	20	R
PFCELDQWLSEDDNHVAIHCK	23	K
YSDTTDSDPENEPFDEDQHTQITK	24	R
MMFETIPMFSGGTCNPQFVVCQLK	24	K
YQEDGFDLDTYIYPNIIAMGFPAER	26	R

Appendices

TVEEPSNPEASSSTSVTPDVSDNEPDHYR	29	K
RYQEDGFDLTLTYIYPNIIAMGFPAER	27	R
VAQYPFEDHNPPQLELIKPFCELDLQWLSEDDN HVAAIHCK	41	R
<i>Trypsin/Glu-C</i>		
LEGVYR	6	R
NNIDDVVR	8	R
DHNPPQLE	8	E
YLVLTLLTK	8	E
KGVTIPSQR	9	K
IYNLCAER	8	K
ALDFYGEVR	9	E
IYSSNSGPTR	10	K
IDSICSIER	9	E
VKIYSSNSGPTR	12	K
FPQPLPVCGLDIK	12	E
YVYYYSYLLK	10	R
AQEALDFYGEVR	12	K
TGVMICAYLLHR	12	R
RYVYYYSYLLK	11	R
FPQPLPVCGLDIKVE	14	E
NEPFDEDQHTQITK	14	E
VAQYPFEDHNPPQLE	15	R
YSDTTDSDPENEPFDE	16	R
MFHFWVNTFFIPGPEE	16	K
FMYFEFPQPLPVCGLDIK	17	K
ASSSTSVTPDVSDNEPDHYR	20	E
DLQWLSEDDNHVAAIHCK	19	E
TIPMFSGGTCNPQFVVCQLK	20	E
FMYFEFPQPLPVCGLDIKVE	19	K
DKFMYFEFPQPLPVCGLDIK	19	E
YSDTTDSDPENEPFDEDQHTQITK	24	R
TVEEPSNPEASSSTSVTPDVSDNEPDHYR	29	K
LIKPFCELDLQWLSEDDNHVAAIHCK	26	E
<i>Chymotrypsin</i>		
RPVALLF	7	Y
DYRPVAL	7	L
CAERHY	6	L
LKNHLDY	7	L
KAQEALDF	8	L
HFWVNTF	7	F
SYLLKNHL	8	Y
LLKNHLDY	8	Y
FSPNFKVKL	9	Y
KAQEALDFY	9	L

Appendices

DYRPVALLF	9	L
SPNFKVKLY	9	F
LDSKHKNHY	9	F
NCRVAQYPF	9	F
EDHNPPQLEL	10	F
LKAQEALDFY	10	F
FSPNFKVKLY	10	Y
RNNIDDVVRFL	10	Y
KNHLDYRPVAL	11	L
RNNIDDVVRFL	11	Y
CAERHYDTAKF	11	L
LKNHLDYRPVAL	12	L
FHKMMFETIPMF	12	L
SGGTCNPQFVVCQL	14	F
NLCAERHYDTAKF	13	Y
LFHKMMFETIPMF	13	L
EDHNPPQLELIKPF	14	F
IYPNIIAMGFPAERL	15	Y
RYSDDTSDPENEPF	15	Y
FIPGPEETSEKVENGL	17	F
TKNDLDKANKDKANRY	16	L
EFQPLPVCGLKVEFF	17	F
TKNDLDKANKDKANRYF	17	L
NCRVAQYPFEDHNPPQL	17	F
TLTKNDLDKANKDKANRY	18	L
IYPNIIAMGFPAERLEGVY	19	Y
SGGTCNPQFVVCQLKVKIY	19	F
TLTKNDLDKANKDKANRYF	19	L
VLTKNDLDKANKDKANRY	20	L
NCRVAQYPFEDHNPPQLEL	19	F
MYFEFPQPLPVCGLKVEFF	20	F
SDTTSDPENEPFDEDQHTQITKV	24	Y
NCRVAQYPFEDHNPPQLELIKPF	23	F
RYSDDTSDPENEPFDEDQHTQITKV	26	Y
TKTVEEPSNPEASSSTSVTPDVSDNEPDHY	30	F
FTKTVEEPSNPEASSSTSVTPDVSDNEPDHY	31	Y
YFTKTVEEPSNPEASSSTSVTPDVSDNEPDHY	32	L
FTKTVEEPSNPEASSSTSVTPDVSDNEPDHYRY	33	Y



Supplementary Figure 2 Uncropped SDS-PAGE Analysis of the Treatment Control Fractions

Supplementary Table 2 PTEN-Specific Interactors Identified by the Pull Down Assay that met the Threshold Parameters

Accession ^l	Protein Name	Uniq ue Pepti des [@]	Confiden ce Score [£]	Anova (p) [§]	Max. Fold Chang e	Highest Abunda nce
ACSF2_H UMAN	Medium-chain acyl-CoA ligase ACSF2, mitochondrial	7	114.47	0.0011	6.6	Control
AFF4_HU MAN	AF4/FMR2 family member 4	2	103.85	0.0375	1.6	Control
AMOT_HU MAN*	Angiomotin	4	69.52	0.0072	5.1	Control
AN32E_HU MAN	Acidic leucine-rich nuclear phosphoprotein 32 family member E	3	175.92	0.0179	2.9	Control
AP3B1_HU MAN	AP-3 complex subunit beta-1	16	1384.51	0.0141	1.7	Control
AP3D1_HU MAN	AP-3 complex subunit delta-1	18	1095.44	0.0235	1.9	Control
AP3M1_H UMAN	AP-3 complex subunit mu-1	5	467.12	0.0104	1.3	Control
ARF1_HU MAN	ADP-ribosylation factor 1	4	411.07	0.0251	1.5	Treated
BOLA2_H UMAN	BolA-like protein 2	2	116.63	0.0163	3.2	Control
BRD2_HU MAN	Bromodomain- containing protein 2	8	655.25	0.0064	2.1	Control

Appendices

CADH6_H UMAN	Cadherin-6	3	79.62	0.0399	4.1	Treated
CD5R1_H UMAN	Cyclin-dependent kinase 5 activator 1	3	68.85	0.0069	1.9	Treated
CHD3_HU MAN	Chromodomain-helicase-DNA-binding protein 3	3	152.11	0.0430	2.6	Treated
CHD7_HU MAN	Chromodomain-helicase-DNA-binding protein 7	5	276.41	0.0212	4.7	Treated
CHD9_HU MAN	Chromodomain-helicase-DNA-binding protein 9	2	335.78	0.0319	28.6	Treated
COA7_HU MAN	Cytochrome c oxidase assembly factor 7	2	155.81	0.0069	18.9	Treated
CSN2_HU MAN	COP9 signalosome complex subunit 2	4	214.29	0.0345	2.1	Control
CWC22_H UMAN	Pre-mRNA-splicing factor CWC22 homolog	24	1118.15	0.0060	2.0	Treated
DDX21_HU MAN*	Nucleolar RNA helicase 2	16	952.54	0.0304	1.7	Control
DEN5A_H UMAN	DENN domain-containing protein 5A	3	77.21	0.0498	1.6	Control
DYHC2_H UMAN	Cytoplasmic dynein 2 heavy chain 1	7	110.81	0.0449	1.4	Treated
EIF3I_HUM AN	Eukaryotic translation initiation factor 3 subunit I	3	161.87	0.0106	2.5	Control
EWS_HUM AN	RNA-binding protein EWS	3	144.01	0.0198	1.6	Treated
FLNC_HU MAN	Filamin-C	5	214.15	0.0133	5.5	Control
H13_HUM AN	Histone H1.3	7	511.1	0.0103	1.3	Control
HDGR2_H UMAN	Hepatoma-derived growth factor-related protein 2	4	384.18	0.0222	2.3	Control
HECD1_H UMAN	E3 ubiquitin-protein ligase HECTD1	34	1847.88	0.0372	5.1	Treated
HP1B3_HU MAN	Heterochromatin protein 1-binding protein 3	5	285.56	0.0428	1.6	Treated
IQEC2_HU MAN	IQ motif and SEC7 domain-containing protein 2	3	71.58	0.0038	3.1	Treated
IQGA2_HU MAN	Ras GTPase-activating-like protein IQGAP2	2	178.05	0.0189	2.4	Treated
LYSC_HU MAN	Lysozyme C	2	53.91	0.0011	6.9	Treated
MAPK2_H UMAN	MAP kinase-activated protein kinase 2	3	74.43	0.0410	1.1	Treated
MP2K3_H UMAN	Dual specificity mitogen-activated protein kinase kinase	3	79.38	0.0256	1.5	Treated

Appendices

NAT10_HU MAN	RNA cytidine acetyltransferase	2	101.89	0.0069	1.5	Control
NCBP1_H UMAN*	Nuclear cap-binding protein subunit 1	4	270.97	0.0310	1.3	Control
OLA1_HU MAN	Obg-like ATPase 1	7	507.79	0.0112	1.7	Control
PERT_HU MAN	Thyroid peroxidase	4	78.77	0.0000	16.2	Control
PIMT_HUM AN	Protein-L-isoaspartate(D-aspartate) O-methyltransferase	4	164.87	0.0472	1.9	Treated
PPP6_HU MAN	Serine/threonine-protein phosphatase 6 catalytic subunit	2	117.27	0.0004	1.8	Treated
PPR29_HU MAN	Protein phosphatase 1 regulatory subunit	2	60.63	0.0083	2.8	Treated
RBBP6_H UMAN	E3 ubiquitin-protein ligase RBBP6	7	241.44	0.0064	1.7	Control
RCN1_HU MAN*	Reticulocalbin-1	4	140.35	0.0033	7.5	Treated
RIC8A_HU MAN	Synembryn-A	3	72.54	0.0016	5.9	Control
RL22L_HU MAN	60S ribosomal protein L22-like 1	2	281.25	0.0077	2.7	Control
RL37A_HU MAN	60S ribosomal protein L37a	3	195.39	0.0024	7.6	Control
RM12_HU MAN	39S ribosomal protein L12, mitochondrial	2	122.66	0.0207	2.0	Treated
RNF39_HU MAN	RING finger protein 39	2	71.35	0.0178	1.8	Treated
RS28_HU MAN	40S ribosomal protein S28	3	205.25	0.0020	19.5	Control
RS29_HU MAN	40S ribosomal protein S29	4	203.77	0.0064	21.7	Control
RT4_HUM AN	28S ribosomal protein S14, mitochondrial	3	261.1	0.0445	6.5	Control
RT24_HU MAN	28S ribosomal protein S24, mitochondrial	2	65.48	0.0001	210.5	Control
SRP09_HU MAN	Signal recognition particle 9 kDa protein	4	241.46	0.0003	7.7	Control
TBCD1_H UMAN	TBC1 domain family member 1	3	58.21	0.0065	13.5	Treated
THS7A_H UMAN	Thrombospondin type-1 domain-containing protein 7A	5	115.89	0.0093	3.0	Treated
TIM50_HU MAN	Mitochondrial import inner membrane translocase subunit TIM50	4	198.77	0.0227	2.1	Treated
TSR1_HU MAN	Pre-rRNA-processing protein TSR1 homolog	4	243.71	0.0117	2.7	Treated
UBR4_HU MAN	E3 ubiquitin-protein ligase UBR4	12	712.75	0.0077	4.4	Treated

USP9X_HUMAN*	Probable ubiquitin carboxyl-terminal hydrolase FAF-X	24	2754.68	0.0170	15.8	Control
VP13B_HUMAN	Vacuolar protein sorting-associated protein 13B	3	74.47	0.0251	15.8	Treated
ZN609_HUMAN	Zinc finger protein 609	2	92.97	0.0426	1.7	Control

Key:

!: SwissProt Protein ID

@: The number of unique peptides used for quantification

£: The protein confidence score for each protein assigned by Mascot

\$: The p-value generated by Progenesis QI for proteomics

*: Previously identified as a PTEN interactor with physical evidence in the BioGRID database (Stark et al., 2006).

Supplementary Table 3 All Specific PTEN-Interactors Identified in the Affinity Pull Down Assay

Accession[!]	Unique Peptides[@]	Confidence Score[£]	Anova (p)[^]	Max. Fold Change	Highest Abundance
ACSF2_HUMAN	7	114.47	0.0011	6.6	Control
ACYP1_HUMAN*	2	97.03	0.0026	65.1	Treated
AFF4_HUMAN	2	103.85	0.0375	1.6	Control
ALBU_HUMAN\$	6	216.21	0.0090	6.2	Control
AMOT_HUMAN	4	69.52	0.0072	5.1	Control
AN32E_HUMAN	3	175.92	0.0179	2.9	Control
AP3B1_HUMAN	16	1384.51	0.0141	1.7	Control
AP3D1_HUMAN	18	1095.44	0.0235	1.9	Control
AP3M1_HUMAN	5	467.12	0.0104	1.3	Control
ARF1_HUMAN	4	411.07	0.0251	1.5	Treated
ARI1A_HUMAN*	3	106.92	0.0487	9.4	Treated
ARI1B_HUMAN*	2	53.9	0.0070	7.0	Treated
ASCC2_HUMAN\$	3	115.94	0.0457	1.5	Control
BOLA2_HUMAN	2	116.63	0.0163	3.2	Control
BRD2_HUMAN	8	655.25	0.0064	2.1	Control
CADH6_HUMAN	3	79.62	0.0399	4.1	Treated
CD5R1_HUMAN	3	68.85	0.0069	1.9	Treated
CHD3_HUMAN	3	152.11	0.0430	2.6	Treated
CHD7_HUMAN	5	276.41	0.0212	4.7	Treated
CHD9_HUMAN	2	335.78	0.0319	28.6	Treated
COA7_HUMAN	2	155.81	0.0069	18.9	Treated
COIA1_HUMAN*	7	364.04	0.0417	2.5	Treated
COX5A_HUMAN\$	2	159.69	0.0414	12.5	Control
CSN2_HUMAN	4	214.29	0.0345	2.1	Control
CUL2_HUMAN*	2	133.35	0.0098	2.4	Control
CWC22_HUMAN	24	1118.15	0.0060	2.0	Treated
CYFP1_HUMAN*	7	1027.2	0.0015	9.5	Treated
DDX21_HUMAN	16	952.54	0.0304	1.7	Control
DEN5A_HUMAN	3	77.21	0.0498	1.6	Control
DHX30_HUMAN\$	17	1184.8	0.0011	8.4	Control

Appendices

DIAP1_HUMAN ^{\$}	7	289.5	0.0051	1.7	Treated
DJB12_HUMAN ^{\$}	2	77.18	0.0149	1.6	Control
DNJA2_HUMAN ^{\$}	12	706.66	0.0337	1.4	Treated
DYHC2_HUMAN	7	110.81	0.0449	1.4	Treated
EF1D_HUMAN ^{\$}	5	399.44	0.0136	1.7	Control
EIF3I_HUMAN	3	161.87	0.0106	2.5	Control
EWS_HUMAN	3	144.01	0.0198	1.6	Treated
F120B_HUMAN ^{\$}	11	424.17	0.0087	2.5	Treated
FAT1_HUMAN*	3	108.07	0.0168	6.2	Treated
FLNA_HUMAN ^{\$}	11	466.43	0.0362	1.5	Control
FLNC_HUMAN	5	214.15	0.0133	5.5	Control
GBRL2_HUMAN*	2	86.05	0.0095	99.3	Treated
H13_HUMAN	7	511.1	0.0103	1.3	Control
HAKAI_HUMAN ^{\$}	3	66.2	0.0059	2.1	Treated
HDGR2_HUMAN	4	384.18	0.0222	2.3	Control
HECD1_HUMAN	34	1847.88	0.0372	5.1	Treated
HNRH3_HUMAN ^{\$}	2	144.69	0.0074	3.4	Treated
HP1B3_HUMAN	5	285.56	0.0428	1.6	Treated
IDE_HUMAN ^{\$}	9	443.65	0.0121	3.1	Treated
IF2P_HUMAN ^{\$}	2	228.11	0.0050	1.3	Control
IQEC2_HUMAN	3	71.58	0.0038	3.1	Treated
IQGA2_HUMAN	2	178.05	0.0189	2.4	Treated
LYSC_HUMAN	2	53.91	0.0011	6.9	Treated
MAPK2_HUMAN	3	74.43	0.0410	1.1	Treated
MCM3_HUMAN ^{\$}	7	523.07	0.0169	1.9	Treated
MP2K3_HUMAN	3	79.38	0.0256	1.5	Treated
NAT10_HUMAN	2	101.89	0.0069	1.5	Control
NCBP1_HUMAN	4	270.97	0.0310	1.3	Control
NDUAD_HUMAN	2	58.96	0.0038	400.7	Control
*					
NONO_HUMAN ^{\$}	42	3474.52	0.0212	1.2	Control
NPS3A_HUMAN ^{\$}	11	655.65	0.0460	2.2	Treated
NUCL_HUMAN ^{\$}	20	1643.72	0.0121	1.7	Control
OLA1_HUMAN	7	507.79	0.0112	1.7	Control
PERT_HUMAN	4	78.77	0.0000	16.2	Control
PHLB2_HUMAN*	6	400.06	0.0002	4.0	Treated
PHS_HUMAN*	4	207.2	0.0097	12.8	Treated
PIMT_HUMAN	4	164.87	0.0472	1.9	Treated
PP1A_HUMAN ^{\$}	3	540.76	0.0094	42.5	Treated
PP1B_HUMAN ^{\$}	3	498.3	0.0080	43.1	Treated
PP1G_HUMAN ^{\$}	3	514.47	0.0086	44.7	Treated
PPP6_HUMAN	2	117.27	0.0004	1.8	Treated
PPR29_HUMAN	2	60.63	0.0083	2.8	Treated
PR38A_HUMAN ^{\$}	6	448.94	0.0222	1.5	Treated
PRP8_HUMAN ^{\$}	13	546.88	0.0069	5.7	Treated
RBBP6_HUMAN	7	241.44	0.0064	1.7	Control
RBM33_HUMAN*	8	397.24	0.0001	7.2	Treated
RCN1_HUMAN	4	140.35	0.0033	7.5	Treated

Appendices

RENT1_HUMAN ^{\$}	2	137.14	0.0056	2.0	Control
RIC8A_HUMAN	3	72.54	0.0016	5.9	Control
RL6_HUMAN ^{\$}	12	776.52	0.0251	1.3	Treated
RL22L_HUMAN	2	281.25	0.0077	2.7	Control
RL23_HUMAN ^{\$}	11	828.8	0.0048	2.4	Control
RL37A_HUMAN	3	195.39	0.0024	7.6	Control
RL38_HUMAN*	5	213.6	0.0001	64.2	Control
RLA0_HUMAN ^{\$}	11	1192.83	0.0252	1.8	Control
RM12_HUMAN	2	122.66	0.0207	2.0	Control
RM14_HUMAN*	3	256.61	0.0393	3.9	Control
RNF39_HUMAN	2	71.35	0.0178	1.8	Treated
RS12_HUMAN ^{\$}	8	620.18	0.0006	5.3	Control
RS15A_HUMAN ^{\$}	10	500.49	0.0366	1.9	Control
RS16_HUMAN ^{\$}	7	752.14	0.0140	2.5	Control
RS21_HUMAN*	4	226.66	0.0087	19.2	Control
RS27A_HUMAN ^{\$}	5	287.24	0.0005	2.4	Control
RS28_HUMAN	3	205.25	0.0020	19.5	Control
RS29_HUMAN	4	203.77	0.0064	21.7	Control
RT14_HUMAN	3	261.1	0.0445	6.5	Control
RT24_HUMAN	2	65.48	0.0001	210.5	Control
RTRAF_HUMAN ^{\$}	16	1398.56	0.0056	1.7	Treated
RUXF_HUMAN*	2	179.46	0.0188	3.2	Treated
RUXGL_HUMAN *	2	153	0.0095	2.2	Treated
S4A7_HUMAN ^{\$}	5	191.33	0.0105	6.0	Control
SAP_HUMAN*	2	79.03	0.0339	15.7	Control
SF3B6_HUMAN ^{\$}	6	596.8	0.0435	4.5	Treated
SMD1_HUMAN ^{\$}	2	221.3	0.0129	2.3	Treated
SMRC2_HUMAN *	4	488.64	0.0031	7.8	Treated
SMUF2_HUMAN* \$	9	523.95	0.0369	2.1	Treated
SRP09_HUMAN	4	241.46	0.0003	7.7	Control
SRSF9_HUMAN ^{\$}	2	106.72	0.0274	11.4	Treated
SSRP1_HUMAN ^{\$}	18	1514.22	0.0328	1.9	Control
STN1_HUMAN*	2	56.96	0.0410	3.8	Treated
TBCD1_HUMAN	3	58.21	0.0065	13.5	Treated
TCPD_HUMAN ^{\$}	11	707.59	0.0104	7.7	Control
THS7A_HUMAN	5	115.89	0.0093	3.0	Treated
TIM50_HUMAN	4	198.77	0.0227	2.1	Treated
TRA2A_HUMAN ^{\$}	2	134.31	0.0441	1.6	Control
TRNK1_HUMAN ^{\$}	4	97.18	0.0336	2.1	Treated
TSR1_HUMAN	4	243.71	0.0117	2.7	Treated
UBR4_HUMAN	12	712.75	0.0077	4.4	Treated
USP9X_HUMAN	24	2754.68	0.0170	15.8	Control
VP13B_HUMAN	3	74.47	0.0251	15.8	Treated
WDR59_HUMAN \$	5	214.8	0.0143	4.0	Treated

Appendices

YTDC1_HUMAN [§]	8	434.54	0.0350	1.9	Control
ZN609_HUMAN	2	92.97	0.0426	1.7	Control

Key

!: SwissProt Protein ID

@: The number of unique peptides used for quantification

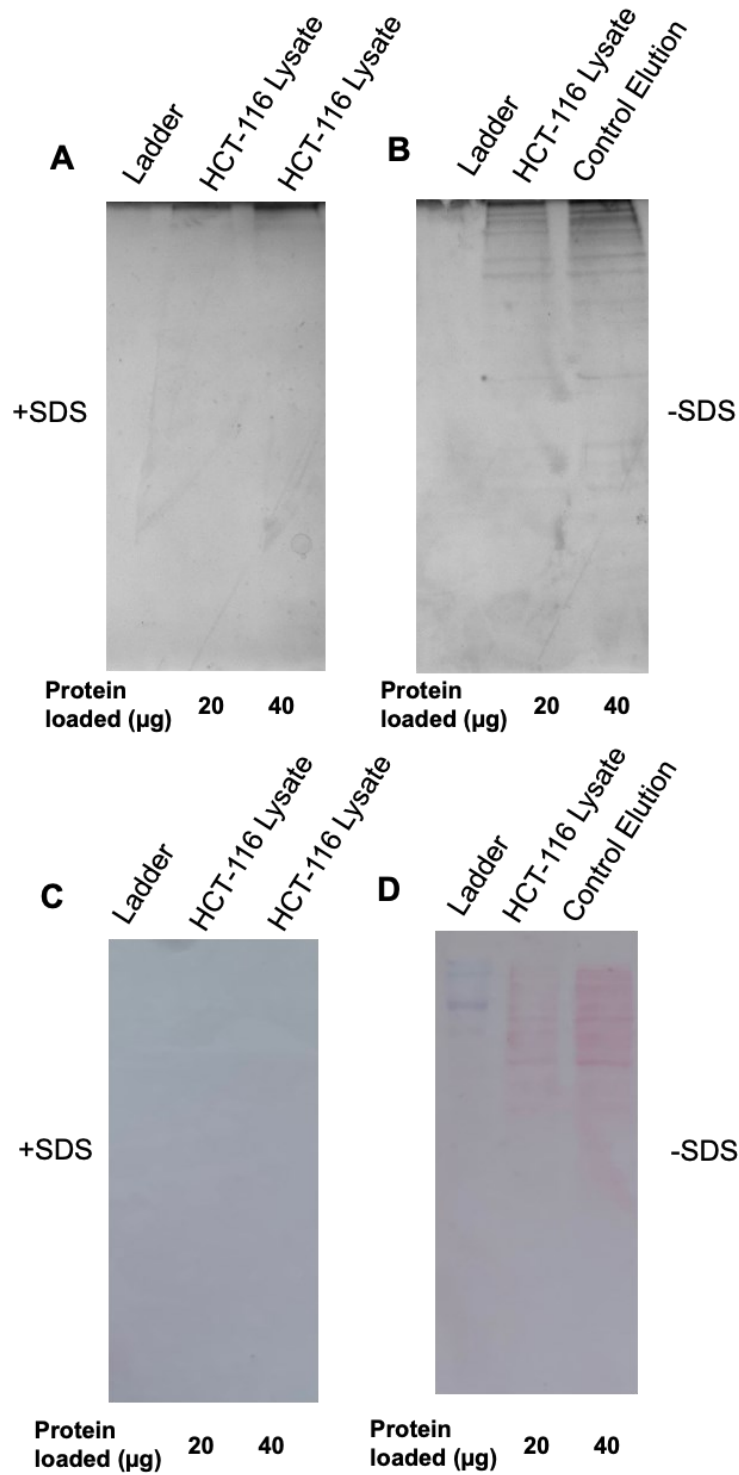
&: The protein confidence score for each protein assigned by Mascot

^: The p-value generated by Progenesis Q1 for proteomics

*: Protein hit identified in the beadome but with a >2 fold maximum change in abundance between the control and treated PTEN.

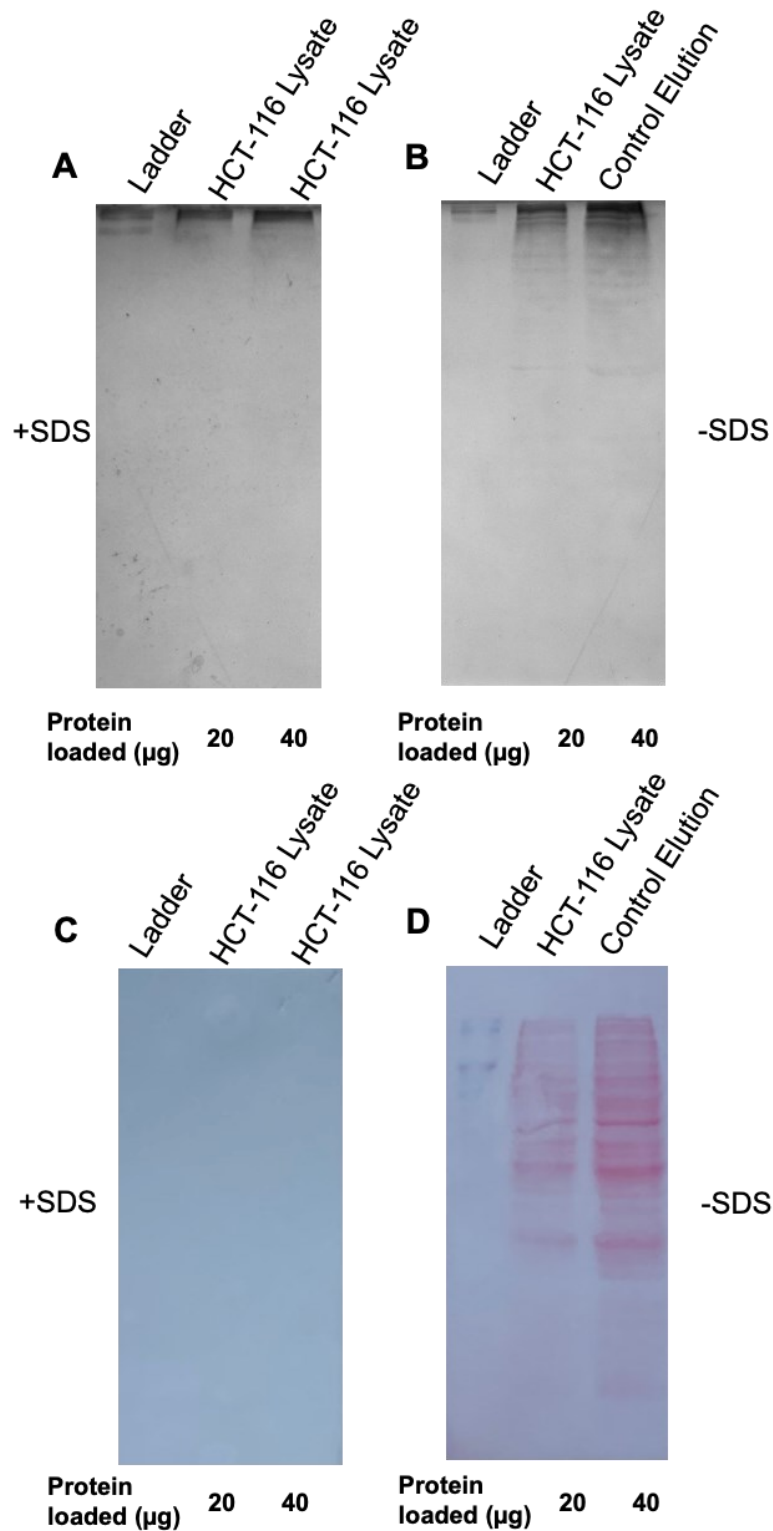
§: Protein hit identified in the beadome with a <2 fold maximum change in abundance between the control and treated PTENome.

£: Protein hit identified in the beadome with a p value < 0.05



Supplementary Figure 3 Western Blot Analysis of HCT-116 WT lysates after a low voltage transfer overnight in the presence and absence of SDS.

Increasing amounts of HCT-116 lysate was resolved on a 10% polyacrylamide gel before transfer with (A and C) and without (B and D) 0.1% SDS in the transfer buffer at 30V overnight at 4°C. The gels were stained post-transfer with Coomassie (A and B) and the blots were stained post-transfer with Ponceau S (C and D).



Supplementary Figure 4 Western Blot Analysis of HCT-116 WT lysates transferred after a high voltage transfer for 1h in the presence and absence of SDS.

Increasing amounts of HCT-116 lysate was resolved on a 10% polyacrylamide gel before transfer with (A and C) and without (B and D) 0.1% SDS in the transfer buffer at 100V for 1h on ice. The gels were stained post-transfer with Coomassie (A and B) and the blots were stained post-transfer with Ponceau S (C and D).

Supplementary Table 4 All PTEN-Interactors Identified with High Throughput Physical Evidence (Modified from BioGRID database (Stark et al., 2006))

Interactor	Description	Accounts of Physical Evidence	
		HTP	LTP
ABCF2	ATP-binding cassette, sub-family F (GCN20), member 2	1	0
ACACA	acetyl-CoA carboxylase alpha	1	0
ACACB	acetyl-CoA carboxylase beta	1	0
ACAP2	ArfGAP with coiled-coil, ankyrin repeat and PH domains 2	1	0
ACAT1	acetyl-CoA acetyltransferase 1	1	0
ACP1	acid phosphatase 1, soluble	1	1
ACTL6A	actin-like 6A	1	0
ADAR	adenosine deaminase, RNA-specific	1	0
AFG3L2	AFG3-like AAA ATPase 2	1	0
AHCYL1	adenosylhomocysteinase-like 1	1	0
AKAP12	A kinase (PRKA) anchor protein 12	1	0
AKT1	v-akt murine thymoma viral oncogene homolog 1	1	1
ALYREF	Aly/REF export factor	1	0
AMOT	angiominin	2	0
ANAPC10	anaphase promoting complex subunit 10	1	0
ANAPC7	anaphase promoting complex subunit 7	1	2
ANG	angiogenin, ribonuclease, RNase A family, 5	1	0
ANKRD11	ankyrin repeat domain 11	1	0
ANP32B	acidic (leucine-rich) nuclear phosphoprotein 32 family, member B	1	0
ANP32E	acidic (leucine-rich) nuclear phosphoprotein 32 family, member E	1	0
ANXA2P2	annexin A2 pseudogene 2	1	0
APOD	apolipoprotein D	1	1
ARAP3	ArfGAP with RhoGAP domain, ankyrin repeat and PH domain 3	1	1

Appendices

ARF4	ADP-ribosylation factor 4	1	0
ARMC2	armadillo repeat containing 2	1	0
ARMCX3	armadillo repeat containing, X-linked 3	1	0
ARRB1	arrestin, beta 1	1	0
ASCC3	activating signal cointegrator 1 complex subunit 3	1	0
ASPRV1	aspartic peptidase, retroviral-like 1	1	0
ATP5A1	ATP synthase, H ⁺ transporting, mitochondrial F1 complex, alpha subunit 1, cardiac muscle	1	0
ATP5C1	ATP synthase, H ⁺ transporting, mitochondrial F1 complex, gamma polypeptide 1	1	0
ATRX	alpha thalassemia/mental retardation syndrome X-linked	1	0
BAG2	BCL2-associated athanogene 2	1	0
BBX	bobby sox homolog (Drosophila)	1	0
BCKDHA	branched chain keto acid dehydrogenase E1, alpha polypeptide	1	0
BEX1	brain expressed, X-linked 1	1	0
BIRC6	baculoviral IAP repeat containing 6	1	0
BOP1	block of proliferation 1	1	0
BUB3	BUB3 mitotic checkpoint protein	1	0
C16ORF13	chromosome 16 open reading frame 13	1	0
C16ORF71	chromosome 16 open reading frame 71	1	0
C2CD4C	C2 calcium-dependent domain containing 4C	1	0
C9ORF156	chromosome 9 open reading frame 156	1	0
CACTIN-AS1	CACTIN antisense RNA 1	1	0
CAD	carbamoyl-phosphate synthetase 2, aspartate transcarbamylase, and dihydroorotase	1	0
CALM1	calmodulin 1 (phosphorylase kinase, delta)	1	0
CAND1	cullin-associated and neddylation-dissociated 1	1	0
CAPRIN2	caprin family member 2	1	0
CCDC180	coiled-coil domain containing 180	1	0
CCDC47	coiled-coil domain containing 47	1	0

Appendices

CCDC7	coiled-coil domain containing 7	1	0
CCND2	cyclin D2	1	0
CCT2	chaperonin containing TCP1, subunit 2 (beta)	1	0
CCT3	chaperonin containing TCP1, subunit 3 (gamma)	1	0
CCT4	chaperonin containing TCP1, subunit 4 (delta)	1	0
CCT6A	chaperonin containing TCP1, subunit 6A (zeta 1)	1	0
CCT8	chaperonin containing TCP1, subunit 8 (theta)	1	0
CDH3	cadherin 3, type 1, P-cadherin (placental)	1	0
CENPL	centromere protein L	1	0
CEP131	centrosomal protein 131kDa	1	0
CEP162	centrosomal protein 162kDa	1	0
CEP170	centrosomal protein 170kDa	1	0
CEP97	centrosomal protein 97kDa	1	0
CFL1	cofilin 1 (non-muscle)	1	0
CHD4	chromodomain helicase DNA binding protein 4	1	0
CHGB	chromogranin B (secretogranin 1)	1	0
CHMP4BP1	charged multivesicular body protein 4B pseudogene 1	1	0
CHTOP	chromatin target of PRMT1	1	0
CIRBP	cold inducible RNA binding protein	1	0
CLCC1	chloride channel CLIC-like 1	1	0
CLNK	cytokine-dependent hematopoietic cell linker	1	0
CMAS	cytidine monophosphate N-acetylneuraminic acid synthetase	1	0
CMTM1	CKLF-like MARVEL transmembrane domain containing 1	1	0
CNBP	CCHC-type zinc finger, nucleic acid binding protein	1	0
CNTROB	centrobin, centrosomal BRCA2 interacting protein	1	0
COPA	coatamer protein complex, subunit alpha	1	0

Appendices

COPB1	coatomer protein complex, subunit beta 1	1	0
COPS6	COP9 signalosome subunit 6	1	0
CSNK2A1	casein kinase 2, alpha 1 polypeptide	1	4
CSNK2A2	casein kinase 2, alpha prime polypeptide	1	2
CUL4A	cullin 4A	1	0
CXCL1	chemokine (C-X-C motif) ligand 1 (melanoma growth stimulating activity, alpha)	1	0
CXXC1	CXXC finger protein 1	1	1
DAP3	death associated protein 3	1	0
DBN1	drebrin 1	1	0
DBT	dihydrolipoamide branched chain transacylase E2	1	0
DCAF11	DDB1 and CUL4 associated factor 11	1	0
DCAF13	DDB1 and CUL4 associated factor 13	1	2
DDOST	dolichyl-diphosphooligosaccharide--protein glycosyltransferase subunit (non-catalytic)	1	0
DDX1	DEAD (Asp-Glu-Ala-Asp) box helicase 1	1	0
DDX21	DEAD (Asp-Glu-Ala-Asp) box helicase 21	1	0
DDX24	DEAD (Asp-Glu-Ala-Asp) box helicase 24	1	0
DDX47	DEAD (Asp-Glu-Ala-Asp) box polypeptide 47	1	0
DDX50	DEAD (Asp-Glu-Ala-Asp) box polypeptide 50	1	0
DGKZ	diacylglycerol kinase, zeta	1	0
DHX15	DEAH (Asp-Glu-Ala-His) box helicase 15	1	0
DHX9	DEAH (Asp-Glu-Ala-His) box helicase 9	1	0
DNAJA1	DnaJ (Hsp40) homolog, subfamily A, member 1	2	0
DNAJA2	DnaJ (Hsp40) homolog, subfamily A, member 2	1	0
DNAJA3	DnaJ (Hsp40) homolog, subfamily A, member 3	1	0
DNAJB6	DnaJ (Hsp40) homolog, subfamily B, member 6	1	0
DNAJC10	DnaJ (Hsp40) homolog, subfamily C, member 10	1	0
DNAJC2	DnaJ (Hsp40) homolog, subfamily C, member 2	1	0

Appendices

DPM1	dolichyl-phosphate mannosyltransferase polypeptide 1, catalytic subunit	1	0
DRG1	developmentally regulated GTP binding protein 1	1	0
DSG1	desmoglein 1	1	0
DSP	desmoplakin	1	0
DUT	deoxyuridine triphosphatase	1	0
EEF2	eukaryotic translation elongation factor 2	1	0
EEFSEC	eukaryotic elongation factor, selenocysteine-tRNA-specific	1	0
EIF4E	eukaryotic translation initiation factor 4E	1	0
EIF6	eukaryotic translation initiation factor 6	1	0
ELAVL1	ELAV like RNA binding protein 1	1	0
EMD	emerin	2	0
EML1	echinoderm microtubule associated protein like 1	1	0
EPHA2	EPH receptor A2	1	0
EPRS	glutamyl-prolyl-tRNA synthetase	1	0
ETS1	v-ets avian erythroblastosis virus E26 oncogene homolog 1	1	0
EXOC5	exocyst complex component 5	1	0
EXOSC1	exosome component 1	1	0
EXOSC2	exosome component 2	1	0
EXOSC4	exosome component 4	1	0
EXOSC7	exosome component 7	1	0
EYA2	EYA transcriptional coactivator and phosphatase 2	1	0
FARSA	phenylalanyl-tRNA synthetase, alpha subunit	1	0
FARSB	phenylalanyl-tRNA synthetase, beta subunit	1	0
FASN	fatty acid synthase	1	0
FBL	fibrillarin	1	0
FBXO22	F-box protein 22	1	1
FEN1	flap structure-specific endonuclease 1	1	0

Appendices

FKBP5	FK506 binding protein 5	1	1
FLNA	filamin A, alpha	1	0
FLNB	filamin B, beta	2	0
FNBP1	formin binding protein 1	1	0
FOXK1	forkhead box K1	1	0
FSBP	fibrinogen silencer binding protein	1	0
FSIP2	fibrous sheath interacting protein 2	1	0
FUBP3	far upstream element (FUSE) binding protein 3	1	0
GEMIN4	gem (nuclear organelle) associated protein 4	1	0
GNAI1	guanine nucleotide binding protein (G protein), alpha inhibiting activity polypeptide 1	1	0
GNAI2	guanine nucleotide binding protein (G protein), alpha inhibiting activity polypeptide 2	1	0
GNB4	guanine nucleotide binding protein (G protein), beta polypeptide 4	1	0
GNL3	guanine nucleotide binding protein-like 3 (nucleolar)	1	0
GPC1	glypican 1	2	0
GPC4	glypican 4	1	0
GPKOW	G patch domain and KOW motifs	1	0
GSTM2	glutathione S-transferase mu 2 (muscle)	1	0
GTF3C2	general transcription factor IIIC, polypeptide 2, beta 110kDa	1	0
GTF3C3	general transcription factor IIIC, polypeptide 3, 102kDa	1	0
GTF3C5	general transcription factor IIIC, polypeptide 5, 63kDa	1	0
H1F0	H1 histone family, member 0	1	0
HADHA	hydroxyacyl-CoA dehydrogenase/3-ketoacyl-CoA thiolase/enoyl-CoA hydratase (trifunctional protein), alpha subunit	1	0
HBA1	hemoglobin, alpha 1	1	0
HDAC6	histone deacetylase 6	1	0
HIST1H2AB	histone cluster 1, H2ab	1	0
HNRNPA1	heterogeneous nuclear ribonucleoprotein A1	1	0

Appendices

HNRNPA3	heterogeneous nuclear ribonucleoprotein A3	1	0
HNRNPAB	heterogeneous nuclear ribonucleoprotein A/B	1	0
HNRNPL	heterogeneous nuclear ribonucleoprotein L	1	0
HNRNPU	heterogeneous nuclear ribonucleoprotein U (scaffold attachment factor A)	1	0
HNRNPUL1	heterogeneous nuclear ribonucleoprotein U-like 1	1	0
HPSE2	heparanase 2 (inactive)	1	0
HSD17B1	hydroxysteroid (17-beta) dehydrogenase 1	1	0
HSD17B10	hydroxysteroid (17-beta) dehydrogenase 10	1	0
HSP90AA1	heat shock protein 90kDa alpha (cytosolic), class A member 1	1	0
HSP90AB1	heat shock protein 90kDa alpha (cytosolic), class B member 1	2	0
HSP90B1	heat shock protein 90kDa beta (Grp94), member 1	1	0
HSPA1A	heat shock 70kDa protein 1A	1	0
HSPA1L	heat shock 70kDa protein 1-like	1	0
HSPA2	heat shock 70kDa protein 2	1	0
HSPA4	heat shock 70kDa protein 4	1	0
HSPA4L	heat shock 70kDa protein 4-like	1	0
HSPA6	heat shock 70kDa protein 6 (HSP70B')	1	0
HSPA8	heat shock 70kDa protein 8	2	0
HSPBP1	HSPA (heat shock 70kDa) binding protein, cytoplasmic cochaperone 1	1	0
HSPD1	heat shock 60kDa protein 1 (chaperonin)	1	0
HSPH1	heat shock 105kDa/110kDa protein 1	1	0
IDE	insulin-degrading enzyme	1	1
IGSF10	immunoglobulin superfamily, member 10	1	0
IKBKAP	inhibitor of kappa light polypeptide gene enhancer in B-cells, kinase complex-associated protein	1	0
IL24	interleukin 24	1	0
ILF2	interleukin enhancer binding factor 2	1	0

Appendices

ILF3	interleukin enhancer binding factor 3, 90kDa	1	0
IPO4	importin 4	1	1
IPO5	importin 5	1	0
IPO7	importin 7	1	0
IQCF2	IQ motif containing F2	1	0
IRS4	insulin receptor substrate 4	1	2
ITGA6	integrin, alpha 6	1	0
ITGB7	integrin, beta 7	1	0
JUP	junction plakoglobin	1	0
KBTBD4	kelch repeat and BTB (POZ) domain containing 4	1	0
KCNAB2	potassium voltage-gated channel, shaker-related subfamily, beta member 2	1	0
KDM1A	lysine (K)-specific demethylase 1A	1	0
KIF11	kinesin family member 11	1	0
KPNB1	karyopherin (importin) beta 1	1	0
KRT3	keratin 3	1	0
KRT39	keratin 39	1	0
LDHA	lactate dehydrogenase A	1	0
LDHB	lactate dehydrogenase B	2	0
LGALS1	lectin, galactoside-binding, soluble, 1	1	0
LIMA1	LIM domain and actin binding 1	1	0
LMNB1	lamin B1	1	0
LRPPRC	leucine-rich pentatricopeptide repeat containing	1	0
LTV1	LTV1 ribosome biogenesis factor	1	0
LUZP1	leucine zipper protein 1	1	0
LYRM1	LYR motif containing 1	1	0
MAGED2	melanoma antigen family D, 2	1	0

Appendices

MAP2K3	mitogen-activated protein kinase kinase 3	1	0
MAPK1	mitogen-activated protein kinase 1	1	0
MARCKS	myristoylated alanine-rich protein kinase C substrate	1	0
MATR3	matrin 3	1	0
MCCC1	methylcrotonoyl-CoA carboxylase 1 (alpha)	1	0
MCCC2	methylcrotonoyl-CoA carboxylase 2 (beta)	1	0
MCM2	minichromosome maintenance complex component 2	1	0
MCM3	minichromosome maintenance complex component 3	1	0
MCM5	minichromosome maintenance complex component 5	1	0
MCM7	minichromosome maintenance complex component 7	2	0
MDN1	MDN1, midasin homolog (yeast)	1	0
METTL16	methyltransferase like 16	1	0
MEX3C	mex-3 RNA binding family member C	1	2
MEX3D	mex-3 RNA binding family member D	1	0
MKI67	marker of proliferation Ki-67	1	0
MPRIP	myosin phosphatase Rho interacting protein	2	0
MRPL11	mitochondrial ribosomal protein L11	1	0
MRPS22	mitochondrial ribosomal protein S22	1	0
MRPS23	mitochondrial ribosomal protein S23	1	0
MRPS27	mitochondrial ribosomal protein S27	1	0
MRPS28	mitochondrial ribosomal protein S28	1	0
MRPS7	mitochondrial ribosomal protein S7	1	0
MRPS9	mitochondrial ribosomal protein S9	1	0
MSH6	mutS homolog 6	1	0
MTHFD1	methylenetetrahydrofolate dehydrogenase (NADP+ dependent) 1, methenyltetrahydrofolate cyclohydrolase, formyltetrahydrofolate synthetase	1	0

Appendices

MTHFD2	methylenetetrahydrofolate dehydrogenase (NADP+ dependent) 2, methenyltetrahydrofolate cyclohydrolase	1	0
MYBBP1A	MYB binding protein (P160) 1a	1	0
MYC	v-myc avian myelocytomatosis viral oncogene homolog	1	0
MYH10	myosin, heavy chain 10, non-muscle	1	0
MYL12A	myosin, light chain 12A, regulatory, non-sarcomeric	1	0
MYO1B	myosin IB	1	0
MYO1C	myosin IC	1	0
MYO1D	myosin ID	1	0
MYOF	myoferlin	1	0
NACA	nascent polypeptide-associated complex alpha subunit	1	0
NCBP1	nuclear cap binding protein subunit 1, 80kDa	1	0
NCF1	neutrophil cytosolic factor 1	1	0
NCOR2	nuclear receptor corepressor 2	1	0
NEDD1	neural precursor cell expressed, developmentally down-regulated 1	1	0
NME1	NME/NM23 nucleoside diphosphate kinase 1	2	0
NOC2L	nucleolar complex associated 2 homolog (<i>S. cerevisiae</i>)	1	0
NOP56	NOP56 ribonucleoprotein	1	0
NOP58	NOP58 ribonucleoprotein	1	0
NPM3	nucleophosmin/nucleoplasmin 3	1	0
NRCAM	neuronal cell adhesion molecule	1	0
OAT	ornithine aminotransferase	1	0
OSGIN1	oxidative stress induced growth inhibitor 1	1	0
P2RY11	purinergic receptor P2Y, G-protein coupled, 11	1	0
PARK2	parkin RBR E3 ubiquitin protein ligase	1	0
PARK7	parkinson protein 7	1	4
PBRM1	polybromo 1	1	0

Appendices

PC	pyruvate carboxylase	1	0
PCCA	propionyl CoA carboxylase, alpha polypeptide	1	0
PCCB	propionyl CoA carboxylase, beta polypeptide	1	0
PCDHGA10	protocadherin gamma subfamily A, 10	1	0
PCNA	proliferating cell nuclear antigen	1	0
PDGFRB	platelet-derived growth factor receptor, beta polypeptide	1	3
PDHA1	pyruvate dehydrogenase (lipoamide) alpha 1	1	0
PDZD9	PDZ domain containing 9	1	0
PELO	pelota homolog (Drosophila)	1	0
PELP1	proline, glutamate and leucine rich protein 1	1	0
PGK1	phosphoglycerate kinase 1	1	3
PHB	prohibitin	1	0
PHB2	prohibitin 2	1	0
PICK1	protein interacting with PRKCA 1	1	1
PKM	pyruvate kinase, muscle	1	0
PLEC	plectin	1	0
PLEKHA1	pleckstrin homology domain containing, family A (phosphoinositide binding specific) member 1	1	0
POLDIP2	polymerase (DNA-directed), delta interacting protein 2	2	0
POLR1A	polymerase (RNA) I polypeptide A, 194kDa	1	0
POLR2A	polymerase (RNA) II (DNA directed) polypeptide A, 220kDa	1	0
POLR2B	polymerase (RNA) II (DNA directed) polypeptide B, 140kDa	1	0
POLR2H	polymerase (RNA) II (DNA directed) polypeptide H	1	0
POP1	processing of precursor 1, ribonuclease P/MRP subunit (<i>S. cerevisiae</i>)	1	0
PPL	periplakin	1	0
PPM1G	protein phosphatase, Mg ²⁺ /Mn ²⁺ dependent, 1G	1	0
PPP1CA	protein phosphatase 1, catalytic subunit, alpha isozyme	1	0
PPP1R10	protein phosphatase 1, regulatory subunit 10	1	0

Appendices

PPP2CA	protein phosphatase 2, catalytic subunit, alpha isozyme	1	0
PPP5C	protein phosphatase 5, catalytic subunit	1	0
PRDX3	peroxiredoxin 3	1	0
PRKDC	protein kinase, DNA-activated, catalytic polypeptide	1	0
PRPF19	pre-mRNA processing factor 19	1	0
PRPF8	pre-mRNA processing factor 8	1	0
PSMD2	proteasome (prosome, macropain) 26S subunit, non-ATPase, 2	1	0
PSMD3	proteasome (prosome, macropain) 26S subunit, non-ATPase, 3	1	0
PSMD7	proteasome (prosome, macropain) 26S subunit, non-ATPase, 7	1	0
PTDSS1	phosphatidylserine synthase 1	1	0
PTEN	phosphatase and tensin homolog	1	1
PTK2	protein tyrosine kinase 2	1	6
PTPN13	protein tyrosine phosphatase, non-receptor type 13 (APO-1/CD95 (Fas)-associated phosphatase)	2	0
PURA	purine-rich element binding protein A	1	0
PURB	purine-rich element binding protein B	1	0
PXN	paxillin	1	1
QPCTL	glutaminy-peptide cyclotransferase-like	1	0
QPRT	quinolinate phosphoribosyltransferase	1	0
RAB7A	RAB7A, member RAS oncogene family	1	0
RAD21	RAD21 homolog (S. pombe)	1	0
RALB	v-ral simian leukemia viral oncogene homolog B	1	0
RAMP2	receptor (G protein-coupled) activity modifying protein 2	1	0
RANBP2	RAN binding protein 2	1	0
RANGAP1	Ran GTPase activating protein 1	1	0
RBBP5	retinoblastoma binding protein 5	1	0
RBM4	RNA binding motif protein 4	1	0

Appendices

RCC2	regulator of chromosome condensation 2	1	0
RCN1	reticulocalbin 1, EF-hand calcium binding domain	1	0
RFC3	replication factor C (activator 1) 3, 38kDa	1	0
RFC4	replication factor C (activator 1) 4, 37kDa	2	0
RFC5	replication factor C (activator 1) 5, 36.5kDa	1	0
RING1	ring finger protein 1	1	0
RIOK1	RIO kinase 1	1	0
RPA1	replication protein A1, 70kDa	1	0
RPF2	ribosome production factor 2 homolog (<i>S. cerevisiae</i>)	1	0
RPL10	ribosomal protein L10	1	0
RPL10A	ribosomal protein L10a	2	0
RPL12	ribosomal protein L12	3	0
RPL13	ribosomal protein L13	1	0
RPL13A	ribosomal protein L13a	1	0
RPL14	ribosomal protein L14	2	1
RPL17	ribosomal protein L17	1	0
RPL18A	ribosomal protein L18a	1	0
RPL21	ribosomal protein L21	1	0
RPL22	ribosomal protein L22	1	0
RPL22L1	ribosomal protein L22-like 1	2	0
RPL23	ribosomal protein L23	2	0
RPL23A	ribosomal protein L23a	2	0
RPL26	ribosomal protein L26	1	0
RPL27	ribosomal protein L27	2	0
RPL27A	ribosomal protein L27a	2	0
RPL28	ribosomal protein L28	1	0
RPL30	ribosomal protein L30	1	0

Appendices

RPL31	ribosomal protein L31	2	0
RPL32	ribosomal protein L32	1	0
RPL34	ribosomal protein L34	1	0
RPL36	ribosomal protein L36	1	0
RPL38	ribosomal protein L38	2	0
RPL5	ribosomal protein L5	1	0
RPL6	ribosomal protein L6	1	0
RPL7	ribosomal protein L7	2	0
RPLP0	ribosomal protein, large, P0	1	0
RPLP2	ribosomal protein, large, P2	1	0
RPN2	ribophorin II	1	0
RPP30	ribonuclease P/MRP 30kDa subunit	1	0
RPP38	ribonuclease P/MRP 38kDa subunit	1	0
RPP40	ribonuclease P/MRP 40kDa subunit	1	0
RPS11	ribosomal protein S11	2	0
RPS13	ribosomal protein S13	2	0
RPS15	ribosomal protein S15	1	0
RPS15A	ribosomal protein S15a	2	0
RPS17	ribosomal protein S17	1	0
RPS2	ribosomal protein S2	1	0
RPS20	ribosomal protein S20	1	0
RPS23	ribosomal protein S23	1	0
RPS25	ribosomal protein S25	2	0
RPS26	ribosomal protein S26	2	0
RPS27	ribosomal protein S27	2	0
RPS27A	ribosomal protein S27a	2	0
RPS3	ribosomal protein S3	1	0

Appendices

RPS4X	ribosomal protein S4, X-linked	2	0
RPS5	ribosomal protein S5	1	0
RPS6	ribosomal protein S6	1	0
RPS9	ribosomal protein S9	2	0
RPTOR	regulatory associated protein of MTOR, complex 1	1	0
RPUSD1	RNA pseudouridylate synthase domain containing 1	1	0
RSL1D1	ribosomal L1 domain containing 1	1	0
RYBP	RING1 and YY1 binding protein	1	0
RYR3	ryanodine receptor 3	1	0
S100A8	S100 calcium binding protein A8	1	0
S100A9	S100 calcium binding protein A9	1	0
SCN10A	sodium channel, voltage-gated, type X, alpha subunit	1	0
SCYL2	SCY1-like 2 (<i>S. cerevisiae</i>)	1	0
SDC1	syndecan 1	1	0
SDC4	syndecan 4	1	0
SDCBP	syndecan binding protein (syntenin)	1	0
SEC61A1	Sec61 alpha 1 subunit (<i>S. cerevisiae</i>)	1	0
SERPINA7	serpin peptidase inhibitor, clade A (alpha-1 antiproteinase, antitrypsin), member 7	1	0
SET	SET nuclear proto-oncogene	1	0
SETX	senataxin	1	0
SFMBT1	Scm-like with four mbt domains 1	1	0
SHROOM3	shroom family member 3	1	0
SIN3A	SIN3 transcription regulator family member A	1	0
SKP1	S-phase kinase-associated protein 1	1	1
SLC12A2	solute carrier family 12 (sodium/potassium/chloride transporter), member 2	1	0
SLC25A1	solute carrier family 25 (mitochondrial carrier; citrate transporter), member 1	1	0
SLC25A13	solute carrier family 25 (aspartate/glutamate carrier), member 13	1	0

Appendices

SLC25A3	solute carrier family 25 (mitochondrial carrier; phosphate carrier), member 3	2	0
SLC25A5	solute carrier family 25 (mitochondrial carrier; adenine nucleotide translocator), member 5	1	0
SLC9A3R1	solute carrier family 9, subfamily A (NHE3, cation proton antiporter 3), member 3 regulator 1	1	7
SMARCA4	SWI/SNF related, matrix associated, actin dependent regulator of chromatin, subfamily a, member 4	1	0
SMARCA5	SWI/SNF related, matrix associated, actin dependent regulator of chromatin, subfamily a, member 5	1	0
SMC2	structural maintenance of chromosomes 2	1	0
SMC4	structural maintenance of chromosomes 4	1	0
SMCHD1	structural maintenance of chromosomes flexible hinge domain containing 1	1	0
SNED1	sushi, nidogen and EGF-like domains 1	1	0
SNRNP200	small nuclear ribonucleoprotein 200kDa (U5)	1	0
SNRPA	small nuclear ribonucleoprotein polypeptide A	1	0
SNRPA1	small nuclear ribonucleoprotein polypeptide A'	1	0
SNRPB2	small nuclear ribonucleoprotein polypeptide B	1	0
SNRPD1	small nuclear ribonucleoprotein D1 polypeptide 16kDa	1	0
SNTB2	syntrophin, beta 2 (dystrophin-associated protein A1, 59kDa, basic component 2)	1	0
SNX27	sorting nexin family member 27	3	4
SOCS1	suppressor of cytokine signaling 1	1	0
SPATA18	spermatogenesis associated 18	1	0
SPTA1	spectrin, alpha, erythrocytic 1	1	0
SPTAN1	spectrin, alpha, non-erythrocytic 1	1	0
SPTBN1	spectrin, beta, non-erythrocytic 1	1	0
SRGAP1	SLIT-ROBO Rho GTPase activating protein 1	1	0
SRP14	signal recognition particle 14kDa (homologous Alu RNA binding protein)	1	0
SRSF7	serine/arginine-rich splicing factor 7	1	0
SSB	Sjogren syndrome antigen B (autoantigen La)	1	0
SSFA2	sperm specific antigen 2	1	0

Appendices

SSR4	signal sequence receptor, delta	2	0
SSRP1	structure specific recognition protein 1	1	0
STAG2	stromal antigen 2	1	0
STIP1	stress-induced phosphoprotein 1	2	0
STK36	serine/threonine kinase 36	1	0
STRAP	serine/threonine kinase receptor associated protein	1	0
SUDS3	suppressor of defective silencing 3 homolog (<i>S. cerevisiae</i>)	1	0
SUGP2	SURP and G patch domain containing 2	2	0
TBC1D31	TBC1 domain family, member 31	1	0
TCF25	transcription factor 25 (basic helix-loop-helix)	1	0
TCL1B	T-cell leukemia/lymphoma 1B	1	0
TCP1	t-complex 1	1	0
TDRD15	tudor domain containing 15	1	0
TECR	trans-2,3-enoyl-CoA reductase	1	0
TERF2IP	telomeric repeat binding factor 2, interacting protein	1	0
THOC2	THO complex 2	1	0
THOC3	THO complex 3	1	0
THOC6	THO complex 6 homolog (<i>Drosophila</i>)	1	0
TMEFF1	transmembrane protein with EGF-like and two follistatin-like domains 1	1	0
TOPAZ1	testis and ovary specific PAZ domain containing 1	1	0
TPK1	thiamin pyrophosphokinase 1	1	0
TRIM28	tripartite motif containing 28	1	0
TRIM37	tripartite motif containing 37	1	0
TSGA10	testis specific, 10	1	0
TUBA1B	tubulin, alpha 1b	1	0
TUBA1C	tubulin, alpha 1c	1	0
TUBA3C	tubulin, alpha 3c	1	0

Appendices

TUBB	tubulin, beta class I	1	0
TUBB2A	tubulin, beta 2A class IIa	1	0
TUBB3	tubulin, beta 3 class III	1	0
TUBB4B	tubulin, beta 4B class IVb	2	0
TUFM	Tu translation elongation factor, mitochondrial	2	0
U2AF1	U2 small nuclear RNA auxiliary factor 1	2	0
UBA1	ubiquitin-like modifier activating enzyme 1	1	0
UBAC2	UBA domain containing 2	1	0
UBE2S	ubiquitin-conjugating enzyme E2S	1	1
UBL7	ubiquitin-like 7	1	0
UBXN1	UBX domain protein 1	1	0
UPF1	UPF1 regulator of nonsense transcripts homolog (yeast)	1	0
USP7	ubiquitin specific peptidase 7 (herpes virus-associated)	1	5
UTP14A	UTP14, U3 small nucleolar ribonucleoprotein, homolog A (yeast)	1	0
UTRN	utrophin	1	0
WWP1	WW domain containing E3 ubiquitin protein ligase 1	1	2
WWP2	WW domain containing E3 ubiquitin protein ligase 2	1	14
XPC	xeroderma pigmentosum, complementation group C	1	0
XRCC5	X-ray repair complementing defective repair in Chinese hamster cells 5 (double-strand-break rejoining)	1	0
XRCC6	X-ray repair complementing defective repair in Chinese hamster cells 6	1	0
YAF2	YY1 associated factor 2	1	0
YES1	YES proto-oncogene 1, Src family tyrosine kinase	1	0
YTHDC2	YTH domain containing 2	1	0
YTHDF2	YTH N(6)-methyladenosine RNA binding protein 2	1	0
ZC3H15	zinc finger CCCH-type containing 15	1	0
ZER1	zyg-11 related, cell cycle regulator	1	0

Appendices

ZNF318	zinc finger protein 318	1	0
ZNF326	zinc finger protein 326	1	0
ZNF391	zinc finger protein 391	1	0
ZSCAN18	zinc finger and SCAN domain containing 18	1	0